



UNIVERSITAT DE
BARCELONA

Sorption of perfluoroalkyl substances and Fluoroquinolone antibiotics in matrices of environmental interest

Joel Fabregat Palau

ADVERTIMENT. La consulta d'aquesta tesi queda condicionada a l'acceptació de les següents condicions d'ús: La difusió d'aquesta tesi per mitjà del servei TDX (www.tdx.cat) i a través del Dipòsit Digital de la UB (diposit.ub.edu) ha estat autoritzada pels titulars dels drets de propietat intel·lectual únicament per a usos privats emmarcats en activitats d'investigació i docència. No s'autoritza la seva reproducció amb finalitats de lucre ni la seva difusió i posada a disposició des d'un lloc aliè al servei TDX ni al Dipòsit Digital de la UB. No s'autoritza la presentació del seu contingut en una finestra o marc aliè a TDX o al Dipòsit Digital de la UB (framing). Aquesta reserva de drets afecta tant al resum de presentació de la tesi com als seus continguts. En la utilització o cita de parts de la tesi és obligat indicar el nom de la persona autora.

ADVERTENCIA. La consulta de esta tesis queda condicionada a la aceptación de las siguientes condiciones de uso: La difusión de esta tesis por medio del servicio TDR (www.tdx.cat) y a través del Repositorio Digital de la UB (diposit.ub.edu) ha sido autorizada por los titulares de los derechos de propiedad intelectual únicamente para usos privados enmarcados en actividades de investigación y docencia. No se autoriza su reproducción con finalidades de lucro ni su difusión y puesta a disposición desde un sitio ajeno al servicio TDR o al Repositorio Digital de la UB. No se autoriza la presentación de su contenido en una ventana o marco ajeno a TDR o al Repositorio Digital de la UB (framing). Esta reserva de derechos afecta tanto al resumen de presentación de la tesis como a sus contenidos. En la utilización o cita de partes de la tesis es obligado indicar el nombre de la persona autora.

WARNING. On having consulted this thesis you're accepting the following use conditions: Spreading this thesis by the TDX (www.tdx.cat) service and by the UB Digital Repository (diposit.ub.edu) has been authorized by the titular of the intellectual property rights only for private uses placed in investigation and teaching activities. Reproduction with lucrative aims is not authorized nor its spreading and availability from a site foreign to the TDX service or to the UB Digital Repository. Introducing its content in a window or frame foreign to the TDX service or to the UB Digital Repository is not authorized (framing). Those rights affect to the presentation summary of the thesis as well as to its contents. In the using or citation of parts of the thesis it's obliged to indicate the name of the author.

Doctoral Program in
ANALYTICAL CHEMISTRY AND ENVIRONMENT

**SORPTION OF PERFLUOROALKYL SUBSTANCES AND
FLUOROQUINOLONE ANTIBIOTICS IN MATRICES OF
ENVIRONMENTAL INTEREST**

A thesis presented to obtain the doctoral degree of the University of Barcelona by

JOEL FABREGAT PALAU

Barcelona, June 2022

Supervisors:

Dr. Anna Rigol Parera (UB)

Dr. Miquel Vidal Espinar (UB)

Dr. Zhiqiang Yu (GIG-CAS)

Tutors:

Dr. Anna Rigol Parera (UB)



UNIVERSITAT DE
BARCELONA



“Man is a part of nature, and his war against nature is inevitably a war against himself”

Rachel Carson

“What are the three most important rules of the chemist?”

“Label clearly. Measure twice. Eat elsewhere.”

Patrick Rothfuss

ACKNOWLEDGEMENTS

Com totes, aquesta tesi no ha estat fàcil. Ha estat un camí llarg i esgotador, però meravellós de recórrer al mateix temps, i que m'ha fet créixer tant professionalment com, vull pensar, personalment. Durant aquests anys diferents persones han fet que això hagi acabat sent una realitat, i m'agradaria adreçar-los unes paraules:

En primer lloc, vull donar les gràcies a la meva família, i sobretot als meus pares, per tot el suport incondicional que m'han donat des de sempre. Sé que a vegades sóc difícil i tinc les meves coses, però espero que us pugeu sentir orgullosos de mi.

En segon lloc, vull donar les gràcies als meus directors. Anna i Miquel, dubto que pugui plasmar amb paraules el que penso, però gràcies per confiar amb mi des del primer dia, pel tracte personal i proper que heu tingut i per dirigir-me de forma tan intel·ligent, sense posar-me més pressió de la que jo mateix em posava i per parar-me els peus quan tocava, així com per trobar sempre un moment per mi quan ho he necessitat tot i les vostres apretades agendes. De veritat que estic molt content i orgullós d'haver tingut uns directors com vosaltres. Professor Yu, thank you very much for all the care and support during my stance in Guangzhou, for all the scientific discussions we could have, and for your contributions in the frame of this PhD thesis.

En tercer lloc, vull donar les gràcies als meus amics. A tots els Sonrisas i Rulleros però sobretot a vosaltres Abel i Víctor per ser-hi des de que tinc memòria. Cris, tenir el teu suport durant aquests últims mesos ha estat imprescindible per poder acabar. Joyce, gracias también a ti, eres una más de la familia, i Miri, gràcies per tot, ets una bona amiga. Luke, Sekey, Mario, Meri, Marina, Miró, Huguet i un llarg etc: sabeu que us estimo molt també. Alfredo, celebraremos esto en Almodévar!! I als companys de laboratori: Yorgos, Joan, Arnau, Isaac i Dídac: gràcies per fer mes amè el dia a dia, ara us toca a vosaltres! También gracias a todos los Jugetones por hacer de los dos años en Guangzhou una experiencia increíble i sobretot gràcies Pablo i Pere per poder compartir tots aquells bons i mals moments amb vosaltres. Also I would like to acknowledge all the international GIG community and to all the lovely people I met in China, with special regards for Jiaxin and Alex.

最后，感谢我所有的 GIG 实验室伙伴，感谢他们给予我的所有帮助。我希望我们能在未来再次见面！

I per últim, gràcies a mi, per demostrar-me que puc amb tot el que em proposi.

SUMMARY

Perfluoroalkyl substances (PFASs) and fluoroquinolone antibiotics (FQs) are pollutants of environmental interest due to their widespread presence in environmental compartments and their high toxicity and disrupting effects of original ecosystems, respectively. PFASs are used in a wide array of applications, and their chemical structure consists in a fluorinated chain attached to a hydrophilic group. Due to their strong C – F bonds, they are hardly photo- and biodegraded, which makes them persist in the environment. On the other hand, FQs are widely used in human and veterinary medicine to treat diseases caused by both Gram positive and Gram negative pathogens. Due to their partial uptake by the organisms and consequent excretion, especially when used in livestock, they have been found in different environmental matrices. High FQ levels may disrupt the microbial communities of the original ecosystems and can generate resistant bacteria strains, thus diminishing their effectiveness for medical purposes.

After a contamination event, an evaluation of the potential threat to humans and ecosystems should be performed, a process which is known as risk assessment. Risk assessment studies require different input data and parameters to quantitatively evaluate the possible outcomes of a contamination episode. Data and parameters include knowing the concentration of the target contaminant in a specific scenario, considering toxicity towards different species and their possible degradation pathways, and taking into account the specific environmental conditions in which the contamination episode occurred (*e.g.*, the physicochemical characteristics of the soil/water system) and predicting the mobility of the contaminant along environmental matrices, among others. If risk assessment studies evidence that intervention actions should be implemented, remediation actions may be taken, including the use of sorbent materials such as biochars and activated carbons for the treatment of contaminated soils and waters aiming to decrease pollutant mobility.

The sorption/desorption process of a contaminant between solid and liquid matrices governs its environmental mobility. Understanding the sorption interaction mechanisms between sorbents and pollutants is important to extrapolate conclusions in other untested but characterized scenarios. Whereas soil OC has been suggested to be the main property affecting PFASs sorption by hydrophobic interactions, recently an additional role of the mineral phase has been highlighted in scenarios with low OC contents. On the other hand, multiple interaction mechanisms have been suggested to occur between FQs and soil organic and mineral phases, revealing a non-linear dependence with pH due to FQ speciation, which makes it difficult the extrapolation of conclusions to bulk soils. A quantitative parameter used in environmental models quantifying the sorption process is the solid-liquid distribution coefficient (K_d). It is necessary to develop K_d prediction models based on key pollutant and sorbent physicochemical properties descriptive of the interaction mechanisms involved in the sorption process. This, in turn may need the creation of robust, critically-reviewed K_d compilation datasets including as much information on physicochemical properties of the system as possible made of literature-gathered data and, if needed, new data derived from ad-hoc laboratory experiments.

Current K_d prediction models for PFASs and FQs in soil pure components, soils and/or carbon-rich materials are scarce, have limitations and require a wider range of applicability. Accordingly, the generation of new models aiming to predict its K_d in these environmental matrices are required for future risk assessment studies. Considering this, the main goal of this thesis has been to identify key parameters affecting PFASs and FQs sorption and to develop K_d prediction models in soils and related environmental matrices (including pure soil components and carbon-rich materials). To reach this main goal, we have performed sorption experiments of PFASs in soils and carbon-rich materials, in addition to sorption experiments of FQs in pure soil phases and soils. Besides, critically-reviewed compilations of K_d data of PFASs and FQs in these matrices have been created to identify the key physicochemical properties responsible

for PFAS and FQs sorption and to develop the K_d prediction models, as well as propose best-estimate K_d values for soils based on relevant soil physicochemical properties.

The results of this work are presented in four chapters. Chapter III focuses on the identification of key soil properties affecting PFAS sorption in soils, and the development of a K_d prediction model based only on few soil and PFAS physicochemical properties. Chapter IV aims to identify the key sorbent properties affecting PFAS sorption in carbon-rich materials (biochar, activated carbon, compost and charcoal fines) and the development of a K_d prediction model for PFAS in these sorbents. Chapter V aims to discuss the sorption of FQs in pure mineral and organic phases present in soils, in order to get insights of the role and the main factors affecting FQ sorption in these phases to latter extrapolate this information to bulk soils. Finally, chapter VI develops a K_d prediction model of FQs in soils, as well as propose best-estimate K_d (FQ) values in soils based on a few physicochemical properties.

Regarding the identification of key parameters governing PFASs and FQs sorption in soils and other environmental matrices, it has been shown that sorption of PFASs in soils is largely governed by soil organic carbon content through hydrophobic interactions, increasing with PFAS chain length. The contribution of the mineral phase can play a significant role in sorption for those soils with a low organic carbon content, but sorption in these scenarios is generally very low. Sorption of PFASs in carbon-rich materials (*e.g.*, biochars and activated carbons) is governed by hydrophobic interactions, increasing with PFAS chain length. Sorption increases when increasing material aromaticity, and additionally, material surface area plays an additional role in sorption providing extra sorption sites. Sorption of FQs in both humic acids and phyllosilicate minerals is strong, although highly pH-dependent. This pH dependence is due to both the speciation of the FQs and the overall surface charge of the phase, and sorption is also dependent on clay nature. On the other hand, sorption of FQs in metal oxides is dependent on the metal nature, but for a specific set of metal oxides sorption increases when

increasing mineral surface area. The identification of key properties affecting FQ sorption in pure soil components allowed to deduce the main phases responsible for sorption in soils. It was confirmed that sorption of FQs in bulk soils is pH-dependent, being soil pH, clay and organic matter content key parameters descriptors of sorption, besides demonstrating the sorption analogy of several widely studied FQs.

Regarding the development of K_d prediction models for PFASs and FQs in environmental matrices, an empiric K_d prediction model for PFASs in soils was developed by accounting the relative contribution of organic and mineral phases on the overall K_d . The model, included only three variables: the organic carbon and the reactive mineral phase (silt + clay) contents, and the number of fluorinated carbons of the PFAS. Besides, a K_d prediction model for PFASs in carbon-rich materials has also been developed. The model included only three variables: the quality and quantity of sorption sites (represented by the C_{ORG}/O molar ratio and the specific surface area, respectively) and the number of fluorinated carbons of the PFAS. In both cases models had a high applicability, and validation procedures using external data confirmed their effectiveness, overcoming previous limitations observed in previous models reported in the literature. Several empirical equations have been proposed here to predict the K_d of FQs in pure soil components. Specifically, the sorption K_d values in humic acids and different phyllosilicate minerals at different pH values were relatively well described by a second-grade polynomial fitting, and besides, a linear model was proposed to predict K_d values for FQs in metal oxides of Fe at neutral pH according to its surface area. Moreover, an empiric K_d prediction model for FQs in soils was developed after multivariate analyses, although it revealed a poor prediction ability when tested against literature data. Alternatively, a set of best-estimate K_d values with associated uncertainty were proposed by refining a K_d dataset for FQs in soils grouped according to specific key properties through cumulative distribution functions.

LIST OF ABBREVIATIONS

ACE: Affinity capillary electrophoresis	HA: Humic acid
ACN: Acetonitrile	HAc: Acetic acid
AEC: Anion exchange capacity	HPLC: High performance liquid chromatography
AFFF: Aqueous firefighting foam	IHSS: International humic substance society
ARG: Antibiotic resistance gene	K_{AW}: Air-water distribution coefficient
BET: Brunauer-Emmett-Teller	K_d: Sorption solid-liquid distribution coefficient
CDF: Cumulative Distribution function	K'_d: Sorption solid-liquid pseudo distribution coefficient
CEC: Cation exchange capacity	K_{d,des}: Desorption solid-liquid distribution coefficient
CIP: Ciprofloxacin	K_{d,SSA}: Surface area normalized sorption distribution coefficient
DNA: Deoxyribonucleic Acid	K_{Humic+Fulvic}: Humic+Fulvic normalized sorption coefficient
DOC: Dissolved organic carbon	K_{Humin}: Humin normalized sorption coefficient
DOM: Dissolved organic matter	K_{MIN}: Mineral normalized sorption coefficient
EDTA: Ethylenediaminetetraacetic acid	K_{oc}: Organic carbon normalized sorption coefficient
ENR: Enrofloxacin	K_{ow}: Octanol-water distribution coefficient
EPA: Environmental protection agency	K_{S+c}: Silt+clay normalized distribution coefficient
ESI: Electrospray ionization	LEV: Levofloxacin
FA: Fulvic acid	LOD: Limit of detection
FLD: Fluorescence detector	LOQ: Limit of quantification
FLSD: Fisher least significant differences	LV: Latent Variable
f_{MIN}: fraction of mineral phase	MeOH: Methanol
f_{oc}: fraction of organic carbon	MRL: Maximum residue limit
FQ: Fluoroquinolone	NH₄OAc: ammonium acetate
f_{S+c}: fraction of silt+clay phase	NMR: Nuclear magnetic resonance
FTIR: Fourier transformed infrared	NOR: Norfloxacin
GAC: Granular activated carbon	OC: Organic carbon
H: hysteresis coefficient	OECD: Organization for Economic Co-operation and Development

OFL: Ofloxacin

OM: Organic matter

PAC: Powdered activated carbon

PCA: Principal Component Analysis

PFAI: Perfluoroalkyl iodides

PFAL: Perfluoroalkyl aldehydes

PFAS: Perfluoroalkyl substances

PFASA: Perfluoroalkyl sulfonamides

PFBA: Perfluorobutanoic acid

PFBS: Perfluorobutane sulfonic acid

PFC: Aliphatic perfluorocarbons

PFCA: Perfluoroalkyl carboxyl acids

PFDA: Perfluorodecanoic acid

PFDoA: Perfluorododecanoic acid

PFDS: Perfluorodecane sulfonic acid

PFHpA: Perfluoroheptanoic acid

PFHpS: Perfluoroheptane sulfonic acid

PFHxA: Perfluorohexanoic acid

PFHxS: Perfluorohexane sulfonic acid

PFNA: Perfluorononanoic acid

PFOA: Perfluorooctanoic acid

PFOM: Pseudo-first order model

PFOS: Perfluorooctane sulfonic acid

PFPeA: Perfluoropentanoic acid

PFPeS: Perfluoropentane sulfonic acid

PFPIa: Perfluoroalkyl phosphinates

PFPrS: Perfluoropropane sulfonic acid

PFSA: Perfluoroalkane sulfonic acid

PFUnA: Perfluoroundecanoic acid

PIPES: 1,4-piperazinedieththanesulfonic acid

PLS: Partial least squares

POP: Persistent organic pollutant

PP: Polypropylene

PSOM: Pseudo-second order model

PTFE: Polytetrafluoroethylene

RMSE: Root mean square error

RPD: Residual predictive deviation

RSD: Relative standard deviation

SEM: Scanning electron microscopy

SMLR: Stepwise multiple linear regression

SOM: Soil organic matter

SPE: Solid phase extraction

SSA: Specific surface area

SUVA: Specific ultraviolet absorbance

USDA: United States department of agriculture

UV-Vis: Ultraviolet-visible

VIP: Variable Importance Projection

WHO: World Health Organization

WWTP: Wastewater treatment plant

TABLE OF CONTENTS

CHAPTER I: INTRODUCTION	Page 21
1.1. Poly- and Perfluoroalkyl Substances (PFASs)	Page 23
1.1.1. Classification and general features	Page 23
1.1.2. PFASs toxicity related to animals and humans	Page 29
1.1.3. PFASs legislation	Page 30
1.1.4. PFASs analysis in environmental samples	Page 31
1.1.5. PFASs input pathways and occurrence in the environment	Page 33
1.2. Fluoroquinolone antibiotics (FQs)	Page 37
1.2.1. Classification and general features	Page 37
1.2.2. FQs toxicity and antibiotic resistance genes	Page 40
1.2.3. FQs legislation	Page 41
1.2.4. FQs analysis in environmental samples	Page 42
1.2.5. FQs input pathways and occurrence in the environment	Page 44
1.3. Environmental risk assessment for PFASs and FQs	Page 48
1.3.1. Environmental risk assessment	Page 48
1.3.2. The sorption/desorption process	Page 49
1.3.3. Theoretical rationale to describe the interaction mechanisms with of organic compounds with environmental matrices	Page 51
1.3.3.1. Electrostatic interactions	Page 51
1.3.3.2. Hydrophobic interactions	Page 52
1.3.3.3. Hydrogen bonding	Page 53
1.3.3.4. Complexation with metals	Page 53
1.3.3.5. Pore filling	Page 54
1.3.3.6. Interactions with π aromatic groups	Page 54
1.3.4. Characteristics of the solid-water system affecting PFASs and FQs sorption	Page 55

1.3.4.1. pH and pH_{ZPC}	Page 55
1.3.4.2. Soil texture and mineralogy	Page 56
1.3.4.3. Soil organic matter	Page 58
1.3.4.4. Cation and anion exchange capacity	Page 61
1.3.4.5. Surface area and porosity	Page 61
1.3.4.6. Water-soluble cations and anions	Page 62
1.3.4.7. Dissolved organic carbon	Page 62
1.4. The solid-liquid distribution coefficient (K_d)	Page 63
1.4.1. Definition and significance of K_d	Page 63
1.4.2. Methods for quantifying sorption	Page 64
1.4.2.1. Laboratory flow-through method	Page 64
1.4.2.2. In-situ method	Page 65
1.4.2.3. Batch method	Page 65
1.4.3. Sorption parameters and information derived from batch experiments	Page 67
1.4.3.1. Sorption kinetics	Page 67
1.4.3.2. Sorption isotherms	Page 68
1.4.4. Sources of K_d variability	Page 72
1.5. Carbon-rich materials as sorbent candidates for the remediation of polluted soil and water bodies	Page 74
1.5.1. Activated carbons	Page 74
1.5.2. Biochars	Page 75
1.5.3. Compost	Page 77
1.5.4. Charcoal Fines	Page 78
1.6. Prediction K_d models and current limitations for PFASs and FQs	Page 79
1.7. References	Page 82

CHAPTER II: MOTIVATION AND OBJECTIVES	Page 111
CHAPTER III: SORPTION OF PFASs IN SOILS	Page 117
3.1. Introduction	Page 119
3.2. Materials and methods	Page 121
3.2.1. Reagents and standards	Page 121
3.2.2. Materials and characterization	Page 122
3.2.3. Sorption and desorption experiments	Page 125
3.2.4. Quality control	Page 126
3.2.5. PFASs analysis by HPLC-MS/MS	Page 127
3.2.6. Quantification of sorption and desorption parameters	Page 129
3.2.7. Construction of the K_d (PFAS) datasets	Page 130
3.3. Results and discussion	Page 135
3.3.1. PFASs sorption and desorption patterns in soils	Page 135
3.3.2. Correlation of sorption and desorption parameters with soil OC	Page 139
3.3.3. Correlation of K_{OC} and K_{MIN} with PFAS physicochemical properties	Page 143
3.3.4. Exploration of the contribution of humic substances in PFASs sorption	Page 146
3.3.5. Development and validation of a PFASs sorption model in soils	Page 151
3.3.6. Assessment of the contribution of organic and mineral phases on K_d	Page 155
3.4. Conclusions	Page 157
3.5. References	Page 158
CHAPTER IV: SORPTION OF PFASs IN CARBON-RICH MATERIALS	Page 169
4.1. Introduction	Page 171
4.2. Materials and methods	Page 173
4.2.1. Reagents and standards	Page 173
4.2.2. Materials and characterization	Page 174

4.2.3. Sorption experiments _____	Page 175
4.2.4. Quality control _____	Page 177
4.2.5. PFASs analysis by HPLC-MS/MS _____	Page 178
4.2.6. Data treatment _____	Page 178
4.2.7. Model construction _____	Page 180
4.3. Results and discussion _____	Page 184
4.3.1. Physicochemical properties of the samples _____	Page 184
4.3.2. Effect of equilibration time on PFOS sorption _____	Page 190
4.3.3. Effect of initial concentration on PFOS sorption _____	Page 191
4.3.4. Effects of pH, Ca concentration and DOC content on PFOS sorption ____	Page 193
4.3.5. Effect of PFASs chain length _____	Page 196
4.3.6. Multivariate analyses between material properties and PFASs sorption parameters _____	Page 198
4.3.7. Development of a prediction model _____	Page 201
4.3.8. External validation of the prediction model _____	Page 202
4.4. Conclusions _____	Page 204
4.5. References _____	Page 205
CHAPTER V: SORPTION OF FQs IN PURE SOIL COMPONENTS _____	Page 213
5.1. Introduction _____	Page 215
5.2. Sorption of FQs in humic substances _____	Page 217
5.2.1. Materials and methods _____	Page 217
5.2.1.1. Reagents and materials characterization _____	Page 217
5.2.1.2. Batch sorption experiments _____	Page 219
5.2.1.3. FQs determination with HPLC-FLD _____	Page 221
5.2.1.4. Data treatment _____	Page 221

5.2.1.5. Creation of a dataset of K_d (FQ) and data treatment	Page 223
5.2.2. Results and discussion	Page 225
5.2.2.1. Sorption kinetics of NOR in humic acids	Page 225
5.2.2.2. Sorption isotherms of NOR in humic acids	Page 226
5.2.2.3. Desorption isotherms of NOR in humic acids	Page 228
5.2.2.4. Effect of Ca concentration and DOC content on NOR sorption in humic acids	Page 229
5.2.2.5. Sorption analogy of FQs in humic substances	Page 232
5.2.2.6. Effect of pH on FQs sorption in humic substances	Page 234
5.3. Sorption of FQs in metal oxides	Page 237
5.3.1. Creation of a K_d (FQ) dataset and data treatment	Page 237
5.3.2. Evaluating the role of metal on FQs sorption in metal oxides	Page 238
5.3.3. Factors affecting FQs sorption: the case of Fe oxides and (hydro)oxides	Page 239
5.4. Sorption of FQ in phyllosilicate minerals	Page 242
5.4.1. Creation of a K_d (FQ) dataset and data treatment	Page 242
5.4.2. Influence of the type of phyllosilicate in FQs sorption	Page 245
5.4.3. Effect of pH on FQs sorption in phyllosilicate minerals	Page 246
5.4.4. Elucidating interaction mechanisms and additional phyllosilicate properties governing FQs sorption	Page 248
5.5. Conclusions	Page 250
5.6. References	Page 251
CHAPTER VI: SORPTION OF FQs IN SOILS	Page 263
6.1. Introduction	Page 265
6.2. Materials and methods	Page 267

6.2.1. Reagents and materials	Page 267
6.2.2. Batch experiments	Page 270
6.2.3. FQs analysis by HPLC-FLD	Page 271
6.2.4. Creation of a K_d (FQ) dataset	Page 272
6.2.5. Data treatment and statistical analysis	Page 275
6.2.6. Development of a partial least squares prediction model	Page 277
6.2.7. Construction of cumulative distribution functions	Page 283
6.3. Results and discussion	Page 284
6.3.1. Sorption and desorption pattern of NOR in soils	Page 284
6.3.2. Assessing the sorption analogy between NOR, CIP, ENR and OFL	Page 288
6.3.3. Development of a multivariate K_d (FQ) prediction model	Page 290
6.3.4. Deriving best-estimate K_d (FQ) values in soils	Page 293
6.4. Conclusions	Page 309
6.5. References	Page 310
CHAPTER VII: CONCLUSIONS	Page 319

CHAPTER I

INTRODUCTION

1.1. Poly- and perfluoroalkyl substances (PFASs)

1.1.1. Classification and general features

Poly- and perfluoroalkyl substances (PFASs) are a complex family of synthetic compounds with an anthropogenic origin, which have been used since the 1940s. The chemical structure of PFASs basically consists in a fluorinated chain (hydrophobic tail) attached to a hydrophilic functional group. Their strong C – F bonds provides a strong thermal resistance, in addition to stunt its breakdown. Besides, both their hydrophobic and hydrophilic parts act as repellent of both water and oils, in addition to provide superior surface tension lowering properties and resistance to thermal, chemical and biological degradation. PFASs are currently used in a wide array of costumer and industrial applications such as additives in electronic devices, fire-fighting foams, inks, lubricants, food containers and oil and water repellents for the leather, paper and textile industries, among others (Prevedouros et al., 2006).

Polytetrafluoroethylene (PTFE), under its commercial name “Teflon”, was accidentally obtained after the polymerization of tetrafluoroethylene in 1938 by Roy J. Plunkett in DuPont’s Jackson Laboratory in Deepwater, New Jersey, USA. After realizing its unique properties, other non-polymeric fluorinated substances started to be investigated. In 1949, 3M started the manufacture of perfluorooctane sulfonic acid (PFOS), and in 1951 began the manufacture of perfluorooctanoic acid (PFOA). Global PFOA emissions from 1951 to 2015 are estimated to being up to 13,000 tones (Wang et al., 2014). Currently, it is estimated that more than 4,700 PFASs have reach the global market (OECD, 2021).

Due to this large amount of compounds, PFASs may be classified according to different criteria. Among them, the classification proposed by Buck and co-workers in 2011 (Buck et al., 2011) has been widely accepted as a standard guideline in terms of their PFASs terminology and classification, although recently the Organization for Economic Co-operation and Development (OECD) issued a new recommendation guideline for their terminology aiming to

fulfill some gaps found in Buck's classification (OECD, 2021). In this document PFASs are defined as "fluorinated substances that contain at least one fully fluorinated methyl or methylene carbon atom (without any H/Cl/Br/I atom attached to it) *i.e.*, with a few noted exceptions, any compound with at least a perfluorinated methyl group (-CF₃) or a perfluorinated methylene group (-CF₂-) is a PFAS". Regardless this new tinge in Buck's terminology, their proposed PFASs classification is still widely used. According to this classification, the PFASs group may be separated into two categories: polymeric and non-polymeric substances. Among polymeric substances we can find fluoropolymers (those with carbon-based backbone with fluorine atoms directly attached; *e.g.*, PTFE), perfluoropolyethers (polymers with carbon- and oxygen-based backbone with fluorine atoms directly attached to carbon) and side-chain fluorinated polymers (polymers with variable composition with non-fluorinated backbone but with fluorinated side chains; *e.g.*, fluorinated urethane polymers, fluorinated oxetane polymers, fluorinated acrylate and methacrylate polymers). On the other hand, non-polymeric PFASs can be classified as perfluoroalkyl and polyfluoroalkyl substances. Perfluoroalkyl substances are those compounds for which all hydrogens on all carbons (except those associated with functional groups) have been replaced by fluorine atoms, and include a wide variety of families: aliphatic perfluorocarbons (PFCs), perfluoroalkyl carboxyl acids (PFCAs), perfluoroalkane sulfonic acids (PFSAs), perfluoroalkane sulfonamides (PFASAs), perfluoroalkyl iodides (PFAIs), perfluoroalkyl aldehydes (PFALs) and perfluoroalkyl phosphinates (PFPIAs), among others. On the other hand, polyfluoroalkyl substances are defined as those compounds for which all hydrogens on at least one (but not all) carbon have been replaced by fluorines, and include a variety of families: perfluoroalkane sulfonamido derivatives, fluorotelomer-based compounds (those with some CF₂ units replaced by CH₂) and semifluorinated *n*-alkanes and alkenes, among others (Buck et al., 2011). **Figure 1.1** summarize the abovementioned classification:

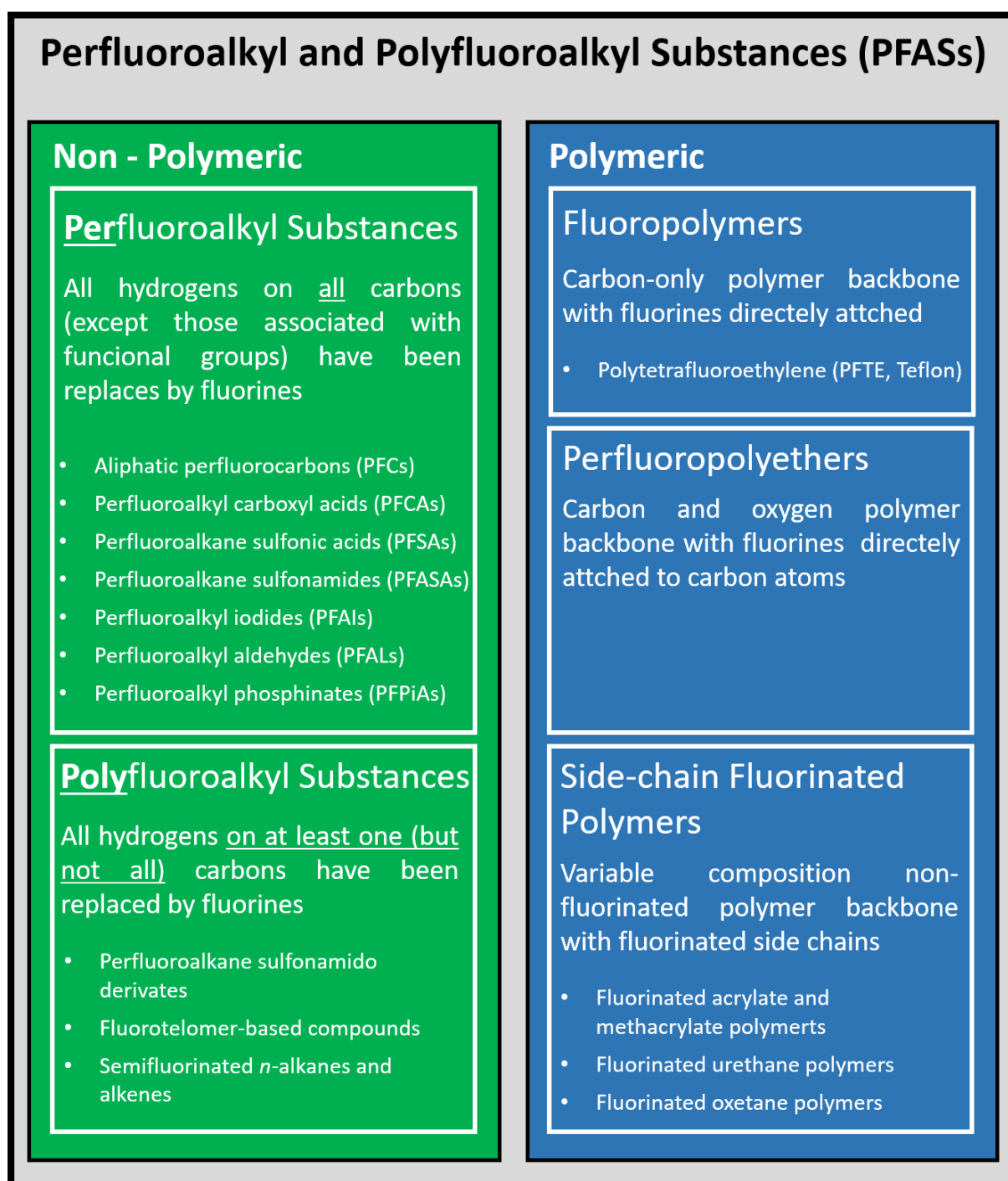


Figure 1.1 Classification of PFASs (adapted from Buck et al., 2011).

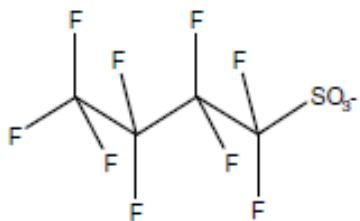
Table 1.1 summarizes the main physicochemical properties of some anionic PFCAs and PFSAs, which are the compounds that will be analysed in this thesis. The chemical structure of some of these anionic PFCAs and PFSAs included in **Table 1.1** are depicted in **Figure 1.2**:

Table 1.1 Main physicochemical properties of target PFASs.

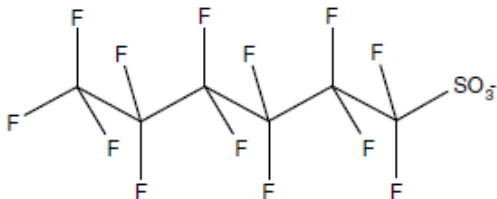
Name	PFAS acronym	Chemical form	CAS number	Molecular weight (g/mol)	Number of CF ₂	log K _{OW}	pK _a	log K _{AW}
Perfluorobutanoic acid	PFBA	C ₄ HF ₇ O ₂	375-22-4	214.0	3	2.3 ^a	0.4 ^a	0.30 ^d
Perfluoropentanoic acid	PFPeA	C ₅ HF ₉ O ₂	2706-90-3	264.1	4	2.9 ^c	N.A.	0.86 ^d
Perfluorohexanoic acid	PFHxA	C ₆ HF ₁₁ O ₂	307-24-4	314.1	5	3.1 ^a	-0.16 ^a	1.43 ^d
Perfluoroheptanoic acid	PFHpA	C ₇ HF ₁₃ O ₂	375-85-9	364.1	6	3.8 ^b	N.A.	2.00 ^d
Perfluorooctanoic acid	PFOA	C ₈ HF ₁₅ O ₂	335-67-1	414.1	7	4.6 ^{a,b}	-0.2 ^a	2.57 ^d
Perfluorononanoic acid	PFNA	C ₉ HF ₁₇ O ₂	375-95-1	464.1	8	5.5 ^b	N.A.	3.14 ^d
Perfluorodecanoic acid	PFDA	C ₁₀ HF ₁₉ O ₂	335-76-2	514.1	9	6.4 ^b	N.A.	3.70 ^d
Perfluoroundecanoic acid	PFUnA	C ₁₁ HF ₂₁ O ₂	2058-94-8	564.1	10	7.4 ^b	N.A.	4.18 ^d
Perfluorododecanoic acid	PFDoA	C ₁₂ HF ₂₃ O ₂	307-55-1	614.1	11	8.1 ^c	N.A.	4.84 ^d
Perfluoropropane sulfonic acid	PFPrS	C ₃ HF ₇ O ₃ S	423-41-6	250.1	3	1.7 ^c	N.A.	N.A.
Perfluorobutane sulfonic acid	PFBS	C ₄ HF ₉ O ₃ S	375-73-5	300.1	4	2.7 ^a	0.14 ^a	1.02 ^d
Perfluoropentane sulfonic acid	PFPeS	C ₅ HF ₁₁ O ₃ S	2706-91-4	350.1	5	3.0 ^c	N.A.	N.A.
Perfluorohexane sulfonic acid	PFHxS	C ₆ HF ₁₃ O ₃ S	355-46-4	400.1	6	4.3 ^a	0.14 ^a	2.15 ^d
Perfluoroheptane sulfonic acid	PFHpS	C ₇ HF ₁₅ O ₃ S	375-92-8	450.1	7	4.3 ^c	N.A.	N.A.
Perfluorooctane sulfonic acid	PFOS	C ₈ HF ₁₇ O ₃ S	1763-23-1	500.1	8	5.3 ^{a,b}	-3.27 ^a	3.29 ^d
Perfluorodecane sulfonic acid	PFDS	C ₁₀ HF ₂₁ O ₃ S	335-77-3	600.1	10	6.4 ^c	N.A.	N.A.

N.A.: not available; ^a Deng et al., 2012; ^b Kelly et al., 2009; ^c Pubchem database (<https://pubchem.ncbi.nlm.nih.gov>); ^d Kim et al., 2015

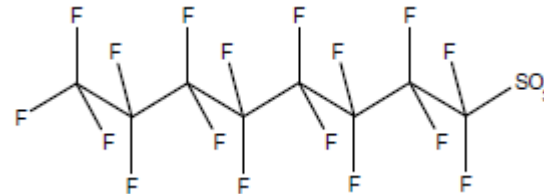
PFBS: Perfluorobutane sulfonic acid



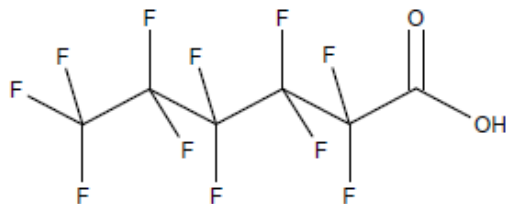
PFHxS: Perfluorohexane sulfonic acid



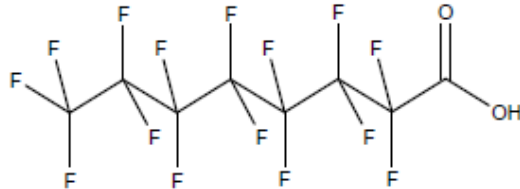
PFOS: Perfluorooctane sulfonic acid



PFHxA: Perfluorohexanoic acid



PFOA: Perfluorohexanoic acid



PFDoA: Perfluorododecanoic acid

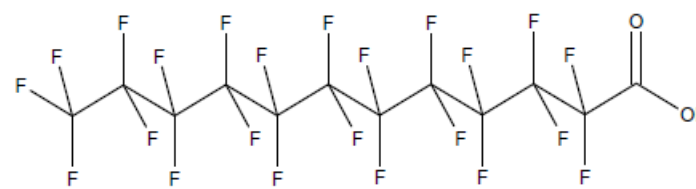


Figure 1.2 Chemical structures of several PFAS.

Different linear, branched and cyclic PFASs have been found in the environment (Xiao, 2017). Whereas the so called “legacy PFASs” species, which mainly includes linear PFCAs and PFSAAs with fluorinated chains ranging 3 – 14, such as PFOA and PFOS, have been widely monitored in environmental compartments since 2001 (Giesy and Kannan, 2001), these only account for a small number of the global PFASs available and, therefore, the environmental exposure to PFASs may be underestimated (Willach et al., 2016). Some PFASs may exist under cationic, zwitterion, anionic or uncharged forms, and although anionic PFASs have gathered the most monitoring attentions in the last years, recent attention has been put for these other “novel PFASs” species (Xiao, 2017; Maizel et al., 2021).

The chain length of the PFASs is usually referred as the number of CF_2 units, including the final $-\text{CF}_3$ moiety. Therefore, PFOS and PFNA have the same number of CF_2 units ($\text{CF}_2 = 8$), while the CF_2 for PFOA, which has the same number of carbons as PFOS, is 7. Buck and co-workers classified PFASs as short- and long-chained according to their number of CF_2 units, being long-chained PFASs those PFCAs with $> 7 \text{ CF}_2$ and those PFSAAs with $> 6 \text{ CF}_2$ (Buck et al., 2011). PFAS hydrophobicity, expressed as its octanol-water partitioning coefficient (K_{ow}), increase with the number of fluorinated carbons. The strong electronegativity of the fluorine atoms stabilizes the negative charge along the fluorinated chain, and hence, pK_a values for these compounds are usually in the range of $-3.3 - 0.4$. Therefore, they are present under their anionic form under most environmental conditions. PFAS accumulation and magnification factors have shown to depend on the chain length. Long-chained PFASs accumulate in the wildlife due to its higher hydrophobicity (Haukås et al., 2007), whereas short-chained PFASs are more prone to accumulate in plants due to its higher water solubility (Lesmeister et al., 2020). Also, PFASs volatility, expressed as its air-water partitioning coefficient (K_{aw}) increases with its fluorinated chain (Kim et al., 2015), suggesting a major atmospheric transport for long-chained PFASs.

1.1.2. PFASs toxicity related to animals and humans

A growing number of reported works studying PFASs toxicity is emerging. Adverse effects concerning acute and chronic effects including hepatotoxicity, reproductive toxicity, neurotoxicity, carcinogenicity and hormonal effects, among others, have been linked to PFASs exposure, and despite these studies have been mainly addressed the effects of legacy PFAS, novel PFASs can exhibit comparable or even more serious potential toxicity (Wang et al., 2019). PFASs have been found in human blood plasma samples worldwide (Olsen et al., 2017; Tian et al., 2018). The presence of PFOS, PFHxS and PFOA in plasma has decreased along 2000 – 2015 in general U.S. population likely due to legislation restrictions, although PFNA and PFDA concentrations remained relatively constant (Olsen et al., 2017). The presence of PFASs in serum has been linked to bone mineral densities alterations in children (Cluett et al., 2019), and in addition, PFASs have also been detected in liver, kidney, heart, muscle and brain tissues (Cao and Ng, 2021). PFASs may disrupt normal reproductive function in women through altering hormone secretion, menstrual period and fertility (Rickard et al., 2022), while their accumulation in brain may cause toxic effects in the central nervous system, including PFAS-induced behavioural and cognitive disorders (Cao and Ng, 2021). The presence of PFASs in hepatic cells have been linked to increasing cytotoxicity with increasing carbon chain lengths (Ojo et al., 2020), while they have been also been suggested to cause hormone disrupting effects in both in vitro and in vivo studies (Bonefeld-Jørgensen et al., 2014). Carcinogenic effects and oxidative deoxyribonucleic acid (DNA) damage have been also linked to PFASs exposure in rats (Chang et al., 2014), although direct evidences between PFASs exposure and cancer outcomes in humans are not clear at date (ATSDR, 2021). Furthermore, PFASs-related adverse effects have been reported to aquatic species and soil bacterial communities (Ahrens and Bundschuh, 2014; Zhang et al., 2019).

1.1.3. PFASs legislation

In May 2000, 3M, the principal worldwide PFAS manufacturer, announced a voluntary phase-out of PFOS, PFHxS, PFOA and related compounds (EPA Docket EPA-HQ-OPPT-2002-0051). In 2006, the Environmental Protection Agency (EPA) invited eight major leading companies to join a global stewardship program aiming to achieve a 95% reduction in emissions of PFOA and related compounds no later than 2010 and committed to eliminate these compounds from emissions and products by 2015 (EPA Docket EPA-HQ-OPPT-2006-0621). The Stockholm convention, which is an international agreement that entered into force in 2004 to protect human health and the environment from the exposure to Persistent Organic Pollutants (POPs, <http://www.pops.int>), limited in 2009 the applications worldwide for PFOS, its salts and its precursor (perfluorooctane sulfonyl fluoride) (UNEP, 2009). Later, the POPs Review Committee also considered a proposal for the potential inclusion of PFOA, its salts, and PFOA-related compounds into the Stockholm convention by restricting production and use, with specific exceptions (UNEP, 2015), and in 2020 were definitely banned in Europe with no exceptions. Currently, PFHxS, its salts and related compounds in addition to C₉-C₁₄ PFCAs have been proposed for restricted production and use (UNEP, 2017; 2021).

In Europe, Directive 2013/39/EU established environmental water quality standards for PFOS and its derivatives with annual average and maximum allowed concentrations in non-inland surface waters established at 0.13 ng L⁻¹ and 7.2 µg L⁻¹, respectively. Besides, a maximum total PFAS concentration of 0.5 µg L⁻¹, with 0.1 µg L⁻¹ for every single compound was recommended for drinking water (Directive 98/83/EC). Currently, there is no dedicated European legislation on PFAS-impacted soil quality other than the Environmental Liability Directive (2004/34/EC) that establishes a framework for preventing and remediating environmental damage (European Commission, 2020).

1.1.4. PFASs analysis in environmental samples

Most of the monitoring studies aiming to determine target PFASs in environmental matrices (*i.e.*, aqueous firefighting foams (AFFF)-impacted soils and freshwater) rely on a liquid extraction and filtration methods for the solid and liquid matrices, respectively, followed by a clean-up and concentration step using solid phase extraction (SPE), and the determination of the PFAS in the eluent by high performance liquid chromatography coupled to tandem mass spectrometry (HPLC-MS/MS) (Higgins et al., 2005; Habibullah-Al-Mamun et al., 2016; Nickerson et al., 2020). For anionic PFASs compounds, electrospray ionization (ESI) working in negative mode is widely applied, whereas for cationic and zwitterion PFASs compounds ESI working in positive mode needs to be applied (Maizel et al., 2021). As long as ESI is known to be susceptible to matrix enhancement/suppression of compounds by co-eluting species, PFAS-labelled internal standard calibration curves are preferred instead of external or standard addition calibration procedures (Washington et al., 2007). Elution time and/or degree of similarity in response to ionization between compounds might affect suitability of compounds that are candidates for use as matrix internal standards (Higgins et al., 2005). Whereas the respective PFAS-labelled compound would be the most suitable internal standard for PFAS quantification purposes, this may be costly and may lead to an overestimation of the PFAS content due to non-labelled impurities in the respective commercial internal standard. Hence, in many studies a few representative PFAS-labelled compounds are used to quantify different chain-length PFCAs and PFSAs. For PFCAs, the decarboxylation reaction is usually monitored, while for PFSAs the usual transition monitored is the formation of the SO_3^- ion. The second most abundant transition is selected as confirmation transition. Linear and branched isomers, can be identified by slight changes in the retention time of the resulting chromatograms (Langlois and Oehme, 2006). **Table 1.2** summarize some of the chromatographic conditions used to quantify PFCAs and PFSAs in aqueous solutions by HPLC-MS/MS.

Table 1.2 Reported HPLC-MS/MS conditions for PFASs analysis in aqueous samples using a triple quadrupole mass spectrometer working in negative ESI mode.

HPLC column	Injection volume (μL)	Flow rate (mL min^{-1})	Aqueous Mobile phase A	Organic Mobile phase B	LOQ (ng mL^{-1})	Reference
C ₁₈ , 2.1×150 mm; 5 μm	3 – 5	0.2	5 mM NH ₄ OAc	5 mM NH ₄ OAc (90% ACN)	N.R.	Brusseau et al., 2019
C ₈ , 2.1×50 mm; 3.5 μm	5	N.R.	0.15 % HAc	0.15 % HAc (ACN)	N.R.	Mejia-Avendaño et al., 2020
C ₁₈ , 2.0×125 mm; 5 μm	10	0.4	2 mM NH ₄ OAc	ACN	N.R.	Gómez-Canela et al., 2012
C ₁₈ , 2.1×150 mm; 5 μm	10	0.2	10 mM NH ₄ OAc	MeOH	0.02 – 0.40	Habibullah-Al-Mamun et al., 2016
C ₁₈ , 2.1×100 mm; 5 μm	5	0.2	5 mM NH ₄ OAc	MeOH	0.10 – 0.55	Lee et al., 2020a
C ₁₈ , 2.0×150 mm; 4 μm	5	0.3	10 mM NH ₄ OAc	10 mM NH ₄ OAc (MeOH)	0.2 – 0.6	Colomer-Vidal et al., 2022
C ₁₈ , 2.1×50 mm; 5 μm	10	0.2	10 mM NH ₄ OAc	10 mM NH ₄ OAc (MeOH)	0.17 – 0.59	Dalahmeh et al., 2018
C ₁₈ , 2.7×100 mm; 5 μm	n.r.	0.2	5 mM NH ₄ OAc	5 mM NH ₄ OAc (MeOH)	0.02– 0.16	Liu et al., 2015

NH₄OAc: ammonium acetate; HAc: acetic acid; ACN: acetonitrile; MeOH: Methanol; LOQ: limit of quantification; N.R.: not reported

1.1.5. PFASs input pathways and occurrence in the environment

PFASs may enter in the environment through different pathways, thus increasing their exposure to human beings. **Figure 1.3** summarizes some of these pathways.

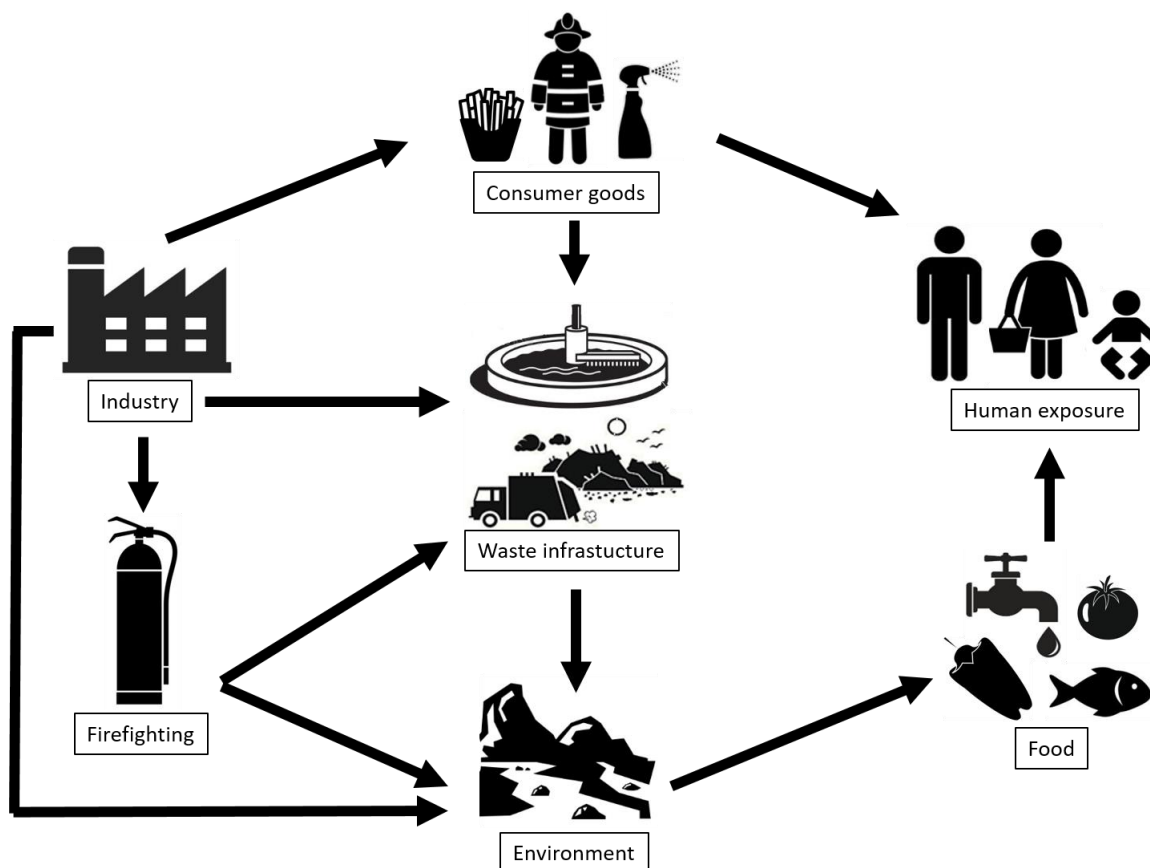


Figure 1.3 Main PFASs input pathways in the environment.

Although PFASs manufacturing processes have been limited in E.U. and U.S., they are still widely produced in other locations. For example, high PFOA concentrations up to $70 \mu\text{g L}^{-1}$ have been found in rivers close to Chinese fluorochemical facilities (Colomer-Vidal et al., 2022). PFASs have a low removal rate in conventional wastewater treatment plants (WWTPs, Lenka et al., 2021), which may lead to low but detectable levels in drinking water (Tan et al., 2017). Another important PFASs input in the environment is the use of AFFF. These foams are used to tackle large hydrocarbon fires, and AFFF formulations include anionic, neutral, cationic and zwitterion PFASs with chain lengths mostly ranging from 4 to 12 (Place and Field, 2012).

Consequently, PFASs have been found at high levels in AFFF-impacted soils (Brusseau et al., 2020). PFASs may be transferred from soils to plants (Lesmeister et al., 2021), which may explain their detection in several vegetable species such as lettuce, carrot, potatoes and tomatoes (Herzke et al., 2013). On the other hand, PFASs may be mobilized from the soil to surface or ground waters (Gellrich et al., 2012), thus increasing their availability towards aquatic species. Consequently, PFASs have been widely detected in finfish and shellfish in U.S. markets (Ruffle et al., 2020). PFASs are also found in several commercial food contact materials (*e.g.*, popcorn, pizza, sandwich and chips bags), and these may migrate to food (Carnero et al., 2021). Overall, the presence of PFASs in daily dietary products may cause a direct intake for human beings. Moreover, their use in building materials, furnishings, consumer products and industrial-strength cleaners may contribute to the PFASs presence in air and dust samples (Savvaides et al., 2021). PFASs have been detected in indoor and outdoor air samples at levels up to hundreds pg m^{-3} , with higher concentrations for fluorotelomer precursors, even in remote areas (Jahnke et al., 2009; Goosey and Harrad, 2012). The presence of PFASs in the atmosphere may contribute to an additional continuous exposure for human beings.

Table 1.3 and **Table 1.4** summarize some of the PFCAs and PFASs concentrations found in freshwaters, sediments and soils worldwide. Among them, PFOS and PFOA have been found at higher concentrations. Specifically, PFOS and PFOA have been found in water bodies including lake, river and coastal areas at levels up to few tens of ng L^{-1} and in the respective sediment cores at levels up to several ng g^{-1} . Besides, PFASs have been detected in background soils at concentrations up to few ng g^{-1} , although higher levels have been detected in AFFF-impacted soils, especially for PFOS (levels up to few $\mu\text{g g}^{-1}$), likely because is the major PFAS component in AFFF formulations (Place and Field, 2012). These high concentrations found in AFFF-impacted sites gather scientific concern and promote the application of remediation actions to reduce PFAS mobility and human exposure (Sørmo et al., 2021).

CHAPTER I: INTRODUCTION

Table 1.3 Worldwide selected PFCAs and PFSAs concentration ranges (min – max) found in water (ng L⁻¹) and sediments (ng g⁻¹).

Location	Matrix	PFBA	PFHxA	PFOA	PFNA	PFDoA	PFBS	PFHxS	PFOS	Reference
Coastal Area (Bangladesh, 2015)	W	<0.01 – 1.82	0.16 – 4.07	3.17 – 27.8	0.46 – 4.17	<0.04 – 3.30	<0.08 – 3.67	<0.04 – 2.59	<0.08 – 5.10	Habibullah et al., 2016
	S	<0.03 – 1.37	0.07 – 0.51	0.09 – 1.49	0.04 – 0.53	<0.03 – 0.49	<0.02 – 0.87	<0.01 – 0.96	0.30 – 3.56	
Coastal Area (Korea, 2020)	W	N.A.	<0.04 – 2.18	0.21 – 16.5	<0.1 – 0.45	<0.1	<0.04 – 3.87	<0.1 – 8.84	<0.04 – 1.92	Lee et al., 2020a
	S	N.A.	<0.002 – 0.06	<0.005 – 0.51	<0.002 – 0.11	<0.005 – 0.04	<0.002 – 0.02	<0.002 – 0.06	<0.005 – 0.33	
Coastal Area (China, 2011)	S	N.D. – 1.34	N.D. – 3.04	N.D. – 1.40	N.D. – 0.43	N.D.	N.D.	N.D. – 0.41	N.D. – 32	Yan et al., 2015
Pearl River (China, 2013)	W	N.A.	<0.03 – 3.54	<0.12 – 9.34	0.24 – 2.97	<0.02 – 0.30	0.34 – 12.0	<0.04 – 1.51	<0.02 – 10.6	Liu et al., 2015
Jiulong River (China, 2015)	W	N.A.	<0.01 – 96	1.08 – 24.8	<0.01 – 0.58	N.A.	<0.01 – 8.61	0.20 – 2.73	0.21 – 14.2	Wang et al., 2022
	S	N.A.	0.02 – 0.20	0.12 – 0.83	<0.001 – 0.06	0.01 – 0.05	<0.002 – 0.19	<0.001 – 0.05	0.02 – 0.95	
Llobregat River (Spain, 2010)	W	0.07 – 111	0.63 – 25.2	0.07 – 146	0.77 – 52.4	N.D.	0.41 – 4.10	14.2 – 33.2	0.01 – 2,710	Campo et al., 2015
	S	0.09 – 12.9	N.D.	0.36 – 1.52	3.87	0.11 – 0.22	0.91 – 3.53	0.03 – 0.29	0.15 – 11.4	
River water (Vietnam, 2014)	W	N.A.	<0.07 – 4.26	0.13 – 54	<0.06 – 4.81	<0.03 – 0.03	<0.30 – 8.28	<0.03 – 5.98	<0.03 – 40	Lam et al., 2017
	S	N.A.	<0.16	<0.20	<0.1	<0.05 – 0.16	<0.34 – 0.57	<0.04 – 18	<0.08 – 6.72	
Nansi Lake (Sweden, 2012)	W	N.A.	N.A.	35 – 85	0.62 – 1.74	N.A.	0.36 – 0.78	0.06 – 0.11	0.49 – 1.79	Cao et al., 2015a
	S	N.A.	N.A.	0.11 – 0.44	0.03 – 0.15	N.A.	N.D.	N.D.	0.17 – 0.83	
Asan Lake (South Korea, 2018)	W	N.A.	2.3 – 105	5.4 – 44	1.8 – 16.3	<0.50	1.4 – 44	2.9 – 25	<0.47 – 18.5	Lee et al., 2020b
	S	N.A.	<0.01 – 0.25	<0.01 – 0.27	<0.02 – 0.47	<0.01 – 1.12	<0.01 – 0.51	<0.05 – 1.48	0.04 – 4.36	

W: water; S: Sediment; N.A.: non analysed; N.D.: non detected (limit of detection, (LOD) not reported)

Table 1.4 Worldwide selected PFCAs and PFSA concentration ranges (min – max) found in background and AFFF-impacted soils (ng g⁻¹).

Status and location	PFBA	PFHxA	PFOA	PFNA	PFDoA	PFBS	PFHxS	PFOS	Reference
Jordan, 2020 ^a	N.D.	N.D.	0.11 – 0.30	N.D.	N.D.	N.D.	0.07	0.51 – 0.92	Shigei et al., 2020
Norway, 2019 ^a	<0.13 – 1.06	<0.04 – 0.18	<0.05 – 0.40	<0.06 – 0.93	<0.09 – 0.40	<0.01 – 0.04	<0.03	<0.04 – 0.64	Grønnestad et al., 2019
Uganda, 2015 ^a	<1.6	0.21 – 0.44	0.25 – 0.91	0.15 – 0.46	0.12 – 0.38	0.04 – 0.12	<0.67	0.60 – 3.0	Dalahmeh et al., 2018
China, 2013 ^a	0.17 – 2.14	0.02 – 0.33	2.84 – 4.99	0.08 – 0.37	0.02 – 0.18	0.01 – 0.10	0.01 – 0.05	0.78 – 4.23	Meng et al., 2018
USA, 2010 ^a	0.07 – 0.49	0.03 – 0.09	0.29 – 0.54	N.A.	N.A.	<0.024 – 0.03	0.03 – 0.11	0.93 – 2.1	Scher et al., 2018
USA, 2021 ^b	0.72 – 46	0.80 – 71	1.4 – 6.2	0.52	0.03 – 0.46	0.53 – 29	0.10 – 190	3.7 – 8,600	Maizel et al., 2021
USA, 2017 ^b	N.A.	54 – 213	237 – 561	0.8 – 8.8	N.D. – 0.8	2.2 – 69	120 – 421	124 – 4,880	Nickerson et al., 2021
Norway, 2015 ^b	<1.8 – 109	<2.5	<2.8 – 207	<1.8	N.A.	<1.8	<1.8	170 – 5,470	Hale et al., 2017
USA, 2014 ^b	0.23 – 14	0.19 – 140	0.26 – 140	0.24 – 23	0.92 – 18	0.20 – 72	0.29 – 180	0.38 – 5,700	Anderson et al., 2016
France, 2014 ^b	<2 – 14	<2 – 58	<2 – 27	<2 – <20	<2 – <20	<2 – 24	<2 – 112	4 – 668	Boiteux et al., 2016

^a Background; ^b AFFF-impacted; N.A.: non analysed; N.D.: non detected (LOD not reported)

1.2. Fluoroquinolone antibiotics (FQs)

1.2.1. Classification and general features

Pharmaceutical and personal care products are considered as emerging contaminants of increasing concern. Among them, antimicrobial agents are substances which are able to kill or inhibit the growth and reproduction of microorganisms such as bacteria, fungi or protozoa, and can have either natural or anthropogenic origin. Currently, they are mainly used in human and veterinary medicine, including a wide range of compounds such as aminoglycosides, β -lactams, macrolides, tetracyclines, quinolones, nitrofurans, nitroimidazoles, penicillin and sulphonamides (Teixidó, 2013). Quinolones are derivatives of quinine, and their antimicrobial applications were discovered in the early 1960s by George Lesher and co-workers after isolating nalidixic acid as a undesired by-product, further synthesizing related compounds (Lesher et al., 1962). Their industrial production was enhanced during the 1970s and 1980s to treat diseases caused by both Gram positive and Gram negative pathogens. The general structure or 'pharmacore' of a quinolone is depicted in **Figure 1.4**.

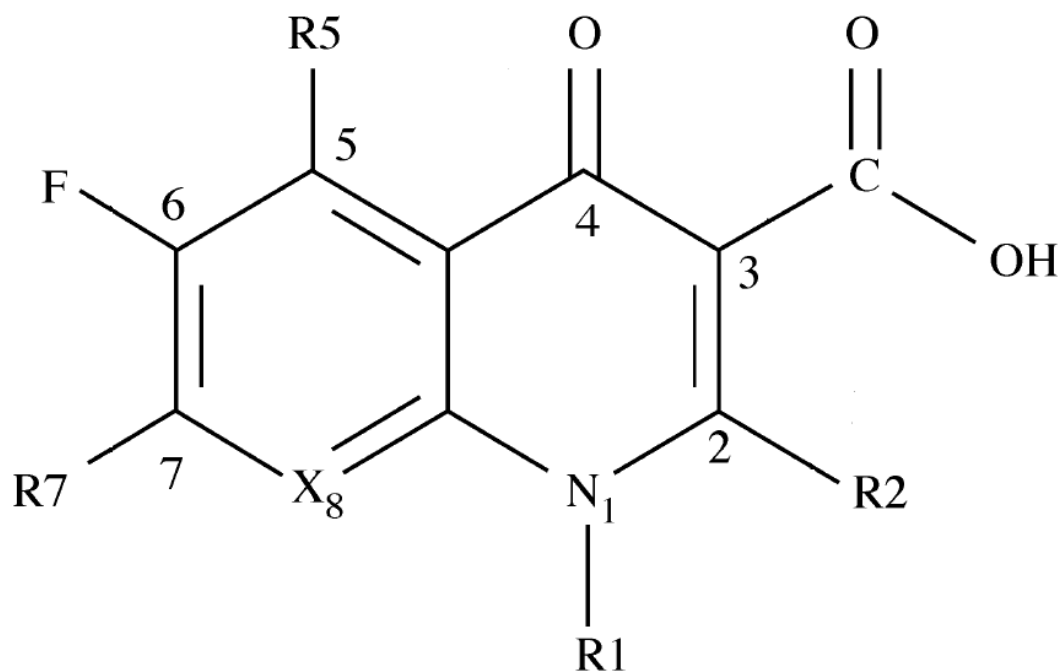

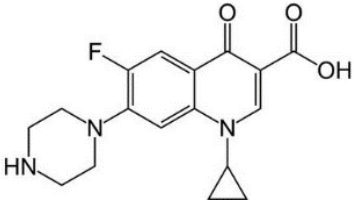
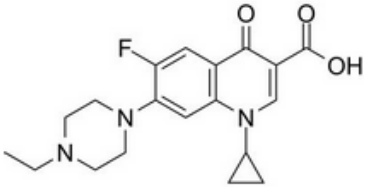
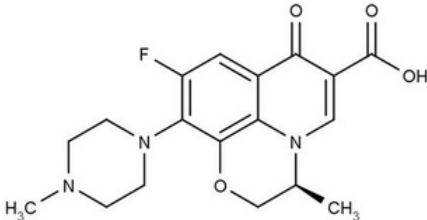


Figure 1.4 General structure of a quinolone antibiotic.

A nitrogen atom in position X₈ resulted in the first naphthyridines compounds, whereas a carbon atom in position X₈ leads to the first quinolone compounds (*e.g.*, cinoxacin, flumequine). The addition of a fluorine atom at position C₆ led to the first fluoroquinolones and was one of the earliest chemical modifications of its structure. The addition of piperazine at position C₇ (*e.g.*, norfloxacin) improved activity against Gram negative organisms, and their antibacterial activity to Gram positive agents was enhanced after adding a cyclopropyl ring or a six-member (pyridobenzoxazine) ring at position N₁ (*e.g.*, ciprofloxacin, ofloxacin). Further improvements in the chemical structure included a five membered or azabicyclic ring at position C₇ (*e.g.*, moxifloxacin, trovafloxacin), which revealed enhanced activity to both Gram positive and especially Gram negative pathogens (Andersson and MacGowan, 2003; Blondeau, 2004).

The physicochemical properties of some FQ antibiotics are summarized in **Table 1.5**. Many of the FQs contain both a carboxyl acid and ternary amine groups in their chemical structure, in addition to an additional secondary amine present in the piperazine group. The pK_a values of the secondary amine present in the piperazine group are around -0.2, thus only being protonated under extreme acid conditions (Rusu et al., 2012). Therefore, under most environmental conditions they may be found under cationic (+), zwitterion (+/-) or anionic (-) forms. Solubility and hydrophobicity of the FQs are pH-dependent. The solubility of the cationic and anionic species is enhanced, reaching values up to 30 g L⁻¹, while a solubility decrease is observed at neutral pH where the zwitterion form is predominant, reaching values up to 0.25 g L⁻¹ (Rivagli et al., 2014). FQ hydrophobicity, expressed as its K_{OW}, suggests a high affinity for remaining in the aqueous solution, even though K_{OW} is decreased at neutral pH where the zwitterion species is predominant (Cárdenas-Youngs and Beltrán, 2015).

Table 1.5 Main physicochemical properties of FQ antibiotics.

FQ	Acronym	CAS number	Molecular formula	Molecular Weight	Chemical structure	pK _{a1} / pK _{a2}	log K _{ow}
Norfloxacin	NOR	70458-96-7	C ₁₆ H ₁₈ FN ₃ O ₃	319.3		6.20 / 8.55 ^a	-1.17 ^b
Ciprofloxacin	CIP	85721-33-1	C ₁₇ H ₁₈ FN ₃ O ₃	331.3		6.30 / 8.61 ^a	-0.81 ^b
Enrofloxacin	ENR	93106-60-6	C ₁₉ H ₂₂ FN ₃ O ₃	359.4		6.22 / 7.90 ^a	-0.43 ^c
Ofloxacin	OFL	82419-36-1	C ₁₈ H ₂₂ FN ₃ O ₄	361.4		6.13 / 8.21 ^a	-0.58 ^b

^a Experimental data from Rusu et al., 2012; ^b Mean log K_{ow} data from Van Doorslaer et al., 2014; ^c Experimental data at pH 5.3 from Cárdenas-Youngs and Beltrán, 2015.

1.2.2. FQs toxicity and generation of antibiotic resistance genes

FQs toxicity tests performed in the laboratory on aquatic organisms revealed a low to moderate risk at relevant FQ environmental concentrations (Robinson et al., 2005), which has been confirmed after risk assessment studies on specific freshwaters systems (Chen et al., 2015; Li et al., 2017; Hu et al., 2018). Besides, they may also affect the growth of soil flora and fauna species at high concentrations (Riaz et al., 2018). Low to moderate effects have been noticed in bacteria communities in constructed wetlands and soils (Kotzerke et al., 2011; Li et al., 2020), although these negative effects may depend on FQ sorption degree and may be dissipated after months (Kotzerke et al., 2011; Xiong et al., 2015). The continuous exposure to these antimicrobials among the bacterial community may lead to the generation and transfer of specific antibiotic resistance genes (ARGs), being one of the most common mechanisms of FQ resistance the mutation in one or more genes that encode the primary and secondary targets of these drugs, the type II topoisomerases enzymes (DNA gyrase and DNA topoisomerase IV) (Redgrave et al., 2014). Mutations in these gens alter the protein structure and subsequently the FQ binding affinity of the enzyme. This may eventually cause a potential threat to humans beings due to the lower effectiveness of these antibiotics to treat infections caused by certain bacteria (WHO, 2017). The amount of ARGs in agricultural soils has been associated with the levels of antibiotics applied (Sun et al., 2020), and therefore, a reduction in the use of antimicrobial agents is crucial to avoid the generation of new resistant bacteria strains. Besides, studying the mobility, degradation, accumulation and dose exposure of FQs to soil bacterial communities is crucial for bacterial risk assessment studies (Parkin, 2007).

1.2.3. FQs legislation

In 2011, the World Health Organization (WHO) Advisory Group on Integrated Surveillance of Antimicrobial Resistance prioritized FQs, among other antibiotic families, as “critically important compounds to monitor and reduce their use due to potential negative long-term negative effects” (WHO, 2011). European Council directive 96/23/EC set measures to monitor certain substances and residues thereof in live animals and animal products, whereas European regulation (EU) No 37/2010 set maximum residue limits (MRLs) in foodstuffs of animal origin. This regulation considers the sum of ENR and CIP as marker residues in animal species including bovine, ovine, caprine, porcine, rabbits, poultry and other food producing species, and set MRLs at levels up to 300 $\mu\text{g kg}^{-1}$ for selected target tissues such as muscle, fat, liver and kidney. However, no current specific regulations for FQ levels affecting soil and water quality are available in the EU.

1.2.4. FQs analysis in environmental samples

Monitoring studies aiming to detect low (among ng L^{-1}) levels of pharmaceuticals in soils, sediments and water samples often require a solid/liquid or liquid/liquid extraction followed up by a clean-up and pre-concentration step using SPE, chromatographic separation and detection using tandem mass spectrometry (USEPA, 2007). However, the fluorescent properties of the FQs allow them to be quantified in soil slurries by HPLC using a fluorescence detector (FLD) at concentrations among hundreds of $\mu\text{g L}^{-1}$ (Leal et al., 2013), or even by Ultraviolet-Visible (UV-Vis) spectrometry at mg L^{-1} levels (Cao et al., 2015b). Nonetheless, the use of HPLC is preferred even when quantifying a single FQ, since it allows the separation of dissolved organic species that may alter the fluorescent properties of FQs through quenching effects (Pan et al., 2012).

Table 1.6 summarize the main characteristics of some reported HPLC methods used to quantify FQs. Reverse-phase C_{18} columns and isocratic elution conditions are usually used, and albeit the composition of the mobile phase A differs among methods, the mobile phase B is mostly composed by ACN or MeOH. Several concerns have been raised in the analysis of FQs by HPLC due to the identification of two peaks corresponding to a single FQ analyte. On one hand, this has been attributed to ternary complexes with dissolved organic matter (DOM) species assisted by calcium cations (FQ-Ca-DOM complexes), which are pH dependent and prone to break down with the addition of a complexing agent such as ethylenediaminetetraacetic acid (EDTA) or oxalic acid, thus avoiding matrix effect in the quantification (Peruchi et al., 2015). However, other authors suggested the presence of an esterification reaction of the protonated carboxyl group of the FQ with MeOH under acid conditions, being the esterified FQ species less retained in the C_{18} column (De Witte et al., 2007). Overall, the combination of formic acid:MeOH as mobile phase seems to lead to a matrix effect that is not observed for other mobile phase combinations.

Table 1.6 Reported HPLC-FLD conditions for the analysis of different FQs in aqueous soil slurries samples.

Injection volume (μL)	Flow rate (mL min^{-1})	Mobile phase composition A:B (%)	LOQ ($\mu\text{g L}^{-1}$)	Detection	Comments	Reference
N.R.	1.0	0.1% formic acid:MeOH (70:30)	10	HPLC-UV-Vis	Addition of EDTA	Peruchi et al., 2015
10	1.0	0.1% formic acid:MeOH (70:30)	10	HPLC-UV-Vis	Addition of EDTA	Martínez-Mejía et al., 2017
N.R.	0.3	0.1% formic acid:MeOH (70:30)	0.05 – 0.06	HPLC-MS/MS	Addition of EDTA	Parpounas et al., 2017
50	1.5	0.01 M oxalic acid (pH 2.2):MeOH (80:20)	2 – 3	HPLC-FLD	No matrix effect	Teixidó et al., 2014
50	1.0	0.1% formic acid:ACN (72:28)	N.R.	HPLC-FLD	No matrix effect	Leal et al., 2013
50	1.0	0.01 M oxalic acid (pH 4):MeOH (72:28)	0.2 – 1.8	HPLC-FLD	No matrix effect	Leal et al., 2012
N.R.	1.0	0.05 M H_3PO_4 (pH 2.7):ACN (70:30)	500	HPLC-UV-Vis	No matrix effect	Vasudevan et al., 2009
20	1.0	Acetate buffer (pH 3):ACN (70:30)	50 - 100	HPLC-UV-Vis	No matrix effect	Conkle et al., 2010
20	0.6	0.025 M H_3PO_4 (pH 3):ACN (83:17)	N.R.	HPLC-FLD	No matrix effect	Zhang et al., 2009
20	0.8	0.1% H_3PO_4 (pH 3):ACN (85:15)	N.R.	HPLC-FLD	No matrix effect	Graouer-Bacart et al., 2015

LOQ: limit of quantification; FLD: Fluorescence detector; MeOH: methanol; ACN: acetonitrile; N.R.: not reported.

1.2.5. FQs input pathways and occurrence in the environment

FQs may reach the environmental compartments through different pathways (**Figure 1.5**). Improper disposals of household waste, expired or unused medicines and solid waste from pharmaceutical industries in dumping sites may lead to detectable levels of FQs in soils (Arun et al., 2020). Besides, their use in aquaculture activities may cause significant pollution issues (Vilca et al., 2021). In addition, due to their widespread use in both human and veterinary medicine, and since antibiotics are only partly metabolized by animal bodies, they can reach the environment after excretion (Rimington, 2020). High levels (up to a hundred $\mu\text{g L}^{-1}$) of FQs have been detected in hot spots such as hospital-effluent wastewaters (Vasconcelos et al., 2009), and although the removal rate of FQs in WWTPs is relatively high (Burch et al., 2019), they are still detected few km far from WWTP effluent discharges (Massey et al., 2010).

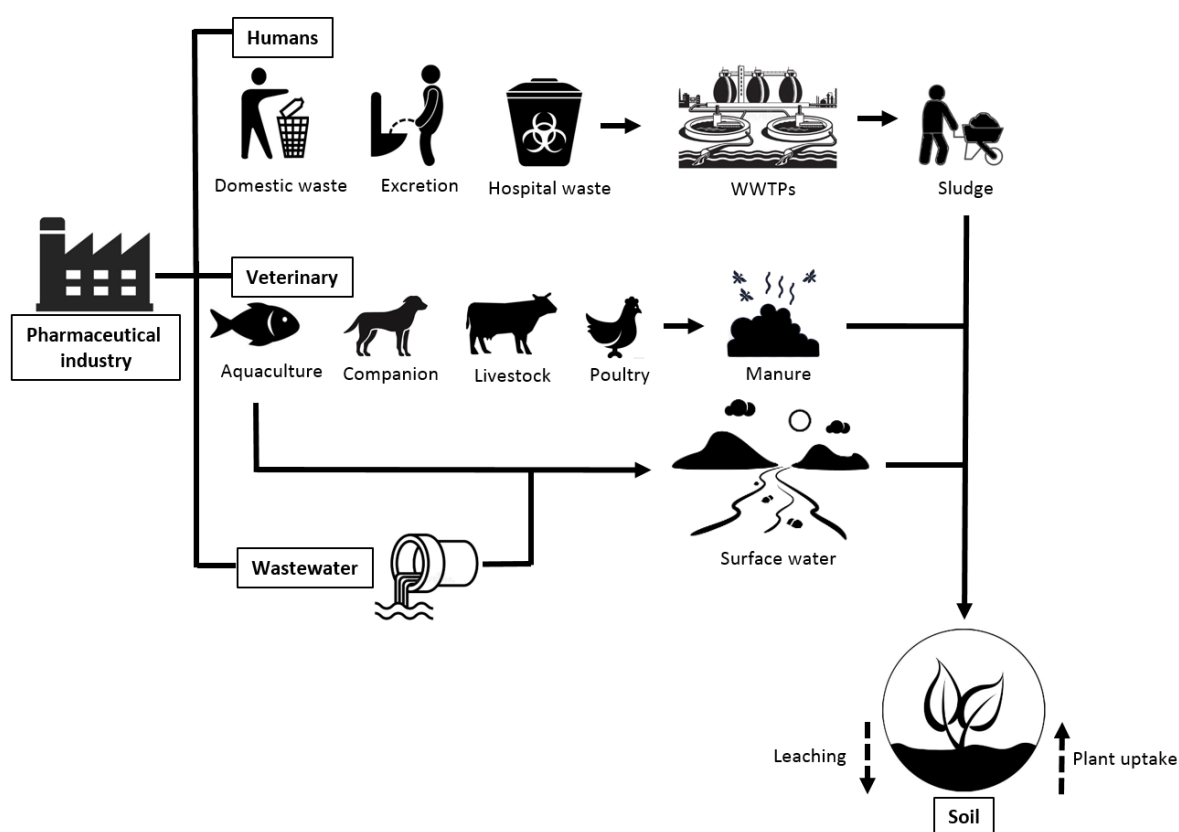


Figure 1.5 Input pathways of FQs in the environment, adapted from Picó and Andreu, 2007.

FQs have been detected in sewage sludge sample at $\mu\text{g kg}^{-1}$ levels (Lillenberg et al., 2009). Hence, both the irrigation of agricultural fields with wastewater and the application of sewage sludge in agricultural soils as amendments may be considered as input pathway of these antibiotics in soils. Also, FQs have been detected at mg kg^{-1} in chicken droppings, poultry, cow litters and pig manure (Riaz et al., 2018), and the use of these amendments in agricultural soils, especially in organic farming, is an important FQ input pathway in the environment (Picó and Andreu, 2007).

Extensive monitoring studies have been conducted to assess the environmental levels of FQs in soil and freshwater systems during the past decade. **Table 1.7** summarizes FQ concentrations in sediments and freshwater systems, while **Table 1.8** summarizes FQ concentrations in soils affected with potential sources of FQs. As can be seen in **Table 1.7**, FQ levels in surface waters range around 5 - 300 ng L^{-1} , thus causing a low to moderate associated risk to aquatic species and disrupting the balance of the original ecosystem (Li et al., 2017). Similarly, concentrations in bed sediments are around 5 - 200 ng g^{-1} in the absence of heavily antibiotic pollutant activities (Vilca et al., 2021). FQ concentrations in impacted soils, however, vary among the FQ input source (**Table 1.8**). The irrigation of agricultural fields with recycled wastewater as well as the addition of sewage sludge as soil amendment may lead to FQ concentrations in soils at levels up to 450 ng g^{-1} , while the addition of animal manure may lead to higher concentrations among few $\mu\text{g g}^{-1}$. Once in the soil, FQs are hardly photo- and biodegraded and tend to accumulate in surface soils, in addition to disrupt soil bacterial communities and eventually be transferred to the plant system or affect its growth (Migliore et al., 2003; Girardi et al., 2011; Hawker et al., 2013; Cui et al., 2014; Chung et al., 2017; Pan and Chu, 2017; Lin et al., 2018; Hu et al., 2021).

Table 1.7 Worldwide selected FQs concentration ranges (min – max) found in water (ng L⁻¹) and sediments (ng g⁻¹).

Location	Matrix	NOR	CIP	ENR	OFL	Reference
Weihe River	W	<1.2 – 23.2	<1.2 – 15.6	<1.2 – 9.8	<1.2 – 12.4	Li et al., 2017
(China, 2014)	S	<2.5 – 28.5	<2.5 – 17.2	<2.5 – 10.4	<2.5 – 20.8	
Hanjiang River	W	<1.3 – 6.4	<1.3 – 4.5	<1.3 – 3.6	<1.3 – 9.5	Hu et al., 2018
(China, 2015)	S	<0.5 – 7.1	<0.5 – 3.7	<0.5 – 2.4	<0.5 – 9.9	
River water	W	N.A.	<0.5 – 116	N.A.	17 – 182	Massey et al., 2010
(USA, 2006)	S	N.A.	6.91 – 74	N.A.	28 – 113	
Jiyun River	W	N.A.	N.A.	1.55 – 57.5	0.36 – 102	Li et al., 2016
(China, 2012)	S	N.A.	N.A.	<0.13 – 11.7	0.46 – 42.2	
Pearl River	W	57 – 227	N.A.	N.A.	5 – 18	Liang et al., 2013
(China, 2011)	S	2.6 – 21	N.A.	N.A.	0.7 – 14	
Urban River	W	<2.53 – 80	<1.71 – 78	N.A.	<2.54 – 69	Valdés et al., 2021
(Argentina, 2016)	S	N.D.	N.A.	N.A.	N.D. – 39	
Bosten Lake	W	N.A.	17.3 – 112	<0.10 – 15.2	1.3 – 32.3	Lei et al., 2015
(China, 2012)	S	N.A.	21.2 – 213	3.42 – 20.0	18.4 – 94	
Taihu Lake	W	<3.6 – 6.5	<3.6 – 43.6	N.A.	<3.6 – 82.8	Xu et al., 2014
(China, 2010)	S	<3.9 – 28.4	<3.9 – 25.3	N.A.	<3.9 – 52.8	
Hailing bay	W	<0.39 – 5.04	<1.05 – 187	<0.33 – 56.7	<0.31 – 13.7	Chen et al., 2015
(China, 2013)	S	<0.82 – 22.2	<1.95 – 4.21	<0.80 – 2.60	<0.73 – 19.4	
Titicaca Lake	W	N.A.	56 – 63	86 – 653	N.A.	Vilca et al., 2021
(Perú, 2016)	S	N.A.	150 – 3,740	950 – 3,010	N.A.	
Dilúvio River	W	<5 – 292	<5 – 344	N.A.	N.A.	Arsand et al., 2020
(Brazil, 2018)						
Senie River	W	<10 – 163	<10	≤ 10	<10 - 55	Tamtam et al., 2008
(France,						
Bohai bay	W	<5.0 – 80.3	N.A.	N.A.	<4.0 – 13.9	Cheng et al., 2016
(China, 2009)	S	<2.0 – 20.9	N.A.	N.A.	<2.0 – 3.54	

W: Water; S: Sediment; N.D.: non detected (LOD not reported); N.A.: non analysed.

Table 1.8 Worldwide selected FQs concentration ranges (min – max) found in agricultural soils (ng g⁻¹) after different fertilization or irrigation processes.

Location	Status	NOR	CIP	ENR	OFL	ref
Mexico, 2009	Agricultural soils irrigated with wastewater	N.A.	0.35 – 2.82	0.03 – 0.64	N.A.	Dalkmann et al., 2012
China, 2008	Agricultural soils irrigated with wastewater	<0.05 – 84	<0.02 – 85	N.A.	N.A.	Shi et al., 2012
China, 2013	Agricultural soils fertilized with sewage sludge	112 – 155	18.4 – 27.5	1.65 – 8.31	111 – 147	Yang et al., 2018
Switzerland, 1999	Agricultural soils fertilized with sewage sludge	350	450	N.A.	N.A.	Golet et al., 2003
France, 2015	Agricultural soils fertilized with sewage sludge	<0.7 – 16.5	<1.4	N.A.	<0.4 – 1.8	Salvia et al., 2015
China, 2011	Agricultural soil fertilized with untreated animal manure	14.9 – 150	5.3 – 120	5.1 – 1,348	N.A.	Li et al., 2011a
China, 2009	Agricultural soils fertilized with poultry manure	N.A.	<5 – 7,220	<5 – 3,059	N.A.	Wei et al., 2016
Turkey, 2009	Agricultural soils fertilized with poultry and cattle manure	N.A.	N.A.	20 – 50	N.A.	Karci and Balcioglu, 2009
China, 2008	Agricultural soils fertilized with livestock manure	N.A.	0.8 – 30	N.A.	0.6 – 1.6	Hu et al., 2010
Italy, 2000	Agricultural soil at several months after fertilization	N.A.	N.A.	33 – 80	N.A.	Sturini et al., 2012
Turkey,	Agricultural soils fertilized with poultry manure	N.A.	N.D. – 53	48 – 222	N.A.	Uslu et al., 2008
Austria, 2004	Agricultural soils fertilized with pig and chicken manure	N.A.	N.A.	130 – 750	N.A.	Martínez-Carballo et al., 2007

N.A.: non analysed; N.D.: non detected.

1.3. Environmental risk assessment for PFASs and FQs

1.3.1. Environmental risk assessment

Once a compound is released in the environment, it is important to assess its associated risk and the possible threats to human beings and ecosystems. The environmental risk assessment is a process that evaluates the likelihood that adverse ecological or health effects may occur as a result of the exposure to one or more stressors. The process is used to systematically evaluate and organize data, information, assumptions and uncertainties in order to help understand and predict the relationships between stressors and adverse effects in a way that is useful for environmental decision making. Defining adversity is important because a stressor may cause adverse effects on one ecosystem component but be neutral or even beneficial to other components. Changes often considered undesirable are those that alter important structural or functional characteristics or components of the general ecosystems. An evaluation of adversity may include a consideration of the type, intensity and scale of the effect as well as the potential for recovery, and the acceptability of adverse effects is determined by risk managers according to professional judgement and available information (USEPA, 1992).

The environmental risk assessment process is based on the characterization of the effects and of the exposure. Therefore, to perform a risk analysis, it is not only important to quantify their presence (levels) in the environment, but also quantify a range of other parameters related to their toxicity to different species, its photo- and biodegradation under environmental conditions, the cumulative risk of a continuous exposure, their mobility through environmental compartments and their related interaction mechanisms, among others. In this sense, the evaluation of the sorption/desorption process of compounds with environmental matrices (*i.e.*, soils and sediments) helps to estimate their potential mobility and therefore potential exposure to organisms. Besides, elucidating the chemical interaction mechanisms with these matrices is important to extrapolate the knowledge to other untested scenarios. Thus, quantitative

parameters descriptors of these sorption/desorption processes are required to assess and predict the derived environmental mobility. With all this information, a proper evaluation of the potential risk can be assessed, and if necessary, remediation actions can be suggested. These may include *in-situ* and *ex-situ* techniques, including soil washing, electrochemical remediation, phytoremediation and the addition of amendment materials in order to sorb, accumulate and immobilize the given pollutant (USEPA, 1992).

1.3.2. The sorption/desorption process

Organic pollutants, such as PFASs and FQs, present in environmental aqueous phases may be mobilized along environmental compartments and eventually end up in drinking waters or be incorporated into the food chain, becoming a potential threat for living organisms. Their binding to solid particles may reduce its mobility, and thus soil and sediment particles play a key role in the overall fate of these pollutants after pollution events. As exposed previously, the understanding of the chemical interaction mechanisms controlling how a pollutant interacts with solid phases, and the estimation of their degree of incorporation and retention (*i.e.*, sorption intensity and reversibility) in different solid matrices are crucial for environmental risk assessment studies. However, their partition and interaction mechanisms may be affected by numerous geochemical processes, in addition to be dependent on various physicochemical parameters related to the pollutant and/or other environmental conditions.

The term “sorption” describes the incorporation of a given compound (sorbate) from a liquid solution to a solid matrix (sorbent), and encompasses all adsorption, absorption, precipitation and related processes. In the case of the soil system, this incorporation may be affected by the nature and amount of the organic and mineral fractions of the soil, in addition to the physicochemical properties of the liquid phase (*e.g.*, pH; concentration of cations and anions; DOM content) and the physicochemical properties of the target sorbate (*e.g.*, speciation;

hydrophobicity). Similarly, the term “desorption” describes the release of the sorbate from the sorbent to a liquid solution. This process may also be affected by similar variables to those affecting sorption. **Figure 1.6** represents the overall sorption/desorption process of a pollutant in the soil/sediment system.

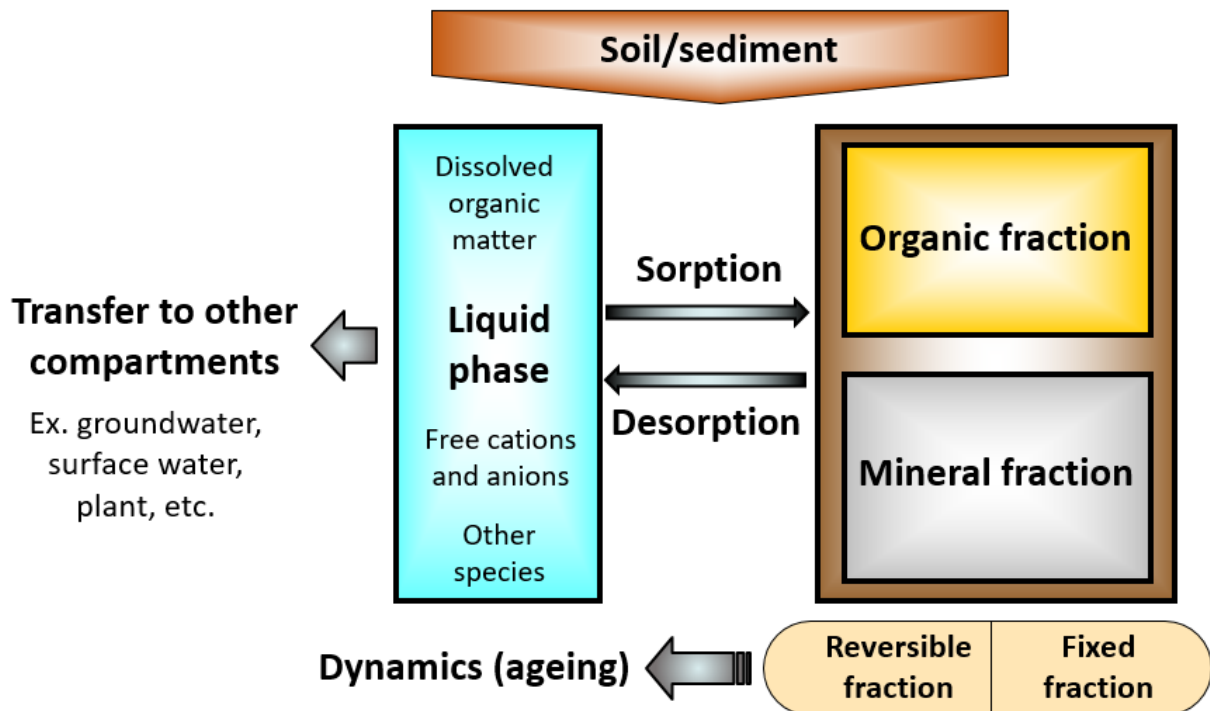


Figure 1.6 Sorption/desorption process of a given pollutant in the soil/sediment system.

Sorption irreversibility may vary along time depending on environmental conditions affecting soil properties and on sorption kinetics and mechanisms governing the sorption process (interaction dynamics). Thus, the time elapsed since contamination may have an impact in the overall sorption process (Ltifi et al., 2014).

1.3.3. Theoretical rationale to describe the interaction mechanisms of organic compounds with environmental matrices

1.3.3.1. Electrostatic interactions

The surfaces of solid environmental matrices may be positively or negatively charged depending on environmental conditions. Hence, non-covalent attractive interactions may occur between charged surfaces and charged organic pollutants of opposite signs, while repulsive interactions may occur between charged surfaces and charged organic pollutants of the same sign. In this sense, clay minerals usually possess a pH-dependent surface charge, being negatively charged under most environmental conditions. The presence of mono and divalent cations may compress the electrical double layer of these sorbents and alter the resulting electrostatic interactions: the presence of cations such as K^+ and Na^+ could shield negative repulsions between anionic sorbents and anionic sorbates, while divalent cations may act as “bridge” to facilitate the formation of anion-cation-anion complexes (Du et al., 2014). Moreover, these clay surfaces may compensate the positive and negative charges with sorbed anions and cations, respectively, which are able to be replaced by charged pollutants through exchange mechanisms. Some of the above mentioned interactions are depicted in **Figure 1.7**.

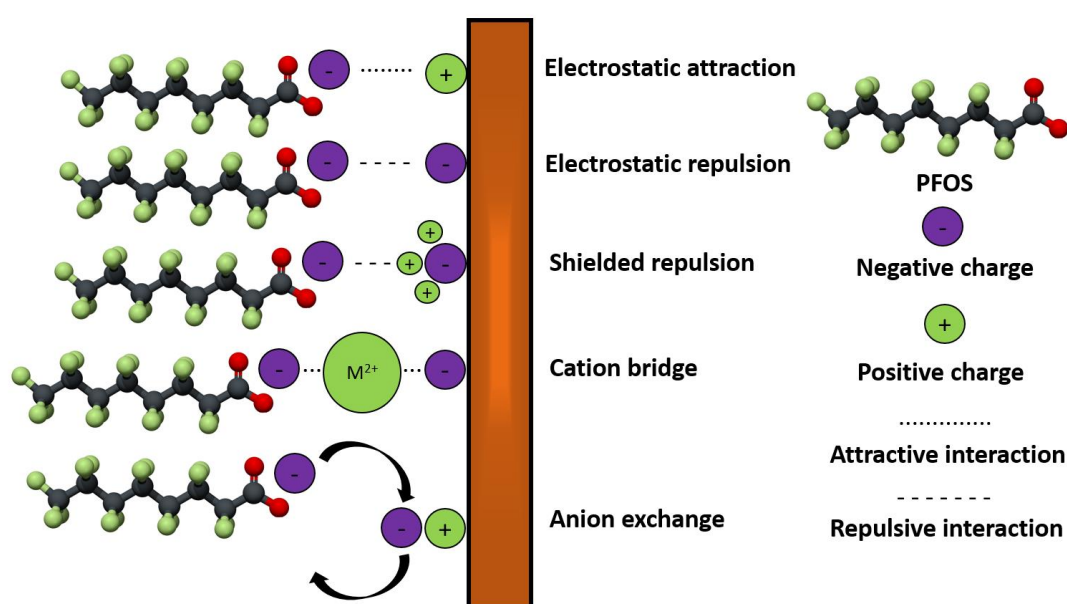


Figure 1.7 Examples of electrostatic interactions between PFOS and solid particles.

1.3.3.2. Hydrophobic interactions

Hydrophobic interactions are the observed tendency of nonpolar substances (hydrophobe) to aggregate among each other and exclude water molecules. Carbon-rich suspended solid particles may also be considered hydrophobes. When a hydrophobe is present in an aqueous medium, hydrogen bonds between water molecules are broken because of its presence, thus being an endothermic reaction ($\Delta H < 0$). The distorted water molecules are likely to create new hydrogen bonds around the hydrophobe, which makes the system more structured with a decrease of the total entropy ($\Delta S < 0$). The resulting ΔH of the system can be negative, zero or positive depending on if the new hydrogen bonds have partially, completely or overcompensated the hydrogen bonds broken after the hydrophobe entry. However, ΔH values are usually insignificant in determining the spontaneity of the reaction because the large ΔS , and therefore, hydrophobic interactions are generally spontaneous ($\Delta G < 0$) (Atkins, 2006).

Figure 1.8 depicts the hydrophobic interaction in aqueous solution.

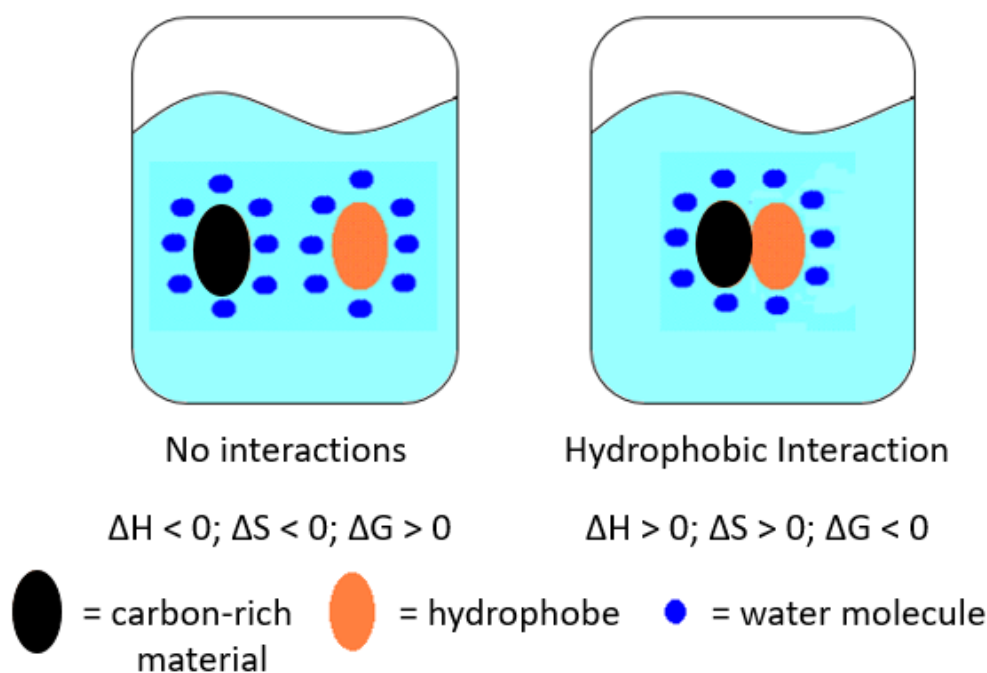


Figure 1.8 Thermodynamic aspects of hydrophobic interactions in aqueous solutions:

the case of the presence of carbon-rich materials.

1.3.3.3. Hydrogen bonding

A hydrogen bond is an attractive electrostatic force between a hydrogen atom which is covalently bound to an electronegative atom or group (hydrogen bond donor, Dn), and another electronegative atom bearing a pair of electrons (hydrogen bond acceptor, Ac). This is generally denoted as: $Dn - H \cdots Ac$, where the solid line indicates a polar covalent bond, and the dotted line indicates the hydrogen bond. The most frequent donor and acceptor atoms are those with a strong electronegativity (*i.e.*, N, O and F). The resulting strength is mainly dependent on the nature of both Dn and Ac: those hydrogen bonds formed by Dn and Ac groups with a similar pK_a will result in a higher bonding strength (Thomas, 2002). Accordingly, FQs could effectively interact with carboxyl and phenol moieties to form hydrogen bonds, whereas PFASs are not likely to form effective hydrogen bonds with functionalities present in environmental matrices due to their very low pK_a values.

1.3.3.4. Complexation with metals

Anionic organic pollutants can be considered as organic ligands (L) that can form complexes with several metallic atoms (M, *i.e.*, Al, Fe, Cu, Zn). These complexes are formed through the interaction of an available electron pair or even an unshared electron pair of the ligand with empty electron orbitals of the metallic atom. Several factors affecting the stability of the resulting complexes include the nature of both ligand and metalling atom, the ionic strength and pH of the aqueous solution, temperature and competing ions. The principal effects on ΔH are the formation of the M – L bond, the charge neutralization energy and the desolvation energy for both M and L when forming the M – L complex (Ribas, 2000). As both PFASs and FQs may be present in anionic forms, both are eligible to be sorbed by complexation mechanisms in environmental matrices and phases such as metal oxides.

1.3.3.5. Pore filling

Pore filling mechanism are physical interactions in which the sorbate is trapped into the porous structure of the sorbent, without the formation of any chemical bond. These interactions may occur in highly porous materials such as carbon-rich materials (*e.g.*, activated carbons and biochars), and key factors affecting its effectiveness are the molecular size of the sorbate and the microporous volumes and width (Du et al., 2014). Those sorbates with a molecular size lower than the microporous width may access in the microporous cavities and be trapped, avoiding its release back to the aqueous solution. Both PFASs and FQs could therefore interact by pore filling mechanism with porous materials.

1.3.3.6. Interactions with π aromatic groups

Aromatic structures may interact with each other by attractive noncovalent interactions between aromatic rings, also called as $\pi - \pi$ stacking, leading to the formation of an electron donor-acceptor complex. The strength of the formation of a benzene dimer by $\pi - \pi$ stacking ranges 8 – 12 kJ mol⁻¹ (Sinnokrot et al., 2002), although the resulting strength is dependent on the respective electron-rich and electron-deficient substituents of the aromatic rings. Here, only FQs could participate in $\pi - \pi$ stacking mechanism as they contain an aromatic ring in their structure. Charged species may also interact with aromatic π structures. Cation – π interactions are noncovalent molecular attractive interactions between the face of an electron-rich π system and a cationic specie. The energetic strength of the interaction range 40 – 90 kJ mol⁻¹ (Zhao et al., 2017) and is dependent on both the presence of electron-donor substituents in the aromatic ring and the acidic strength of the sorbate. Thus, under acidic pH, FQs could participate in cation – π mechanism with highly aromatic sorbents. Besides, anion – π interactions have also been described in the literature: they are defined as favourable noncovalent contacts between an electron deficient (π acidic) aromatic system and an anion, dominated by electrostatic and

anion-induced polarization contributions, being the final binding strength affected by charge density, polarity and hydration effect (Schottel et al., 2008). Although these interactions are suggested to participate in supramolecular chemistry and catalysis (Schottel et al., 2008), its contribution in the binding process of anionic organic pollutants in environmental matrices is unclear, although both PFASs and FQs may interact through anion – π interactions with aromatic sorbents.

1.3.4. Characteristics of the solid-water system affecting PFAS and FQ sorption

The sorption of organic pollutants in environmental matrices may be affected by some relevant physicochemical properties of the sorbent, and the identification of key sorbent properties responsible of sorption may help to elucidate the interaction mechanisms driving the sorption process. Some relevant sorbent physicochemical characteristics participating in sorption of PFASs and FQs are detailed below.

1.3.4.1. pH and pH_{ZPC}

For some organic compounds, especially those containing ionisable groups, their sorption to solid particles may be affected by both their speciation and the overall surface charge of the solid matrix. Whereas soil pH would determine the predominant sorbate species in solution, the difference between pH and pH_{ZPC} (the pH in which the solid matrix has a net zero charge) would rule the overall surface charge able to undergo electrostatic attractions/repulsions and other related mechanisms. Increasing pH leads to a higher number of negative charges, mainly present in pH charge dependent minerals such as kaolinite or goethite and deprotonated acidic functional groups of the soil organic matter components such as humic acids. Hence, the sorption of organic pollutants containing acidic functional groups such as FQs and PFASs in soils and sediments is usually pH-dependent, decreasing when increasing pH due to increasing electrostatic repulsions between the negative charges present in both the sorbent and sorbate (Higgins and Luthy, 2006; Zhang et al., 2009).

1.3.4.2. Soil texture and mineralogy

Soil mineral particles often play a role in the sorption of organic compounds. These particles comprise clay minerals, oxides, sesquioxides and (hydro)oxides of metals. The soil texture is an operational classification related with the particle size of the mineral particles, defined as the relative proportion of clay (< 0.002 mm), silt (0.002 – 0.05 mm) and sand (0.05 – 2 mm). Clay minerals are usually found in the clay and, to a lesser extent, silt fractions, whereas the sand fraction is usually composed by crystalline quartz. A given soil may be therefore classified according to this classification proposed by the United States Department of Agriculture (USDA) depending on the relative proportion of clay, silt and sand referred to the bulk mineral content (**Figure 1.9**). Soils with high OM content, such as peat soils, are unlikely to be classified according to this classification due to their low mineral content.

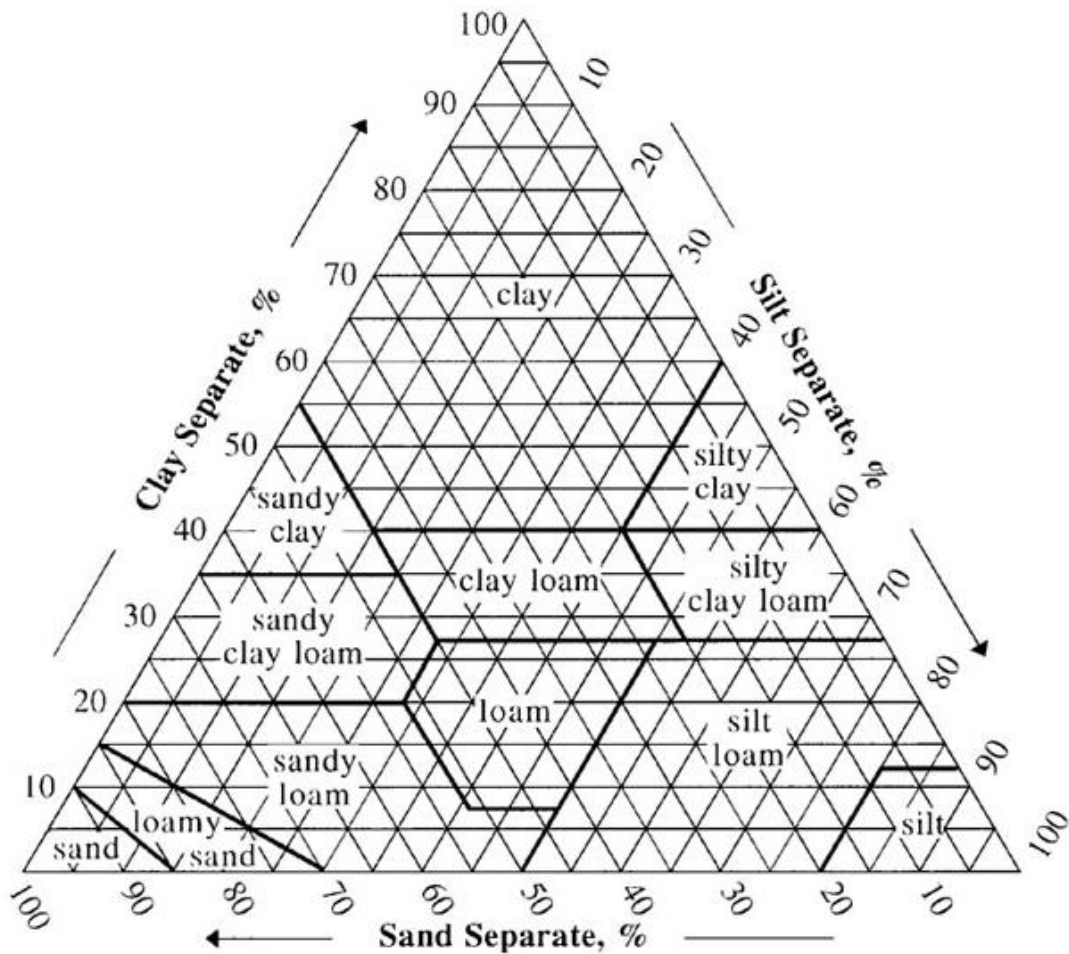


Figure 1.9 USDA soil classification depending on the relative mineral proportion.

The phyllosilicates are the major clay minerals found in soils. These minerals comprise 1:1 phyllosilicates (*e.g.*, kaolinite), which consist in one silica tetrahedral layer bonded to an aluminium octahedral sheet, and 1:2 phyllosilicates (*e.g.*, vermiculite, montmorillonite), which consist in two silica tetrahedral layers surrounding an aluminium octahedral layer. Kaolinite has a pH-dependent surface charge and lower surface area and cation exchange capacity compared to 1:2 phyllosilicates, that have a higher surface area and cation exchange capacity. Contrarily to 1:1 phyllosilicates, only weak van der Waals forces exist between these two layers in 1:2 phyllosilicates. Therefore, water and hydrated cations can readily enter into the interlayer region and be immobilized, thus expanding this interlayer and providing additional sorption sites able to bind organic pollutants (Uddin, 2017).

Sorption of FQs have been shown to have a high sorption affinity to clay minerals such as kaolinite and montmorillonite, especially at acid to neutral pH (Wan et al., 2013). Moreover, sorption on 1:2 phyllosilicates, especially montmorillonite, has been shown to be two orders of magnitude higher than 1:1 phyllosilicates such as kaolinite, due to the intercalation of fluoroquinolone molecules in the interlayer (Nowara et al., 1997). The main sorption mechanisms between FQs and phyllosilicates are electrostatic and cation exchange interactions. Unlike FQs, sorption of PFASs in phyllosilicate minerals seems to be poor, revealing a low sorption affinity to both kaolinite and montmorillonite (Johnson et al., 2007; Jeon et al., 2011).

Besides clay minerals, Fe and Al oxides and (hydro)oxides are commonly found in soils in several mineralogical forms (*e.g.*, hematite, goethite, gibbsite and bohemite). These minerals have also a pH-dependent surface charge, thus allowing them to interact through electrostatic mechanisms with ionic or ionisable organic pollutants. Sorption of FQs in goethite at neutral and basic pH is driven by the formation of complexes with the Fe atoms in the goethite surface (Paul et al., 2014). On the other hand, PFASs have also been shown to have a weak complexation affinity to goethite and bohemite (Johnson et al., 2007; Wang et al., 2012).

1.3.4.3. Soil organic matter

The soil organic matter (SOM) includes high molecular weight organic materials, such as polysaccharides and proteins, and other simpler substances, such as sugars, amino acids and other small molecules, in addition to humic substances (Ahmed et al., 2015). Humic substances account for approximately 85 – 90 % of the total organic carbon (OC) in soils. They are formed as a result of the decay and transformation of plant residues and consist in a heterogeneous mixture of compounds for which no single structural formula can be attributed, as their physicochemical properties are highly dependent on feedstock type and humidification conditions. It is assumed that they consist of a skeleton of alkyl/aromatic units cross-linked mainly by oxygen and nitrogen groups with the major functional groups being carboxyl acid, phenolic and alcohol hydroxyls, ketone and quinone groups. Humic substances are operationally classified into fulvic acids (soluble at any pH), humic acids (soluble at basic pH) and humin (insoluble at any pH). Humic acids (**Figure 1.10A**) have a larger average molecular size than those of fulvic acids (**Figure 1.10B**) and are usually found aggregated to mineral particles, especially with those of the clay fraction, thus coating mineral particles. Fulvic acids have a higher number of alkyl groups than humic acids and their aromatic core is less developed. Humin, on the other hand, accounts up to 50% of the total SOM and have a polymeric furanic type structure, with a few hydroxyl, aldehyde and ketone functionalities (Stevson, 1982).

SOM is a key property affecting sorption of certain organic compounds, especially PFASs. Their sorption in soils is suggested to be mainly driven by the SOM fraction through hydrophobic interactions, although their affinity to the different SOM fractions may be affected by their chain length (Higgins and Luthy, 2006). On the other hand, FQs have a stronger sorption affinity to all SOM fractions compared to PFASs (Aristilde and Sposito, 2013), although the interaction mechanisms among them are not totally understood at date.

through hydrophobic interactions, even at neutral pH when $\log K_{OW}$ is maximized, and accordingly, such interactions have been suggested to play a minor role in FQ sorption, such as NOR, in humic acids (Zhang et al., 2012). Whereas PFASs barely form hydrogen bonds with hydrogen atoms bonded to functional groups of most environmental matrices (Du et al., 2014), likely due to its very strong acidity ($pK_a < 1$), the carboxylate moiety of FQs may participate in sorption by hydrogen bonds with protonated functional groups. In addition, such functional groups may also bind the F atom of the FQ through hydrogen bonding, as revealed by Fourier transformed infrared (FTIR) spectroscopic data run in sorption residues of CIP to humic acids (Liu et al., 2017).

Contrarily to PFAS, FQs may interact with aromatic structures of SOM components through $\pi - \pi$ stacking. Both the fluorine moiety and N-substituents groups adjacent to the aromatic ring, in addition to the charge stabilization of the π electrons by the ketone and carboxylate groups, may facilitate $\pi - \pi$ stacking interactions with other aromatic substituents containing electron-donor groups. Besides, anionic PFAS are unable to interact by cation - π interactions, but this mechanism is supposed to mainly drive sorption of cationic and zwitterion FQ species in graphene (Zhao et al., 2017). Moreover, both PFASs and FQs could interact through anion - π interactions with aromatic patches of organic materials such as biochars or humic acids. However, no evidences of the relevance of anion - π interactions have been reported at date in the literature regarding both FQs and PFASs.

1.3.4.4. Cation and anion exchange capacity

Part of the charges present in the solid surfaces may be balanced by cations or anions of opposite charge. Cation and anion exchange capacity (CEC and AEC, respectively) are empirical determinations at a certain pH aiming to determine the total negative and positive charges, respectively, present in the surface of solid particles. This determination relies on the saturation of the material with specific cations and anions that are then exchanged with other cations and anions with a higher affinity for the respective charged sites (Sparks, 1996). Charged pollutants such as PFASs and FQs may replace sorbed cations and anions balancing surface charges during the sorption process. The presence of cation exchange interactions has been observed for cationic CIP in kaolinite clay after monitoring the amount of cations released along the sorption process (Li et al., 2011b), while anion exchange resins have been suggested to be effective sorbents for PFASs removal (Liu et al., 2022).

1.3.4.5. Surface area and porosity

The specific surface area (SSA) of a given material may be related with the number of sorption sites able to bind organic pollutants. SSA gains relevance for those highly porous materials such as biochars and activated carbons, which can achieve areas up to $2,000 \text{ m}^2 \text{ g}^{-1}$ after a proper pyrolysis/activation process (Du et al., 2015). Consequently, their well-developed porous structure leads to an enhancement of the number of sorption sites able to interact with the pollutants if their size can fit into the porous structure. Both pore width and molecular size would determine the accessibility of a compound to the microporous structure, in which pore filling or other sorption mechanisms may take place. Regarding PFASs and FQs, their sorption in biochars increase when increasing sorbent SSA (Guo et al., 2017; Yang et al., 2019).

1.3.4.6. Water-soluble cations and anions

Water-soluble cations and anions can affect the partitioning of PFASs and FQs in soils. Some common soluble cations present in soils include Na^+ , K^+ , Mg^{2+} and Ca^{2+} , whereas some common soluble anions include CO_3^{2-} , Cl^- , NO_3^- and SO_4^{2-} . PFASs sorption in soils increased with metal concentration in solution likely due to cation bridge mechanisms and the shielding effect of electrostatic repulsions (Higgins and Luthy, 2006; Xiao et al., 2011), whereas for FQs cations may compete for cation exchange sites and therefore suppress FQ sorption under acid and neutral conditions (Kong et al., 2014). On the other hand, although water soluble anions may compete for anion exchange sites, only PO_4^{3-} has been found to decrease PFAS sorption in activated carbon at very high concentrations (Qian et al., 2017), and to compete for complexation sites present in the goethite surface able to bind FQs (Qin et al., 2014).

1.3.4.7. Dissolved organic carbon

Dissolved organic carbon (DOC) species, sometimes present in colloidal forms, may affect the sorption of organic pollutants in soil matrices, likely due to three main mechanisms: (i) the blockage of sorption sites present in the microporous structure of the solid matrix; (ii) the sorption of colloidal particles to sorption sites of the solid matrix able to bind the target compound; (iii) the sorption of the target compound to DOC species, thus competing and decreasing sorption. Both PFASs and FQs can interact with DOC, and DOC presence has been shown to decrease PFASs and FQs sorption to activated carbons beyond certain DOC concentration (Yu et al., 2012; Zhang et al., 2018).

1.4. The solid-liquid distribution coefficient (K_d)

1.4.1 Definition and significance of K_d

A useful empirical parameter to quantify the sorption processes under equilibrium conditions is the solid-liquid distribution coefficient (K_d , L kg⁻¹). This parameter is defined as the ratio between the concentration of a compound sorbed in the solid phase (C_s , g kg⁻¹) and the concentration in the aqueous phase (C_{eq} , g L⁻¹) as defined in Equation 1.1:

$$K_d = \frac{C_s}{C_{eq}} \quad (1.1)$$

This approach constitutes the simplest sorption model available, and it does not provide information about the chemical interaction mechanisms affecting the phase partitioning of the target compound. K_d values may be highly sensitive to environmental conditions, including the physicochemical properties of both sorbate and sorbent as well as the nature of the aqueous solution, and therefore are site-specific. K_d values can vary along several orders of magnitude. K_d values < 10 L kg⁻¹ and especially < 1 L kg⁻¹ are indicative of a very weak sorption in the solid phase, and thus the compound is expected to have high mobility to other environmental compartments and associated risk. Compounds with K_d values ranging 10 – 100 L kg⁻¹ possess higher sorption but still can be considered as mobile, whereas K_d values ranging 100 – 1,000 L kg⁻¹ indicate strong sorption and thus low expected mobility. Lastly, those sorbates with K_d values > 1,000 L kg⁻¹ are essentially immobile.

Similarly to K_d , desorption processes may also be described by a “desorption” solid-liquid distribution coefficient ($K_{d,des}$, L kg⁻¹), which is defined as the ratio between the sorbed concentration in the solid phase after desorption equilibrium is reached ($C_{s,des}$, mg kg⁻¹) and the concentration in the solution ($C_{eq,des}$, mg kg⁻¹) desorbed from the solid phase:

$$K_{d,des} = \frac{C_{s,des}}{C_{eq,des}} \quad (1.2)$$

The hysteresis coefficient (H, dimensionless) is defined as the ratio between $K_{d,des}$ and K_d :

$$H = \frac{K_{d,des}}{K_d} \quad (1.3)$$

A hysteresis coefficient for a given substance higher than 1 is indicative of an irreversible sorption process. PFASs and FQs sorption in soils is expected to be generally irreversible, with H coefficients higher than 1 (Drillia et al., 2005; Miao et al., 2017).

1.4.2. Methods for quantifying sorption

The sorption process of organic pollutants in environmental matrices can be evaluated through different experimental approaches. The most widely applied include flow-through experiments, batch sorption experiments and *in-situ* experiments, which are described below.

1.4.2.1. Laboratory flow-through method

Also known as “column” method, it consists in a solution containing a known amount of the target analyte which passes through a column containing a packed sorbent of a known bulk density and porosity, which permits to evaluate its maximum sorption capacity. The analyte concentration in the effluent is monitored as a function of time. A known amount of non-sorbing tracer may also be introduced into the column and its time-varying concentration provides information about the pore-water velocity. The resulting data are plotted as a break-through curve, and the velocity of each constituent is calculated as the length of the column divided by the constituent’s mean residence time. The calculation of a retardation factor (defined as the ratio between pore-water velocity to contaminant velocity) may allow the derivation of K_d (USEPA, 1999).

1.4.2.2. In-situ method

A method for evaluating the distribution coefficient in a field scale is the *in-situ* method (Kim and Carlson, 2007). This method is generally used to analyse sorption in aquifers (then implying sediments), although it can also be applied for soils. In brief, both sediment and overlaying water are sampled, and the concentration of the given analyte in each phase is determined. This method also applies to soils after extracting their interstitial pore water. Later, distribution coefficients can be derived from the ratio between the concentrations found in both phases. Evaluating sorption by the *in-situ* method does not necessarily imply that the system is under equilibrium. Therefore, the distributions coefficients obtained by the in-situ method are often referred as pseudo-partitioning coefficients (K'_d) and may better describe real environmental dynamic scenarios.

1.4.2.3. Batch method

The most common procedure to quantify the sorption/desorption process in a laboratory scale is through batch experiments, performed according to the OECD-based guidelines (OECD, 2000). In these experiments, a given amount of sorbent material is placed in a centrifuge tube and later a given amount of solution is added in the tube, leading to a solid suspension of the sorbent. The optimum soil-to-solution ratio used is determined according to preliminary tests and the sorption strength of the sorbate in the sorbent, aiming to achieve sorption percentages > 50% but also being able to perform a reliable determination (*e.g.*, final concentration two orders of magnitude higher than method LOQ). The contact solution is recommended to be composed by 0.01 M CaCl₂ in order to keep a constant ionic strength and facilitate comparisons among studies, unless the effect of ionic strength or composition is aimed to be evaluated. In addition, several antimicrobial agents such as HgCl₂ or NaN₃ can be added in the solution if the sorbate is likely to suffer biodegradation, whereas applying dark conditions is recommended if the sorbate is likely to suffer photodegradation.

The suspension is then shaken at a given temperature during a given amount of time to achieve a pre-equilibrium state between both phases, and after, a known volume of working solution containing the sorbate is added in the tube. It is recommended that spiked concentrations do not exceed half of the solubility limit. In case that the sorbate solution is prepared in other solvents rather than water, spiking volumes should preferably not exceed 1% to avoid co-solvent effects (*e.g.*, partitioning among three phases). Once the sorbate has been added in the suspension, the tubes are shaken during a given amount of time (established after analysing the sorption kinetics) until sorption equilibrium is reached, and then, the suspension is centrifuged ($> 3,000\text{ g}$) and the supernatant removed and preferably filtered. Checking changes in the liquid phase (*e.g.*, pH, amount of soluble cations) before and after the sorption process is recommended, since changes may contribute to elucidating sorption mechanisms.

Quality controls must be run in parallel to each batch. These includes blank samples to ensure that no target chemical was previously present in the sorbent and aqueous samples (without sorbent material) spiked at representative concentrations used in the experiments to account for possible losses during the experimental setup. Although it is recommended to analyse the concentration of the sorbate in both solid and liquid matrices through validated analytical methods, the concentration sorbed in the solid phase can also be calculated by mass balance if negligible losses are observed in the aqueous control experiments.

A similar experimental approach can be applied to quantify the desorption process. The solid residues after sorption experiments or samples originated from contaminated sites can be analysed to quantify desorption, after adding fresh contact solution but without the presence of the target analyte. The tubes are shaken for a pre-established time, and the supernatants analysed for quantitating the amount of analyte desorbed from the solid phase (**Figure 1.11**).

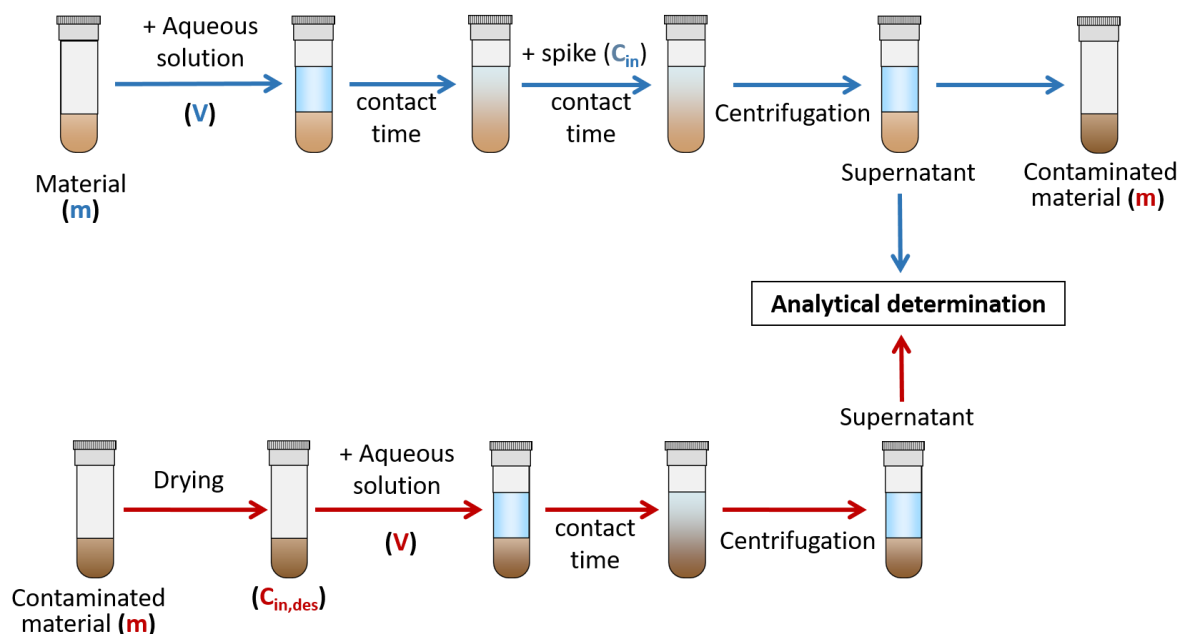


Figure 1.11 General set-up to run batch sorption and desorption experiments.

1.4.3. Sorption parameters and information derived from batch experiments

Sorption experiments performed in the laboratory allow to evaluate several sorption features that may affect the overall process (OECD, 2000). These include the optimization of contact/shaking time, which is related to sorption kinetics; the evaluation of the effect of the initial concentration of the analyte, which may recommend the construction of sorption isotherms; the effect of solution composition (*i.e.*, pH, ionic strength, DOC content), which may lead to the evaluation of the effect of these properties in the sorption; and the effect of temperature. Some of the abovementioned factors are discussed below.

1.4.3.1. Sorption kinetics

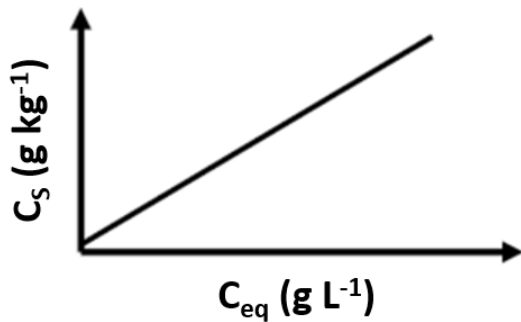
Sorption kinetics affect the optimum contact/shaking time at which sorption reach equilibrium conditions. Kinetic experiments can be performed by monitoring changes in the sorbed concentration in the solid phase and the related concentration in the liquid phase along

time. Several mathematical models can then be applied to fit experimental data to obtain mechanistic information. Some widely used models to fit kinetics data are the pseudo-first-order model (PFOM), the pseudo-second-order model (PSOM), and the Elovich and Boyd models, among others (Qiu et al., 2009). Sorption equilibrium time may vary for a single system if modifying experimental parameters such as temperature, shaking speed, pH, status of the aqueous solution and initial pollutant concentrations (Ho and McKay, 1998). Once the optimum contact time is established, sorption tests can be carried on under the assumption of equilibrium conditions.

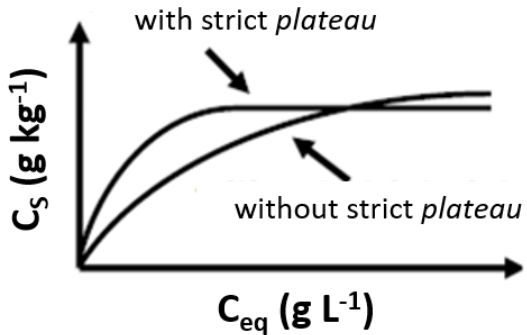
1.4.3.2. Sorption isotherms

The sorbent used in the sorption experiments has a certain number of sorption sites able to interact with the sorbate. The number of sites able to participate in the sorption process depends on the characteristics of the sorbent, as well as the nature of the sorbent-sorbate mechanistic interactions. Higher analyte concentrations than the amount of available sorption sites can lead to a sorption saturation of the sorbent. A useful approach to determine the amount and nature of the sorption sites is based on the construction of sorption isotherms, which are built up by evaluating the sorption at different analyte initial concentrations at a constant temperature and soil-to-solution ratio. Sorption isotherms are therefore defined as the observed pattern between the sorbed concentrations in the solid phase in respect to the remaining concentration in the aqueous phase for different analyte initial concentrations. Sorption isotherms may generally be displayed plotting C_S vs. C_{eq} for the different initial concentrations tested, although other plots are also possible (*e.g.*, K_d vs. C_{eq}). Regarding C_S vs. C_{eq} plots, four main types of patterns (C, L, H and S; see **Figure 1.12**, Limousin et al., 2007) can be found.

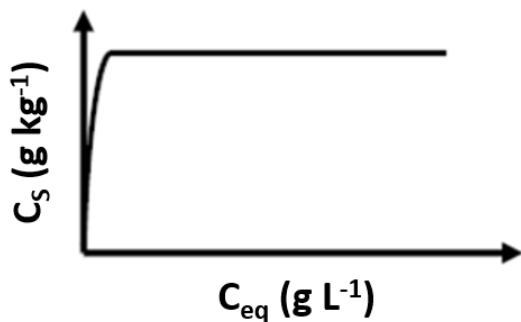
The “C” isotherm



The “L” isotherm



The “H” isotherm



The “S” isotherm

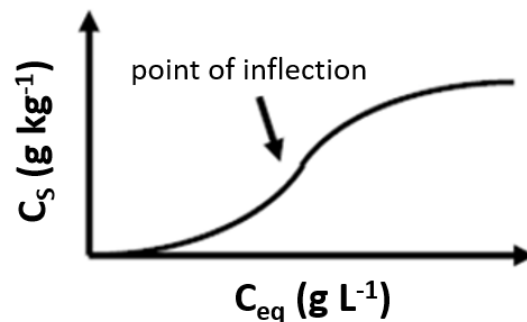


Figure 1.12 Common types of sorption isotherms, adapted from Limousin et al., (2007).

C-type isotherms are characterized by a linear trend with a null y-intercept. In these situations, it is assumed that the sorbent possesses a sufficient and accessible amount of sorption sites with equivalent affinity able to interact with the sorbate. This type of isotherm is often observed in those scenarios with both a high sorbent dosage (high solid-to-solution ratio) and low initial concentrations, leading to trace concentrations in the remaining solution. It ensures the derivation of K_d values from the slope of the isotherm. L-type isotherms are indicative that the sorbent has a limited amount of sorption sites. The sorbate firstly interact with high affinity sorption sites, and when higher initial concentrations of sorbate are tested, other sorption sites with less affinity participate in the sorption process. Due to this limitation, increasing initial concentrations beyond a certain threshold does not lead to a significant sorbate uptake in the solid phase, and the isotherm reaches a *plateau*. This *plateau* can be more or less evident

according to the nature of the sorption sites and the interaction mechanisms between sorbent and sorbate. Similarly, H-type isotherms are a particular case of L-type isotherms, in which a clear *plateau* is obtained and the initial slope of the isotherm is very high. S-shape isotherms are a result of at least two opposite mechanisms, and usually have at least one inflection point due to a phenomenon which is called “cooperative sorption”. Initially, it is observed a low sorption affinity, but as soon as the material surface is covered, sorption becomes more favoured (Limousin et al., 2007).

The data obtained from the experiments aiming at the construction of sorption isotherms can be fitted to different mathematical models, thus obtaining information about the nature of the sorption sites and sorption parameters related to the physicochemical processes taking place during sorption. C-type isotherms may be fitted to a Linear model with a null y-intercept (see Equation 1.1). Therefore, the slope of the isotherm can be considered a reliable K_d of the system. This model assumes that the sorbent has a sufficient number of equally-affinity sorption sites, thus obtaining a constant partition along different the initial concentrations tested. L-type isotherms can be fitted to different models depending on the resulting shape of the isotherm. For those isotherms without a strict *plateau*, usually the Freundlich equation describes better the experimental data. This model (Equation 1.4) considers a parameter ($K_F, (\text{mg kg}^{-1}) / (\text{mg L}^{-1})^N$) related to the affinity of the sorbate-sorbent interaction and a dimensionless parameter, N , related to the heterogeneity of sorption sites:

$$C_S = K_F (C_{eq})^N \quad (1.4)$$

For $N = 1$, the model assumes that the sorbent has a sufficient amount of equally-affine sorption sites able to bind the sorbate, and therefore, Equation 1.4 equals to Equation 1.1 and K_F equals to K_d . However, $N < 1$ values are indicative of sorption sites with different affinity for the sorbate, which is assumed to sorb at high-affinity sites during the first stage of the sorption process, while other low-affinity sorption sites take part in the sorption process when

higher initial concentrations are tested, without reaching a strict *plateau* due to material saturation (Limousin et al., 2007). Contrarily, L-type isotherms with a strict *plateau* are usually well fitted by the Langmuir model (Equation 1.5):

$$C_S = \frac{K_L C_{S,MAX} C_{eq}}{1 + (K_L C_{eq})} \quad (1.5)$$

This model assumes a limited number of sorption sites that are identical, energetically and sterically independent of the sorbed quantity and that retain one molecule per site. Thus, the sorbate interacts with the sorption sites until they gradually become occupied and an increase in the initial concentration does not lead to an increase in the sorbed concentration, thus provoking a *plateau* in the sorption isotherm. Langmuir fitted parameters are K_L ($L\ kg^{-1}$), related to the affinity of the sorbent-sorbate interaction, and $C_{S,MAX}$ ($kg\ kg^{-1}$), related to the number of sites of the sorbent. (Limousin et al., 2007).

Lastly, S-type isotherms can be fitted with the Freundlich fitting within the C_e range prior to reach the inflection point. In these cases, an $N > 1$ coefficient is obtained, suggesting a cooperative sorption. Once the inflection point is reached, increasing initial concentrations leads to a sorption site saturation, being the Sigmoidal or Sigmoidal-Langmuir model a suitable descriptor of the isotherm (Limousin et al., 2007).

PFASs sorption in soils have often been described by non-linear isotherms well fitted by the Freundlich model, although few cases of linear isotherms have also been described (Sima and Jaffé, 2021). Contrarily, sorption isotherms of PFASs in biochars and activated carbons are usually fitted by the Langmuir model, as deriving $C_{S,MAX}$ values for different sorbents is of interest for water remediation purposes (Gagliano et al., 2020). Similarly, FQs sorption in soils is also described by both linear and non-linear isotherms well fitted by the Linear and Freundlich models, respectively (Riaz et al., 2018), whereas L-type, H-type and in few occasions S-type sorption isotherms have also been observed in pure mineral phases such as kaolinite and montmorillonite (Li et al., 2011; Rivagli et al., 2014).

1.4.4. Sources of K_d variability

According to previous discussions, K_d values are affected by various sources of variability. **Figure 1.13** summarizes some of these, including the applied methodology and the physicochemical properties of the solid phase and the aqueous solution, in addition to target compound properties and speciation and time elapsed since contamination.

The characteristics of the solid and liquid phases of natural environmental matrices may extraordinarily differ among sites to be assessed. Therefore, modellers assessing risk have to either use site-specific data or, better, to know the multivariate dependence of the K_d with relevant solid and liquid properties (some of them not always available in routine characterization analyses) and thus to predict K_d values based on those correlations. However, the lack of a fully characterization of the environmental matrices and/or the absence of knowledge of such correlations often only permits to use a best-estimate K_d value representative for a group of soils according to the values of a general property.

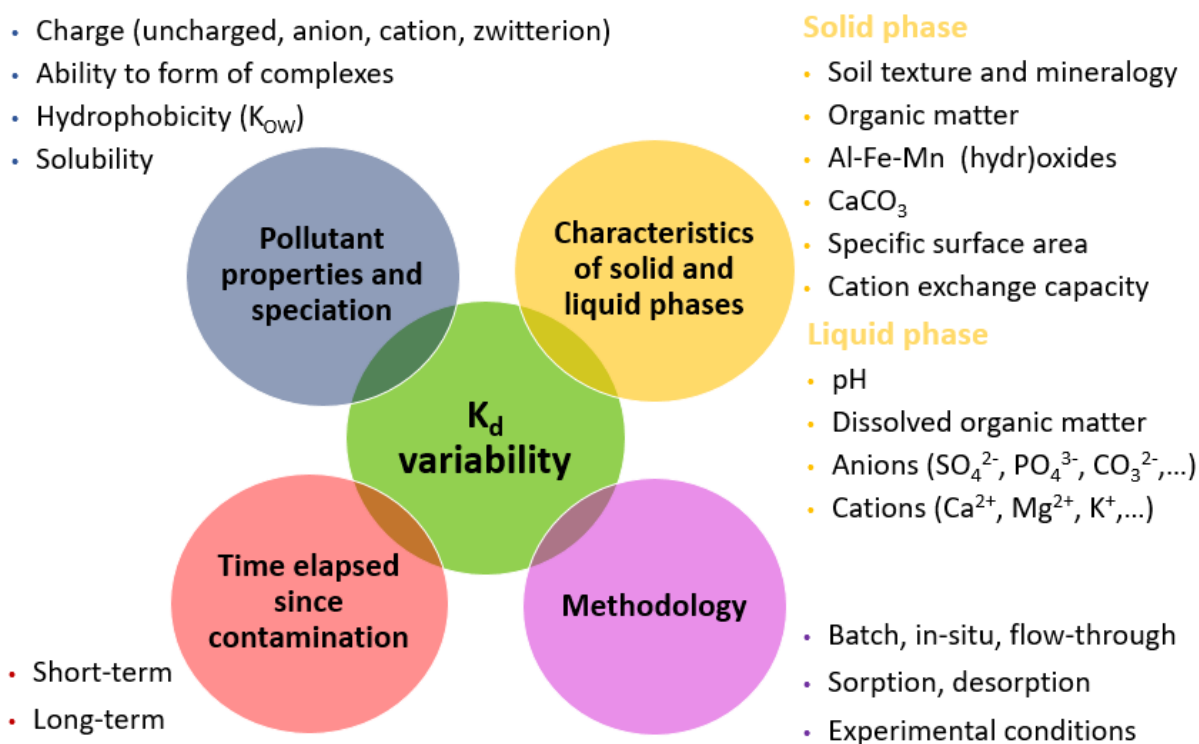


Figure 1.13 Sources of K_d variability.

As stated, K_d is affected by multiple sources of variability. In addition to the variability caused by the differences in the physicochemical properties of the respective solid and aqueous phases (*i.e.*, soil texture and OC content; solution pH and DOC), these include the methodology used to derive these K_d values (*e.g.*, K_d data derived from batch, flow through or in-situ methods, may vary among applied methodology), the physicochemical properties of the target compound (*i.e.*, prediction models based on pK_a and K_{OW} values) and the interaction dynamics due to the time elapsed since contamination (*i.e.*, short or long term after the contamination event).

Due to the above described main sources affecting K_d variability, ancillary information accompanying the K_d values reported in the literature plays a major role. When considering to use data from the literature, acceptance criteria is crucial for constructing datasets. Besides the sorption parameters (basically K_d itself), these datasets have to include the main physicochemical properties of the sorbent and sorbate, in addition to the methodology and experimental conditions used to obtain such information. Acceptance criteria may be applied to materials (*i.e.*, decision about including analogous geological materials to soils and sediments, such as pure organic and inorganic soil phases), methodology (*i.e.*, decision about including only sorption data derived from batch experiments; acceptance of characterization data based only on specific, official characterization methods) or other expert-judgment based criteria.

1.5. Carbon-rich materials as sorbent candidates for the remediation of polluted soil and water bodies

When environmental risk assessment studies point at a potential threat to organisms due to harmful effects of a given compound, specific remediation actions should be taken. A common strategy to reduce the associated risk is the use of organic and/or inorganic materials as sorbents to immobilize the pollutant. Ideally, a good remediation sorbent material should have the following features: (i) to have a high sorbent affinity (high K_d), fast sorption kinetics, high sorption capacity and high sorption irreversibility towards the target pollutant; (ii) to be stable along time and changes in environmental conditions; (iii) to require low dosages to be applied; (iv) to be geographically available, sustainable and economic.

Several organic and inorganic materials, among them carbon-rich materials, have been tested to immobilize both PFASs and FQs from polluted waters (Genç and Dogan, 2014; Inyang and Dickenson, 2015) and they have been shown effective to remediate them in contaminated soils in comparison to other materials such as bentonites, hydrotalcites and zeolites (Sleep and Juhasz, 2021). Therefore, some of these carbon-rich materials and their potentiality as PFASs and FQs sorbents are described below.

1.5.1. Activated carbons

Activated carbons are produced from carbonaceous materials, such as bamboo, coconut husk, lignite, coal or petroleum pitch, through pyrolysis at temperatures up to 2,000 °C. Activated carbons have a black appearance, a high carbon content and a developed porous structure, which give them prominent sorption properties towards organic pollutants due to their large surface area.

Activated carbons can be produced either by physical or chemical activation processes. In the physical activation, the material is pyrolyzed at temperatures within the range of 600 – 1,200 °C in an inert atmosphere with gases such as N₂, followed by its exposure to oxidising agents. On the other hand, in the chemical activation the material is impregnated with an acid, strong base or a salt (*e.g.*, 25% H₃PO₄, 5% NaOH or 25% ZnCl₂) and subjected to high temperatures (250 – 600 °C). In both processes, the carbonaceous structure is forced to open up, thus increasing its surface area due to increasing developed porous structure.

Activated carbons are therefore complex products that can be classified on the basis of their behaviour, surface characteristics, preparation methods and industrial application. Two of the most used types of activated carbons are powdered activated carbon (PAC), which are based on fine granules made up of crushed carbon particles that pass through a given mesh sieve, and granulated activated carbon (GAC), that have larger particle size compared to PAC.

Activated carbons are often used in several types of WWTPs and have been successfully used to remove both PFASs and FQs from aqueous solutions in a laboratory scale, revealing fast sorption kinetics ($> 87 \cdot 10^3 \text{ mg kg}^{-1} \text{ h}^{-1}$) and high sorption capacities ($> 100 \text{ mg g}^{-1}$) (Yu et al., 2009; Ahmed and Theydan, 2014).

1.5.2. Biochars

Biomass waste may be transformed to other materials with higher environmental interest through several thermal processes, thus deriving a number of added-value residues such as biochar (solid residue), bio-oil (liquid residue) and biogas (gas residue). The thermal process applied vary depending on the desired by-product proportions. Among these, torrefaction processes lead to the highest biochar rates, although pyrolysis treatments are often preferred since higher carbon contents are achieved. Two main pyrolysis processes are used for the obtention of biochar: the “slow pyrolysis”, which achieves temperatures up to 400°C during

residences times ranging from minutes to days, and the “fast pyrolysis”, which achieves higher temperatures up to 800°C during faster residence times, usually within the time interval of seconds or minutes. Slow pyrolysis processes usually achieve higher biochar yields with higher carbon contents (Meyer et al., 2011). The decomposition of hemicellulose, cellulose and lignin occurs at 250 – 350°C, being lignin the most thermally stable component. Therefore, in addition to the release of water and other volatile compounds, at this temperature range a decrease in the original feedstock mass is expected, and the result is an amorphous material where a mixture of polyaromatic and altered biopolymers coexist (Barskov et al., 2019). This graphene-like aromatic structures, which also contain functional groups such as carboxylic acids, carbonyls, lactones and phenols, aggregate with each other forming crystalline composites, which are aleatory distributed in the final material. Their final relative percentages of %C, %N and %O as well as other properties such as specific surface area and porous distribution are highly dependent on both feedstock properties and pyrolysis conditions (Hassan et al., 2020). Some biomass waste materials often transformed to biochars are wood and pine chips, rice husk or straw, hardwood litter, and bamboo, sugarcane, eucalyptus and pericarp coconut wastes, although biochars derived from sewage sludge and animal manure have been also described (Ahmad et al., 2014).

Biochar may be applied to soils either as conditioner or amendment, in order to improve selected soil physicochemical properties. Some environmental advantages of the addition of biochars in soils are the decrease of nutrient runoff, the increase in soil organic carbon and the improvement of soil fertility and ease of tillage practices. In addition to this, biochar production is considered a carbon negative process: the carbonization of the biomass to a stable carbon form reduces CO₂ emissions, with the benefit of obtaining energy through the process.

Biochar can achieve similar values of relevant physicochemical properties, such as carbon content, surface area and porous volumes, to those reported for activated carbons, thus

having the possibility to achieve comparable sorption yields for both organic and inorganic pollutants (Ahmad et al., 2014). Therefore, they have been suggested as alternative, cheaper substitutes for activated carbons in WWTPs (Inyang and Dickenson, 2015). Their ability to immobilize both PFAS and FQs has been demonstrated in laboratory (Yi et al., 2016; Guo et al., 2017), but their sorption potential and affinity is highly dependent on biochar properties, and the main interaction mechanisms among them are not totally understood at date. Also, they have also been applied to polluted soils to immobilize both organic and inorganic pollutants, and in the context of soil remediation biochar are prominent sorbents candidates in the design of remediation actions due to their sustainable and economic advantages (Ahmad et al., 2014; Inyang and Dickenson, 2015; Tan et al., 2015).

1.5.3. Compost

Organic wastes can be revalorized after composting processes. These are based on a biological degradation of the organic matter and occur under aerobic conditions, being compost (solid residue) and biogas the main resulting by-products of the composting process. Some of the environmental benefits of using compost is the enhancement of soil quality, as compost contributes to retain moisture and suppress plant diseases and pests, to reduce the need of fertilizers and to enhance the production of beneficial bacteria and fungi that degrade soil organic matter to create humus. The composting process at industrial scale is usually performed in aerated static piles, since it does not need intensive physical manipulation.

Alike biochars, compost may also be considered as a soil remediation candidate material. A compost sample obtained from municipal organic waste revealed a prominent ability for remediating metal-contaminated soils after observing its strong sorption properties (Venegas et al., 2015). Although limited data regarding sorption of organic pollutants in compost samples exist at date, some explorations of composted materials derived from wood

fibres and barks revealed a relatively low sorption affinity for PFASs (Söregård et al., 2020). Therefore, the generation of new sorption data regarding PFASs sorption in extensively characterized compost samples is of interest to assess its potential remediation ability for PFASs-polluted soils.

1.5.4. Charcoal fines

Charcoal fines, or non-magnetic fines, are one of the main by-products of the metallurgical industry, for which they are unsuitable for reuse because their small particle size (< 9.2 mm) causes clogging of gas passages, hence decreasing the efficiency of blast furnaces (Angelo et al., 2014). Due to their large waste generation and scarce applicability, they usually end up in landfills, and therefore, their applicability for remediation is of interest to support circular economy. Although literature data examining charcoal fines sorption affinity to organic pollutants are scarce, their application to low organic carbon soil at low amendment doses revealed a considerable decrease in PFASs leaching, albeit no significant immobilization was noticed in high organic carbon soils with much higher doses (Zhang et al., 2022). Therefore, the generation of new PFASs sorption data in these materials may help to better assess their potential remediation effectiveness.

1.6. Prediction K_d models and current limitations for PFASs and FQs

Prediction K_d models should determine the objectives and the type of the model to be built up and applied, in addition to set its relevant boundary conditions and domain of applicability. Besides, peer-reviewed data criteria acceptance to build up model calibration and validation datasets have to be clearly defined (USEPA, 2009).

Environmental models may be classified according to different criteria, depending on the processes the model attempt to reproduce, the time and spatial scale of the processes and the mathematical nature of the model. Probabilistic models, sometimes also referred to as statistical or stochastic models, are often used in the description and prediction of environmental variables (USEPA, 2009). They use the entire range of available data to develop a probability distribution of the variable to be modelled (here, K_d) rather than to derive a single value result. They can be used to evaluate and describe the variability of datasets and to derive best-estimate values of the target variable, according to selected physicochemical properties. In this context, cumulative distribution functions (CDFs) have been used to decrease and describe data variability and derive best-estimate K_d values, associated with the central value of the distribution (50th percentile), for inorganic pollutants and radionuclides by classifying soils according to relevant properties affecting the sorption process, such as texture, pH and/or OC contents (Ramirez-Guinart et al., 2020a; 2020b; 2020c). According to our knowledge no probabilistic K_d models are available for PFASs or FQs in the current literature.

On the other hand, deterministic models provide a numeric solution rather than a set of probabilistic outcomes, and therefore, do not necessarily simulate the effects of data uncertainty and variability (USEPA, 2009). Thus, changes in model outputs are solely due to changes in model components, boundary conditions or initial conditions, and repeated simulations under constant conditions will result in consistent results. Among these models, empirical models include very little information on the underlying mechanisms and rely upon the observed

relationships among experimental data and material properties. Therefore, they are extremely sensitive to the ranges of values of the variables used for their construction. Their parameters may or may not have real-world interpretation and often suffer from lack of extrapolation. Different mathematical tools may be used for fitting purposes, such as single or multiple linear, polynomial, potential, or exponential correlations.

An example of this in the context of this doctoral thesis is the prediction of the sorption of PFOA by running a multiple linear regression between a set of 100 K_d values derived from soils and their physicochemical properties (Knight et al., 2021). The resulting model included only significant correlations with OC, clay and pH. However, due to the range of variation of the soil properties of the data used for the model calibration, its applicability was only limited to soils with OC < 3.5%. Similarly, an empirical K_d prediction model was proposed to predict the sorption of NOR (Gong et al., 2012). The model was developed by a partial least squares (PLS) regression after deriving K_d values in 23 soils of different physicochemical properties. The final model variables included pH, clay, Fe, OM and calcium contents. However, the model failed to predict data representative for scenarios different to those used in the calibration step, and it could not be extrapolated to cases in which higher sorption was noticed (Leal et al., 2013).

On the other hand, mechanistic models, another subtype of empirical models, aim at providing description about the sorption mechanisms, being the model parameters related to relevant mechanisms, and these models usually permit extrapolation. In the case of K_d prediction models, these could use specific sorbent and sorbate properties that describe certain interaction mechanisms (*e.g.*, soil properties such as OC responsible for hydrophobic interactions and pollutant hydrophobicity, expressed as K_{ow}). An example of a mechanistic model in the frame of this doctoral thesis is the prediction of the sorption of anionic surfactants, including PFAS, in soil organic matter (Higgins and Luthy, 2007). Such model included both hydrophobic and electrostatic components and estimates the contribution of each in K_d using

Gibbs free energy terms. The inclusion of non-easily measurable input parameters (*e.g.*, density and electrostatic potential of the organic matter and its fraction accessible to the sorbate) and their mathematical complexity makes it difficult to apply such model for early risk assessment studies. Regarding K_d (FQ) prediction models, a charge distribution-multisite complexation model was developed to model the surface complexation of zwitterion OFL in goethite by separately accounting for interactions of charged surface with the positively and negatively charged functional groups (Paul et al., 2014). The model incorporated a basic Stern layer approach, goethite surface mineralogy characteristics, surface acid-base reactions, binding of electrolyte ions to the goethite surface, aqueous acid-base equilibrium reactions for OFL and surface complexation reactions involving different OFL species.

As stated, current available K_d prediction models in environmental matrices for PFASs and FQs in the literature are scarce and have limitations. In addition, prediction models in pure soil components, which may help to assess their overall fate in bulk soils, are also scarce. Besides, the applicability of some models developed for soils has not been assessed to a wider range of scenarios and they have not been yet externally validated. Furthermore, the use of soil properties in the model which are not totally descriptive of sorption may difficult the model applicability.

According to all the previous discussions, the understanding of the chemical interactions between PFASs and FQs with different environmental matrices such as bulk soils, pure soil organic and inorganic soil components and carbon-rich materials, in addition to the construction of K_d prediction models based on key sorbent and sorbate physicochemical properties governing sorption, are important stages previous to environmental risk assessment analyses. However, the K_d prediction models for PFASs and FQs in environmental matrices available at date are scarce and have limitations, and therefore, the development of new models is required, an overall objective that will be explored in this thesis.

1.7. References

- Ahmad, M., Upamali, A., Eun, J., Zhang, M., Bolan, N., Mohan, D., Vithanage, M., Soo, S., Sik, Y., 2014. Biochar as a sorbent for contaminant management in soil and water: A review. *Chemosphere*, 99, 19–33. <https://doi.org/10.1016/j.chemosphere.2013.10.071>
- Ahmed, M. J., Theydan, S. K., 2014. Fluoroquinolones antibiotics adsorption onto microporous activated carbon from lignocellulosic biomass by microwave pyrolysis. *J. Taiwan Inst. Chem. Eng.* 45 (1), 219–226. <https://doi.org/10.1016/j.jtice.2013.05.014>
- Ahmed, A. A., Thiele-Bruhn, S., Aziz, S. G., Hilal, R. H., Elroby, S. A., Al-Youbi, A. O., Leinweber, P., Kühn, O., 2015. Interaction of polar and nonpolar organic pollutants with soil organic matter: Sorption experiments and molecular dynamics simulation. *Sci. Total Environ.* 508, 276–287. <https://doi.org/10.1016/j.scitotenv.2014.11.087>
- Ahrens, L., Bundschuh, M., 2014. Fate and effects of poly- and perfluoroalkyl substances in the aquatic environment: A review. *Environ. Toxicol. Chem.* 33 (9), 1921–1929. <https://doi.org/10.1002/etc.2663>
- Anderson, R. H., Long, G. C., Porter, R. C., Anderson, J. K., 2016. Occurrence of select perfluoroalkyl substances at U.S. Air Force aqueous film-forming foam release sites other than fire-training areas: Field-validation of critical fate and transport properties. *Chemosphere*, 150, 678–685. <https://doi.org/10.1016/j.chemosphere.2016.01.014>
- Andersson, M. I., MacGowan, A. P., 2003. Development of the quinolones. *J. Antimicrob. Chemoth.* 51 (90001), 1–11. <https://doi.org/10.1093/jac/dkg212>
- Angelo, L. C., Mangrich, A. S., Mantovani, K. M., Santos, S., 2014. Loading of VO²⁺ and Cu²⁺ to partially oxidized charcoal fines rejected from Brazilian metallurgical industry. *J. Soils Sed.* 14, 353–359. <https://doi.org/10.1007/s11368-013-0764-5>

- Aristilde, L., Sposito, G., 2013. Complexes of the antimicrobial ciprofloxacin with soil, peat, and aquatic humic substances. *Environ. Toxicol. Chem.* 32 (7), 1467–1478. <https://doi.org/10.1002/etc.2214>
- Arsand, J. B., Hoff, R. B., Jank, L., Bussamara, R., Dallegrave, A., Bento, F. M., Kmetzsch, L., Falção, D. A., do Carmo Ruaro Peralba, M., de Araujo Gomes, A., Pizzolato, T. M., 2020. Presence of antibiotic resistance genes and its association with antibiotic occurrence in Dilúvio River in southern Brazil. *Sci. Total Environ.* 738, 139781. <https://doi.org/10.1016/j.scitotenv.2020.139781>
- Arun, S., Kumar, R. M., Ruppa, J., Mukhopadhyay, M., Ilango, K., Chakraborty, P., 2020. Occurrence, sources and risk assessment of fluoroquinolones in dumpsite soil and sewage sludge from Chennai, India. *Environ. Toxicol. Phar.* 79, 103410. <https://doi.org/10.1016/j.etap.2020.103410>
- Atkins, P., de Paula, J., 2006. *Physical Chemistry*. 8th Ed. Oxford, UK: Oxford University Press. ISBN: 0-7167-8759-8.
- ATSDR, 2021. Toxicological Profile for Perfluoroalkyls. U.S. Department of Health and Human Services; Agency for Toxic Substances and Disease Registry. ATSDR, 205, 24. <http://dx.doi.org/10.1155/2013/286524>
- Barskov, S., Zappi, M., Buchireddy, P., Dufreche, S., Guillory, J., Gang, D., Hernandez, R., Bajpai, R., Baudier, J., Cooper, R., Sharp, R., 2019. Torrefaction of biomass: A review of production methods for biocoal from cultured and waste lignocellulosic feedstocks. *Renew. Energ.* 142, 624–642. <https://doi.org/10.1016/j.renene.2019.04.068>
- Blondeau, J. M., 2004. Fluoroquinolones: Mechanism of action, classification, and development of resistance. *Surv. Ophthalmol.*, 49, 1–6. <https://doi.org/10.1016/j.survophthal.2004.01.005>

-
- Boiteux, V., Bach, C., Sagres, V., Hemard, J., Colin, A., Rosin, C., Munoz, J. F., Dauchy, X., 2016. Analysis of 29 per- and polyfluorinated compounds in water, sediment, soil and sludge by liquid chromatography–tandem mass spectrometry. *Int. J. Environ. An. Ch.* 96 (8), 705–728. <https://doi.org/10.1080/03067319.2016.1196683>
- Bonefeld-Jørgensen, E. C., Ghisari, M., Wielsøe, M., Bjerregaard-Olesen, C., Kjeldsen, L. S., Long, M., 2014. Biomonitoring and hormone-disrupting effect biomarkers of persistent organic pollutants in vitro and ex vivo. *Basic Clin. Pharmacol.* 115 (1), 118–128. <https://doi.org/10.1111/bcpt.12263>
- Brusseau, M. L., Khan, N., Wang, Y., Yan, N., Van Glubt, S., Carroll, K. C., 2019. Nonideal Transport and Extended Elution Tailing of PFOS in Soil. *Environ. Sci. Technol.* 53 (18), 10654–10664. <https://doi.org/10.1021/acs.est.9b02343>
- Brusseau, M. L., Anderson, R. H., Guo, B., 2020. PFAS concentrations in soils: Background levels versus contaminated sites. *Sci. Total Environ.* 740, 140017. <https://doi.org/10.1016/j.scitotenv.2020.140017>
- Buck, R. C., Franklin, J., Berger, U., Conder, J. M., Cousins, I. T., Voogt, P. De, Jensen, A. A., Kannan, K., Mabury, S. A., van Leeuwen, S. P. J., 2011. Perfluoroalkyl and polyfluoroalkyl substances in the environment: Terminology, classification, and origins. *Integr. Environ. Assess.* 7 (4), 513–541. <https://doi.org/10.1002/ieam.258>
- Burch, K. D., Han, B., Pichtel, J., Zubkov, T., 2019. Removal efficiency of commonly prescribed antibiotics via tertiary wastewater treatment. *Environ. Sci. Pollut. R.* 26 (7), 6301–6310. <https://doi.org/10.1007/s11356-019-04170-w>
- Campo, J., Pérez, F., Masiá, A., Picó, Y., Farré, M., Barceló, D., 2015. Perfluoroalkyl substance contamination of the Llobregat River ecosystem (Mediterranean area, NE Spain). *Sci. Total Environ.* 503–504, 48–57. <https://doi.org/10.1016/j.scitotenv.2014.05.094>

- Cao, Yuanxin, Cao, X., Wang, H., Wan, Y., Wang, S., 2015a. Assessment on the distribution and partitioning of perfluorinated compounds in the water and sediment of Nansi Lake, China. *Environ. Monit. Assess.* 187:611. <https://doi.org/10.1007/s10661-015-4831-9>
- Cao, X., Pang, H., Yang, G., 2015b. Sorption behaviour of norfloxacin on marine sediments. *J. Soil Sediment.* 15, 1635–1643. <https://doi.org/10.1007/s11368-015-1124-4>
- Cao, Y., Ng, C., 2021. Absorption, distribution, and toxicity of per- and polyfluoroalkyl substances (PFAS) in the brain: A review. *Environ. Sci-Proc. Imp.* 23 (11), 1623–1640. <https://doi.org/10.1039/d1em00228g>
- Cárdenas-Youngs, G. M., Beltrán, J. L., 2015. Dissociation Constants and Octanol-Water Partition Equilibria for Several Fluoroquinolones. *J. Chem. Eng. Data*, 60 (11), 3327–3332. <https://doi.org/10.1021/acs.jced.5b00556>
- Carnero, A. R., Lestido-Cardama, A., Loureiro, P. V., Barbosa-Pereira, L., de Quirós, A. R. B., Sendón, R., 2021. Presence of perfluoroalkyl and polyfluoroalkyl substances (PFAS) in food contact materials (FCM) and its migration to food. *Foods*, 10 (7). <https://doi.org/10.3390/foods10071443>
- Chang, E. T., Adami, H. O., Boffetta, P., Cole, P., Starr, T. B., Mandel, J. S., 2014. A critical review of perfluorooctanoate and perfluorooctanesulfonate exposure and cancer risk in humans. *Crit. Rev. Toxicol.* 44, 1–81. <https://doi.org/10.3109/10408444.2014.905767>
- Chen, H., Liu, S., Xu, X. R., Zhou, G. J., Liu, S. S., Yue, W. Z., Sun, K. F., Ying, G. G., 2015. Antibiotics in the coastal environment of the Hailing Bay region, South China Sea: Spatial distribution, source analysis and ecological risks. *Mar. Pollut. Bull.* 95 (1), 365–373. <https://doi.org/10.1016/j.marpolbul.2015.04.025>
- Cheng, D., Xie, Y., Yu, Y., Liu, X., Zhao, S., Cui, B., Bai, J., 2016. Occurrence and Partitioning of Antibiotics in the Water Column and Bottom Sediments from the Intertidal Zone in the Bohai Bay, China. *Wetlands*, 36, 167–179. <https://doi.org/10.1007/s13157-014-0561-y>

- Chung, H. S., Lee, Y. J., Rahman, M. M., Abd El-Aty, A. M., Lee, H. S., Kabir, M. H., Kim, S. W., Park, B. J., Kim, J. E., Hacımüftüoğlu, F., Nahar, N., Shin, H. C., Shim, J. H., 2017. Uptake of the veterinary antibiotics chlortetracycline, enrofloxacin, and sulphathiazole from soil by radish. *Sci. Total Environ.* 605–606, 322–331. <https://doi.org/10.1016/j.scitotenv.2017.06.231>
- Cluett, R., Seshasayee, S. M., Rokoff, L. B., Rifas-Shiman, S. L., Ye, X., Calafat, A. M., Gold, D. R., Coull, B., Gordon, C. M., Rosen, C. J., Oken, E., Sagiv, S. K., Fleisch, A. F., 2019. Per- and Polyfluoroalkyl Substance Plasma Concentrations and Bone Mineral Density in Midchildhood: A Cross-Sectional Study (Project Viva, United States). *Environ. Health Persp.* 127 (8), 1–7. <https://doi.org/10.1289/EHP4918>
- Colomer-Vidal, P., Jiang, L., Mei, W., Luo, C., Lacorte, S., Rigol, A., Zhang, G., 2022. Plant uptake of perfluoroalkyl substances in freshwater environments (Dongzhulong and Xiaoqing Rivers, China). *J. Hazard. Mater.* 421, 126768. <https://doi.org/10.1016/j.jhazmat.2021.126768>
- Conkle, J. L., Lattao, C., White, J. R., Cook, R. L., 2010. Competitive sorption and desorption behavior for three fluoroquinolone antibiotics in a wastewater treatment wetland soil. *Chemosphere*, 80 (11), 1353–1359. <https://doi.org/10.1016/j.chemosphere.2010.06.012>
- Cui, H., Wang, S. P., Fu, J., Zhou, Z. Q., Zhang, N., Guo, L., 2014. Influence of ciprofloxacin on microbial community structure and function in soils. *Biol. Fert. Soils*, 50 (6), 939–947. <https://doi.org/10.1007/s00374-014-0914-y>
- Dalahmeh, S., Tirgani, S., Komakech, A. J., Niwagaba, C. B., Ahrens, L., 2018. Per- and polyfluoroalkyl substances (PFASs) in water, soil and plants in wetlands and agricultural areas in Kampala, Uganda. *Sci. Total Environ.* 631–632, 660–667. <https://doi.org/10.1016/j.scitotenv.2018.03.024>

- Dalkmann, P., Broszat, M., Siebe, C., Willaschek, E., Sakinc, T., Huebner, J., Amelung, W., Grohmann, E., Siemens, J., 2012. Accumulation of pharmaceuticals, enterococcus, and resistance genes in soils irrigated with wastewater for zero to 100 years in central Mexico. *PLoS ONE*, 7 (9). <https://doi.org/10.1371/journal.pone.0045397>
- De Witte, B., Dewulf, J., Demeestere, K., De Ruyck, M., Van Langenhove, H., 2007. Critical points in the analysis of ciprofloxacin by high-performance liquid chromatography. *J. Chromatogr. A*, 1140 (1–2), 126–130. <https://doi.org/10.1016/j.chroma.2006.11.076>
- Deng, S., Zhang, Q., Nie, Y., Wei, H., Wang, B., Huang, J., Yu, G., Xing, B., 2012. Sorption mechanisms of perfluorinated compounds on carbon nanotubes. *Environ. Pollut.* 168, 138–144. <https://doi.org/10.1016/j.envpol.2012.03.048>
- Drillia, P., Stamatelatou, K., Lyberatos, G., 2005. Fate and mobility of pharmaceuticals in solid matrices. *Chemosphere*, 60 (8), 1034–1044. <https://doi.org/10.1016/j.chemosphere.2005.01.032>
- Du, Z., Deng, S., Bei, Y., Huang, Q., Wang, B. 2014. Adsorption behavior and mechanism of perfluorinated compounds on various adsorbents — A review. *J. Hazard. Mater.* 274, 443–454. <https://doi.org/10.1016/j.jhazmat.2014.04.038>
- Du, Z., Deng, S., Chen, Y., Wang, B., Huang, J., Wang, Y., Yu, G., 2015. Removal of perfluorinated carboxylates from washing wastewater of perfluorooctanesulfonyl fluoride using activated carbons and resins. *J. Hazard. Mater.* 266, 136–143. <https://doi.org/10.1016/j.jhazmat.2014.12.037>
- European Commission, 2020. Poly- and perfluoroalkyl substances (PFAS): Chemicals Strategy for Sustainability Towards a Toxic-Free Environment. Commission Staff Working Document, 1–22. <https://op.europa.eu/en/publication-detail/-/publication/2614f1f2-0f02-11eb-bc07-01aa75ed71a1/language-en>. Accessed 10 June 2022.

-
- Gagliano, E., Sgroi, M., Falciglia, P. P., Vagliasindi, F. G. A., Roccaro, P., 2020. Removal of poly- and perfluoroalkyl substances (PFAS) from water by adsorption: Role of PFAS chain length, effect of organic matter and challenges in adsorbent regeneration. *Water Res.* 171, 115381. <https://doi.org/10.1016/j.watres.2019.115381>
- Gellrich, V., Stahl, T., Knepper, T. P., 2012. Behavior of perfluorinated compounds in soils during leaching experiments. *Chemosphere*, 87 (9), 1052–1056. <https://doi.org/10.1016/j.chemosphere.2012.02.011>
- Genç, N., Dogan, E. C., 2013. Adsorption kinetics of the antibiotic ciprofloxacin on bentonite, activated carbon, zeolite and pumice. *Desal. Water Treat.* <https://doi.org/10.1080/19443994.2013.84504>
- Giesy, J. P., Kannan, K., 2001. Global distribution of perfluorooctane sulfonate in wildlife. *Environ. Sci. Technol.* 35 (7), 1339–1342. <https://doi.org/10.1021/es001834k>
- Girardi, C., Greve, J., Lamshöft, M., Fetzer, I., Miltner, A., Schäffer, A., Kästner, M., 2011. Biodegradation of ciprofloxacin in water and soil and its effects on the microbial communities. *J. Hazard. Mater.* 198, 22–30. <https://doi.org/10.1016/j.jhazmat.2011.10.004>
- Golet, E. M., Xifra, I., Siegrist, H., Alder, A. C., Giger, W., 2003. Environmental exposure assessment of fluoroquinolone antibacterial agents from sewage to soil. *Environ. Sci. Technol.* 37 (15), 3243–3249. <https://doi.org/10.1021/es0264448>
- Gómez-Canela, C., Barth, J. A. C., Lacorte, S., 2012. Occurrence and fate of perfluorinated compounds in sewage sludge from Spain and Germany. *Environ. Sci. Pollut. R.* 19 (9), 4109–4119. <https://doi.org/10.1007/s11356-012-1078-7>
- Gong, W., Liu, X., He, H., Wang, L., Dai, G., 2012. Quantitatively modeling soil-water distribution coefficients of three antibiotics using soil physicochemical properties. *Chemosphere*, 89 (7), 825–831. <https://doi.org/10.1016/j.chemosphere.2012.04.064>

- Goosey, E., Harrad, S., 2012. Perfluoroalkyl substances in UK indoor and outdoor air: Spatial and seasonal variation, and implications for human exposure. *Environ. Int.* 45 (1), 86–90. <https://doi.org/10.1016/j.envint.2012.04.007>
- Graouer-Bacart, M., Sayen, S., Guillon, E., 2015. Adsorption of enrofloxacin in presence of Zn (II) on a calcareous soil. *Ecotox. Environ. Safe.* 122, 470–476. <https://doi.org/10.1016/j.ecoenv.2015.09.019>
- Grønnestad, R., Vázquez, B. P., Arukwe, A., Jaspers, V. L. B., Jenssen, B. M., Karimi, M., Lyche, J. L., Krøkje, Å., 2019. Levels, Patterns, and Biomagnification Potential of Perfluoroalkyl Substances in a Terrestrial Food Chain in a Nordic Skiing Area. *Environ. Sci. Technol.* 53 (22), 13390–13397. <https://doi.org/10.1021/acs.est.9b02533>
- Guo, W., Huo, S., Feng, J., Lu, X., 2017. Adsorption of perfluorooctane sulfonate (PFOS) on corn straw-derived biochar prepared at different pyrolytic temperatures. *J. Taiwan Inst. Chem. Eng.* 78, 265–271. <https://doi.org/10.1016/j.jtice.2017.06.013>
- Habibullah-Al-Mamun, M., Ahmed, M. K., Raknuzzaman, M., Islam, M. S., Negishi, J., Nakamichi, S., Sekine, M., Tokumura, M., Masunaga, S., 2016. Occurrence and distribution of perfluoroalkyl acids (PFAAs) in surface water and sediment of a tropical coastal area (Bay of Bengal coast, Bangladesh). *Sci. Total Environ.* 571, 1089–1104. <https://doi.org/10.1016/j.scitotenv.2016.07.104>
- Hale, S. E., Arp, H. P. H., Slinde, G. A., Wade, E. J., Bjørseth, K., Breedveld, G. D., Straith, B. F., Moe, K. G., Jartun, M., Høisæter, Å., 2017. Sorbent amendment as a remediation strategy to reduce PFAS mobility and leaching in a contaminated sandy soil from a Norwegian firefighting training facility. *Chemosphere*, 171, 9–18. <https://doi.org/10.1016/j.chemosphere.2016.12.057>

-
- Hassan, M., Liu, Y., Naidu, R., Parikh, S. J., Du, J., Qi, F., Willett, I. R., 2020. Influences of feedstock sources and pyrolysis temperature on the properties of biochar and functionality as adsorbents: A meta-analysis. *Sci. Total Environ.* 744, 140714. <https://doi.org/10.1016/j.scitotenv.2020.140714>
- Haukås, M., Berger, U., Hop, H., Gulliksen, B., Gabrielsen, G. W., 2007. Bioaccumulation of per- and polyfluorinated alkyl substances (PFAS) in selected species from the Barents Sea food web. *Environ. Pollut.* 148 (1), 360–371. <https://doi.org/10.1016/j.envpol.2006.09.021>
- Hawker, D. W., Cropp, R., Boonsaner, M., 2013. Uptake of zwitterionic antibiotics by rice (*Oryza sativa* L.) in contaminated soil. *J. Hazard. Mater.* 263, 458–466. <https://doi.org/10.1016/j.jhazmat.2013.09.066>
- Herzke, D., Huber, S., Bervoets, L., D'Hollander, W., Hajslova, J., Pulkrabova, J., Brambilla, G., De Filippis, S. P., Klenow, S., Heinemeyer, G., de Voogt, P., 2013. Perfluorinated alkylated substances in vegetables collected in four European countries; occurrence and human exposure estimations. *Environ. Sci. Pollut. R.* 20 (11), 7930–7939. <https://doi.org/10.1007/s11356-013-1777-8>
- Higgins, C. P., Field, J. A., Criddle, C. S., Luthy, R. G., 2005. Quantitative determination of perfluorochemicals in sediments and domestic sludge. *Environ. Sci. Technol.* 39 (11), 3946–3956. <https://doi.org/10.1021/es048245p>
- Higgins, C. P., Luthy, R. G., 2006. Sorption of Perfluorinated Surfactants on Sediments. *Environ. Sci. Technol.* 40, 7251–7256. <https://doi.org/10.1021/es061000n>
- Higgins, C. P., Luthy, R. G., 2007. Modeling Sorption of Anionic Surfactants onto Sediment Materials: An a priori Approach for Perfluoroalkyl Surfactants and Linear Alkylbenzene Sulfonates. *Environ. Sci. Technol.* 41, 3254–3261. <https://doi.org/10.1021/es062449j>
- Ho, Y. S., McKay, G., 1998. Sorption of dye from aqueous solution by peat. *Chem. Eng. J.* 70 (2), 115–124. [https://doi.org/10.1016/S1385-8947\(98\)00076-X](https://doi.org/10.1016/S1385-8947(98)00076-X)

-
- Hu, X., Zhou, Q., Luo, Y., 2010. Occurrence and source analysis of typical veterinary antibiotics in manure, soil, vegetables and groundwater from organic vegetable bases, northern China. *Environ. Pollut.* 158 (9), 2992–2998. <https://doi.org/10.1016/j.envpol.2010.05.023>
- Hu, Y., Yan, X., Shen, Y., Di, M., Wang, J., 2018. Antibiotics in surface water and sediments from Hanjiang River, Central China: Occurrence, behavior and risk assessment. *Ecotox. Environ. Safe.* 157, 150–158. <https://doi.org/10.1016/j.ecoenv.2018.03.083>
- Hu, Y., Habibul, N., Hu, Y. Y., Meng, F. L., Sheng, G. P., 2021. Chemical speciation of ciprofloxacin in aqueous solution regulates its phytotoxicity and uptake by rice (*Oryza sativa* L.). *Sci. Total Environ.* 771, 144787. <https://doi.org/10.1016/j.scitotenv.2020.144787>
- Inyang, M., Dickenson, E., 2015. The potential role of biochar in the removal of organic and microbial contaminants from potable and reuse water: A review. *Chemosphere*, 134, 232–240. <https://doi.org/10.1016/j.chemosphere.2015.03.072>
- Jahnke, A., Barber, J. L., Jones, K. C., Temme, C., 2009. Quantitative trace analysis of polyfluorinated alkyl substances (PFAS) in ambient air samples from Mace Head (Ireland): A method intercomparison. *Atmos. Environ.* 43 (4), 844–850. <https://doi.org/10.1016/j.atmosenv.2008.10.049>
- Jeon, J., Kannan, K., Lim, B. J., An, K. G., Kim, S. D., 2011. Effects of salinity and organic matter on the partitioning of perfluoroalkyl acid (PFAAs) to clay particles. *J. Environ. Monitor.* 13 (6), 1803–1810. <https://doi.org/10.1039/c0em00791a>
- Johnson, R. L., Anschutz, A. J., Smolen, J. M., Simcik, M. F., Lee Penn, R., 2007. The adsorption of perfluorooctane sulfonate onto sand, clay, and iron oxide surfaces. *J. Chem. Eng. Data.* 52 (4), 1165–1170. <https://doi.org/10.1021/je060285g>

-
- Karci, A., Balcioğlu, I. A., 2009. Investigation of the tetracycline, sulfonamide, and fluoroquinolone antimicrobial compounds in animal manure and agricultural soils in Turkey. *Sci. Total Environ.* 407 (16), 4652–4664. <https://doi.org/10.1016/j.scitotenv.2009.04.047>
- Kelly, B. C., Ikonomou, M. G., Blair, J. D., Hoover, D., Surridge, B., Grace, R., Gobas, F. A. P. C., 2009. Perfluoroalkyl Contaminants in an Arctic Marine Food Web: Trophic Magnification and Wildlife Exposure. *Environ. Sci. Technol.* 43, 4037 - 4043. <https://doi.org/10.1021/es9003894>.
- Kim, M., Li, L. Y., Grace, J. R., Yue, C., 2015. Selecting reliable physicochemical properties of perfluoroalkyl and polyfluoroalkyl substances (PFASs) based on molecular descriptors. *Environ. Pollut.* 196, 462–472. <https://doi.org/10.1016/j.envpol.2014.11.008>
- Kim, S. C., Carlson, K., 2007. Temporal and spatial trends in the occurrence of human and veterinary antibiotics in aqueous and river sediment matrices. *Environ. Sci. Technol.* 41 (1), 50–57. <https://doi.org/10.1021/es060737+>
- Knight, E. R., Janik, L. J., Navarro, D. A., Kookana, R. S., McLaughlin, M. J., 2019. Predicting partitioning of radiolabelled ¹⁴C-PFOA in a range of soils using diffuse reflectance infrared spectroscopy. *Sci. Total Environ.* 686, 505 - 513. <https://doi.org/10.1016/j.scitotenv.2019.05.339>
- Kong, X., Feng, S., Zhang, X., Li, Y., 2014. Effects of bile salts and divalent cations on the adsorption of norfloxacin by agricultural soils. *J. Environ. Sci-China.* 26 (4), 846–854. [https://doi.org/10.1016/S1001-0742\(13\)60480-5](https://doi.org/10.1016/S1001-0742(13)60480-5)
- Kotzerke, A., Hammesfahr, U., Kleinedam, K., Lamshöft, M., Thiele-Bruhn, S., Schloter, M., Wilke, B. M., 2011. Influence of difloxacin-contaminated manure on microbial community structure and function in soils. *Biol. Fert. Soils*, 47 (2), 177–186. <https://doi.org/10.1007/s00374-010-0517-1>

-
- Lam, N. H., Cho, C. R., Kannan, K., Cho, H. S., 2017. A nationwide survey of perfluorinated alkyl substances in waters, sediment and biota collected from aquatic environment in Vietnam: Distributions and bioconcentration profiles. *J. Hazard. Mater.* 323, 116–127. <https://doi.org/10.1016/j.jhazmat.2016.04.010>
- Langlois, I., Oehme, M., 2006. Structural identification of isomers present in technical perfluorooctane sulfonate by tandem mass spectrometry. *Rapid Commun. Mass Sp.* 20 (5), 844–850. <https://doi.org/10.1002/rcm.2383>
- Leal, R. M. P., Figueira, R. F., Tornisielo, V. L., Regitano, J. B., 2012. Occurrence and sorption of fluoroquinolones in poultry litters and soils from São Paulo State, Brazil. *Sci. Total Environ.* 432, 344–349. <https://doi.org/10.1016/j.scitotenv.2012.06.002>
- Leal, R. M. P., Alleoni, L. R. F., Tornisielo, V. L., Regitano, J. B., 2013. Sorption of fluoroquinolones and sulfonamides in 13 Brazilian soils. *Chemosphere*, 92 (8), 979–985. <https://doi.org/10.1016/j.chemosphere.2013.03.018>
- Lee, J. W., Lee, H. K., Lim, J. E., Moon, H. B., 2020a. Legacy and emerging per- and polyfluoroalkyl substances (PFASs) in the coastal environment of Korea: Occurrence, spatial distribution, and bioaccumulation potential. *Chemosphere*, 251, 126633. <https://doi.org/10.1016/j.chemosphere.2020.126633>
- Lee, Y. M., Lee, J. Y., Kim, M. K., Yang, H., Lee, J. E., Son, Y., Kho, Y., Choi, K., Zoh, K. D., 2020b. Concentration and distribution of per- and polyfluoroalkyl substances (PFAS) in the Asan Lake area of South Korea. *J. Hazard. Mater.* 381, 120909. <https://doi.org/10.1016/j.jhazmat.2019.120909>
- Lei, X., Lu, J., Liu, Z., Tong, Y., Li, S., 2015. Concentration and distribution of antibiotics in water–sediment system of Bosten Lake, Xinjiang. *Environ. Sci. Pollut. R.* 22 (3), 1670–1678. <https://doi.org/10.1007/s11356-014-2994-5>

-
- Lenka, S. P., Kah, M., Padhye, L. P., 2021. A review of the occurrence, transformation, and removal of poly- and perfluoroalkyl substances (PFAS) in wastewater treatment plants. *Water Res.* 199, 117187. <https://doi.org/10.1016/j.watres.2021.117187>
- Leshner, G. Y., Froelich, E. J., Gruett, M. D., Bailey, J. H., Brundage, R. P., 1962. 1,8-Naphthyridine Derivatives. A New Class of Chemotherapeutic Agents. *J. Med. Pharmaceut. Ch.* 5 (5), 1063–1065. <https://doi.org/10.1021/jm01240a021>
- Lesmeister, L., Lange, F. T., Breuer, J., Biegel-Engler, A., Giese, E., Scheurer, M., 2020. Extending the knowledge about PFAS bioaccumulation factors for agricultural plants – A review. *Sci. Total Environ.* 766, 142640. <https://doi.org/10.1016/j.scitotenv.2020.142640>
- Li, Y. W., Wu, X. L., Mo, C. H., Tai, Y. P., Huang, X. P., Xiang, L., 2011a. Investigation of sulfonamide, tetracycline, and quinolone antibiotics in vegetable farmland soil in the pearl river delta area, Southern China. *J. Agr. Food Chem.* 59 (13), 7268–7276. <https://doi.org/10.1021/jf1047578>
- Li, Z., Hong, H., Liao, L., Ackley, C. J., Schulz, L. A., Macdonald, R. A., Mihelich, A. L., Emard, S. M., 2011b. A mechanistic study of ciprofloxacin removal by kaolinite. *Colloid. Surface. B.* 88 (1), 339–344. <https://doi.org/10.1016/j.colsurfb.2011.07.011>
- Li, Y., Liu, B., Zhang, X., Wang, J., Gao, S., 2016. The distribution of veterinary antibiotics in the river system in a livestock-producing region and interactions between different phases. *Environ. Sci. Pollut. R.* 23 (16), 16542–16551. <https://doi.org/10.1007/s11356-016-6677-2>
- Li, Q., Gao, J., Zhang, Q., Liang, L., Tao, H., 2017. Distribution and Risk Assessment of Antibiotics in a Typical River in North China Plain. *B. Environ. Contam. Tox.* 98 (4), 478–483. <https://doi.org/10.1007/s00128-016-2023-0>
- Li, X., Lu, S., Liu, S., Zheng, Q., Shen, P., Wang, X., 2020. Shifts of bacterial community and molecular ecological network at the presence of fluoroquinolones in a constructed wetland system. *Sci. Total Environ.* 708, 135156. <https://doi.org/10.1016/j.scitotenv.2019.135156>

-
- Liang, X., Chen, B., Nie, X., Shi, Z., Huang, X., Li, X., 2013. The distribution and partitioning of common antibiotics in water and sediment of the Pearl River Estuary, South China. *Chemosphere*, 92 (11), 1410–1416. <https://doi.org/10.1016/j.chemosphere.2013.03.044>
- Lillenberg, M., Yurchenko, S., Kipper, K., Herodes, K., Pihl, V., Sepp, K., Lõhmus, R., Nei, L., 2009. Simultaneous determination of fluoroquinolones, sulfonamides and tetracyclines in sewage sludge by pressurized liquid extraction and liquid chromatography electrospray ionization-mass spectrometry. *J. Chromatogr. A.* 1216 (32), 5949–5954. <https://doi.org/10.1016/j.chroma.2009.06.029>
- Limousin, G., Gaudet, J. P., Charlet, L., Szenknect, S., Barthès, V., Krimissa, M., 2007. Sorption isotherms: A review on physical bases, modeling and measurement. *Appl. Geochem.* 22, 249–275. <https://doi.org/10.1016/j.apgeochem.2006.09.010>
- Lin, Y. C., Hsiao, K. W., Lin, A. Y. C., 2018. Photolytic degradation of ciprofloxacin in solid and aqueous environments: kinetics, phototransformation pathways, and byproducts. *Environ. Sci. Pollut. R.* 25 (3), 2303–2312. <https://doi.org/10.1007/s11356-017-0666-y>
- Liu, B., Zhang, H., Xie, L., Li, J., Wang, X., Zhao, L., Wang, Y., Yang, B., 2015. Spatial distribution and partition of perfluoroalkyl acids (PFAAs) in rivers of the Pearl River Delta, southern China. *Sci. Total Environ.* 524–525, 1–7. <https://doi.org/10.1016/j.scitotenv.2015.04.004>
- Liu, X., Lu, S., Liu, Y., Meng, W., Zheng, B., 2017. Adsorption of sulfamethoxazole (SMZ) and ciprofloxacin (CIP) by humic acid (HA): characteristics and mechanism. *RSC Adv.*, 7 (80), 50449–50458. <https://doi.org/10.1039/C7RA06231A>
- Liu, C., Chu, J., Natalie, L. C., Fortner, J. D., Pennell, K. D., 2022. In-situ sequestration of perfluoroalkyl substances using polymer-stabilized ion exchange resin. *J. Hazard. Mater.* 422. <https://doi.org/10.1016/j.jhazmat.2021.126960>

-
- Ltifi, M., Abichou, T., Tisot, J. P., 2014. Effects of Soil Aging on Mechanical and Hydraulic Properties of a Silty Soil. *Geotech. Geol. Eng.* 32 (4), 1101–1108. <https://doi.org/10.1007/s10706-014-9784-1>
- Maizel, A. C., Shea, S., Nickerson, A., Schaefer, C., Higgins, C. P., 2021. Release of Per- And Polyfluoroalkyl Substances from Aqueous Film-Forming Foam Impacted Soils. *Environ. Sci. Technol.* 55 (21), 14617–14627. <https://doi.org/10.1021/acs.est.1c02871>
- Martínez-Carballo, E., González-Barreiro, C., Scharf, S., Gans, O., 2007. Environmental monitoring study of selected veterinary antibiotics in animal manure and soils in Austria. *Environ. Pollut.* 148 (2), 570–579. <https://doi.org/10.1016/j.envpol.2006.11.035>
- Martínez-Mejía, M. J., Sato, I., Rath, S., 2017. Sorption mechanism of enrofloxacin on humic acids extracted from Brazilian soils. *Environ. Sci. Pollut. R.* 24, 15995–16006. <https://doi.org/10.1007/s11356-017-9210-3>
- Massey, L. B., Haggard, B. E., Galloway, J. M., Loftin, K. A., Meyer, M. T., Green, W. R., 2010. Antibiotic fate and transport in three effluent-dominated Ozark streams. *Ecol. Eng.* 36 (7), 930–938. <https://doi.org/10.1016/j.ecoleng.2010.04.009>
- Mejia-Avendaño, S., Zhi, Y., Yan, B., Liu, J., 2020. Sorption of Polyfluoroalkyl Surfactants on Surface Soils: Effect of Molecular Structures, Soil Properties, and Solution Chemistry. *Environ. Sci. Technol.* 54 (3), 1513–1521. <https://doi.org/10.1021/acs.est.9b04989>
- Meng, J., Wang, T., Song, S., Wang, P., Li, Q., Zhou, Y., Lu, Y., 2018. Tracing perfluoroalkyl substances (PFASs) in soils along the urbanizing coastal area of Bohai and Yellow Seas, China. *Environ. Pollut.* 238, 404–412. <https://doi.org/10.1016/j.envpol.2018.03.056>
- Meyer, S., Glaser, B., Quicker, P., 2011. Technical , Economical , and Climate-Related Aspects of Biochar Production Technologies: A Literature Review. *Environ. Sci. Technol.* 45, 9473–9483. <https://doi.org/10.1021/es201792c>

-
- Miao, Y., Guo, X., Peng, D., Fan, T., Yang, C., 2017. Rates and equilibria of perfluorooctanoate (PFOA) sorption on soils from different regions of China. *Ecotox. Environ. Safe.* 139, 102–108. <https://doi.org/10.1016/j.ecoenv.2017.01.022>
- Migliore, L., Cozzolino, S., Fiori, M., 2003. Phytotoxicity to and uptake of enrofloxacin in crop plants. *Chemosphere*, 52 (7), 1233–1244. [https://doi.org/10.1016/S0045-6535\(03\)00272-8](https://doi.org/10.1016/S0045-6535(03)00272-8)
- Milinic, J., Lacorte, S., Vidal, M., Rigol, A., 2015. Sorption behaviour of perfluoroalkyl substances in soils. *Sci. Total Environ.* 511, 63–71. <https://doi.org/10.1016/j.scitotenv.2014.12.017>
- Nickerson, A., Maizel, A. C., Kulkarni, P. R., Adamson, D. T., Kornuc, J. J., Higgins, C. P., 2020. Enhanced Extraction of AFFF-Associated PFASs from Source Zone Soils. *Environ. Sci. Technol.* 54 (8), 4952–4962. <https://doi.org/10.1021/acs.est.0c00792>
- Nickerson, A., Rodowa, A. E., Adamson, D. T., Field, J. A., Kulkarni, P. R., Kornuc, J. J., Higgins, C. P., 2021. Spatial Trends of Anionic, Zwitterionic, and Cationic PFASs at an AFFF-Impacted Site. *Environ. Sci. Technol.* 55 (1), 313–323. <https://doi.org/10.1021/acs.est.0c04473>
- Nowara, A., Burhenne, J., Spiteller, M., 1997. Binding of Fluoroquinolone Carboxylic Acid Derivatives to Clay Minerals. *J. Agric. Food Chem.* 45 (4), 1459–1463. <https://doi.org/10.1021/jf9602151>
- OECD, 2000. OECD 106 Adsorption - Desorption Using a Batch Equilibrium Method. OECD Guideline for the Testing of Chemicals, 1–44. <https://doi.org/10.1787/9789264069602-en>
- OECD, 2021. OECD 61 Reconciling Terminology of the Universe of Per- and Polyfluoroalkyl Substances: Recommendations and Practical Guidance, OECD Series on Risk Management. OECD Publishing, Paris.

-
- Ojo, A. F., Peng, C., Ng, J. C., 2020. Combined effects and toxicological interactions of perfluoroalkyl and polyfluoroalkyl substances mixtures in human liver cells (HepG2). *Environ. Pollut.* 263, 114182. <https://doi.org/10.1016/j.envpol.2020.114182>
- Olsen, G. W., Mair, D. C., Lange, C. C., Harrington, L. M., Church, T. R., Goldberg, C. L., Herron, R. M., Hanna, H., Nobiletti, J. B., Rios, J. A., Reagen, W. K., Ley, C. A., 2017. Per- and polyfluoroalkyl substances (PFAS) in American Red Cross adult blood donors, 2000–2015. *Environ. Res.* 157, 87–95. <https://doi.org/10.1016/j.envres.2017.05.013>
- Pan, B., Liu, Y., Xiao, D., Wu, F., Wu, M., Zhang, D., Xing, B., 2012. Quantitative identification of dynamic and static quenching of ofloxacin by dissolved organic matter using temperature-dependent kinetic approach. *Environ. Pollut.* 161, 192–198. <https://doi.org/10.1016/j.envpol.2011.10.026>
- Pan, M., Chu, L. M., 2017. Leaching behavior of veterinary antibiotics in animal manure-applied soils. *Sci. Total Environ.* 579, 466–473. <https://doi.org/10.1016/j.scitotenv.2016.11.072>
- Parkin, R. T., 2007. Foundations and Frameworks for Microbial Risk Assessment. Center for Risk Science and Public Health School of Public Health and Helath Services, The George Washington University Medical Center, Washington, DC. Prepared for the U.S. Environmental Protection Agency (USEPA) National Cernter for Environmental Assessment.
- Parpounas, A., Litskas, V., Hapeshi, E., Michael, C., Fatta-Kassinou, D., 2017. Assessing the presence of enrofloxacin and ciprofloxacin in piggery wastewater and their adsorption behaviour onto solid materials, with a newly developed chromatographic method. *Environ. Sci. Pollut. R.* 24, 23371–23381. <https://doi.org/10.1007/s11356-017-9849-9>

- Paul, T., Liu, J., Machesky, M. L., Strathmann, T. J., 2014. Adsorption of zwitterionic fluoroquinolone antibacterials to goethite: A charge distribution-multisite complexation model. *J. Colloid Inter. Sci.* 428, 63–72. <https://doi.org/10.1016/j.jcis.2014.04.034>
- Peruchi, L. M., Fostier, A. H., Rath, S., 2015. Sorption of norfloxacin in soils: Analytical method, kinetics and Freundlich isotherms. *Chemosphere*, 119, 310–317. <https://doi.org/10.1016/j.chemosphere.2014.06.008>
- Picó, Y., Andreu, V., 2007. Fluoroquinolones in soil-risks and challenges. *Anal. Bioanal. Chem.* 387 (4), 1287–1299. <https://doi.org/10.1007/s00216-006-0843-1>
- Place, B. J., Field, J. A., 2012. Identification of novel fluorochemicals in aqueous film-forming foams used by the US military. *Environ. Sci. Technol.* 46 (13), 7120–7127. <https://doi.org/10.1021/es301465n>
- Prevedouros, K., Cousins, I. T., Buck, R. C., Korzeniowski, S. H., 2006. Sources, fate and transport of perfluorocarboxylates. *Environ. Sci. Technol.* 40 (1), 32–44. <https://doi.org/10.1021/es0512475>
- Qian, J., Shen, M., Wang, P., Wang, C., Li, K., Liu, J., Lu, B., Tian, X., 2017. Perfluorooctane sulfonate adsorption on powder activated carbon: Effect of phosphate (P) competition, pH, and temperature. *Chemosphere*, 182, 215–222. <https://doi.org/10.1016/j.chemosphere.2017.05.033>
- Qin, X., Liu, F., Wang, G., Weng, L., Li, L., 2014. Adsorption of levofloxacin onto goethite: Effects of pH, calcium and phosphate. *Colloid. Surf. Biointer.* 116, 591–596. <https://doi.org/10.1016/j.colsurfb.2013.09.056>
- Qiu, H., Lv, L., Pan, B., Zhang, Q., Zhang, W., Zhang, Q., 2009. Critical review in adsorption kinetic models. *J. Zhejiang Univ. Sci. A.* 10 (5), 716–724. <https://doi.org/10.1631/jzus.A0820524>

- Ramirez-Guinart, O., Kaplan, D., Rigol, A., Vidal, M., 2020a. Deriving probabilistic soil distribution coefficients (K_d). Part 1: General approach to decreasing and describing variability and example using uranium K_d values. *J. Environ. Radioac.* 222, 106362. <https://doi.org/10.1016/j.jenvrad.2020.106362>.
- Ramirez-Guinart, O., Kaplan, D., Rigol, A., Vidal, M., 2020b. Deriving probabilistic soil distribution coefficients (K_d). Part 2: Reducing caesium K_d uncertainty by accounting for experimental approach and soil properties. *J. Environ. Radioac.* 223-224, 106407. <https://doi.org/10.1016/j.jenvrad.2020.106407>.
- Ramirez-Guinart, O., Kaplan, D., Rigol, A., Vidal, M., 2020c. Deriving probabilistic soil distribution coefficients (K_d). Part 3: Reducing variability of americium K_d best estimates using soil properties and chemical and geological material analogues. *J. Environ. Radioac.* 223-224, 106378. <https://doi.org/10.1016/j.jenvrad.2020.106378>.
- Redgrave, L. S., Sutton, S. B., Webber, M. A., Piddock, L. J. V., 2014. Fluoroquinolone resistance: Mechanisms, impact on bacteria, and role in evolutionary success. *Trends Microbiol.* 22 (8), 438–445. <https://doi.org/10.1016/j.tim.2014.04.007>
- Riaz, L., Mahmood, T., Khalid, A., Rashid, A., Ahmed Siddique, M. B., Kamal, A., Coyne, M. S., 2018. Fluoroquinolones (FQs) in the environment: A review on their abundance, sorption and toxicity in soil. *Chemosphere*, 191, 704–720. <https://doi.org/10.1016/j.chemosphere.2017.10.092>
- Ribas, J. G., 2000. Química de Coordinación (in spanish). 1st Ed. Ediciones Omega S.A. ISBN: 9788428212106
- Rickard, B. P., Rizvi, I., Fenton, S. E., 2022. Per- and poly-fluoroalkyl substances (PFAS) and female reproductive outcomes: PFAS elimination, endocrine-mediated effects, and disease. *Toxicology*, 465, 153031. <https://doi.org/10.1016/j.tox.2021.153031>

-
- Rimington, F., 2020. Pharmacokinetics and pharmacodynamics. *South. Afr. J. Anaesth. Analg.* 26 (6), S153–S156. <https://doi.org/10.36303/SAJAA.2020.26.6.S3.2562>
- Rivagli, E., Pastorello, A., Sturini, M., Maraschi, F., Speltini, A., Zampori, L., Setti, M., Malavasi, L., Profumo, A., 2014. Clay minerals for adsorption of veterinary FQs : Behavior and modeling. *J. Environ. Chem. Eng.* 2 (1), 738–744. <https://doi.org/10.1016/j.jece.2013.11.017>
- Robinson, A. A., Belden, J. B., Lydy, M. J., 2005. Toxicity of fluoroquinolone antibiotics to aquatic organisms. *Environ. Toxicol. Chem.* 24 (2), 423–430. <https://doi.org/10.1897/04-210R.1>
- Ruffle, B., Vedagiri, U., Bogdan, D., Maier, M., Schwach, C., Murphy-Hagan, C., 2020. Perfluoroalkyl Substances in U.S. market basket fish and shellfish. *Environ. Res.* 190, 109932. <https://doi.org/10.1016/j.envres.2020.109932>
- Rusu, A., Tóth, G., Szocs, L., Kökösi, J., Kraszni, M., Gyéresi, Á., Noszál, B., 2012. Triprotic site-specific acid-base equilibria and related properties of fluoroquinolone antibacterials. *J. Pharmaceut. Biomed.*, 66, 50–57. <https://doi.org/10.1016/j.jpba.2012.02.024>
- Salvia, M. V., Fieu, M., Vulliet, E., 2015. Determination of tetracycline and fluoroquinolone antibiotics at trace levels in sludge and soil. *Appl. Environ. Soil Sci.* Vol 2015, 1 - 10. <https://doi.org/10.1155/2015/435741>
- Savvaides, T., Koelmel, J. P., Zhou, Y., Lin, E. Z., Stelben, P., Aristizabal-Henao, J. J., Bowden, J. A., Pollitt, K. J. G., 2021. Prevalence and Implications of Per- and Polyfluoroalkyl Substances (PFAS) in Settled Dust. *Curr. Environ. Health Rep.* 8 (4), 323–335. <https://doi.org/10.1007/s40572-021-00326-4>

-
- Scher, D. P., Kelly, J. E., Huset, C. A., Barry, K. M., Hoffbeck, R. W., Yingling, V. L., Messing, R. B., 2018. Occurrence of perfluoroalkyl substances (PFAS) in garden produce at homes with a history of PFAS-contaminated drinking water. *Chemosphere*, 196, 548–555. <https://doi.org/10.1016/j.chemosphere.2017.12.179>
- Schottel, B. L., Chifotides, H. T., Dunbar, K. R., 2008. Anion- π interactions. *Chem. Soc. Rev.* 37, 68 - 83. <https://doi.org/10.1039/b614208g>
- Shi, Y., Gao, L., Li, W., Liu, J., Cai, Y., 2012. Investigation of fluoroquinolones, sulfonamides and macrolides in long-term wastewater irrigation soil in Tianjin, China. *B. Environ. Contam. Tox.* 89 (4), 857–861. <https://doi.org/10.1007/s00128-012-0761-1>
- Shigei, M., Ahren, L., Hazaymeh, A., Dalahmeh, S. S., 2020. Per- and polyfluoroalkyl substances in water and soil in wastewater-irrigated farmland in Jordan. *Sci. Total Environ.* 716, 137057. <https://doi.org/10.1016/j.scitotenv.2020.137057>
- Sima, M. W., Jaffé, P. R., 2021. A critical review of modeling Poly- and Perfluoroalkyl Substances (PFAS) in the soil-water environment. *Sci. Total Environ.* 757, 143793. <https://doi.org/10.1016/j.scitotenv.2020.143793>
- Sinnokrot, M., O., Valeev, E., F., Sherrill, C. D., 2002. Estimates of the ab initio limit for π - π interactions: The benzene dimer. *J. Am. Chem. Soc.* 124, 10887–10893. <https://doi.org/10.1021/ja025896h>
- Sleep, J. A., Juhasz, A. L., 2021. A Review of Immobilisation-Based Remediation of Per- and Poly-Fluoroalkyl Substances (PFAS) in Soils. *Curr. Pollut. Rep.* 7 (4), 524–539. <https://doi.org/10.1007/s40726-021-00199-z>
- Söregård, M., Östblom, E., Köhler, S., Ahrens, L., 2020. Adsorption behavior of per- And polyfluoroalkyl substances (PFASs) to 44 inorganic and organic sorbents and use of dyes as proxies for PFAS sorption. *J. Environ. Chem. Eng.* 8 (3), 103744. <https://doi.org/10.1016/j.jece.2020.103744>

-
- Sørmo, E., Silvani, L., Bjerkli, N., Hagemann, N., Zimmerman, A. R., Hale, S. E., Hansen, C. B., Hartnik, T., Cornelissen, G., 2021. Stabilization of PFAS-contaminated soil with activated biochar. *Sci. Total Environ.* 763. <https://doi.org/10.1016/j.scitotenv.2020.144034>
- Sparks, D. L., 1996. *Methods of Soil Analysis Part 3: Chemical Methods*. Soil Science Society of America, American Society of Agronomy, Madison, USA. ISBN: 0-89118-825-8.
- Stevenson, F. J., 1994. *Humus Chemistry: Genesis, Composition, Reactions* (2nd Edition). Wiley, New York, USA. ISBN: 978-0-471-59474-1.
- Sturini, M., Speltini, A., Maraschi, F., Profumo, A., Pretali, L., Fasani, E., Albini, A., 2012. Sunlight-induced degradation of soil-adsorbed veterinary antimicrobials Marbofloxacin and Enrofloxacin. *Chemosphere*, 86 (2), 130–137. <https://doi.org/10.1016/j.chemosphere.2011.09.053>
- Sun, J., Jin, L., He, T., Wei, Z., Liu, X., Zhu, L., Li, X., 2020. Antibiotic resistance genes (ARGs) in agricultural soils from the Yangtze River Delta, China. *Sci. Total Environ.* 740, 140001. <https://doi.org/10.1016/j.scitotenv.2020.140001>
- Tamtam, F., Mercier, F., Le Bot, B., Eurin, J., Tuc Dinh, Q., Clément, M., Chevreuil, M., 2008. Occurrence and fate of antibiotics in the Seine River in various hydrological conditions. *Sci. Total Environ.* 393 (1), 84–95. <https://doi.org/10.1016/j.scitotenv.2007.12.009>
- Tan, X., Liu, Y., Zeng, G., Wang, X., Hu, X., Gu, Y., 2015. Application of biochar for the removal of pollutants from aqueous solutions. *Chemosphere*, 125, 70–85. <https://doi.org/10.1016/j.chemosphere.2014.12.058>
- Tan, K. Y., Lu, G. H., Piao, H. T., Chen, S., Jiao, X. C., Gai, N., Yamazaki, E., Yamashita, N., Pan, J., Yang, Y. L., 2017. Current Contamination Status of Perfluoroalkyl Substances in Tapwater from 17 Cities in the Eastern China and Their Correlations with Surface Waters. *B. Environ. Contam. Tox.* 99 (2), 224–231. <https://doi.org/10.1007/s00128-017-2109-3>

-
- Teixidó, M., 2006. Agents antimicrobians en el sistema sòl-aigua: estudis de sorció. Doctoral Thesis (in catalan), University of Barcelona. <http://hdl.handle.net/2445/46803>
- Teixidó, M., Medeiros, J., Beltrán, J., Prat, M. D., Granados, M., 2014. Sorption of enrofloxacin and ciprofloxacin in agricultural soils: Effect of organic matter. *Adsorpt. Sci. Technol.* 32 (2–3), 153–163. <https://doi.org/10.1260/0263-6174.32.2-3.153>
- Thomas, S., 2002. The Hydrogen Bond in the Solid State. *Angew. Chem. Int. Ed.* 41, 48–76.
- Tian, Y., Zhou, Y., Miao, M., Wang, Z., Yuan, W., Liu, X., Wang, X., Wang, Z., Wen, S., Liang, H., 2018. Determinants of plasma concentrations of perfluoroalkyl and polyfluoroalkyl substances in pregnant women from a birth cohort in Shanghai, China. *Environ. Int.* 119, 165–173. <https://doi.org/10.1016/j.envint.2018.06.015>
- Uddin, M. K., 2017. A review on the adsorption of heavy metals by clay minerals, with special focus on the past decade. *Chem. Eng. J.* 308, 438–462. <https://doi.org/10.1016/j.cej.2016.09.029>
- UNEP, 2009. Stockholm Convention on persistent organic pollutants (POPs). United Nations Environment Programme. http://chm.pops.int/Portals/0/Repository/convention_text/UNEP-POPS-COP-CONVTEXT-FULL.English.PDF. Accessed 10 June 2022.
- UNEP, 2015. Stockholm Convention on persistent organic pollutants (POPs). United Nations Environment Programme. <http://chm.pops.int/TheConvention/POPsReviewCommittee/Meetings/POPRC11/Overview/tabid/4558/ctl/Download/mid/14594/Default.aspx?id=5&ObjID=21458>. Accessed 10 June 2022.
- UNEP, 2017. Stockholm Convention on persistent organic pollutants (POPs). United Nations Environment Programme. POPRC-13/3: Perfluorohexane sulfonic acid (CAS No : 355-46-4 , PFHxS), its salts and PFHxS-related compounds Annex to decision POPRC-13/3. <http://chm.pops.int/Convention/POPsReviewCommittee/Chemicals/tabid/243/Default.aspx>. Accessed 10 June 2022.

- UNEP, 2021. Stockholm Convention on persistent organic pollutants (POPs). United Nations Environment Programme. Proposal to list long-chain perfluorocarboxylic acids, their salts and related compounds in Annexes A, B and/or C to the Stockholm Convention on Persistent Organic Pollutants. <http://chm.pops.int/Convention/POPsReviewCommittee/Chemicals/tabid/243/Default.aspx>. Accessed 10 June 2022.
- USEPA, 1992. A framework for ecological risk assessment. U.S. Environmental Protection Agency, EPA/630/R-92/001.
- USEPA, 1999. Understanding variation in partition coefficient, K_d , values. Volume I: The K_d Model, Methods of Measurement, and Application of Chemical Reaction Codes. U.S. Environmental Protection Agency, EPA 402-R-99-004A, 212.
- USEPA, 2007. Method 1694 : Pharmaceuticals and Personal Care Products in Water , Soil , Sediment and Biosolids by HPLC-MS/MS. U.S. Environmental Protection Agency Method, EPA-821-R-08-002.
- USEPA, 2009. Guidance on the development, evaluation, and application of environmental models. U.S. Environmental Protection Agency. EPA/100/K-09/003.
- Uslu, M. Ö., Yediler, A., Balcıoğlu, I. A., Schulte-Hostede, S., 2008. Analysis and sorption behavior of fluoroquinolones in solid matrices. *Water Air Soil Poll.* 190 (1–4), 55–63. <https://doi.org/10.1007/s11270-007-9580-0>
- Valdés, M. E., Santos, L. H. M. L. M., Rodríguez Castro, M. C., Giorgi, A., Barceló, D., Rodríguez-Mozaz, S., Amé, M. V., 2021. Distribution of antibiotics in water, sediments and biofilm in an urban river (Córdoba, Argentina, LA). *Environ. Pollut.* 269. <https://doi.org/10.1016/j.envpol.2020.116133>
- Van Doorslaer, X., Dewulf, J., Van Langenhove, H., Demeestere, K., 2014. Fluoroquinolone antibiotics: An emerging class of environmental micropollutants. *Sci. Total Environ.* 500–501, 250–269. <https://doi.org/10.1016/j.scitotenv.2014.08.075>

-
- Vasconcelos, T. G., Kümmerer, K., Henriques, D. M., Martins, A. F., 2009. Ciprofloxacin in hospital effluent: Degradation by ozone and photoprocesses. *J. Hazard. Mater.* 169 (1–3), 1154–1158. <https://doi.org/10.1016/j.jhazmat.2009.03.143>
- Vasudevan, D., Bruland, G. L., Torrance, B. S., Upchurch, V. G., Mackay, A. A., 2009. pH-dependent ciprofloxacin sorption to soils: Interaction mechanisms and soil factors influencing sorption. *Geoderma* 151, 68–76. <https://doi.org/10.1016/j.geoderma.2009.03.007>
- Venegas, A., Rigol, A., Vidal, M., 2015. Viability of organic wastes and biochars as amendments for the remediation of heavy metal-contaminated soils. *Chemosphere*, 119, 190–198. <https://doi.org/10.1016/j.chemosphere.2014.06.009>
- Vilca, F. Z., Galarza, N. C., Tejedo, J. R., Cuba, W. A. Z., Quiróz, C. N. C., Tornisielo, V. L., 2021. Occurrence of residues of veterinary antibiotics in water, sediment and trout tissue (*Oncorhynchus mykiss*) in the southern area of Lake Titicaca, Peru. *J. Great Lakes Res.* 47 (4), 1219–1227. <https://doi.org/10.1016/j.jglr.2021.04.012>
- Wan, M., Li, Z., Hong, H., Wu, Q., 2013. Enrofloxacin uptake and retention on different types of clays. *J. Asian Earth Sci.* 77, 287–294. <https://doi.org/10.1016/j.jseaes.2013.02.032>
- Wang, F., Liu, C., Shih, K., 2012. Adsorption behavior of perfluorooctanesulfonate (PFOS) and perfluorooctanoate (PFOA) on boehmite. *Chemosphere*, 89 (8), 1009–1014. <https://doi.org/10.1016/j.chemosphere.2012.06.071>
- Wang, Z., Cousins, I. T., Scheringer, M., Buck, R. C., Hungerbühler, K., 2014. Global emission inventories for C₄-C₁₄ perfluoroalkyl carboxylic acid (PFCA) homologues from 1951 to 2030, Part I: Production and emissions from quantifiable sources. *Environ. Int.*, 70, 62–75. <https://doi.org/10.1016/j.envint.2014.04.013>

-
- Wang, Y., Chang, W., Wang, L., Zhang, Y., Zhang, Y., Wang, M., Wang, Y., Li, P., 2019. A review of sources, multimedia distribution and health risks of novel fluorinated alternatives. *Ecotox. Environ. Safe.* 182, 109402. <https://doi.org/10.1016/j.ecoenv.2019.109402>
- Wang, S., Cai, Y., Ma, L., Lin, X., Li, Q., Li, Y., Wang, X., 2022. Perfluoroalkyl substances in water, sediment, and fish from a subtropical river of China: Environmental behaviors and potential risk. *Chemosphere*, 288, 132513. <https://doi.org/10.1016/j.chemosphere.2021.132513>
- Washington, J. W., Ellington, J. J., Jenkins, T. M., Evans, J. J., 2007. Analysis of perfluorinated carboxylic acids in soils: Detection and quantitation issues at low concentrations. *J. Chromatogr. A.* 1154 (1–2), 111–120. <https://doi.org/10.1016/j.chroma.2007.03.107>
- Wei, R., Ge, F., Zhang, L., Hou, X., Cao, Y., Gong, L., Chen, M., Wang, R., Bao, E., 2016. Occurrence of 13 veterinary drugs in animal manure-amended soils in Eastern China. *Chemosphere*, 144, 2377–2383. <https://doi.org/10.1016/j.chemosphere.2015.10.126>
- WHO, 2011. Report of the 3rd meeting of the WHO Advisory Group on integrated surveillance of Antimicrobial Resistance (AGISAR 3), 1–68. World Health Organization, Geneva. https://apps.who.int/iris/bitstream/handle/10665/75198/9789241504010_eng.pdf. Accessed 10 June 2022.
- WHO, 2017. Global Priority list of antibiotic-resistance bacteria to guide research, discovery, and development of new antibiotics. World Health Organization, Geneva. <https://www.who.int/news/item/27-02-2017-who-publishes-list-of-bacteria-for-which-new-antibiotics-are-urgently-needed>. Accessed 10 June 2022.

-
- Xiao, F., Zhang, X., Penn, L., Gulliver, J. S., Simcik, M. F., 2011. Effects of monovalent cations on the competitive adsorption of perfluoroalkyl acids by kaolinite: Experimental studies and modeling. *Enviro. Sci. Technol.* 45 (23), 10028–10035. <https://doi.org/10.1021/es202524y>
- Xiao, F., 2017. Emerging poly- and perfluoroalkyl substances in the aquatic environment: A review of current literature. *Water Res.* 124, 482–495. <https://doi.org/10.1016/j.watres.2017.07.024>
- Xiong, W., Sun, Y., Ding, X., Zhang, Y., Zhong, X., Liang, W., Zeng, Z., 2015. Responses of plasmid-mediated quinolone resistance genes and bacterial taxa to (fluoro)quinolones-containing manure in arable soil. *Chemosphere*, 119, 473–478. <https://doi.org/10.1016/j.chemosphere.2014.07.040>
- Xu, J., Zhang, Y., Zhou, C., Guo, C., Wang, D., Du, P., Luo, Y., Wan, J., Meng, W., 2014. Distribution, sources and composition of antibiotics in sediment, overlying water and pore water from Taihu Lake, China. *Sci. Total Environ.* 497–498, 267–273. <https://doi.org/10.1016/j.scitotenv.2014.07.114>
- Yan, H., Zhang, C., Zhou, Q., Yang, S., 2015. Occurrence of perfluorinated alkyl substances in sediment from estuarine and coastal areas of the East China Sea. *Environ. Sci. Pollut. R.* 22 (3), 1662–1669. <https://doi.org/10.1007/s11356-014-2838-3>
- Yang, L., Wu, L., Liu, W., Huang, Y., Luo, Y., Christie, P., 2018. Dissipation of antibiotics in three different agricultural soils after repeated application of biosolids. *Environ. Sci. Pollut. R.* 25 (1), 104–114. <https://doi.org/10.1007/s11356-016-8062-6>
- Yang, Z., Xing, R., Zhou, W., 2019. Adsorption of ciprofloxacin and Cu²⁺ onto biochars in the presence of dissolved organic matter derived from animal manure. *Environ. Sci. Pollut. R.* 14382–14392. <https://doi.org/10.1007/s11356-019-04760-8>

-
- Yi, S., Gao, B., Sun, Y., Wu, J., Shi, X., Wu, B., Hu, X., 2016. Removal of levofloxacin from aqueous solution using rice-husk and wood-chip biochars. *Chemosphere*, 150, 694-701. <https://doi.org/10.1016/j.chemosphere.2015.12.112>
- Yu, Q., Zhang, R., Deng, S., Huang, J., Yu, G., 2009. Sorption of perfluorooctane sulfonate and perfluorooctanoate on activated carbons and resin: Kinetic and isotherm study. *Water Res.* 43 (4), 1150–1158. <https://doi.org/10.1016/j.watres.2008.12.001>
- Yu, J., Lv, L., Lan, P., Zhang, S., Pan, B., Zhang, W., 2012. Effect of effluent organic matter on the adsorption of perfluorinated compounds onto activated carbon. *J. Hazard. Mater.* 225–226, 99–106. <https://doi.org/10.1016/j.jhazmat.2012.04.073>
- Zhang, J., Li, Z., Ge, G., Sun, W., Liang, Y., Wu, L., 2009. Impacts of soil organic matter, pH and exogenous copper on sorption behavior of norfloxacin in three soils. *J. Environ. Sci.* 21 (5), 632–640. [https://doi.org/10.1016/S1001-0742\(08\)62318-9](https://doi.org/10.1016/S1001-0742(08)62318-9)
- Zhang, Q., Zhao, L., Dong, Y. hua, Huang, G., 2012. Sorption of norfloxacin onto humic acid extracted from weathered coal. *J. Environ. Manage.* 102, 165–172. <https://doi.org/10.1016/j.jenvman.2011.12.036>
- Zhang, J., Lu, M., Wan, J., Sun, Y., Lan, H., Deng, X., 2018. Effects of pH, dissolved humic acid and Cu^{2+} on the adsorption of norfloxacin on montmorillonite-biochar composite derived from wheat straw. *Biochem. Eng. J.* 130, 104–112. <https://doi.org/10.1016/j.bej.2017.11.018>
- Zhang, D., Zhang, W., Liang, Y., 2019. Distribution of eight perfluoroalkyl acids in plant-soil-water systems and their effect on the soil microbial community. *Sci. Total Environ.* 697, 134146. <https://doi.org/10.1016/j.scitotenv.2019.134146>

- Zhang, Y., Cornelissen, G., Silvani, L., Zivanovic, V., Smebye, A. B., Sørmo, E., Thune, G., Okkenhaug, G., 2022. Industrial byproducts for the soil stabilization of trace elements and per- and polyfluorinated alkyl substances (PFASs). *Sci. Total Environ.* 820, 153188. <https://doi.org/10.1016/j.scitotenv.2022.153188>
- Zhao, Q., Zhang, S., Zhang, X., Lei, L., Ma, W., Ma, C., Song, L., 2017. Cation–Pi Interaction: A Key Force for Sorption of Fluoroquinolone Antibiotics on Pyrogenic Carbonaceous Materials. *Environ. Sci. Technol.* 51, 13659 - 13667. <https://doi.org/10.1021/acs.est.7b02317>

CHAPTER II

MOTIVATION AND OBJECTIVES

Poly- and perfluoroalkyl substances (PFASs) are anthropogenic pollutants which may cause severe adverse health effects, and have been widely found in different environmental matrices. On the other hand, fluoroquinolone antibiotics (FQs) are synthetic pharmaceutical compounds and their use in veterinary medicine has led to high levels of FQs in manure and droppings. These materials can be then used as amendments to improve soil physicochemical properties, especially organic carbon and nitrogen content, which then leads to the incorporation of FQs in soils.

After a contamination event it is mandatory to assess its associated risk and estimate pollutant exposure to animal and human beings, which requires the quantification of a number of interaction parameters. These include, among others, pollutant concentration, toxicity, and potential mobility within environmental compartments. This latter requires the evaluation of the sorption and desorption process of pollutants in environmental matrices such as soils and sediments. A widely used parameter in environmental models to estimate pollutant mobility is the solid-liquid distribution coefficient (K_d), which quantifies the equilibrium of the pollutant between solid and liquid phases. Low K_d values are associated with a high mobility, being the pollutant present mainly in the aqueous phase, and thus able to be transported along environmental compartments (*e.g.*, plant and groundwater).

To better describe the sorption and desorption process, and extrapolate this information to other untested but characterized scenarios, the identification of key sorbent properties affecting K_d , in addition to the elucidation of the chemical mechanisms responsible for the pollutant binding in the solid phase, are required. Elucidating sorption mechanisms in pure soil phases, such as humic substances, phyllosilicate minerals and metal oxides may also be of interest to later extrapolate the drawn conclusions to bulk soils, in where all these phases may coexist.

The identification of the key sorbent properties affecting sorption can be assessed by examining the correlation of K_d values with single or multiple soil/sediment properties. This approach relies on robust, critically-reviewed compilations of K_d values, covering diverse scenarios and wide ranges of property values, and made of literature-gathered data and, if needed, new data derived from ad-hoc laboratory experiments.

Models derived from calibration datasets built-up with data from contrasted scenarios have a wider range of applicability than those obtained under narrower conditions, which may be only applicable to selected scenarios. Unfortunately, current K_d prediction models for PFASs and FQs in soils suffer from certain limitations in their applicability, and there is a need of developing new prediction models with a wider range of applicability.

After assessing the environmental risk, remediation actions may be needed. These can include the application of carbon-rich materials such as activated carbons, biochars or compost to soils in order to sorb and immobilize the pollutant in the new solid phase. The effectiveness of this strategy depends on the physicochemical properties of the carbon-rich material. Thus, prediction K_d models in these sorbents are of interest for screening purposes of their potential sorption affinity for organic pollutants. In this context, no current sorption K_d models for PFASs in these materials are available at date.

Considering this, the main goal of this thesis has been to identify key parameters affecting PFASs and FQs sorption and to develop K_d prediction models in soils and related environmental matrices (including pure soil components and carbon-rich materials). To reach this main goal, the following work has been carried out:

- Performing sorption experiments of PFASs in soils and carbon-rich materials.
- Performing sorption experiments of FQs in pure soil phases and soils.
- Construction of critically-reviewed compilations of K_d data of PFASs and FQs, with own and literature-gathered data in these environmental matrices.
- Identification of the key physicochemical properties responsible for PFASs and FQs sorption in these matrices by using univariate and multivariate correlation tools.
- Development and validation of prediction models of K_d (PFAS) in soils and in carbon-rich materials.
- Development and validation, when feasible, of prediction models of K_d (FQ) in pure soil phases and bulk soils.
- Proposal of best-estimate K_d (FQ) values for soils based on relevant soil physicochemical properties.

The results of this work are presented in four chapters. Chapter III focuses on the identification of key soil properties affecting PFASs sorption in soils, and the development of a K_d prediction model based only on a few soil and PFAS physicochemical properties. Chapter IV aims to identify the key sorbent properties affecting PFASs sorption in carbon-rich materials (including biochar, activated carbon, compost and charcoal fines) and the development of a K_d prediction model for PFAS in these sorbents. Chapter V discusses the sorption of FQs in pure mineral and organic phases present in soils, in order to get insights of the role and the main factors affecting FQs sorption in these phases to latter extrapolate this information to bulk soils. Finally, chapter VI aims to develop a K_d prediction model of FQs in soils, as well as to propose best-estimate K_d (FQ) values in soils based on a few physicochemical properties.

CHAPTER III

SORPTION OF PFASs IN SOILS

3.1. Introduction

PFASs, among them PFCAs and PFSAAs, are anthropogenic organic pollutants with a fluorinated carbon chain attached to a functional group. These substances have been used for more than 50 years in a variety of applications including fire-fighting foams, inks, lubricants, and oil and water repellents for the leather, paper and textile industries (Prevedouros et al., 2006). Because they are widely used, highly toxic, and can bioaccumulate and persist in the environment, PFASs have garnered considerable scientific attention in recent years (Kannan, 2011). They have been found in environmental matrices such as soil, sediment, and biological samples, as well as in rain, freshwater, seawater, and groundwater (Prevedouros et al., 2006). Specifically, they have often been detected at levels of up to a few mg kg^{-1} in contaminated soils and at levels of up to several hundred $\mu\text{g L}^{-1}$ in groundwater of contaminated sites (Brusseau et al., 2020; McGuire et al., 2014). Given these high concentrations, it is important to evaluate PFASs sorption in soils in order to develop sorption prediction models and to assess their mobility in the environment more accurately.

Several soil properties have been suggested to affect PFAS sorption in soils, including OC, silt and clay phases, pH and status of divalent metals. Higgins and Luthy (Higgins and Luthy, 2006) found that soil OC content was the main parameter affecting the sorption behaviour of PFASs in sediments, suggesting that most sorption occurred via hydrophobic interactions, although soil pH and the concentration of divalent cations might also play a role in the sorption process via electrostatic interactions. The presence of hydrophobic interactions in soils was further addressed by Milinovic et al. (Milinovic et al., 2015), and the effect of salinity and pH on sorption to sediments with $\text{OC} < 1\%$ has also been evaluated elsewhere (You et al., 2010). However, even though pH and ionic strength may play a role in the sorption process in mineral soils under controlled scenarios, these effects are minor compared to the effect of OC content. Moreover, studies exploring the sorption of PFASs on low OC soils (<

5%) have suggested that the mineral phase may have a positive influence on the sorption process (Knight et al., 2019; Martz et al., 2019). A literature review evaluating the role of soil and sediment properties in the sorption of PFASs concluded that OC alone could not satisfactorily account for the sorption of PFASs and suggested that other parameters, such as soil pH and clay content, should also be considered (Li et al., 2018). However, these conclusions were based on a data set that included mostly studies of soils or sediments with OC content < 10% and very few samples of soils with higher OC content, which may be representative of environmental scenarios such as meadows, forest soil layers or peat soils. In addition, the sorption pattern was deduced from the widely-evaluated PFOS and PFOA, while only limited sorption data are available for other shorter or longer-chained PFASs in soils and sediments.

Among the models for predicting the sorption behaviour of PFASs currently in use, a mechanistic model was developed to predict the sorption of PFCAs, PFSAAs, and linear alkylbenzenes in sediments with OC ranging from 0.6 to 9.7% via both electrostatic and hydrophobic interactions with the organic matter (Higgins and Luthy, 2007). The model was tested for its ability to predict the sorption parameters of PFCAs and PFSAAs with 7–11 fluorinated carbons under specific experimental conditions. Moreover, Knight et al. (Knight et al., 2019) developed a model based on OC and soil silt and clay content, able to predict the sorption of PFOA under selected experimental conditions in soils with OC content ranging from 0.1–3.5%, thus excluding organic soils. Therefore, new experimental data for deriving PFAS sorption and desorption parameters in a diversity of soil types are required to improve current sorption models, making them less site-specific and covering a wide variety of PFASs, including the least commonly regulated species (especially short-chained PFASs, Sima and Jaffé, 2021).

In this chapter, we aim to construct a simple and global parametric model, based on a small number of easily-measurable physicochemical properties of soil and- PFASs, to predict the sorption solid-liquid distribution coefficient (K_d) of any PFCAs and PFSAAs with a number of fluorinated carbon units between 3 and 11, and applicable to both mineral and organic soils. First, sorption parameters (K_d , $K_{d,des}$, %S, %D) of eight PFASs in seven soils with OC ranging from 1.6 to 41% were determined to enrich an overall dataset of K_d values of PFASs created with literature data. Then, normalized sorption coefficients (with respect to soil OC and mineral phase contents, K_{OC} and K_{MIN} , respectively) were deduced by correlating K_d values with the soil organic fraction. Moreover, normalized sorption coefficients with respect to the humin and humic+fulvic fractions (K_{Humin} and $K_{Humic+Fulvic}$, respectively) were deduced. The correlation of K_{OC} and K_{MIN} with specific PFAS physicochemical properties allowed the deduction of the main interaction mechanisms in each phase and set the basic equations to construct a parametric K_d prediction model. The model was validated with external data and the contribution of both mineral and organic soil phases on the overall K_d was quantified.

3.2. Materials and methods

3.2.1. Reagents and standards

Milli-Q double deionized water ($18.2 \text{ M}\Omega \text{ cm}^{-1}$) was obtained from a water purification system (USF PureLaB Plus, Spain). HPLC-grade acetonitrile ($\geq 99.9\%$), as well as extra-pure sodium azide ($\geq 99.0\%$) and calcium chloride dihydrate (99%), were supplied by Merck (Germany), and ammonium acetate (96%) was supplied by Panreac (Spain). Analytical standards of PFBA (98%), PFHxA (97%), PFOA (96%), PFNA (97%), PFDoA (95%), and PFHxS (98%) were supplied by Sigma-Aldrich (Germany). Analytical standards of PFBS (98%) and PFOS (95%) were supplied by Fluka (Austria). Isotope-labelled sodium perfluoro-1-[1,2,3,4,- $^{13}\text{C}_4$]-octane sulfonate (MPFOS) and perfluoro-n-[1,2,3,4,- $^{13}\text{C}_4$]-octanoic acid

(MPFOA), both at concentrations of $50 \mu\text{g mL}^{-1}$ in methanol, were supplied by Wellington Laboratories (Canada). An ACN-based solution of 500 ng mL^{-1} for both MPFOS and MPFOA was prepared by appropriate dilution of the commercial standard. Working solutions of $1,000 \mu\text{g mL}^{-1}$ containing the individual PFAS were prepared in acetonitrile, whereas working solutions of MPFOS and MPFOA were prepared separately at $20 \mu\text{g mL}^{-1}$ in ACN by diluting the commercial stock solutions. All solutions were stored at -18°C in glass vials with polyethylene caps (Sigma-Aldrich, Germany).

The main physicochemical properties of all PFASs considered in this study, including those not used in our experiments but incorporated in the database for our parametric model, are summarized in **Table 1.1**. Buck and co-workers suggested a unified classification of PFASs into short- and long-chained groups (Buck et al., 2011). However, according to the differences in the log K_{ow} (see **Table 1.1**), in this study we decided to adapt the PFASs definition by grouping the PFASs in short-, mid- and long-chained. We considered PFASs with $\leq 5 \text{ CF}_2$ (PFBA, PFBS, PFPeA, and PFHxA) to be short-chained PFASs. PFASs with 6-9 CF_2 (PFHpA, PFHxS, PFOA, PFNA, PFOS, and PFDA) and $> 9 \text{ CF}_2$ (PFUnA, PFDS, and PFDoA) were considered to be mid- and long-chained PFASs, respectively.

3.2.2. Materials and characterization

Seven field soil samples (topsoils; taken at 0–10 cm depth) with physicochemical properties varying within a wide range were selected for our PFASs sorption and desorption experiments (**Table 3.1**). The soil samples generally had an acidic pH ranging from 5.2 to 5.8 and a CaCO_3 content below 3%, with the exception of the DELTA2 soil, which had a slightly basic pH of 8.0 likely due to its higher CaCO_3 content. The OC content of the soil samples ranged from 1.6 to 41%; four samples having an OC content above 25%. Amorphous Fe, Al and Mn contents ranged $1,000 - 20,000$; $170 - 1,700$ and $200 - 1,400 \text{ mg kg}^{-1}$, respectively.

DOC contents ranged 15 – 290 mg C L⁻¹, with higher content for the organic soils, and SSA values ranged 0.5 – 6.5 m² g⁻¹.

The pH of the soil was determined in a 40 g L⁻¹ Milli-Q water suspension slurry after being shaken during 48 hours, whereas OC content was determined by elemental analysis (EA-1108 C.E Instruments, Thermo Fisher Scientific). Soil texture (sand, silt and clay contents) was determined by the pipette method (Burt, 2004). The amount of amorphous Fe was determined by ascorbic extraction (Kotska and Luther, 1994), whereas the amount of amorphous Al and Mn was determined by oxalate extraction (Carter and Gregorich, 2006). The calcium carbonate content, CaCO₃, was determined by the Bernard method (Müller and Gastner, 1971). The DOC in the soil suspensions was determined using a DOC analyser (Shimadzu TOC-5000 A, Japan) after acidification to pH 2.0 using HCl 1 N. SSA was determined by Nitrogen adsorption using the Brunauer-Emmett-Teller (BET) method (TriStar 3000, Micromeritics). Additional information about the soil samples is provided elsewhere (Ramírez-Guinart et al., 2017).

Additional characterizations in BRA and KOM soils were performed elsewhere (Rigol et al., 1998). Briefly, fats and waxes contents of the soil were extracted after refluxing the soil with an ethanol/toluene mixture. Then, soil humic and fulvic acid fractions were quantified after three consecutive extractions with 0.2 M NaOH, and the resulting residue (containing humin + mineral fractions) was neutralized, washed and freeze-dried. The humin fraction was then purified by removing the mineral fraction after consecutively digesting the resulting residue with HF. Detailed information about these procedures are provided in Rigol et al. (1998).

Table 3.1 Main soil physicochemical properties.

Soil	pH	OC ^a (%)	Clay ^b (%)	Silt ^b (%)	Fe ^c (mg kg ⁻¹)	Al ^c (mg kg ⁻¹)	Mn ^c (mg kg ⁻¹)	CaCO ₃ (%)	DOC ^d (mg L ⁻¹)	SSA ^e (m ² g ⁻¹)
ALM	5.5	1.6	11	35	1.01 · 10 ³	400	200	2.0	15	2.0
DELTA2	8.0	7.7	34	52	2.97 · 10 ³	230	330	51	39	6.5
OVI01	5.2	9.4	19	40	4.52 · 10 ³	380	390	3.0	250	1.8
UIAR	5.8	27	3.0	51	6.50 · 10 ³	1.73 · 10 ³	560	0.2	180	0.5
BRA	5.7	32	2.0	63	1.24 · 10 ⁴	1.03 · 10 ³	600	2.0	175	0.6
DUBLIN	5.7	39	1.3	78	1.06 · 10 ⁴	170	1.44 · 10 ³	1.6	290	0.6
KOM	5.7	41	1.1	79	1.97 · 10 ⁴	480	390	0.5	190	0.8

^a OC: Organic Carbon; ^b Clay and Silt contents referred to mineral phase; ^c Amorphous metal content; ^d DOC: Dissolved Organic Carbon;

^e SSA: Specific Surface Area.

3.2.3. Sorption and desorption experiments

To test the sorption behaviour of each PFAS in each soil, three grams of dried soil were placed in 80-mL polypropylene (PP) centrifuge tubes with 30 mL of 0.01 mol L⁻¹ CaCl₂ solution containing 1 g L⁻¹ of NaN₃ as a biodegradation inhibitor (OECD, 2000). The resulting suspensions were end-over-end shaken at 30 rpm for 24 h, and then known volumes of individual PFAS stock solutions were added to the suspensions. The initial spiked concentrations of each PFAS (**Table 3.2**) were selected to ensure that: (i) the K_d value fell within the linear range of the sorption isotherm according to previous studies of PFAS sorption in soils performed by our research group (Milinovic et al., 2015); (ii) the final sorbed concentrations were representative of concentrations that might be found in contaminated soils (Brusseau et al., 2020); (iii) PFAS concentrations in the final liquid solution were below 70 µg L⁻¹, a value also representative of concentrations found in groundwater of PFAS-impacted sites (McGuire et al., 2014); and (iv) the final concentration in the liquid solution led to reliable results after their analytical determination. After being spiked with a PFAS, tubes were shaken again at 30 rpm for 24 h to ensure that the equilibrium was reached in accordance with previous kinetic studies (Li et al., 2019; Miao et al., 2017; Wei et al., 2017; Xiang et al., 2018). Then, tubes were centrifuged for 30 min at 4 °C and 7,800 g (AJ2-HS, Beckman Coulter, USA) and supernatants were removed using a plastic syringe, filtered through 0.45 µm and stored in 50 mL glass vials at 4 °C until analysis. For the desorption experiments, soil residues from the sorption experiment were dried at 40°C and then tested using the same procedure as above, but without PFAS spiking, except for PFBA and PFBS that presented, in general, very low sorption levels. Shaking desorption time was 24 hours, in agreement with previous kinetic desorption experiments on soils and sediments with varying OC content (Miao et al., 2017; Zhi and Liu, 2018). The pH of the resulting supernatants from sorption and desorption experiments did not significantly differ (± 0.2) from the soil pH reported in **Table 3.1**.

Table 3.2 Spiked PFAS initial concentrations (ng mL⁻¹) in each soil for the sorption experiments.

Soil	PFBA	PFBS	PFHxA	PFHxS	PFOA	PFNA	PFOS	PFD _o A
ALM	30	30	35	50	50	60	170	330
DELTA2	30	30	35	50	50	170	170	500
OVI01	30	30	35	50	50	170	170	500
UIAR	30	50	50	140	150	570	670	1,000
BRA	30	50	50	140	150	570	670	1,000
DUBLIN	30	50	50	140	150	570	670	1,000
KOM	30	50	50	140	150	570	670	1,000

3.2.4. Quality control

All sorption and desorption batch experiments were performed in duplicate. The relative standard deviation (% RSD) between replicates was approximately 20% in the worst scenarios. Quality control of the analyses included blank soil samples that were tested using the same procedure described in Section 3.2.3, but without PFAS spiking, to test whether PFASs were present in the soil samples. In addition to this, aqueous control samples at PFAS concentrations representative of the tested concentration range were assayed to quantify PFAS losses during the experimental stages of the batch test. Results from the analyses of blank soil samples showed that no PFASs were present in the soils prior to the analysis. Regarding aqueous control samples, although some authors have reported sorption of PFOA on common laboratory equipment (Lath et al., 2019), our results agree with those reporting negligible losses for short- and mid-chained PFASs (Ahrens et al., 2011; Milinovic et al., 2015; Campos Pereira et al., 2018). However, for the long-chained PFD_oA only 40% was recovered, and the results were corrected accordingly.

3.2.5. PFASs analysis by HPLC-MS/MS

To quantify the PFASs concentration resulting from the sorption and desorption experiments, 750 μL aliquots of the supernatants were transferred into a 2-mL chromatographic vial. 10 μL of either the MPFOS or MPFOA internal standard working solution and 240 μL of ACN were then added into the vial to reach a final volume of 1 mL, and the PFASs were subsequently analysed via HPLC-MS/MS. The HPLC was equipped with an auto-sampler (Agilent 1100 Wellplate) thermostated at 10 °C and a pump and solvent system (Agilent 1100 LC). A Luna C₁₈ (2)-HST reverse phase column (2.5 μm , 100 x 2.00 mm, Phenomenex) thermostated at 45°C was used for the chromatographic separation. The chromatographic separation conditions were adapted from elsewhere (Gómez-Canela et al., 2012) and briefly consisted in an injection volume of 10 μL (full loop) with a mobile phase A composed of 10 mmol L⁻¹ ammonium acetate and a mobile phase B composed of ACN. The flow rate was set at 300 $\mu\text{L min}^{-1}$ while the elution gradient was set at 75% A during one minute and then reached until 85% B during 5 minutes. After, mobile phase reached 100% B during the next 30 seconds and this percentage was hold during 30 more seconds being reduced at 25% B during the next minute. This elution grade of 25 % B was held during the next 7 minutes to condition the column for the next analysis.

Detection was performed using a triple quadrupole mass spectrometer (API3000 Perkin-Elmer Sciex Instruments) provided with a ionization chamber (Turblon SprayTM) located at 10 mm from the analyser and working in the negative mode, ESI(-). The most significant m/z transition of each PFAS was used for quantification while the second one was used for confirmation. The dwell time for each transition was established at 30 ms, and the software used for the determination was Absciex Analyst. Experimental parameters of the mass spectrometer are specified in **Table 3.3**.

Table 3.3. Experimental parameters of the mass spectrometer.

PFAS	Transition (m/z)	Declustering Potential (V)	Focusing Potential (V)	Potential (V)	Collision Energy (V)
PFBA	213 > 169	-17	-91		-18
PFH _x A	313 > 269, 119	-20	-104		-21
PFOA	413 > 369, 169	-23	-122		-20
PFNA	463 > 419, 169	-27	-123		-21
PFD _o A	613 > 569, 319	-32	-110		-24
PFBS	299 > 80, 99	-40	-121		-45
PFH _x S	399 > 80, 119	-43	-133		-58
PFOS	499 > 80, 130	-44	-131		-68
MPFOA	417 > 372, 172	-23	-122		-20
MPFOS	503 > 80, 99	-44	-131		-68

Quantification was performed using 1/x weighted calibration curves with standards of 0; 0.5; 2; 5; 10; 20; 50; 100 and 200 ng mL⁻¹ for each PFAS, together with the inner standards MPFOS and MPFOA spiked at 5 ng mL⁻¹. The Pearson coefficients of the resulting calibration lines were up to 0.999. The LOD and LOQ were determined as a signal-to-noise ratio set at 1:3 and 1:10 respectively, and were similar to other LODs and LOQs reported elsewhere (Liu et al., 2015; Habibullah-Al-Mamun et al., 2016). Repeatability was determined after ten consecutive injections at a concentration of 20 ng mL⁻¹. The quality figures of the method are reported in **Table 3.4**.

Table 3.4 Quality figures of the method.

PFAS	Repeatability at 20 ng mL ⁻¹ (%RSD)	LOD (ng L ⁻¹)	LOQ (ng L ⁻¹)	Pearson coefficient of calibration curves	Recovery of controls (%)
PFBA	4	0.10	0.30	0.999	> 98
PFH _x A	5	0.04	0.10	0.991	> 98
PFOA	3	0.02	0.08	0.997	> 95
PFNA	4	0.01	0.05	0.998	> 95
PFD _o A	4	0.01	0.04	0.995	40
PFBS	5	0.03	0.10	0.997	> 98
PFH _x S	5	0.03	0.10	0.998	> 98
PFOS	5	0.06	0.20	0.999	> 95

3.2.6. Quantification of sorption and desorption parameters

K_d ($L\ kg^{-1}$), was calculated as the ratio between the concentration of the target PFAS sorbed at the solid phase, C_S ($ng\ g^{-1}$), and the concentration of the target PFAS in the aqueous phase at equilibrium, C_{eq} ($ng\ mL^{-1}$):

$$K_d = \frac{C_S}{C_{eq}} \quad (3.1)$$

where C_{eq} values were directly determined by HPLC-MS/MS, and C_S was calculated using the following equation:

$$C_S = \frac{(C_{in} - C_{eq}) \cdot V}{m} \quad (3.2)$$

where C_{in} ($ng\ mL^{-1}$) represents the initial concentration of PFAS in the suspension (**Table 3.2**), V (mL) is the total volume of contact solution, and m (g) refers to the dry mass of soil.

As with K_d (Equation 3.1), $K_{d,des}$ ($L\ kg^{-1}$), was calculated as follows:

$$K_{d,des} = \frac{C_{S,des}}{C_{eq,des}} \quad (3.3)$$

where $C_{S,des}$ ($ng\ g^{-1}$) and $C_{eq,des}$ ($ng\ mL^{-1}$) are PFAS concentrations in the solid and aqueous phases, respectively, after the desorption experiments. $C_{eq,des}$ values were directly determined by HPLC-MS/MS, whereas $C_{S,des}$ values were calculated as the difference between the initial PFAS concentration in the solid residue resulting from the sorption experiments ($C_{in,des}$, $ng\ g^{-1}$) and the PFAS desorbed with regard to the mass of soil, as follows:

$$C_{S,des} = C_{in,des} - \frac{C_{eq,des} \cdot V}{m} \quad (3.4)$$

$C_{in,des}$ depends on C_S and the amount of PFAS present in the residual volume (V_{res} , mL^{-1}) of solution that remained in the soil after the sorption experiment:

$$C_{in,des} = C_S + \frac{C_{eq} \cdot V_{res}}{m} \quad (3.5)$$

The sorption and desorption percentages (%S and %D, respectively) were calculated as follows:

$$\% S = \frac{(C_{in} - C_{eq})}{C_{in}} \cdot 100 \quad (3.6)$$

$$\% D = \frac{(C_{eq,des} \cdot V)}{C_{in,des} \cdot m} \cdot 100 \quad (3.7)$$

3.2.7. Construction of the PFASs K_d datasets

Three datasets including K_d (PFAS) values in soils and analogous geological materials (*i.e.*, subsoils and sediments) were constructed using our own experimental data and additional data gathered from the literature. Ancillary information about the soils, such as sand, silt, clay, and OC content, was also included in all datasets. The acceptance criteria to include a K_d value from the literature were: (i) data was originated from batch experiments, given that K_d values obtained from *in situ* experiments have been shown to be significantly higher due to the non-equilibrium nature of natural systems (Li et al., 2018); (ii) only studies in which a K_d value could be confidently derived (*i.e.*, linear isotherms with constant K_d ; non-linear isotherms, but with the reported K_d falling within the linear range of the isotherm; K_d values calculated from a low initial concentration, assuming that sorption saturation was not reached) were considered; (iii) we only included data for PFCAs and PFSAAs that contained from 3 to 11 fluorinated carbons; (iv) for those studies reporting K_d values at varying pH, the K_d value at ± 1 pH unit of the native soil pH was considered; (v) for those studies reporting K_d values at varying ionic strength, the lowest ionic strength was considered.

The first dataset, hereinafter referred as “own dataset” included only our experimental data, consisted of 56 entries and was used to preliminary evaluate the key soil parameters affecting PFASs sorption. The second dataset hereinafter referred as “overall dataset”, included our experimental data and 379 additional K_d data in 222 soil and sediment samples gathered

from the literature, and comprised a total of 435 entries. **Table 3.5** provides the references and information for the calibration dataset used to build the PFASs sorption model. Of the 222 samples, 167 were soils, 171 had an OC content less than 2%, and only 10 had an OC content above 10%. Among these 222 samples, 183 reported additional soil texture characterization. **Figure 3.1** displays the USDA soil classification of these samples according to both the relative proportion of sand/silt/clay and the OC contents. As the USDA classification only classifies soils according to the relative sand/silt/clay percentages of the bulk soil, the OC of the soils was labelled in different colours. The samples covered a wide range of soil types, with a majority of samples with OC contents < 2%, and only 7 soil samples had an OC content greater than 10%. PFOS and PFOA were the two PFASs with the highest number of entries, whereas limited data were available in the literature for other PFASs.

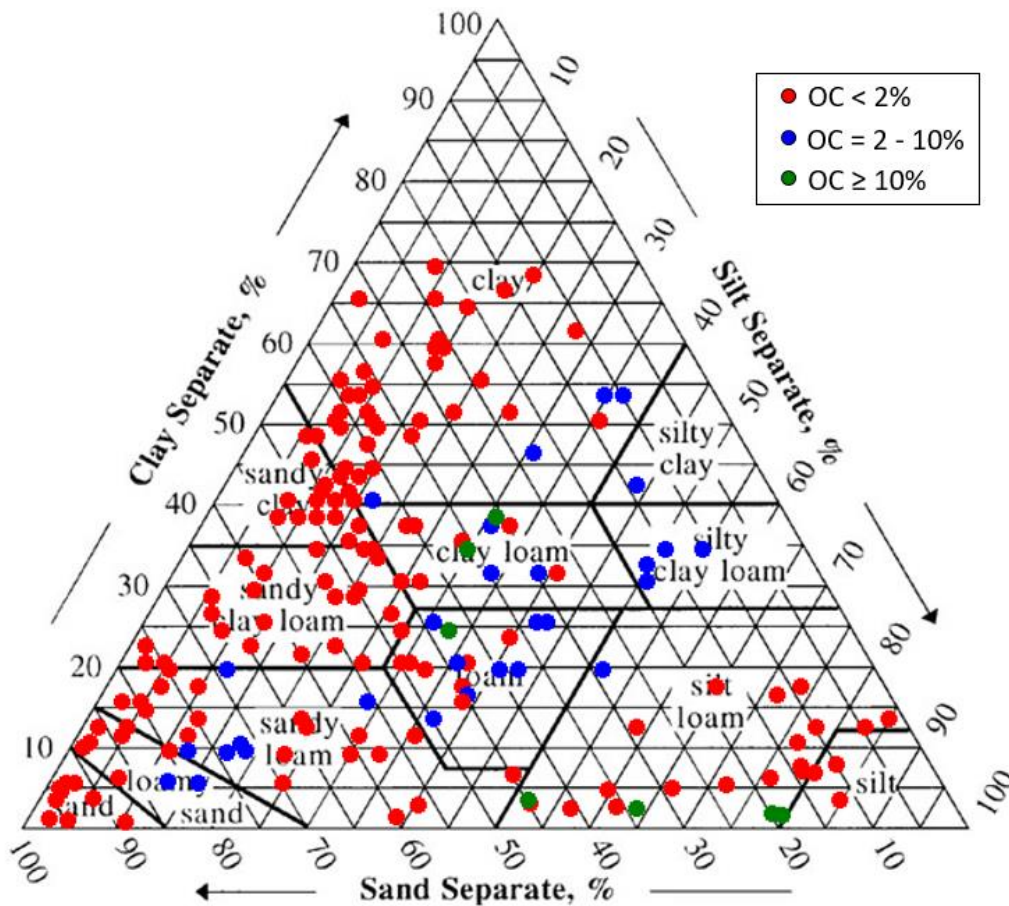


Figure 3.1 USDA classification of the 183 soil/sediment samples included in the calibration dataset according to its OC content and sand/silt/clay relative percentages.

Table 3.5 List of references including information about which PFASs were used to construct the overall dataset.

Reference	Number of samples (total entries)	OC range (%)	PFBA	PFBS	PFPeA	PFHxA	PFHpA	PFHxS	PFOA	PFNA	PFOS	PFDA	PFUnA	PFDS	PFDoA
Chen et al., 2012	5 (5)	0.42 – 1.43									X				
Mejia-Avendaño et al., 2020	5 (15)	1.7 – 7.3							X		X	X			
Chen et al., 2013	5 (10)	0.52 – 16							X		X				
Enevoldsen and Juhler, 2010	2 (12)	0.42 – 1.0		X			X		X	X	X	X			
Guelfo and Higgins, 2013	3 (30)	0.8 – 4.5	X	X	X	X	X	X	X	X	X	X	X		
Higgins and Luthy, 2006	5 (24)	0.56 – 9.66							X	X	X	X	X	X	
Higgins and Luthy, 2007	1 (1)	4.34													X
Ellefson, 2000	4 (4)	1.3 – 2.8									X				
Du Pont, 2003	4 (4)	0.8 – 5.76							X						
Jeon et al., 2011	3 (6)	0.21 – 0.55							X		X				
Johnson et al., 2007	1 (1)	2.5									X				
Milinovic et al., 2015	2 (6)	0.2 – 3.9		X					X		X				
Knight et al., 2019	100 (100)	0.1 – 3.5							X						
You et al., 2010	15 (15)	0.16 – 1.49									X				
Kwadijk et al., 2013	1 (1)	2.6									X				
Martz et al., 2019	5 (5)	0.05 – 11.7							X						
Miao et al., 2017	10 (10)	0.52 – 5.76							X						
Ahrens et al., 2011	3 (5)	0.03 – 1.6							X		X				
Oliver, et al., 2020	19 (57)	0.1 – 11						X	X		X				
Wei et al., 2017	6 (6)	0.87 – 2.71									X				
Gredelj et al., 2020	1 (9)	1.43	X	X	X	X	X		X	X	X	X			
Pan et al., 2009	1 (1)	0.75									X				
Chen et al., 2009	1 (1)	0.91									X				
Brusseau et al., 2019	2 (2)	0.10 – 0.38									X				
Xiao et al., 2019	5 (5)	0.10 – 5.3							X						
Chen et al., 2016	1 (5)	2.52						X	X	X	X	X			
McLachlan et al., 2019	2 (24)	0.40 – 0.93	X	X	X	X	X	X	X	X	X	X	X		X
Aly et al., 2019	1 (6)	1.44		X				X	X	X	X				
Campos Pereira et al., 2018	1 (6)	45	X	X	X	X	X		X						
Xiang et al., 2018	1 (1)	0.69							X						
Zhi and Liu, 2018	1 (2)	47							X		X				
This study	7 (56)	1.6 – 41	X	X		X		X	X	X	X				X

The final model was externally validated elsewhere (Fabregat-Palau et al., 2021) in terms of excluding a representative third of the calibration data using the Kennard and Stone algorithm and use it as validation data (Kennard and Stone, 1969), while remaining two thirds of the data in calibration set. In this chapter, however, a third dataset, hereinafter referred as “validation dataset” was constructed with new sorption data available in the literature not included previously in the calibration dataset (**Table 3.6**).

Table 3.6 List of references informing which PFAS were included in the validation dataset.

Reference \ PFAS	Nguyen et al., 2020	Cai et al., 2022	Wang et al., 2022	Yin et al., 2022
Number of samples (total entries)	10 (154)	2 (16)	3 (6)	1 (7)
OC range (%)	0.08 – 4.9	2.6 – 4.9	2.0 – 4.0	0.37
PFBA	X			
PFPeA	X			
PFHxA	X	X		
PFHpA	X	X		
PFOA	X	X		X
PFNA	X	X		X
PFDA	X	X	X	X
PFUnA	X			X
PFDoA	X		X	
PFBS	X	X		
PFPeS	X	X		
PFHxS	X	X		
PFHpS	X	X		X
PFOS	X	X		X
PFNS	X	X		
PFDS	X			X

Acceptance criteria to include data in the validation dataset mimicked the abovementioned criteria. This dataset consisted in a total of 183 entries, including data from 16 soils in which both OC and silt+clay contents were reported. The database also included sorption data for PFCAs and PFSAAs with CF₂ units ranging 3 – 11 and 4 – 10, respectively.

To evaluate the predictive accuracy of the model, the root square mean error (RMSE) and the residual predictive deviation (RPD) were calculated as:

$$\text{RMSE} = \sqrt{\frac{\sum_{i=1}^n (\log K_{d,\text{measured},i} - \log K_{d,\text{predicted},i})^2}{N}} \quad (3.8)$$

where $\log K_{d,\text{measured}}$ and $\log K_{d,\text{predicted}}$ are the measured and predicted $\log K_d$ values, respectively, i is the entry being tested and N is the total number of entries included in the model. The RPD was calculated as:

$$\text{RPD} = \frac{\text{SD}}{\text{RMSE}} \quad (3.9)$$

where SD is the standard deviation of the original $\log K_{d,\text{measured}}$ data. RPD values therefore relate the variability of the original data to the variability of the prediction errors, and are indicative of the quality of the model. Despite RPD thresholds are subjective and dependent on imposed quality requirements, usually RPD values < 1.5 are considered as models with poor prediction ability; RPD values ranging from 1.5 to 2.0 are considered as models with acceptable prediction ability; RPD values ranging from 2.0 to 3.0 are considered as models with good prediction ability, and RPD values > 3.0 are considered as models with excellent prediction ability (Knight et al., 2019).

3.3. Results and discussion

3.3.1. PFASs sorption and desorption patterns in soils

K_d and $K_{d,des}$ values for each PFAS in each of the seven soils examined are summarized in **Table 3.7**, while sorption and desorption percentages are summarized in **Table 3.8**. Short-chained PFASs (PFBA, PFBS and PFHxA) generally had K_d values below 7 L kg^{-1} , regardless of the soil characteristics or the PFAS functional group, indicating their low sorption affinity in soils and their potentially high mobility (Gellrich et al., 2012). On the other hand, mid-chained PFASs (PFHxS, PFOA, PFOS and PFNA) had higher K_d values ranging from 2 to 295 L kg^{-1} depending on the PFAS and the soil characteristics, indicating higher sorption affinity in the examined soils and therefore a lower potential mobility. Sorption in low OC soils, as exemplified by the ALM soil, was significantly lower than in the rest of soils, and in general, K_d values increased with OC content. The long-chained PFAS, PFDoA, had the highest K_d values ($> 400 \text{ L kg}^{-1}$) among the PFASs tested, with a high K_d even for the low OC ALM soil, indicating a very low mobility of these PFASs.

K_d values for short-chained PFAS agreed with those obtained for $\leq 5 \text{ CF}_2$ in both mineral ($\text{OC} < 2\%$) soils and a single organic ($\text{OC} = 45\%$) soil sample, which ranged from 0.10 to 9.0 L kg^{-1} (Campos-Pereira et al., 2018; McLachlan et al., 2019). K_d values for the mid-chained PFHxS, PFOA and PFOS in ALM, DELTA2 and OVI01 soils were comparable to those previously reported values ($0.35 - 8.2 \text{ L kg}^{-1}$, $0.93 - 15 \text{ L kg}^{-1}$ and $3.8 - 103 \text{ L kg}^{-1}$ for PFHxS, PFOA and PFOS, respectively) in soils and sediments with $\text{OC} < 10\%$ (Higgins and Luthy, 2006; Oliver et al., 2020). Besides, PFHxS, PFOA and PFOS K_d values for the organic soils DUBLIN and KOM were within the K_d values range found in peat soils and pure humic acid samples ($10 - 15 \text{ L kg}^{-1}$, $18 - 71 \text{ L kg}^{-1}$ and $77 - 324 \text{ L kg}^{-1}$ for PFHxS, PFOA and PFOS, respectively) with OC contents ranging 45 – 54% (Campos-Pereira et al., 2022; Zhi and Liu, 2018).

Table 3.7 K_d and $K_{d,des}$ values of PFASs in the seven examined soils. The number of CF_2 in each PFAS is indicated into brackets.

Parameter	Soil	PFBA (3)	PFBS (4)	PFHxA (5)	PFHxS (6)	PFOA (7)	PFNA (8)	PFOS (8)	PFDoA (11)
K_d (L kg ⁻¹)	ALM	0.55	0.60	2.9	2.4	2.6	11	32	422
	DELTA2	0.89	1.6	2.5	4.1	3.9	35	76	623
	OVI01	0.33	1.4	1.2	5.4	7.1	39	110	738
	UIAR	0.91	1.5	2.6	18	26	96	144	$1.38 \cdot 10^3$
	BRA	1.2	3.0	5.4	17	27	117	171	$2.03 \cdot 10^3$
	DUBLIN	1.7	6.8	5.1	21	38	122	295	$1.84 \cdot 10^3$
	KOM	1.2	3.0	6.5	18	37	128	207	$3.08 \cdot 10^3$
$K_{d,des}$ (L kg ⁻¹)	ALM	N.Q.	N.Q.	N.Q.	4.4	18	35	43	761
	DELTA2	N.Q.	N.Q.	N.Q.	16	11	43	83	$6.59 \cdot 10^3$
	OVI01	N.Q.	N.Q.	9.1	7.7	12	57	107	$7.12 \cdot 10^3$
	UIAR	N.Q.	N.Q.	25	18	38	177	437	$9.38 \cdot 10^3$
	BRA	N.Q.	N.Q.	29	29	41	226	560	$1.27 \cdot 10^4$
	DUBLIN	N.Q.	N.Q.	32	41	61	262	760	$1.32 \cdot 10^4$
	KOM	N.Q.	N.Q.	23	37	48	297	749	$1.79 \cdot 10^4$

N.Q.: Not quantifiable

K_d values for mid-chained PFASs were higher than the corresponding short-chain PFASs, indicating that sorption was favoured by greater PFAS hydrophobicity. Despite having the same CF_2 , PFOS had higher K_d values than PFNA, suggesting an additional influence of the hydrophilic functional group in sorption, with a slightly higher affinity of the sulfonate group than the carboxylate group. These differences between the sorption affinity for PFOS and PFNA have also been described elsewhere (Higgins and Luthy, 2006; Enevoldsen and Juhler, 2010) and confirm that PFCAs have a higher mobility than PFASs (Sepulvado et al., 2011). K_d values for PFDoA agreed with those reported in both mineral ($OC < 2\%$) soils and an organic ($OC = 45\%$) soil sample, which ranged $150 - 9,000 \text{ L kg}^{-1}$ (Campos-Pereira et al., 2018; McLachlan et al., 2019).

Sorption percentages reported in **Table 3.8** followed the same trend as the respective K_d values, with PFAS sorption percentages increasing as the number of CF_2 units increased. Sorption percentages were as low as $< 10\%$ for short-chained PFASs and reached values $> 99\%$ for PFDoA. The reversibility of the sorption process was also quantified in terms of the hysteresis coefficient (Equation 1.3). $K_{d,des}$ values derived from the batch experiments are reported in **Table 3.7** and were higher than the corresponding K_d values. As with K_d values, $K_{d,des}$ increased with increasing PFASs chain length. The hysteresis coefficient was larger than one in all cases. Desorption percentages therefore decreased from $25 - 50\%$ for short-chained PFAS to less than 1% for PFDoA (see **Table 3.8**). These results indicate the irreversibility of PFAS sorption in soils and sediments, and are in agreement with previous studies (Enevoldsen and Juhler, 2010; Miao et al., 2017).

Table 3.8 %S and %D of PFASs in the seven examined soils. The number of CF₂ in each PFAS is indicated into brackets.

Parameter	Soil	PFBA (3)	PFBS (4)	PFHxA (5)	PFHxS (6)	PFOA (7)	PFNA (8)	PFOS (8)	PFDoA (11)
%S	ALM	5.2	5.7	23	19	21	52	76	98
	DELTA2	8.2	14	20	29	28	78	88	98
	OVI01	3.2	12	11	35	42	80	92	98
	UIAR	8.3	13	21	64	72	91	94	> 99
	BRA	11	23	35	63	73	92	95	> 99
	DUBLIN	15	41	34	68	79	92	97	> 99
	KOM	11	23	39	64	79	93	95	> 99
%D	ALM	N.Q.	N.Q.	N.Q.	70	36	23	19	0.70
	DELTA2	N.Q.	N.Q.	N.Q.	39	48	19	11	0.05
	OVI01	N.Q.	N.Q.	53	57	45	15	8.6	0.05
	UIAR	N.Q.	N.Q.	29	38	21	5.3	2.3	0.03
	BRA	N.Q.	N.Q.	26	25	20	4.3	1.8	0.03
	DUBLIN	N.Q.	N.Q.	24	20	13	3.7	1.3	0.03
	KOM	N.Q.	N.Q.	30	21	18	3.2	1.3	0.02

N.Q.: Not quantifiable

3.3.2. Correlation of sorption and desorption parameters with soil OC

Given the importance of soil OC content for PFASs sorption and desorption parameters, especially for mid- and long-chained PFASs, K_d values reported in **Table 3.7** were further examined for their dependence on the fraction of OC (f_{OC}), expressed as kg of OC per kg of soil. We additionally examined the relative contribution of OC and mineral binding sites to the overall sorption. Specifically, iron, aluminium and titanium oxides have all been reported to be able to interact with PFASs and to participate in PFAS sorption (Lu et al., 2016). Although a preliminary overview of our results showed that K_d values were correlated with extracted amorphous Fe content, this correlation might be attributed to the correlation between extracted Fe and soil OC ($r^2 = 0.81$, $p < 0.01$, data derived from **Table 3.1**). This conclusion agrees with previous studies which observed no correlation between K_d and Fe content in soils where OC was the primary driver of PFASs sorption (Higgins and Luthy, 2006; Miao et al., 2017).

The OC-normalized sorption coefficient (K_{OC} , L kg OC⁻¹) is defined as the ratio between K_d and the soil f_{OC} (OECD, 2000).

$$K_{OC} = \frac{K_d}{f_{OC}} \quad (3.10)$$

According to Equation 3.10, a K_{OC} value can be derived for a single soil sample, or contrarily, as the slope of the K_d vs. f_{OC} plot when considering different soils with a wide range of OC. However, Equation 3.10 considers that the sorption is driven entirely by soil OC, and it may overestimate K_{OC} if the soil mineral fraction plays a role in the sorption, a situation that several authors have pointed out for PFASs in mineral soils (Li et al., 2018; Knight et al., 2019; Wang et al., 2021). Thus, a constant term has to be added in equation 3.10 referring to the sorption contribution of non-OC soil fractions, which may be attributed to the soil mineral fraction ($K_{d,MIN}$, L kg⁻¹) (Milinovic et al., 2015; Sorengard et al., 2019):

$$K_d = K_{d,ORG} + K_{d,MIN} = K_{OC} f_{OC} + K_{d,MIN} \quad (3.11)$$

Hence, $K_{d,MIN}$ can be quantified by the y-intercept of the correlation at $f_{OC} = 0$. In this scenario, sorption is driven entirely by the mineral fraction ($f_{MIN} = 1$) and thus $K_{d,MIN}$ could be directly considered as the normalized sorption coefficient referring to the mineral phase ($K_{d,MIN} \approx K_{MIN}$, L kg mineral⁻¹). **Figure 3.2** show the application of Equation 3.11 for deriving K_{OC} and K_{MIN} for a set of soils with a given OC range.

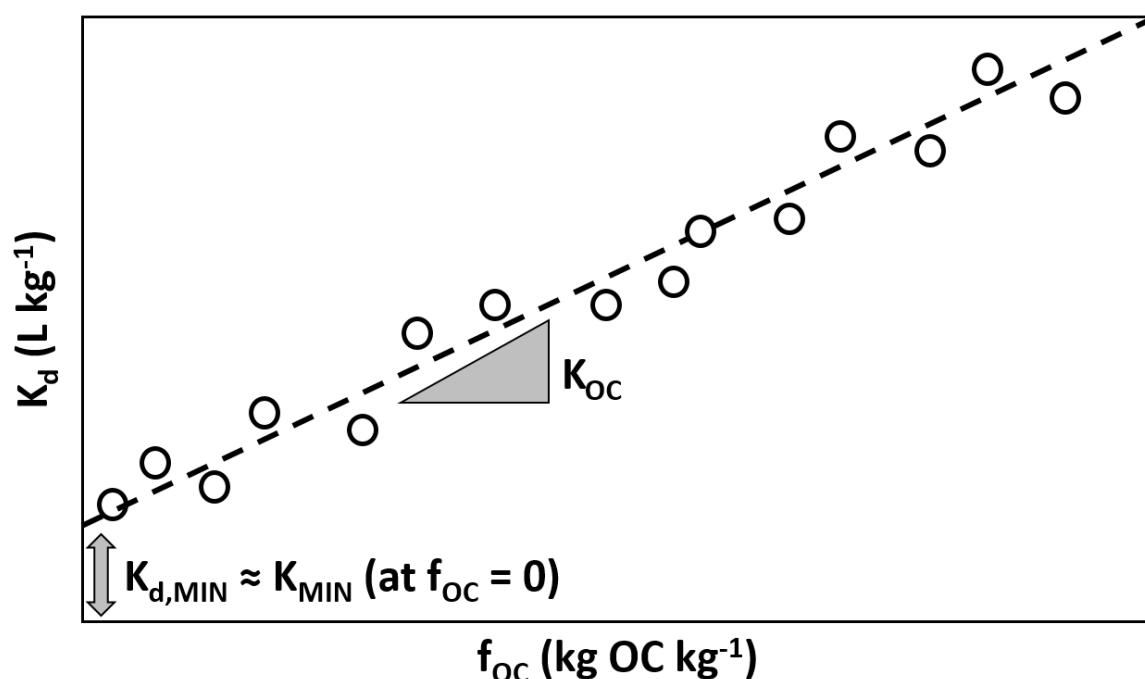


Figure 3.2 Derivation of K_{OC} and K_{MIN} values for a set of soils with a given OC range.

The K_{OC} and K_{MIN} values obtained for each PFAS after applying Equation 3.11 using both the own and overall datasets are summarized in **Table 3.9**. To our knowledge, although other authors have attempted to calculate different mineral-normalized sorption coefficients (Sorengard et al., 2019; Wang et al., 2021), this is the first time that mineral-normalized sorption coefficients values have been calculated from data assembled from the literature. Significant correlations for each PFAS ($p < 0.05$) were obtained between K_d and f_{OC} for both datasets.

Table 3.9 K_{OC} and K_{MIN} values for PFASs derived from the own and overall datasets. Standard errors of parameters are given into brackets.

PFAS	Own dataset (n=7)		Overall dataset		
	K_{OC}	K_{MIN}	K_{OC}	K_{MIN}	n
PFBA	2.3 (0.7)	0.44 (0.19)	2.9 (0.6)	0.43 (0.13)	13
PFBS	10 (3.8)	0.41 (0.11)	11 (1.5)	0.44 (0.29)	19
PFPeA	N.A.	N.A.	15 (2.4)	0.46 (0.42)	7
PFHxA	10 (3.1)	1.5 (0.83)	15 (1.8)	0.46 (0.41)	14
PFHpA	N.A.	N.A.	50 (1.3)	N.Q.	10
PFHxS	47 (5.6)	1.6 (1.5)	50 (2.2)	1.2 (0.29)	33
PFOA	94 (5.7)	N.Q.	107 (4.5)	3.3 (0.34)	182
PFOS	496 (98)	36 (27)	609 (19)	9.4 (1.8)	95
PFNA	300 (16)	11 (4.4)	324 (10)	2.0 (1.7)	20
PFDA	N.A.	N.A.	604 (221)	14 (7.7)	19
PFUnA	N.A.	N.A.	2,450 (510)	25 (20)	8
PFDS	N.A.	N.A.	4,600 (560)	N.Q.	5
PFDoA	5,440 (1,030)	208 (178)	5,370 (670)	229 (152)	10

N.A.: Not analysed; N.Q.: Not quantifiable;

Derived K_{MIN} values of PFASs were lower than the respective K_{OC} values, indicating that PFASs have a higher sorption affinity to the OC sites present in the soil. The application of Equation 3.11 to the overall dataset allowed us to derive K_{OC} and K_{MIN} for PFASs not included in our experiments, such as PFPeA, PFHpA, PFDA, PFUnA, and PFDS. Since the K_d values of the overall dataset were obtained under a wide range of experimental conditions, the K_{OC} and K_{MIN} values derived were affected by the intrinsic variability of the literature data. Besides, K_{MIN} values derived from the overall dataset can be considered more representative than those derived from ours, as the overall dataset contained a higher number of soils with low OC.

The K_{OC} values of PFASs we obtained were lower than K_{OC} values calculated solely based on Equation 3.10 reported elsewhere (Enevoldsen and Juhler, 2010; Guelfo and Higgins, 2013; McLachlan et al., 2019) but comparable to reported K_{OC} derived by considering sorption at mineral sites as well (Higgins and Luthy, 2006; Milinovic et al., 2015). Direct comparisons with previously reported K_{MIN} values were not possible. However, K_d data of PFASs are available for pure mineral phases, such as phyllosilicate minerals, which can serve as analogues for soils with $f_{OC} = 0$. The overall K_d in these materials therefore equals $K_{d,MIN}$ and, consequently, K_{MIN} . For the mid-chained PFOS and PFOA, two of the most frequently studied PFAS, the K_{MIN} values that we derived from the overall dataset were 9.4 and 3.3 respectively. These values are in agreement with the range of K_d values obtained for PFAS on pure phyllosilicate minerals (**Table 3.10**), but slightly lower than other silt+clay normalized sorption coefficient reported for PFOS (19 L kg silt + clay⁻¹, Wang et al., 2021). Furthermore, K_{MIN} values for PFOS were higher than for PFNA, in agreement with previous observations (Xiao et al., 2011). Besides, K_{MIN} values for PFASs with ≤ 5 CF₂ were lower than 1; this is consistent with the hypothesis that sorption of short-chained PFASs is not thermodynamically favourable under systems with low ionic strength (1 - 10 mM) (Xiao et al., 2011), which are the most common scenarios of the experiments used to construct the overall database.

Table 3.10 K_d values (equivalent to K_{MIN}) for PFAS in pure clay minerals.

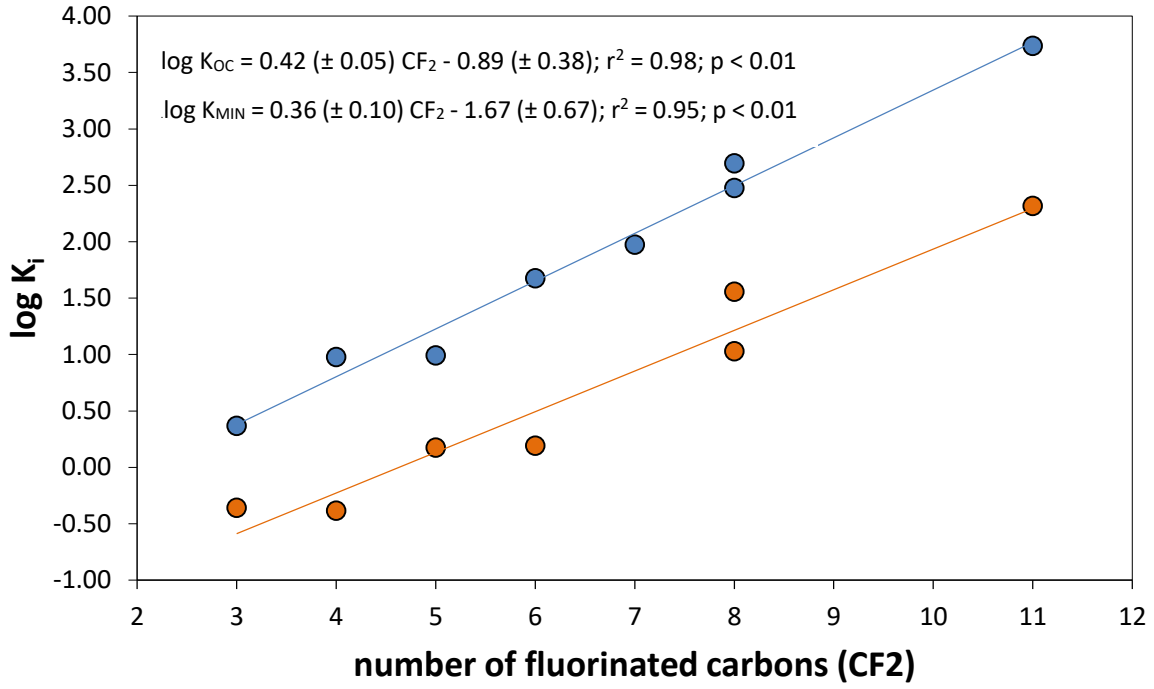
PFAS	Mineral	K_d (L kg ⁻¹)	Reference
PFOA	Kaolinite	0.40	Jeon et al., 2011
	Kaolinite	2.3	Xiao et al., 2011
	Montmorillonite	1.3	Jeon et al., 2011
	Montmorillonite	4.4	Tian et al., 2016
	Illite	0.13	Li et al., 2012
PFOS	Kaolinite	2.7	Jeon et al., 2011
	Kaolinite	5.3	Johnson et al., 2007
	Kaolinite	14	Xiao et al., 2011
	Montmorillonite	5.0	Jeon et al., 2011
PFNA	Kaolinite	5.5	Xiao et al., 2011
PFDA	Kaolinite	20	Xiao et al., 2011
PFUnA	Kaolinite	50	Xiao et al., 2011

$K_{OC,des}$ and $K_{MIN,des}$ were calculated similarly using our own desorption data. For all PFAS, $K_{OC,des}$ and $K_{MIN,des}$ values were higher than the respective K_{OC} and K_{MIN} values, further demonstrating sorption irreversibility. Besides, $K_{OC,des}$ values were similar to other reported values in the literature (Enevoldsen and Juhler, 2010; Sepulvado et al., 2011). No similar comparison could be performed for PFAS $K_{MIN,des}$ as no data on either the $K_{MIN,des}$ or $K_{d,des}$ of pure mineral phases were available in the literature. Because desorption data were scarce in the literature and only available for a few PFASs, all subsequent analyses focus solely on sorption data.

3.3.3. Correlation of K_{OC} and K_{MIN} with PFAS physicochemical properties

As shown in **Table 1.1**, the hydrophobicity of the PFASs, expressed as $\log K_{OW}$, increased linearly with each fluorinated carbon added to the alkyl chain ($\log K_{OW} = 0.71 (\pm 0.08) \times \text{number of } CF_2$, $r^2 = 0.97$, $p < 0.001$, $n = 13$). Due to this strong correlation, the effect of PFAS properties on K_{OC} and K_{MIN} can reasonably be evaluated based on either the number of CF_2 or $\log K_{OW}$. In principle, K_{OW} values better differentiate PFASs that have the same number of CF_2 but different functional groups, such as PFOS and PFNA, but $\log K_{OW}$ values vary significantly in the literature depending if they are experimental or calculated values. Therefore, correlations were performed using the number of CF_2 , an easily available parameter that is descriptive of PFAS hydrophobicity. As shown in **Figure 3.3**, the K_{OC} and K_{MIN} values derived from both our experimental and literature-assembled datasets were logarithmically correlated with the number of CF_2 of the PFASs.

A)



B)

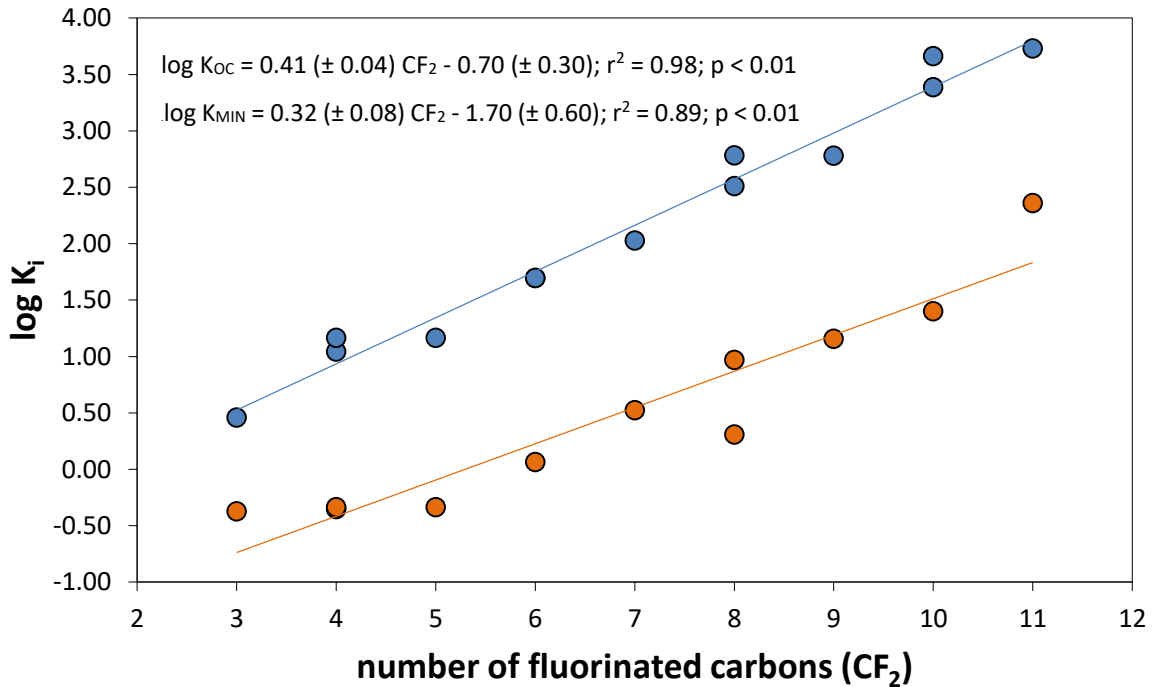


Figure 3.3 Correlations between K_{OC} (blue) and K_{MIN} (orange) values and PFAS CF_2 derived from the own (A) and overall (B) dataset.

The correlations were significant, and both the slope and the y-intercept were comparable between datasets. Equation 3.12 and Equation 3.13 show the relationships between the number of fluorinated carbons and each of K_{OC} and K_{MIN} derived from the overall dataset:

$$\log K_{OC} = 0.41 (\pm 0.04) \times \text{number of CF}_2 - 0.70 (\pm 0.30); r^2 = 0.98; p < 0.001 \quad (3.12)$$

$$\log K_{MIN} = 0.32 (\pm 0.08) \times \text{number of CF}_2 - 1.70 (\pm 0.60); r^2 = 0.89; p < 0.001 \quad (3.13)$$

The high quality of these correlations allowed us to derive predicted K_{OC} and K_{MIN} values for PFASs for which only the number of CF_2 units were available. In agreement with previous findings (Milinovic et al., 2015), K_{OC} values increased with higher PFAS hydrophobicity, which strongly suggested that sorption to OC was mainly driven by hydrophobic interactions. Humic substances, which are the main organic compounds present in the soil organic phase, often possess hydrophilic moieties that can also interact with PFASs through mechanisms such as hydrogen bonding or divalent cation bridging (Du et al., 2014). However, experiments testing the sorption of PFASs on humic acids extracted from soils have shown that these hydrophilic contributions are not predominant, thus confirming that hydrophobic interactions are the main sorption mechanism (Xiang et al., 2018; Zhao et al., 2014).

K_{MIN} values also increased with increasing PFAS chain length, a finding that is comparable to the K_d increase reported for the C_7 – C_{10} PFAS series on kaolinite clay (Xiao et al., 2011). The interaction between the negatively charged kaolinite surface and the negatively charged PFAS could be explained by the presence of divalent cations either acting as an intermediate bridge in electrostatic interactions (Du et al., 2014), which may explain the positive effects of the presence of calcium on the K_d (PFAS) (Higgins and Luthy, 2006), or inhibiting the negative repulsions within the electrical double layer of the mineral surface (Xiao

et al., 2011). However, spectroscopic studies pointed to ligand exchange and acid/base interactions with clay surfaces, being sorption affected by both PFAS hydrophobic chain length and functional group (Zhang et al., 2014). In agreement with these findings, recent computational studies pointed to a direct coordination of carboxylate and sulfonate groups with hydroxyl groups present in the kaolinite surface, thus avoiding hydrophobic domains, and the formation of aggregated clusters of PFAS molecules varying in size (Loganathan and Wilson, 2022). The hydrophobic interactions among PFAS molecules, stabilized with increasing chain length, may therefore favour the formation of clusters of PFAS molecules and explain the increase in K_{MIN} values with the CF_2 of the PFAS. Contrarily, computational studies have identified the hydrophobic patches of montmorillonite clay as the primary adsorption domains and the stabilization of adsorption enthalpy in the presence of cations (Willemsen and Bourg, 2021). Nevertheless, further mechanistic insights between negatively charged PFASs and different clay minerals are still required.

Overall, these results suggest that both sorption of the PFASs in the mineral and organic phases of the soil become more favourable as the PFAS chain length increases. However, the ratio between K_{OC} and K_{MIN} values also increased with increasing PFAS chain length, indicating that long-chained PFASs have a higher affinity for the organic phases than mid- and short-chained PFASs.

3.3.4. Exploration of the contribution of humic substances in PFASs sorption

According to the importance of soil OC on the sorption of PFASs in soils, we aimed to evaluate the specific contributions of each organic species (humins and humic+fulvic acids) on the overall K_d (PFAS). This evaluation was performed in two organic soil samples previously tested for PFAS sorption (BRA and KOM) since its humin and humic+fulvic contents have been previously characterized (Rigol et al., 1998).

Table 3.11 summarize these additional characterizations performed in both BRA and KOM soils. Both soils had a similar humic and fulvic acid content (about 50% w/w) but KOM soil presented a higher humin content. Fat and waxes contents were negligible ($\leq 3\%$) in both soils.

Table 3.11 Additional fat, waxes, humin, humic and fulvic acids characterizations.

Soil	OC	OM	Fats and waxes	Humic+fulvic acids	Humin	Mineral matter
	(%)	(%)	(%)	(%)	(%)	(%)
BRA	32	67	2.2	52.9	10.1	34.8
KOM	41	84	3.1	54.5	21.8	20.7

It has been previously hypothesized in the literature for a peat soil sample that short-chain PFASs are more prone to sorb in the humic and fulvic fractions of the soil, whereas long-chained PFASs have a higher sorption affinity to the humin fraction (Campos-Pereira et al., 2018). In order to confirm this hypothesis, the relative contribution of the humin and humic+fulvic acids on the overall sorption were assessed by deriving humin (K_{Humin} , L kg humin⁻¹) and humic+fulvic ($K_{\text{Humic+Fulvic}}$, L kg humic + fulvic acids⁻¹) normalized sorption coefficients for each PFAS using a two compartment distribution sorption model. This approach to derive normalized sorption coefficients has been previously used for PFOS to derive normalized sorption coefficients to the OC and silt + clay fractions of the soil (Wang et al., 2021).

Due to the organic nature of these peat soils, the relative contribution of the mineral phase in sorption is expected to play a minor role (Campos-Pereira et al., 2022; Wang et al., 2021). Therefore, the organic phase is expected to be the only sorption domain for PFASs, and accordingly, K_d in these scenarios may be expressed for each PFAS in each soil as shown in Equations 3.14 and 3.15:

$$K_{d,BRA} = K_{Humin} \times f_{Humin (BRA)} + K_{Humic+Fulvic} \times f_{Humic+Fulvic (BRA)} \quad (3.14)$$

$$K_{d,KOM} = K_{Humin} \times f_{Humin (KOM)} + K_{Humic+Fulvic} \times f_{Humic+Fulvic (KOM)} \quad (3.15)$$

where f_{Humin} and $f_{Humic+Fulvic}$ are the humin and humic+fulvic acids fractions, respectively, expressed as grams of each fraction per gram of organic matter. Both, K_{Humin} and $K_{Humic+Fulvic}$ were deduced for each PFAS by solving the respective system of equations, and results are summarized in **Table 3.12**:

Table 3.12 Derived K_{Humin} and $K_{Humic+Fulvic}$ values for different chain-length PFAS.

	K_{Humin}	$K_{Humic+Fulvic}$
PFBA	1.1	1.2
PFBS	2.9	3.0
PFH _x A	12	4.1
PFH _x S	18	17
PFOA	90	15
PFOS	191	103
PFNA	404	126
PFDoA	8,806	744

Despite the lack of sorption data of different chain-length PFAS in humic substances, the obtained K_{Humin} and $K_{Humic+Fulvic}$ values for PFH_xS, PFOA and PFOS were relatively close to those reported in a humin sample and humic acid samples extracted from soils (Jia et al., 2010; Xiang et al., 2018; Zhao et al., 2014; Zhi and Liu, 2018). K_{Humin} and $K_{Humic+Fulvic}$ are affected by intrinsic sources of variability, including the chemical nature of each fraction (*i.e.*, OC content; amount of functionalities), the experimental conditions used to derive the sorption data (*i.e.*, composition of the aqueous solution) and the methodology used to derive such coefficients. Whereas K_{Humin} and $K_{Humic+Fulvic}$ normalized sorption coefficients could be reliably derived by correlating soil K_d values with its respective varying humin and humic+fulvic contents, as well as performing sorption experiments with pure organic isolates,

the lack of soil characterization data in this regard and the limited number of studies evaluating sorption of different chain-length PFASs in soil organic components, respectively, hamper this analysis. Hence, here we used a two compartment distribution sorption model as an approach to preliminary derive K_{Humin} and $K_{\text{Humic+Fulvic}}$ values, although a deeper analysis with a higher number of soils would be required. The resulting K_{Humin} and $K_{\text{Humic+Fulvic}}$ reported in **Table 3.12** were logarithmically correlated with the number of CF_2 of the PFAS (**Figure 3.4**). As with K_{OC} , significant linear correlations between both $\log K_{\text{Humin}}$ and $\log K_{\text{Humic+Fulvic}}$ with CF_2 were obtained. This further confirmed that hydrophobic interactions are the main interaction mechanisms between PFASs and SOM (Zhao et al., 2014). Besides, **Figure 3.4** revealed a stronger sorption affinity of mid- (CF_2 6 – 9) and long-chained ($\text{CF}_2 > 9$) PFAS on the humin fraction of the soil, while short-chained ($\text{CF}_2 \leq 5$) PFAS had comparable or even higher sorption affinity for the humic and fulvic soil fractions, thus confirming previous hypothesis (Campos Pereira et al., 2018).

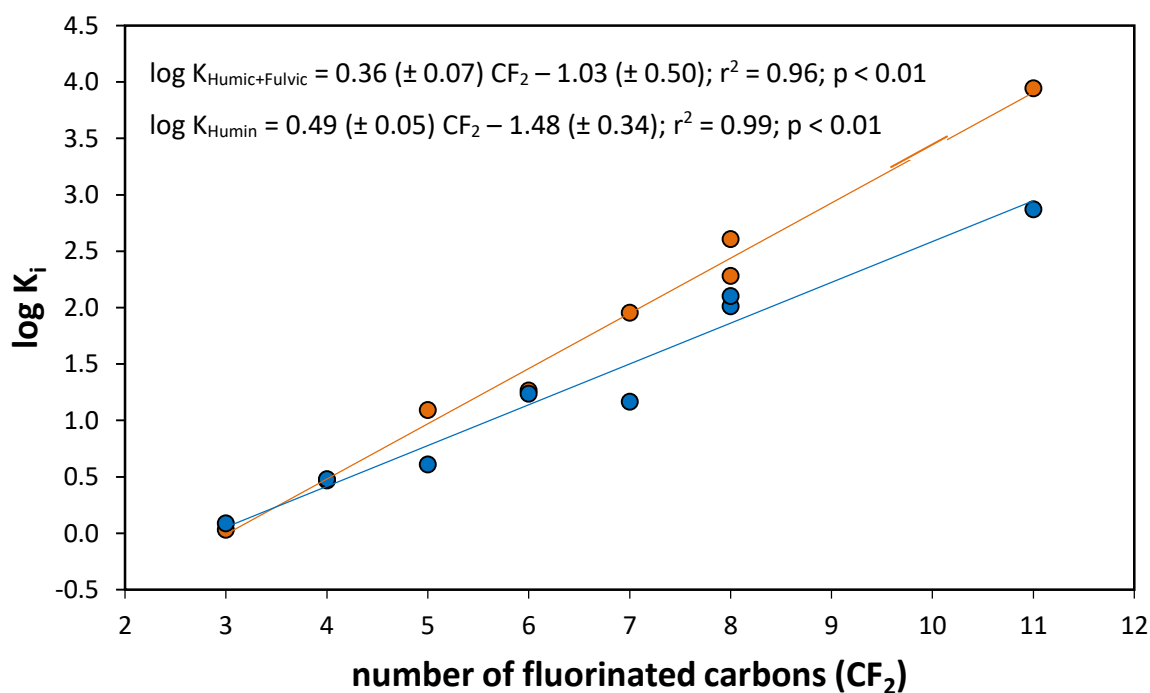


Figure 3.4 Correlations between $\log K_{\text{Humin}}$ (orange) and $\log K_{\text{Humic+Fulvic}}$ (blue) with PFAS CF_2 .

Lastly, we used the relationships between K_{Humin} and $\log K_{\text{Humic+Fulvic}}$ with CF_2 to calculate the relative contribution of these fractions on the overall K_d for KOM and BRA soils. We selected PFBA, PFOA, PFOS and PFDoA as representatives of short-, mid- and long-chained PFASs (**Figure 3.5**). The humin fraction contributed up to 30% for PFBA, and increased up to 80% for PFDoA. The contribution of the humin fraction in K_d for KOM soil was higher than BRA due to its higher humin content. The relative contribution of different humic substances on the overall K_d of different chain-length PFASs may be of interest to better assess the influence of the soil OC in the sorption process of PFASs, especially in organic soils.

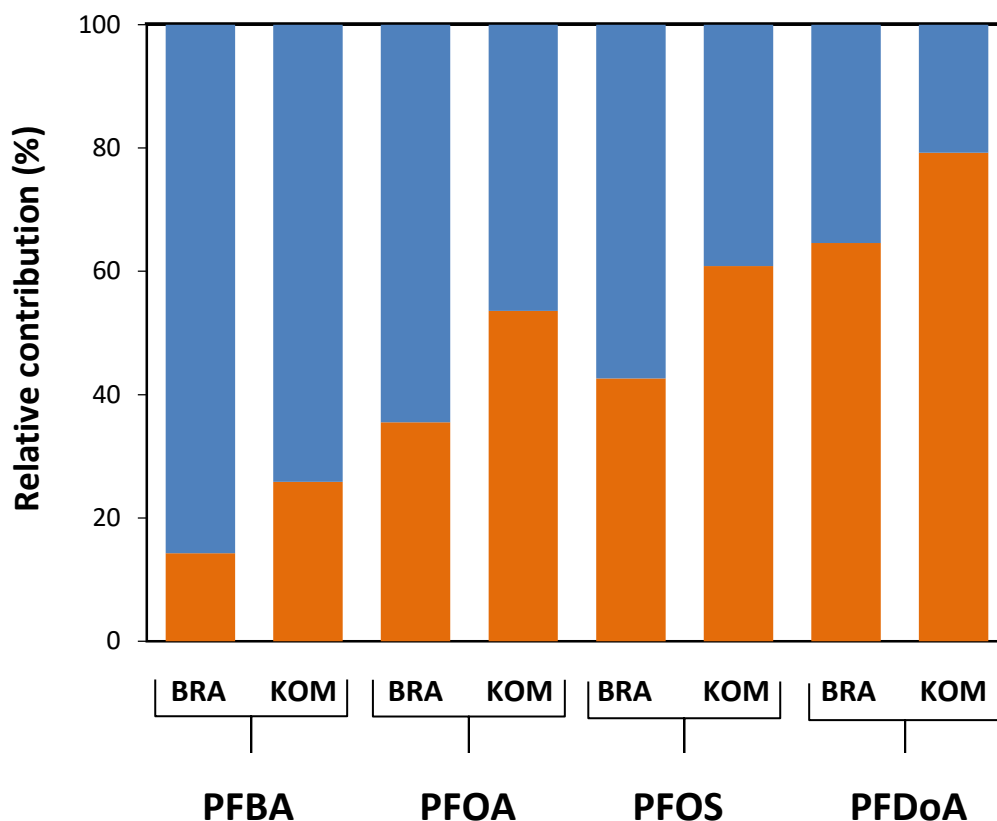


Figure 3.5 Contributions of the humin (orange) and humic + fulvic acids (blue) fractions in the overall K_d for PFBA, PFOA, PFOS and PFDoA.

3.3.5. Development and validation of a PFASs sorption model in soils

To develop a parametric model to predict K_d (PFCA) and K_d (PFSA) in soils based only on the number of CF_2 of PFAS and on a few physicochemical properties of the soil, we used the correlations presented in Equation 3.12 and Equation 3.13 as descriptors of the sorption on the OC and mineral pool sites, respectively. Based on a multiple regression analysis, Li et al. concluded that soil OC, clay content, and pH all have a significant effect on the K_d (PFAS) (Li et al., 2018). Similarly, Knight et al. found that OC and the mineral silt and clay fractions contributed significantly to the sorption of PFOA in a large number of mineral soils (Knight et al., 2019). The silt and clay fractions have also been reported to have a positive effect on the K_d of PFOS, PFOA and PFHxS in sediments (Oliver et al., 2020), and a study of PFOA sorption on various soil size fractions confirmed that K_d decreases along the sequence: clay > fine silt > coarse silt > fine sand > coarse sand (Xiang et al., 2018). Indeed, Wang and co-workers derived a silt+clay normalized sorption coefficient using a three-compartment distribution model to account for the contribution of the mineral fraction to the overall K_d (Wang et al., 2021).

Preliminary attempts to model the K_d values of PFASs in soils based only on CF_2 and OC led to an underestimation of K_d values in mineral soils, thus highlighting that the mineral contribution needed to be considered in the modelling. K_{MIN} values were derived in Section 3.3.2 at $f_{OC} = 0$ after correlating K_d values derived from soil with their respective f_{OC} , as detailed in Equation 3.11. However, to quantify the contribution of the mineral phase on the overall K_d , K_{MIN} values needs to be weighted by the amount of mineral fraction (f_{MIN} , expressed as kg of mineral phase per kg of soil).

Therefore, the K_d of PFASs was further modelled from a separate contribution of the organic and mineral phases ($K_{d,ORG}$ and $K_{d,MIN}$ respectively), regardless of the f_{OC} value:

$$K_d = K_{OC} f_{OC} + K_{MIN} f_{MIN} \quad (3.16)$$

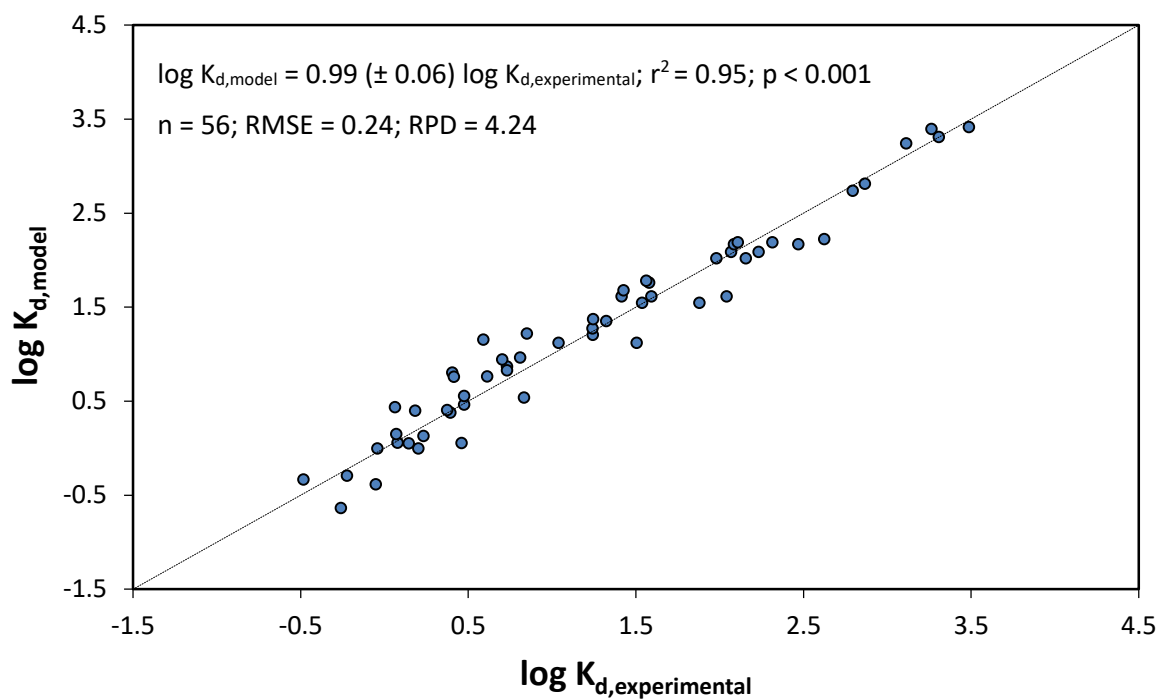
According to the above discussion, the mineral phases mainly responsible for PFAS sorption are silt and clay. Then, f_{MIN} should be limited to the silt+clay fraction, $f_{\text{S+C}}$, expressed as kg of silt+clay per kg of soil, and the K_{MIN} values reported in **Table 3.9** could be considered as silt+clay normalized sorption coefficients ($K_{\text{S+C}}$, L kg silt+clay⁻¹), leading to the following model based on the CF₂ of the PFAS and OC, and silt+clay content s:

$$K_d = K_{\text{OC}} f_{\text{OC}} + K_{\text{MIN}} f_{\text{S+C}} = 10^{(0.41 \text{ number of CF}_2 - 0.70)} f_{\text{OC}} + 10^{(0.32 \text{ number of CF}_2 - 1.70)} f_{\text{S+C}} \quad (3.17)$$

We preliminary tested the predictive ability of this model using only the entries from our datasets that contained data for both soil OC and textural fractions. The predictive accuracy for the model was quite satisfactory both for our experimental data and for the overall dataset (see **Figure 3.6A** and **Figure 3.6B**, respectively). The model's RMSE and RPD values when tested with the overall data (0.39 and 1.90, respectively) indicated that its quality was acceptable. Moreover, the model's predictive ability increased if the K_{OC} and K_{MIN} values for each PFAS, reported in **Table 3.9**, were used rather than the K_{OC} and K_{MIN} values predicted from the correlations with the number of CF₂ ($\log K_{d,\text{model}} = 0.92 (\pm 0.05) \times \log K_{d,\text{experimental}}$, $r^2 = 0.78$, $p < 0.001$, $n = 353$). In that case, RMSE and RPD values were 0.37 and 1.94, respectively. However, such model cannot be applied to PFASs for which no K_{OC} and K_{MIN} data are available.

Although the inclusion of other soil properties (*e.g.*, the status of divalent metal ions, pH, or metal oxide content) could be examined to further improve the established prediction model, this would also increase the model's complexity without enhancing its range of application. According to the RPD of the model derived from the overall dataset (**Figure 3.6B**), and although some scattering of the data was observed, this model is useful to estimate K_d values for categorizing scenarios with very low ($K_d < 10$ L kg⁻¹), medium (K_d of 10 – 1,000 L kg⁻¹), and high ($K_d > 1,000$ L kg⁻¹) sorption.

A)



B)

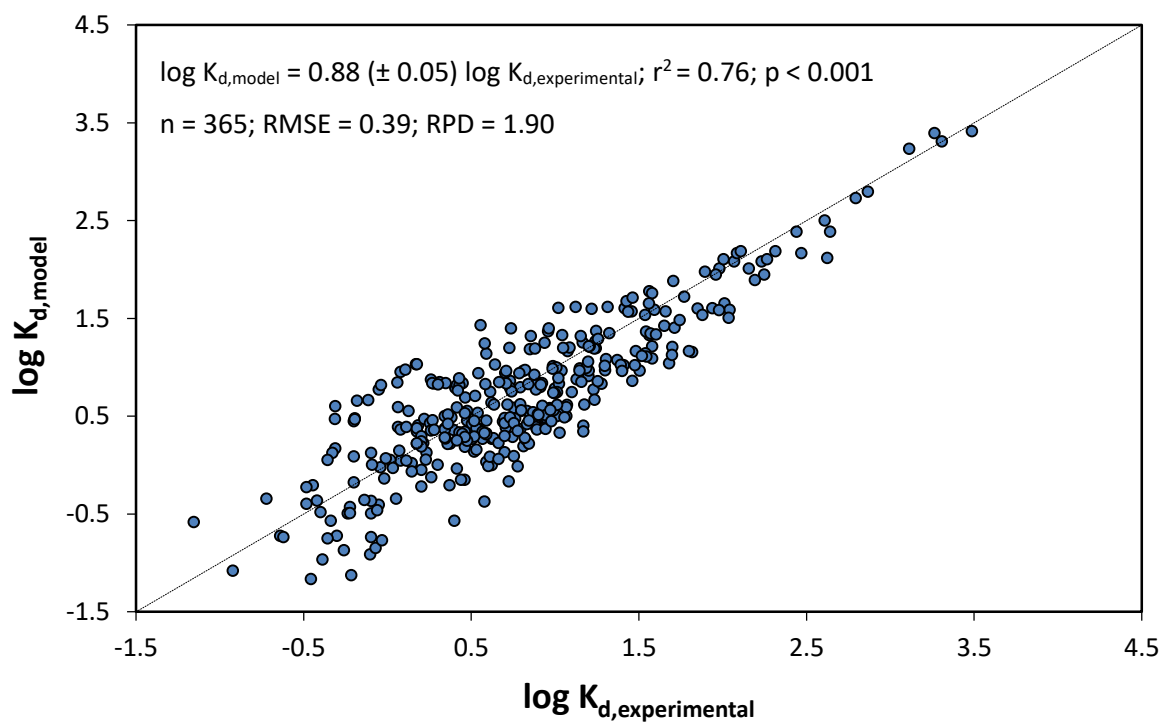


Figure 3.6 Prediction ability of the model for the own (A) and overall (B) datasets.

The resulting K_d (PFAS) prediction model (Equation 3.17) was then tested against the validation dataset (which gathered data not contemplated for the model construction, see **Table 3.6**) and resulted in the following prediction (**Figure 3.7**):

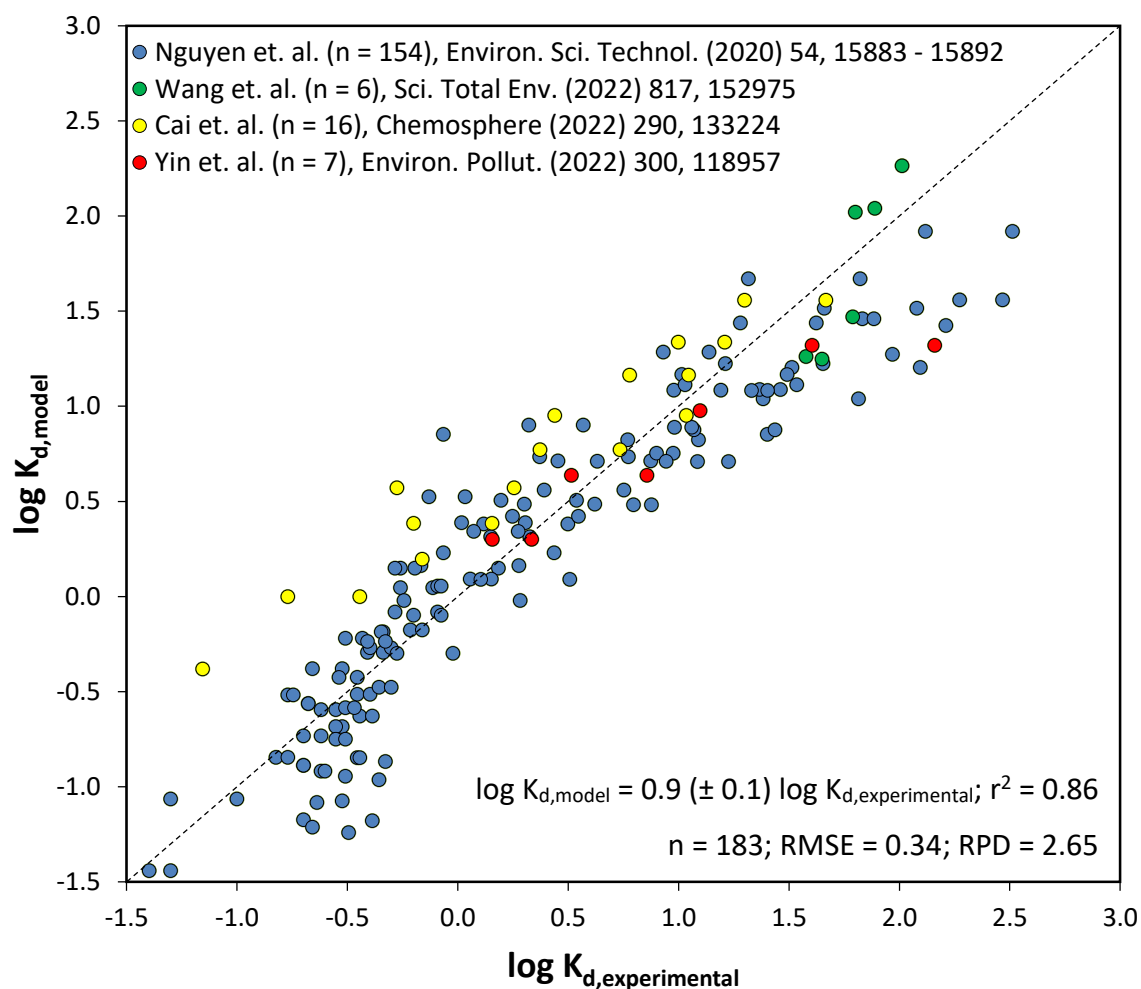


Figure 3.7 Prediction ability of Equation 12 against the external validation dataset.

The prediction ability of Equation 3.17 against the external validation data resulted in a slope and y-intercept statistically equal to one and zero, respectively, described 86% of the data variance and obtained RMSE and RPD values of 0.40 and 2.25, respectively, indicating that the model resulted in a good prediction quality. This further ensured the applicability of the model to roughly predict K_d (PFAS) values in soils using only a few soil and PFAS physicochemical properties.

3.3.6. Assessment of the contribution of organic and mineral phases on K_d

Although OC sites have a higher affinity for PFASs sorption than silt+clay sites (that is, K_{OC} is higher than K_{MIN}), the relative amount of OC and mineral sites also influences the total K_d (PFAS) in a given soil. Thus, mineral sites may govern PFAS sorption in mineral soils with low OC, especially in the case of short and mid-chained PFASs. We therefore used our well-established prediction model to quantify the actual distribution of PFASs among OC and silt+clay sites. The proportional contribution of mineral sites, which we quantified as the percentage of $K_{d,MIN}$ with respect to the overall K_d ($\% K_{d,MIN}$), was calculated using the K_d values predicted from the overall dataset. We specifically evaluated $\% K_{d,MIN}$ for PFBS, PFOA, PFOS and PFDoA, which served as representatives of short-, mid-, and long-chained PFASs. Results were grouped by soil classes defined by their OC content, as shown in **Table 3.13**.

Sorption at OC sites was predominant ($\% K_{d,MIN} \leq 3$) for all the PFASs in soils with OC > 10%. In soils with a lower OC content, especially < 2%, the contribution of mineral sites ($\% K_{d,MIN}$) varied significantly with the soil and PFAS properties, as the $\% K_{d,MIN}$ values depended on the silt+clay content (higher $\% K_{d,MIN}$ for soils with higher silt+clay content). Thus, $\% K_{d,MIN}$ increased with the silt+clay content, especially for the soils with OC < 2% and the short-chained PFASs. Hence, the model was not only capable of roughly predicting K_d (PFAS) values in soils, but also allowed to quantify the contribution of the organic and mineral soil phases to the overall K_d . Despite this relatively higher PFASs affinity for mineral sites in low OC soils, we note that low OC soils had generally low overall K_d values of PFASs, indicating that in these soils PFASs contamination might result in a higher environmental risk.

Table 3.13 Contribution of the mineral sorption sites to the overall K_d for different OC-content soils and PFASs.

Soil group (% OC)	PFBS			PFOA			PFOS			PFDoA		
	n	K_d	% $K_{d,MIN}$	n	K_d	% $K_{d,MIN}$	n	K_d	% $K_{d,MIN}$	n	K_d	% $K_{d,MIN}$
< 2	8	0.07-0.8	20-95	119	0.5-15	3 - 93	44	1.8-48	3 - 90	2	156-422	12 - 13
2 – 10	4	0.8-2.4	18-37	28	0.9-20	3 - 43	23	14-110	3 - 37	3	407-738	3 – 7
> 10	4	1.5-6.8	≤ 3	6	27-41	< 3	6	144-295	< 3	4	1,300-3,080	< 3

3.4. Conclusions

The results presented in this chapter confirm that the overall sorption behaviour of PFASs in soils of varying OC content increase with increasing both soil OC content and PFAS chain length, being this sorption more irreversible for long-chained PFASs. Short-chain PFASs are more likely to sorb in the humic and fulvic fractions of the soil, whereas mid- and long chained PFASs have a higher affinity for the humin fraction. Sorption in mineral phases also contribute to the sorption process, being important to explain the low K_d values observed for PFASs in mineral soils. Hence, these K_d values of PFASs in soils can be estimated by modelling the relative sorption at OC and mineral sites for each PFAS specie. The validation of the model ensured that it is able to predict, with acceptable accuracy, scenarios from very low to high sorption of target PFCAs and PFASs (with a total number of fluorinated carbons ranging from 3 to 11), based on only a few physicochemical properties of the soil (OC and silt+clay content) and the number of fluorinated carbons of the target PFAS. This information may be relevant for an early evaluation of the potential PFAS mobility after a contamination event. Although soil OC content is the main parameter governing PFASs sorption, the relative contribution of the sorption at mineral sites can be significant when short-chained PFASs are sorbed in soils with low OC and high silt+clay content. However, the associated K_d (PFAS) for these scenarios are generally very low, and therefore a high related PFAS mobility is expected, and remediation actions might be required.

3.5. References

- Ahrens, L., Yeung, L. W. Y., Taniyasu, S., Lam, P. K. S., Yamashita, N., 2011. Partitioning of perfluorooctanoate (PFOA), perfluorooctane sulfonate (PFOS) and perfluorooctane sulfonamide (PFOSA) between water and sediment. *Chemosphere*, 85 (5), 731–737. <https://doi.org/10.1016/j.chemosphere.2011.06.046>
- Aly, Y. H., McInnis, D. P., Lombardo, S. M., Arnold, W. A., Pennell, K. D., Hatton, J., Simcik, M. F., 2019. Enhanced adsorption of perfluoro alkyl substances for: In situ remediation. *Environ. Sci. Water Res.* 5 (11), 1867–1875. <https://doi.org/10.1039/c9ew00426b>
- Brusseau, M. L., Khan, N., Wang, Y., Yan, N., Van Glubt, S., Carroll, K. C., 2019. Nonideal Transport and Extended Elution Tailing of PFOS in Soil. *Environ. Sci. Technol.* 53 (18), 10654–10664. <https://doi.org/10.1021/acs.est.9b02343>
- Brusseau, M. L., Anderson, R. H., Guo, B., 2020. PFAS concentrations in soils: Background levels versus contaminated sites. *Sci. Total Environ.* 740, 140017. <https://doi.org/10.1016/j.scitotenv.2020.140017>
- Buck, R.C., Franklin, J., Berger, U., Conder, J.M., Cousins, I.T., de Voogt, P., Jensen, A.A., Kannan, K., Mabury, S.A., van Leeuwen, S.P.J., 2011. Perfluoroalkyl and polyfluoroalkyl substances in the environment: Terminology, classification, and origins. *Integr. Environ. Assess.* 7 (4), 513–541. <https://doi.org/10.1002/ieam.258>
- Burt, R., 2004. Soil survey laboratory methods manual. Investigation report No 42, Version 4.0, Natural resources Conservation Service. USDA, Washington, USA.
- Cai, W., Navarro, D. A., Du, J., Ying, G., Yang, B., McLaughlin, M. J., Kookana, R. S., 2022. Increasing ionic strength and valency of cations enhance sorption through hydrophobic interactions of PFAS with soil surfaces. *Sci. Total Environ.* 817, 152975. <https://doi.org/10.1016/j.scitotenv.2022.152975>

- Campos-Pereira, H., Ullberg, M., Kleja, D. B., Gustafsson, J. P., Ahrens, L., 2018. Sorption of perfluoroalkyl substances (PFASs) to an organic soil horizon – Effect of cation composition and pH. *Chemosphere*, 207, 183–191. <https://doi.org/10.1016/j.chemosphere.2018.05.012>
- Campos-Pereira, H., Makselon, J., Kleja, D. B., Prater, I., Kögel-Knabner, I., Ahrens, L., Gustafsson, J. P., 2022. Binding of per- and polyfluoroalkyl substances (PFASs) by organic soil materials with different structural composition – Charge- and concentration-dependent sorption behavior. *Chemosphere*, 297, 134167. <https://doi.org/10.1016/j.chemosphere.2022.134167>
- Carter, M. R., Gregorich, E. G., 2006. Extractable Al, Fe, Mn and Si. From: *Soil Sampling and Methods of Analysis*, second edition. Canadian Society of Soil Science, CRC Press, Boca Raton, USA. <https://doi.org/10.1201/9781420005271>
- Chen, H., Chen, S., Quan, X., Zhao, Y., Zhao, H., 2009. Sorption of perfluorooctane sulfonate (PFOS) on oil and oil-derived black carbon: Influence of solution pH and $[Ca^{2+}]$. *Chemosphere*, 77 (10), 1406–1411. <https://doi.org/10.1016/j.chemosphere.2009.09.008>
- Chen, H., Zhang, C., Yu, Y., Han, J., 2012. Sorption of perfluorooctane sulfonate (PFOS) on marine sediments. *Mar. Pollut. Bull.* 64 (5), 902–906. <https://doi.org/10.1016/j.marpolbul.2012.03.012>
- Chen, Y. C., Lo, S. L., Li, N. H., Lee, Y. C., Kuo, J., 2013. Sorption of perfluoroalkyl substances (PFASs) onto wetland soils. *Desalin. Water Treat.* 51 (40–42), 7469–7475. <https://doi.org/10.1080/19443994.2013.792145>
- Chen, H., Reinhard, M., Tung, V., Gin, K. Y., 2016. Reversible and irreversible sorption of perfluorinated compounds (PFCs) by sediments of an urban reservoir. *Chemosphere*, 144, 1747–1753. <https://doi.org/10.1016/j.chemosphere.2015.10.055>

- Du, Z., Deng, S., Bei, Y., Huang, Q., Wang, B., 2014. Adsorption behavior and mechanism of perfluorinated compounds on various adsorbents — A review. *J. Hazard. Mater.* 274, 443–454. <https://doi.org/10.1016/j.jhazmat.2014.04.038>
- du Pont, 2003. Adsorption/Desorption of ammonium Perfluorooctane to Soil (OECD 106), E.I. du Pont de Nemours and Company EMSE report no. 17-03, U.S. Environmental Protection Agency docket OPPT-2003-0012-0401.
- Enevoldsen, R., Juhler, R. K., 2010. Perfluorinated compounds (PFCs) in groundwater and aqueous soil extracts: Using inline SPE-LC-MS/MS for screening and sorption characterisation of perfluorooctane sulphonate and related compounds. *Anal. Bioanal. Chem.* 398 (3), 1161–1172. <https://doi.org/10.1007/s00216-010-4066-0>
- Ellefson, M., 2001. Soil adsorption/desorption study of potassium perfluorooctane sulfonate (PFOS); EPA Docket AR226-1030a030; 3M Company: Maplewood, MN.
- Fabregat-Palau, J., Vidal, M., Rigol, A., 2021. Modelling the sorption behaviour of perfluoroalkyl carboxylates and perfluoroalkane sulfonates in soils. *Sci. Total Environ.* 801, 149343. <https://doi.org/10.1016/j.scitotenv.2021.149343>
- Gellrich, V., Stahl, T., Knepper, T. P., 2012. Behavior of perfluorinated compounds in soils during leaching experiments. *Chemosphere*, 87 (9), 1052–1056. <https://doi.org/10.1016/j.chemosphere.2012.02.011>
- Gómez-Canela, C., Barth, J. A. C., Lacorte, S., 2012. Occurrence and fate of perfluorinated compounds in sewage sludge from Spain and Germany. *Environ. Sci. Pollut. R.* 19 (9), 4109–4119. <https://doi.org/10.1007/s11356-012-1078-7>

- Gredeļj, A., Nicoletto, C., Valsecchi, S., Ferrario, C., Polesello, S., Lava, R., Zanon, F., Barausse, A., Palmeri, L., Guidolin, L., Bonato, M., 2020. Uptake and translocation of perfluoroalkyl acids (PFAA) in red chicory (*Cichorium intybus* L.) under various treatments with pre-contaminated soil and irrigation water. *Sci. Total Environ.* 708, 134766. <https://doi.org/10.1016/j.scitotenv.2019.134766>
- Guelfo, J. L., Higgins, C. P., 2013. Subsurface transport potential of perfluoroalkyl acids at aqueous film-forming foam (AFFF)-impacted sites. *Environ. Sci. Technol.* 47 (9), 4164–4171. doi:10.1021/es3048043
- Habibullah-Al-Mamun, M., Ahmed, M. K., Raknuzzaman, M., Islam, M. S., Negishi, J., Nakamichi, S., Sekine, M., Tokumura, M., Masunaga, S., 2016. Occurrence and distribution of perfluoroalkyl acids (PFAAs) in surface water and sediment of a tropical coastal area (Bay of Bengal coast, Bangladesh). *Sci. Total Environ.* 571, 1089–1104. <https://doi.org/10.1016/j.scitotenv.2016.07.104>
- Higgins, C. P., Luthy, R. G., 2006. Sorption of Perfluorinated Surfactants on Sediments. *Environ. Sci. Technol.* 40, 7251–7256. <https://doi.org/10.1021/es061000n>
- Higgins, C. P., Luthy, R. G., 2007. Modeling sorption of anionic surfactants onto sediment materials: an a priori Approach for perfluoroalkyl substances and linear alkylbenzene sulfonates. *Environ. Sci. Technol.* 41 (9), 3254–3261.
- Jeon, J., Kannan, K., Lim, B. J., An, K. G., Kim, S. D., 2011. Effects of salinity and organic matter on the partitioning of perfluoroalkyl acid (PFAs) to clay particles. *J. Environ. Monitor.* 13 (6), 1803–1810. <https://doi.org/10.1039/c0em00791a>
- Jia, C., You, C., Pan, G., 2010. Effect of temperature on the sorption and desorption of perfluorooctane sulfonate on humic acid. *J. Environ. Sci.* 22 (3), 355–361. [https://doi.org/10.1016/S1001-0742\(09\)60115-7](https://doi.org/10.1016/S1001-0742(09)60115-7)

- Johnson, R. L., Anschutz, A. J., Smolen, J. M., Simcik, M. F., Lee Penn, R., 2007. The adsorption of perfluorooctane sulfonate onto sand, clay, and iron oxide surfaces. *J. Chem. Eng. Data*, 52 (4), 1165–1170. <https://doi.org/10.1021/je060285g>
- Kannan, K., 2011. Perfluoroalkyl and polyfluoroalkyl substances: current and future perspectives. *Environ. Chem.* 8, 333–338. <https://doi.org/10.1071/EN11053>
- Kennard, R. W., Stone, L. A., 1969. Computer Aided Design of Experiments. *Technometrics*, 11 (1), 137–148. <https://doi.org/10.1080/00401706.1969.10490666>.
- Knight, E. R., Janik, L. J., Navarro, D. A., Kookana, R. S., McLaughlin, M. J., 2019. Predicting partitioning of radiolabelled ^{14}C -PFOA in a range of soils using diffuse reflectance infrared spectroscopy. *Sci. Total Environ.* 686, 505–513. <https://doi.org/10.1016/j.scitotenv.2019.05.339>
- Kotska, J. E., Luther III, G. W., 1994. Partitioning and speciation of solid phase Fe in saltmarsh sediments. *Geochim. Cosmochim. Acta*, 58 (7), 1701 - 1710. [https://doi.org/10.1016/0016-7037\(94\)90531-2](https://doi.org/10.1016/0016-7037(94)90531-2)
- Kwadijk, C. J. A. F., Velzeboer, I., Koelmans, A. A., 2013. Sorption of perfluorooctane sulfonate to carbon nanotubes in aquatic sediments. *Chemosphere*, 90 (5), 1631–1636. <https://doi.org/10.1016/j.chemosphere.2012.08.041>
- Lath, S., Knight, E. R., Navarro, D. A., Kookana, R. S., McLaughlin, M. J., 2019. Sorption of PFOA onto different laboratory materials: Filter membranes and centrifuge tubes. *Chemosphere*, 222, 671–678. <https://doi.org/10.1016/j.chemosphere.2019.01.096>
- Li, C., Ji, R., Schäffer, A., Sequaris, J. M., Amelung, W., Vereecken, H., Klumpp, E., 2012. Sorption of a branched nonylphenol and perfluorooctanoic acid on Yangtze River sediments and their model components. *J. Environ. Monitor.* 14 (10), 2653–2658. <https://doi.org/10.1039/c2em30394a>

- Li, Y., Oliver, D. P., Kookana, R. S., 2018. A critical analysis of published data to discern the role of soil and sediment properties in determining sorption of per and polyfluoroalkyl substances (PFASs). *Sci. Total Environ.* 628–629, 110–120. <https://doi.org/10.1016/j.scitotenv.2018.01.167>
- Li, F., Fang, X., Zhou, Z., Liao, X., Zou, J., Yuan, B., Sun, W., 2019. Adsorption of perfluorinated acids onto soils: Kinetics, isotherms, and influences of soil properties. *Sci. Total Environ.* 649, 504–514. <https://doi.org/10.1016/j.scitotenv.2018.08.209>
- Liu, B., Zhang, H., Xie, L., Li, J., Wang, X., Zhao, L., Wang, Y., Yang, B., 2015. Spatial distribution and partition of perfluoroalkyl acids (PFAAs) in rivers of the Pearl River Delta, southern China. *Sci. Total Environ.* 524–525, 1–7. <https://doi.org/10.1016/j.scitotenv.2015.04.004>
- Loganathan, N., Wilson, A. K., 2022. Adsorption, Structure, and Dynamics of Short- and Long-Chain PFAS Molecules in Kaolinite: Molecular-Level Insights. *Environ. Sci. Technol.* 56, 8043-8052. <https://doi.org/10.1021/acs.est.2c01054>
- Lu, X., Deng, S., Wang, B., Huang, J., Wang, Y., Yu, G., 2016. Adsorption behavior and mechanism of perfluorooctane sulfonate on nanosized inorganic oxides. *J. Colloid Interf. Sci.* 474, 199–205. <https://doi.org/10.1016/j.jcis.2016.04.032>
- Martz, M., Heil, J., Marschner, B., Stumpe, B., 2019. Effects of soil organic carbon (SOC) content and accessibility in subsoils on the sorption processes of the model pollutants nonylphenol (4-n-NP) and perfluorooctanoic acid (PFOA). *Sci. Total Environ.* 672, 162–173. <https://doi.org/10.1016/j.scitotenv.2019.03.369>

- McGuire, M. E., Schaefer, C., Richards, T., Backe, W. J., Field, J. A., Houtz, E., Sedlak, D. L., Guelfo, J. L., Wunsch, A., Higgins, C. P., 2014. Evidence of remediation-induced alteration of subsurface poly- and perfluoroalkyl substance distribution at a former firefighter training area. *Environ. Sci. Technol.* 48 (12), 6644–6652. <https://doi.org/10.1021/es5006187>
- McLachlan, M. S., Felizeter, S., Klein, M., Kotthoff, M., De Voogt, P., 2019. Fate of a perfluoroalkyl acid mixture in an agricultural soil studied in lysimeters. *Chemosphere*, 223, 180–187. <https://doi.org/10.1016/j.chemosphere.2019.02.012>
- Mejia-Avendaño, S., Zhi, Y., Yan, B., Liu, J., 2020. Sorption of Polyfluoroalkyl Surfactants on Surface Soils: Effect of Molecular Structures, Soil Properties, and Solution Chemistry. *Environ. Sci. Technol.* 54 (3), 1513–1521. <https://doi.org/10.1021/acs.est.9b04989>
- Miao, Y., Guo, X., Dan Peng, Fan, T., Yang, C., 2017. Rates and equilibria of perfluorooctanoate (PFOA) sorption on soils from different regions of China. *Ecotox. Environ. Saf.* 139, 102–108. <https://doi.org/10.1016/j.ecoenv.2017.01.022>
- Milinovic, J., Lacorte, S., Vidal, M., Rigol, A., 2015. Sorption behaviour of perfluoroalkyl substances in soils. *Sci. Total Environ.* 511, 63–71. <https://doi.org/10.1016/j.scitotenv.2014.12.017>
- Müller, G., Gastner, M., 1971. The "Karbonate-bomber", a simple device for the determination of the carbonate content in sediments, soils, and other materials. *Neues Jb. Mineral. Monat.* 10, 466-469.
- Nguyen, T. M. H., Bräunig, J., Thompson, K., Thompson, J., Kabiri, S., Navarro, D. A., Kookana, R. S., Grimison, C., Barnes, C. M., Higgins, C. P., Mclaughlin, M. J., Mueller, J. F., 2020. Influences of Chemical Properties, Soil Properties, and Solution pH on Soil-Water Partitioning Coefficients of Per- And Polyfluoroalkyl Substances (PFASs). *Environ. Sci. Technol.* 54 (24), 15883–15892. <https://doi.org/10.1021/acs.est.0c05705>

- OECD, 2000. OECD 106 Adsorption - Desorption Using a Batch Equilibrium Method. OECD Guideline for the Testing of Chemicals. <https://doi.org/10.1787/9789264069602-en>
- Oliver, D. P., Navarro, D. A., Baldock, J., Simpson, S. L., Kookana, R. S., 2020. Sorption behaviour of per- and polyfluoroalkyl substances (PFASs) as affected by the properties of coastal estuarine sediments. *Sci. Total Environ.* 720, 137263. <https://doi.org/10.1016/j.scitotenv.2020.137263>
- Pan, G., Jia, C., Zhao, D., You, C., Chen, H., Jiang, G., 2009. Effect of cationic and anionic surfactants on the sorption and desorption of perfluorooctane sulfonate (PFOS) on natural sediments. *Environ. Pollut.* 157 (1), 325–330. <https://doi.org/10.1016/j.envpol.2008.06.035>
- Prevedouros, K., Cousins, I. T., Buck, R. C., Korzeniowski, S. H., 2006. Sources, fate and transport of perfluorocarboxylates. *Environ. Sci. Technol.* 40 (1), 32–44. <https://doi.org/10.1021/es0512475>
- Ramírez-Guinart, O., Salaberria, A., Vidal, M., Rigol, A., 2017. Assessing soil properties governing radiosamarium sorption in soils: Can trivalent lanthanides and actinides be considered as analogues?. *Geoderma*, 290, 33–39. <https://doi.org/10.1016/j.geoderma.2016.12.010>
- Rigol, A., Vidal, M., Rauret, G., Shand, C. A., Cheshire, M. V., 1998. Competition of organic and mineral phases in radiocesium partitioning in organic soils of Scotland and the area near Chernobyl. *Environ. Sci. Technol.* 32 (5), 663–669. <https://doi.org/10.1021/es970672y>
- Sepulvado, J. G., Blaine, A. C., Hundal, L. S., Higgins, C. P., 2011. Occurrence and fate of perfluorochemicals in soil following the land application of municipal biosolids. *Environ. Sci. Technol.* 45 (19), 8106–8112. <https://doi.org/10.1021/es103903d>

- Sima, M.W., Jaffé, P.R., 2021. A critical review of modeling Poly- and Perfluoroalkyl Substances (PFAS) in the soil-water environment. *Sci. Total Environ.* 757, 143793. <https://doi.org/10.1016/j.scitotenv.2020.143793>
- Sorengard, M., Berggren, D., Ahrens, L., 2019. Stabilization of per- and polyfluoroalkyl substances (PFASs) with colloidal activated carbon (PlumeStop ®) as a function of soil clay and organic matter content. *J. Environ. Manag.* 249, 109345. <https://doi.org/10.1016/j.jenvman.2019.109345>
- Tian, H., Gao, J., Li, H., Boyd, S. A., Gu, C., 2016. Complete Defluorination of Perfluorinated Compounds by Hydrated Electrons Generated from 3-Indole-acetic-acid in Organomodified Montmorillonite. *Sci. Rep.* 6, 1–9. <https://doi.org/10.1038/srep32949>
- Wang, Y., Khan, N., Huang, D., Carroll, K. C., Brusseau, M. L., 2021. Transport of PFOS in aquifer sediment: Transport behavior and a distributed-sorption model. *Sci. Total Environ.* 779, 146444. <https://doi.org/10.1016/j.scitotenv.2021.146444>
- Wang, W., Rhodes, G., Zhang, W., Yu, X., Teppen, B. J., Li, H., 2022. Implication of cation-bridging interaction contribution to sorption of perfluoroalkyl carboxylic acids by soils. *Chemosphere*, 290, 133224. <https://doi.org/10.1016/j.chemosphere.2021.133224>
- Wei, C., Song, X., Wang, Q., Hu, Z., 2017. Sorption kinetics, isotherms and mechanisms of PFOS on soils with different physicochemical properties. *Ecotox. Environ. Saf.* 142, 40–50. <https://doi.org/10.1016/j.ecoenv.2017.03.040>
- Willemsen, J. A. R., Bourg, I. C., 2021. Molecular dynamics simulation of the adsorption of per- and polyfluoroalkyl substances (PFASs) on smectite clay. *J. Colloid Inter. Sci.* 585, 337–346. <https://doi.org/10.1016/j.jcis.2020.11.071>

- Xiang, L., Xiao, T., Yu, P. F., Zhao, H. M., Mo, C. H., Li, Y. W., Li, H., Cai, Q. Y., Zhou, D. M., Wong, M. H., 2018. Mechanism and Implication of the Sorption of Perfluorooctanoic Acid by Varying Soil Size Fractions. *J. Agr. Food Chem.* 66 (44), 11569–11579. <https://doi.org/10.1021/acs.jafc.8b03492>
- Xiao, F., Zhang, X., Penn, L., Gulliver, J. S., Simcik, M. F., 2011. Effects of monovalent cations on the competitive adsorption of perfluoroalkyl acids by kaolinite: Experimental studies and modeling. *Environ. Sci. Technol.* 45 (23), 10028–10035. <https://doi.org/10.1021/es202524y>
- Xiao, F., Jin, B., Golovko, S. A., Golovko, M. Y., Xing, B., 2019. Sorption and Desorption Mechanisms of Cationic and Zwitterionic Per- and Polyfluoroalkyl Substances in Natural Soils: Thermodynamics and Hysteresis. *Environ. Sci. Technol.* 53 (20), 11818–11827. <https://doi.org/10.1021/acs.est.9b05379>
- Yin, C., Pan, C. G., Xiao, S. K., Wu, Q., Tan, H. M., Yu, K., 2022. Insights into the effects of salinity on the sorption and desorption of legacy and emerging per- and polyfluoroalkyl substances (PFASs) on marine sediments. *Environ. Pollut.* 300. <https://doi.org/10.1016/j.envpol.2022.118957>
- You, C., Jia, C., Pan, G., 2010. Effect of salinity and sediment characteristics on the sorption and desorption of perfluorooctane sulfonate at sediment-water interface. *Environ. Pollut.* 158 (5), 1343–1347. <https://doi.org/10.1016/j.envpol.2010.01.009>
- Zhang, R., Yan, W., Jing, C., 2014. Mechanistic study of PFOS adsorption on kaolinite and montmorillonite. *Colloid. Surface A.* 462, 252–258. <https://doi.org/10.1016/j.colsurfa.2014.09.019>
- Zhao, L., Zhang, Y., Fang, S., Zhu, L., Liu, Z., 2014. Comparative sorption and desorption behaviors of PFHxS and PFOS on sequentially extracted humic substances. *J. Environ. Sci.* 26 (12), 2517–2525. <https://doi.org/10.1016/j.jes.2014.04.009>

Zhi, Y., Liu, J., 2018. Sorption and desorption of anionic, cationic and zwitterionic polyfluoroalkyl substances by soil organic matter and pyrogenic carbonaceous materials. *Chem. Eng. J.* 346, 682–691. <https://doi.org/10.1016/j.cej.2018.04.042>

CHAPTER IV

SORPTION OF PFASs IN

CARBON-RICH MATERIALS

4.1. Introduction

PFASs, such as PFCAs and PFSAAs, have gained attention in recent years due to their high persistence in the environment, their bioaccumulation, and their toxicity. PFASs have been widely used for more than 50 years in industrial applications such as fire-fighting foams, inks, lubricants, surfactants, and oil and water repellents for leather, paper and textile goods. Their strong C-F bonds contribute to their high resistance to thermal, biological and photolytic degradation, and they are found in a range of environmental matrices (Prevedouros et al., 2006).

PFASs have been detected at levels up to several mg kg^{-1} and $\mu\text{g L}^{-1}$ in soils and freshwater environments respectively (Brusseau et al., 2020; Colomer-Vidal et al., 2022). They can be transferred from soil to plants through root uptake and bioaccumulate in these organisms (Lesmeister et al., 2020). PFASs can also reach groundwater by soil run-off (Gellrich et al., 2012). Hence, remediation techniques to decrease PFASs mobility in the environment are of attracting increasing attention. In this regard, activated carbon has been shown to be an effective sorbent for PFASs removal from residual waters (Ochoa-Herrera and Sierra-Alvarez, 2008; Qian et al., 2017), and is occasionally tested in the laboratory to remediate contaminated soils (Kupryianchyk et al., 2016). Biochars are a sustainable alternative to activated carbon, given their similar sorption properties towards organic pollutants (Ahmad et al., 2014), and they may be considered a cost-effective alternative for soil remediation (Silvani et al., 2019; Askeland et al., 2020; Sørmo et al., 2021). Additionally, other organic by-products such as charcoal-based materials rejected by the steel industry and compost have been reported to be capable of sorbing PFASs (Söregård et al., 2020).

It has been suggested that sorbent properties such as SSA and surface chemistry may play important roles in PFASs sorption in activated carbons (Saeidi et al., 2020a). Furthermore, PFASs sorption generally increases with greater fluorinated chain length (Söregård et al., 2020). Other factors such as pH, ionic strength and DOC levels can also modify sorption in

activated carbons (Saeidi et al., 2020a; Xiao et al., 2017; Yu et al., 2012). However, new systematic studies are required to evaluate the role of different factors governing PFASs sorption in biochars of contrasted properties, as well as to obtain sorption parameters for PFASs with different chain lengths in other carbon-rich materials such as compost and charcoal fines. The current literature on PFASs sorption by carbon-rich materials mainly focuses on the evaluation of the maximum loading capacities of the materials, aiming to determine their efficiency in the context of wastewater remediation (Zhang et al., 2020). The estimation of K_d may be a suitable parameter to assess the sorption affinity of PFASs for a given material, helping to assess its potential remediation effectiveness. However, descriptions in the literature of K_d prediction models for PFASs sorption by these carbon-rich sorbents are scarce.

The aim of this chapter is to evaluate the sorption kinetics, sorption isotherms and the effects of pH, calcium concentration and DOC content on PFASs sorption by several carbon-rich materials eligible to be used for remediation purposes (including biochars, compost, charcoal fines and activated carbon) in order to assess its sorption affinity for PFASs. These effects will be evaluated for PFOS as PFAS-representative, and additionally, K_d values for PFCAs and PFSAAs that contain fluorinated carbons ranging from 4 to 11 will be derived in a set of ten carbon-rich materials. The key sorbent properties affecting PFASs sorption will be identified by principal component analysis (PCA), which will set the basis to develop a multivariate linear K_d prediction model. The model will be based on robust stepwise multiple linear regression and will be validated using external sorption data gathered from the literature. The developed model may help to identify the most promising carbon-rich materials for the remediation of areas contaminated with PFASs.

4.2. Materials and methods

4.2.1. Reagents and standards

Milli-Q double deionized water ($18.2 \text{ M}\Omega \text{ cm}^{-1}$) was obtained from a water purification system (USF PureLaB Plus, Spain). HPLC-grade ACN ($\geq 99.9\%$) as well as extra pure sodium azide ($\geq 99.0\%$) and calcium chloride dihydrate (99%) were purchased from Merck (Germany), while ammonium acetate (96%) was obtained from Panreac (Spain). Analytical standards of PFHxA (97%), PFOA (96%), PFNA; (97%), PFDoA (95%) and PFHxS (98%) were obtained from Sigma-Aldrich (Germany). Analytical standards of PFBS (98%) and PFOS (95%) were purchased from Fluka (Austria). The physicochemical properties of the PFASs, including those PFASs used to test the developed model, are summarized in **Table 1.1**.

Individual PFAS stock solutions of 1 g L^{-1} were prepared in ACN, while the working solutions for the sorption experiments were prepared by the dilution of the stock standards in acetonitrile. Isotopically labelled standard solutions of MPFOS and MPFOA, both at concentrations of $50 \mu\text{g mL}^{-1}$ in MeOH, were purchased from Wellington Laboratories (Canada). Working standard solutions of both MPFOS and MPFOA were prepared at 500 ng mL^{-1} of each PFAS in ACN. All solutions were stored at 5°C in glass vials with polyethylene caps (Sigma-Aldrich, Germany).

Based on the pK_a values reported in **Table 1.1**, all the PFASs were expected to be in their anionic form in the experimental conditions of the sorption tests. The PFASs chain length in this study refers to the total number of fluorinated carbons in the alkyl chain (CF_2), including the final $-\text{CF}_3$ moiety.

4.2.2. Materials and characterization

Six biochar, one coal fines, one compost and two activated carbon samples were examined. Biochar obtained from tree barks (TB) was provided by a wine factory after pyrolyzing the feedstock under a nitrogen atmosphere at 400°C for 3 hours, while biochars from crop eucalyptus (CE), sugarcane bagasse (SB), castor meal (CM), pericarp of coconut (PC) and water hyacinth (WH) were obtained after pyrolyzing each feedstock at 350°C for 70 minutes as described elsewhere (Doumer et al., 2015). The coal fines (CF) sample was provided by a Brazilian metallurgical company, while municipal organic waste (MOW) compost was provided by a waste management treatment plant in Barcelona (Spain). The initial carbon-rich bulk samples of a few kg were sieved at < 2 mm. The sample mass was homogenized and representatively reduced using riffle splitters before sorption tests. Two granular activated charcoal, GAC (C2889) and NGAC (Norit® 1240W), were purchased from Sigma-Aldrich (Steinheim, Germany). These materials were tested without any further treatment.

Total carbon (%TC), nitrogen (%TN), hydrogen (%TH), sulphur (%TS) and oxygen (%TO) contents were determined all by elemental analysis (EA-1108 C.E Instruments, Thermo Fisher Scientific). The pH of the materials was measured in a 40 g L⁻¹ 0.01 M CaCl₂ suspension after being equilibrated during 48 hours. Total organic carbon content (%C_{ORG}) was also determined by elemental analysis with previous acidification with 2.0 mol L⁻¹ HCl. The pH_{ZPC} was determined adding one gram of material in a 80 mL PP centrifuge tube containing 40 mL of a 0.01 M NaCl solution adjusted at pH ranging 2 – 12 using 0.5 N NaOH and 0.5 N HCl. The final pH was recorded after shaking the tubes for 24 hours and the differences between the initial and final pH were used to determine pH_{ZPC} (Yu et al., 2009). Ash content was determined after calcination of the samples at 750°C during 4 hours (ASTM D3174-02).

CEC was determined by the barium exchange method at material initial pH (UNE-EN ISO 11260:2018). Water soluble cations and anions were extracted using a 40 g L⁻¹ Milli-Q water suspension and analysed by inductively coupled plasma – optical emission spectrometry (ICP-OES, Perkin Elmer, Optima 3200RL) and anionic chromatography (Jasco 2000 Plus), respectively. Detection wavelength (nm) and LOQ (mg L⁻¹) for the selected metals were: 590 nm / 0.5 mg L⁻¹ for Na; 766 nm / 0.5 mg L⁻¹ for K; 279 nm / 0.05 mg L⁻¹ for Mg and 318 nm / 0.05 mg L⁻¹ for Ca. Anionic chromatography was performed using a IC-Pak™ Anion HR (4.6 x 75 mm) column and a gluconate-borate mobile phase at a flow rate of 0.8 mL min⁻¹. Particle size distribution was determined by laser diffraction (Beakman Coulter LS 13320) using the dry method, while SSA and average pore width were determined by nitrogen adsorption (TriStar 3000, Micromeritics) using the BET method. DOC content of the blank supernatants was measured using a DOC analyser (Analytic Jena Multi N/C 3100) with previous acidification to pH 2.0 using HCl. The UV-Vis spectra of the blank supernatants was recorded (Varian Cary 100) using a 1 cm optical cell, and the specific ultraviolet absorbance at 254 nm (SUVA₂₅₄), which has been related to the degree of aromaticity of the DOC, was calculated for those materials with DOC contents above 20 mg L⁻¹ according to elsewhere (Weishaar et al., 2003). FTIR spectra of the materials was obtained by solid KBr dilution (Thermo Nicolet 5700). The surface morphology of the solid particles was examined by scanning electron microscopy (SEM, JEOL JSM 7001F) at 15 kV.

4.2.3. Sorption experiments

Two biochars (TB and CE), a compost sample (MOW) and a charcoal fines sample (CF) were selected to assess PFAS sorption kinetics, sorption isotherms and the effects of pH, calcium concentration and DOC content on sorption. TB and CE were selected due to their different physicochemical properties compared to other reported biochars (Fagbayigbo et al.,

2017; Guo et al., 2017), whereas the evaluation of compost and charcoal fines has been barely studied in the literature. Additionally, the activated charcoal sample NGAC was used for comparison purposes of the sorption isotherms obtained by the other selected materials. PFOS was selected as the PFAS-representative. Once the equilibration time and initial concentrations were optimized, sorption experiments of seven PFASs were performed in the 10 carbon-rich materials.

To run all the sorption experiments (OECD, 2000), one gram of dried material was introduced into 80-mL PP centrifuge tubes before the addition of 25 mL of a 1 g L^{-1} NaN_3 solution (pH 7.7 unless specified otherwise). The resulting suspension was shaken in an end-over-end shaker at 30 rpm and room temperature (18-20°C) for 24 h to obtain a pre-equilibrium state between the solid material and the solution. Selected volumes of individual PFAS working solutions were then added to the suspensions to achieve a given initial concentration. All experiments were run in triplicate.

For the sorption kinetics, PFOS was spiked at 400 ng mL^{-1} , while the initial concentrations for PFOS sorption isotherms ranged from 10 to 600 ng mL^{-1} for TB, CE, MOW and CF, and 500 to $10,000 \text{ ng mL}^{-1}$ for NGAC, as higher sorption coefficients were expected for NGAC. The pH of all the resulting experiments did not differ (± 0.2) from the initial sample pH. For the evaluation of the effects of pH and calcium concentration, specific contact solutions were adjusted according to previous acid/base tests using 0.5 N HCl and 0.5 N NaOH to achieve a final suspension pH of 5, 7 or 11 after the pre-equilibration step, with the final volume being 25 mL. For each pH, several compositions of the contact solutions were tested. These solutions contained NaN_3 at 1 g L^{-1} and calcium at a natural concentration, 10 mM or 100 mM. The suspensions were spiked with 400 ng mL^{-1} of PFOS after the pre-equilibration step, and the DOC content in the supernatants of these experiments was also monitored.

For the remaining PFASs, sorption experiments were conducted to derive K_d values at a single spiking concentration (**Table 4.1**). In view of the results from the PFOS sorption isotherms in the five representative materials, it was assumed that the derived K_d values were within the linear range of PFAS sorption. In all the experiments, after each individual PFAS spike, tubes were shaken at 30 rpm for 48 hours and centrifuged for 30 min at 4°C and 7,800 *g* (AJ2-HS, Beckman Coulter, USA). After centrifugation, the supernatants were removed using a plastic syringe, passed through 0.45 µm filters and stored at 4°C in glass vials until analysis.

Table 4.1 PFASs initial concentrations (ng mL⁻¹) for the batch experiments.

Material	PFBS	PFHxA	PFHxS	PFOA	PFNA	PFOS	PFDoA
TB	100	100	100	100	400	N.A.	500
CE	100	100	100	100	400	N.A.	500
SB	100	100	100	100	400	400	500
WH	100	100	100	100	400	400	500
CM	100	100	100	100	400	400	500
PC	100	100	100	100	400	400	500
MOW	100	100	100	100	400	N.A.	500
CF	100	100	100	100	400	N.A.	500
GAC	2,000	2,000	2,500	2,500	4,500	4,500	5,000
NGAC	2,000	2,000	2,500	2,500	4,000	N.A.	5,000

N.A.: Non Analysed (K_d data was derived from the isotherm experiments)

4.2.4. Quality control

The %RSD between the replicates was generally lower than 15%, and up to 30% in few worst-case scenarios. Quality control of the analyses included blank samples that were tested using the same procedure described in 4.2.3, but without PFAS spiking, to test for the presence

of PFAS in the samples. In addition, aqueous control samples with a PFAS concentration representative of the tested concentration range were assayed to quantify PFAS losses during the experimental stages of the batch test. Results from the analyses of the blanks showed that no PFAS were present in the samples prior to the analysis. Regarding the aqueous control samples, negligible losses were observed for all the PFAS, except for PFDoA, of which only 40% was recovered, and results were corrected accordingly.

4.2.5. PFASs analysis by HPLC-MS/MS

To quantify the PFASs after the sorption experiments, a 750- μ L aliquot of the supernatant was transferred to a 2-mL chromatography vial. 10 μ L of the MPFOS and MPFOA internal standard working solution and 240 μ L of ACN were added to the vial to obtain a final volume of 1 mL. The PFASs were subsequently analysed by HPLC-MS/MS. Details about the chromatography methods can be found Section 3.2.5 of this thesis.

4.2.6. Data treatment

The K_d (mL g^{-1}), was calculated as the ratio of the concentration of the target PFAS sorbed into the solid phase, C_S (ng g^{-1}), to the concentration in the aqueous phase at equilibrium, C_{eq} (ng mL^{-1}):

$$K_d = \frac{C_S}{C_{\text{eq}}} \quad (4.1)$$

C_{eq} values were directly determined by HPLC-MS/MS, whereas C_S was calculated with the following equation:

$$C_S = \frac{(C_{\text{in}} - C_{\text{eq}}) \cdot V}{m} \quad (4.2)$$

where C_{in} (ng mL^{-1}) corresponds to the initial concentration of PFAS added to the suspension, V (mL) is the volume of solution and m (g) refers to the dry mass of the material. The sorption percentage, S (%), was calculated as follows:

$$S (\%) = \frac{(C_{in} - C_{eq})}{C_{in}} \cdot 100 \quad (4.3)$$

The kinetic data were fitted to the PSOM equation:

$$\frac{t}{C_{S,t}} = \frac{1}{K_2 C_{S,eq}^2} + \frac{t}{C_{S,eq}} = \frac{1}{V_0} + \frac{t}{C_{S,eq}} \quad (4.4)$$

where $C_{S,t}$ (ng g^{-1}) is the sorbed concentration at time t (h), K_2 ($\text{g ng}^{-1} \text{h}^{-1}$) is the PSOM rate constant, $C_{S,eq}$ (ng g^{-1}) is the sorbed concentration at equilibrium and V_0 is the initial sorption rate ($\text{ng g}^{-1} \text{h}^{-1}$) (Yu et al., 2009).

The isotherm data was fitted to the Linear (Equation 4.1) and Freundlich (Equation 4.5) model. This last model considers a parameter (K_F , $(\text{mg kg}^{-1}) / (\text{mg L}^{-1})^N$) related to the affinity of the sorbate-sorbent interaction and a dimensionless parameter, N , related to the heterogeneity of sorption sites. For $N = 1$, the model assumes that the sorbent has a sufficient amount of equally-affine sorption sites able to bind the sorbate, and therefore, Equation 4.5 equals to Equation 4.1 and K_F equals to K_d (Limousin et al., 2007).

$$C_S = K_F (C_{eq})^N \quad (4.5)$$

Both the kinetic and isotherm data were fitted using the least-squares method (cftoolbox, Matlab® R2009a (MathWorks Inc., USA)). Fisher's least significant difference (FLSD) test was run, using Statgraphics Centurion 18.1.14 (Statgraphics Technologies, USA) and \log_{10} -transformed data. To identify the key sorbent properties affecting PFAS sorption, a principal component analysis (PCA) was performed (PLS Toolbox 703, Matlab® R2009a (MathWorks Inc., USA)) after autoscaling and performing a \log_{10} transformation of the data (with the exception of pH, pH_{ZPC} and $\log K_{OW}$).

4.2.7. Model construction

The K_d prediction model was constructed using a calibration set based on our 70 own experimental K_d data in addition to 15 additional literature entries (Deng et al., 2015; Xiao et al., 2017; Siriwardena et al., 2019) selected to enlarge the range values of the relevant properties used as model variables. These additional entries also permitted to obtain a better distribution of the K_d values along the calibration set, regardless the type of material. Additional data gathered from the literature was used as a validation set (**Table 4.2**). The acceptance criteria for including literature data were: (i) data must originate from batch experiments with PFAS and carbon-rich sorbents with experimental conditions similar to OECD 106 test (OECD, 2000); (ii) tested materials should be similar to those used in our work, such as biochars or activated carbons, but excluding data derived from studies using modified/doped materials or material mixtures (*i.e.*, soil + biochar); (iii) the characterization data of the sorbents must be available; (iv) the K_d values for the PFAS should be reported or be derivable from the information reported in the study, resulting in K_d values within the linear sorption range.

Contrarily to soils, in which linear and Freundlich-type isotherms (reporting K_d values within the linear sorption range) for PFASs are commonly observed, many sorption studies in carbon-rich materials aims to identify the maximum sorption capacity of the sorbents, and thus the sorption isotherm reaches a *plateau*, being well described by the Langmuir equation. However, K_d values within the linear range of the sorption isotherms in these cases are barely reported. Hence, in this study we had to derive K_d values from the literature using other reported sorption data such as Langmuir, Freundlich, kinetic and sorption percentage parameters.

K_d values in this section were mostly derived from reported Langmuir parameters. K_d values derived from non-linear isotherms are concentration-dependent, thus hampering the selection of a given concentration to derive a K_d value representative of the linear range of the sorption isotherm.

Table 4.2 List of references used to build up the validation dataset

Material information (number of samples)	Target PFAS	Number of entries	Reference
<i>Activated Carbons</i>			
Synthetic magnetic Activated Carbon (1)	PFCA: PFOA; PFSA: PFBS, PFHxS, PFOS	4	Meng et al., 2019
Commercial Activated Carbon (Filtrisorb 300 *) (1)	PFSA: PFOS	1	Steigerwald and Ray, 2021
Commercial Activated Carbon (Filtrisorb 400 **) (1)	PFCA: PFOA; PFSA: PFOS	2	Yao et al., 2014
Commercial Activated Carbon (Filtrisorb 400 **) (1)	PFCA: PFPeA, PFHpA, PFOA PFSA: PFPeS, PFHxS, PFHpS, PFOS	7	Yan et al., 2020
Commercial Activated Carbon (Filtrisorb 400 **) (1)	PFSA: PFOS	1	Senevirathna et al., 2010
Commercial Activated Carbon (Filtrisorb 400 **) (1)	PFCA: PFOA; PFSA: PFBS, PFOS	3	Ochoa-Herrera et al., 2008
Commercial Activated Carbon (Filtrisorb 400 **) (1)	PFSA: PFBS, PFOS	2	Carter and Farrell, 2010
Commercial Activated Carbon (NORIT ® 1240W ***) (1)	PFCA: PFBA, PFPeA, PFHxA, PFHpA, PFOA, PFNA PFSA: PFBS, PFHxS	8	Stebel et al., 2019
Commercial Activated Carbon (NORIT ® 830) (1)	PFCA: PFBA	1	Inyang and Dickenson, 2017
<i>Biochars</i>			
Biochars derived from maize straw and willow sawdust (2)	PFSA: PFOS	2	Chen et al., 2011
Biochars derived from different feedstocks (3)	PFCA: PFBA, PFOA	6	Inyang and Dickenson, 2017
Biochars derived from Spend Coffee Grounds and Mountain Crest Gardens (2)	PFSA: PFOS	2	Steigerwald and Ray, 2021
Commercial hardwood biochar (1)	PFCA: PFOA; PFSA: PFOS	2	Zhi and Liu, 2018
Bamboo-derived biochar (1)	PFCA: PFHxA, PFHpA, PFOA	3	Du et al., 2015

* additional characterization data from Ulrich et al. (2015); ** additional characterization data from Morlay et al. (2012); *** characterization data derived from this study.

Nonetheless, a concentration independent K_d value may be derived from Langmuir parameters as the product of K_L (indicative of the affinity of the sorbate for the sorption sites) and $C_{S,MAX}$ (indicative of the quantity of sorption sites), as shown in Equation 4.6, as a result of forcing the sorption isotherm at very low C_{eq} levels, in which the sorption isotherm is assumed to behave linearly.

$$\lim_{C_{eq} \rightarrow 0} K_d = \frac{C_S}{C_{eq}} = \frac{K_L C_{S,MAX} C_{eq}}{1 + (K_L C_{eq})} = K_L C_{S,MAX} \quad (4.6)$$

A few data was also derived from reported Freundlich (Equation 4.5) parameters. Deriving K_d values from Freundlich parameters at very low environmental concentrations could in some cases lead to anomaly high K_d values for isotherms with $N < 1$ coefficients, as K_d in these scenarios tends to infinitive when lowering C_{eq} . In the cases in which K_d values needed to be derived from reported Freundlich isotherms, expert judgment was applied to select a given aqueous concentration that felt within the linear range of the reported sorption isotherm.

Additionally, a few K_d data was derived from reported kinetic and sorption percentages data. One of the fitted parameters in the PSOM (Equation 4.4) is the maximum sorption ($C_{S,PSOM}$) at a given initial concentration at equilibrium. With the reported solid-to-solution ratio, $C_{S,PSOM}$ values may be expressed with respect to the liquid phase, allowing the calculation of C_{eq} by mass balance with C_{in} . With $C_{S,PSOM}$ and C_{eq} , a K_d value can be calculated. Similarly, K_d values can be derived from reported sorption percentages (Equation 4.3, sometimes also referred as removal rates). Using the reported percentage and the given C_{in} , C_{eq} values can be derived, and with the given solid-to-solution ratio, C_S values referred to the solid phase can be calculated by mass balance. With C_{eq} and C_S , a given K_d value can be derived. In either cases is then dependent on further experimental evidences or expert judgement the quality acceptance of the derived K_d (*i.e.*, felts within the linear range of the sorption isotherm) to be included in the database.

The model was constructed by stepwise multiple linear regressions (SMLR), and the least squares of the regressions were iteratively weighted with a bisquare weighting function to avoid the potential skewness provoked by data in the calibration set. Once the model was built up, it was tested against the validation dataset. This included the sorption K_d data from biochars and activated carbon for both PFCA and PFSA with a fluorinated alkyl chain number ranging from 3 to 8. The total number of accepted entries of the validation set was 44 (15 for biochars and 29 for activated carbons).

To evaluate the predictive accuracy of the model, RMSE and RPD values were calculated as:

$$\text{RMSE} = \sqrt{\frac{\sum_{i=1}^n (\log K_{d,\text{measured},i} - \log K_{d,\text{predicted},i})^2}{N}} \quad (4.7)$$

where $\log K_{d,\text{measured}}$ and $\log K_{d,\text{predicted}}$ are the measured and predicted $\log K_d$ values, respectively, i is the entry being tested and N is the total number of entries included in the model. The RPD was calculated as:

$$\text{RPD} = \frac{\text{SD}}{\text{RMSE}} \quad (4.8)$$

where SD is the standard deviation of the original $\log K_{d,\text{measured}}$ data. RPD values therefore relate the variability of the original data to the variability of the prediction errors, and are indicative of the quality of the model. Despite RPD thresholds are subjective and dependent on imposed quality requirements, usually RPD values < 1.5 are considered as models with poor prediction ability; RPD values ranging from 1.5 to 2.0 are considered as models with acceptable prediction ability; RPD values ranging from 2.0 to 3.0 are considered as models with good prediction ability, and RPD values > 3.0 are considered as models with excellent prediction ability (Knight et al., 2019).

4.3. Results and discussion

4.3.1. Physicochemical properties of the samples

The main physicochemical properties of the materials are summarized in **Table 4.3**. The %TC of the biochars ranged from 27 to 80%, and the presence of inorganic carbon species was minor (< 7%) according to the differences between %C_{ORG} and %TC. Total nitrogen and hydrogen content ranged 0.47 – 7.0% and 2.2 – 4.4%, respectively, and the presence of sulphur was minor (< 0.5%) in all materials. The C_{ORG} differed among the biochars obtained under the same pyrolysis conditions likely due to differences in the feedstocks (Doumer et al., 2015). The C_{ORG}/O molar ratio of the biochar and compost samples ranged from 1.3 to 8.6 and correlated well ($r^2 = 0.91$, $p < 0.001$, $n = 7$) with the percentages of aromatic carbon revealed by ¹³C nuclear magnetic resonance (¹³C-NMR, Doumer et al., 2016; Venegas et al., 2015) and therefore, this parameter was chosen as an indicator of the aromaticity of the material. The median particle size distribution of the samples ranged from 40 to 1,010 μm (see **Figure 4.1**). With the exception of TB, the SSA of the biochars was $\leq 3 \text{ m}^2 \text{ g}^{-1}$, with average pore width 250 – 4,800 Å. By contrast, the commercial GAC and NGAC samples presented both developed porosity and a high SSA, reaching SSA values up to $1,000 \text{ m}^2 \text{ g}^{-1}$, and with pore widths ranging 20 – 30 Å. Despite the low SSA of some of these sorbent materials, SEM images revealed a relatively well-developed porous structure (see **Figure 4.2**).

CEC of the materials ranged 4.7 – 63 cmol_c kg⁻¹. The pH and pH_{ZPC} of the samples ranged from 6 to 10 and from 5 to 11, respectively. Since pH_{ZPC} is defined as the pH at which the material presents a net neutral charge, positively-charged surfaces may be expected for pH_{ZPC} > pH, whereas negatively-charged surfaces may be expected for pH_{ZPC} < pH. Therefore, the difference between pH_{ZPC} and pH was considered a qualitative indicator of the overall bulk net surface charge. Ash contents ranged 4 – 15% for most materials, although increased up to 35% for WH, MOW and CF. The main water-soluble cation and anion levels in the blank

samples are reported in **Table 4.4** and their sum ranged 0.2 – 12 and 0.1 – 14 meq L⁻¹, respectively, with the exception of WH, that presented higher water-soluble cations and anions levels. With the exception of TB, the DOC content of the biochars was relatively high (> 100 mg L⁻¹). The SUVA₂₅₄ of the biochars ranged 1.0 – 3.8 L mg⁻¹ m⁻¹, which was within the range of other values reported elsewhere for biochars pyrolyzed at < 400 °C (Jamieson et al., 2014). The aromaticity of these DOC species, roughly calculated according to elsewhere (Weishaar et al., 2003), ranged 12 – 30% and indicated a fulvic acid-like structure, although it increased up to 40% for the compost sample. These high DOC contents, which may be attributed to the presence of unpyrolyzed carbon species, were confirmed by the FTIR bands at 2,860 and 2,930 cm⁻¹ (see **Figure 4.3**) that were related to symmetric and asymmetric aliphatic C – H stretch vibrations, respectively. The 800 – 2,000 cm⁻¹ region of the FTIR spectra for the biochar samples agreed with the pattern observed for a woody powder sample with different lignin, cellulose and hemicellulose contents (Horikawa et al., 2019), while MOW spectra, that did not present this pattern, was similar to the FTIR spectra reported for a municipal solid waste compost (Carballo et al., 2008).

Table 4.3 Main physicochemical properties of the sorbent materials.

	TB	CE	SB	WH	CM	PC	MOW	CF	GAC	NGAC
<i>Solid phase</i>										
TC (%)	80	70	65	45	55	65	27	50	76	79
C _{ORG} (%)	77	65	60	43	55	63	27	43	73	79
TN (%)	0.65	0.57	0.60	4.0	7.0	1.0	1.8	1.4	0.47	0.38
TH (%)	2.2	4.0	4.4	3.3	5.4	4.0	2.9	2.3	0.59	0.49
TS (%)	<0.10	<0.10	<0.10	0.25	<0.10	<0.10	0.47	<0.10	0.17	0.45
TO (%)	12	26	22	25	22	24	27	21	8.5	2.3
C _{ORG} /O molar ratio	8.6	3.3	3.6	2.3	3.3	3.5	1.3	2.7	12	46
pH	8.9	7.2	6.0	9.2	7.3	8.9	8.3	8.0	10.1	8.7
pH _{ZPC}	9.3	6.3	5.2	9.1	6.4	5.7	9.3	7.5	10.4	10.9
(pH _{ZPC} – pH)	0.4	-0.9	-0.8	0.1	-0.9	-3.2	-1.0	-0.5	0.3	2.2
Ash (%)	4.0	4.5	5.0	31	11	5.5	35	24	6.6	14
CEC (cmol _c kg ⁻¹)	4.7	9.6	5.2	48	10	10	51	63	17	4.5
Median particle size (µm)	40	378	226	87	482	381	1010	386	N.A.	1135
SSA (m ² g ⁻¹)	162	0.61	1.3	3.0	0.06	0.97	9.2	7.3	580	964
Pore width (Å)	N.Q.	334	246	4771	290	2203	346	300	28	22
<i>Liquid phase</i>										
DOC (mg L ⁻¹)	8.4	185	122	827	832	125	134	13	2.7	1.9
SUVA ₂₅₄	N.Q.	2.4	1.2	3.8	1.6	1.0	5.4	N.Q.	N.Q.	N.Q.
∑ Soluble anions (meq L ⁻¹)	0.89	3.9	0.10	60	3.6	14	11	2.2	2.2	0.10
∑ Soluble cations (meq L ⁻¹)	1.5	3.6	1.2	70	5.8	8.4	12	2.3	3.6	0.20

N.A.: not analysed; N.Q.: not quantifiable.

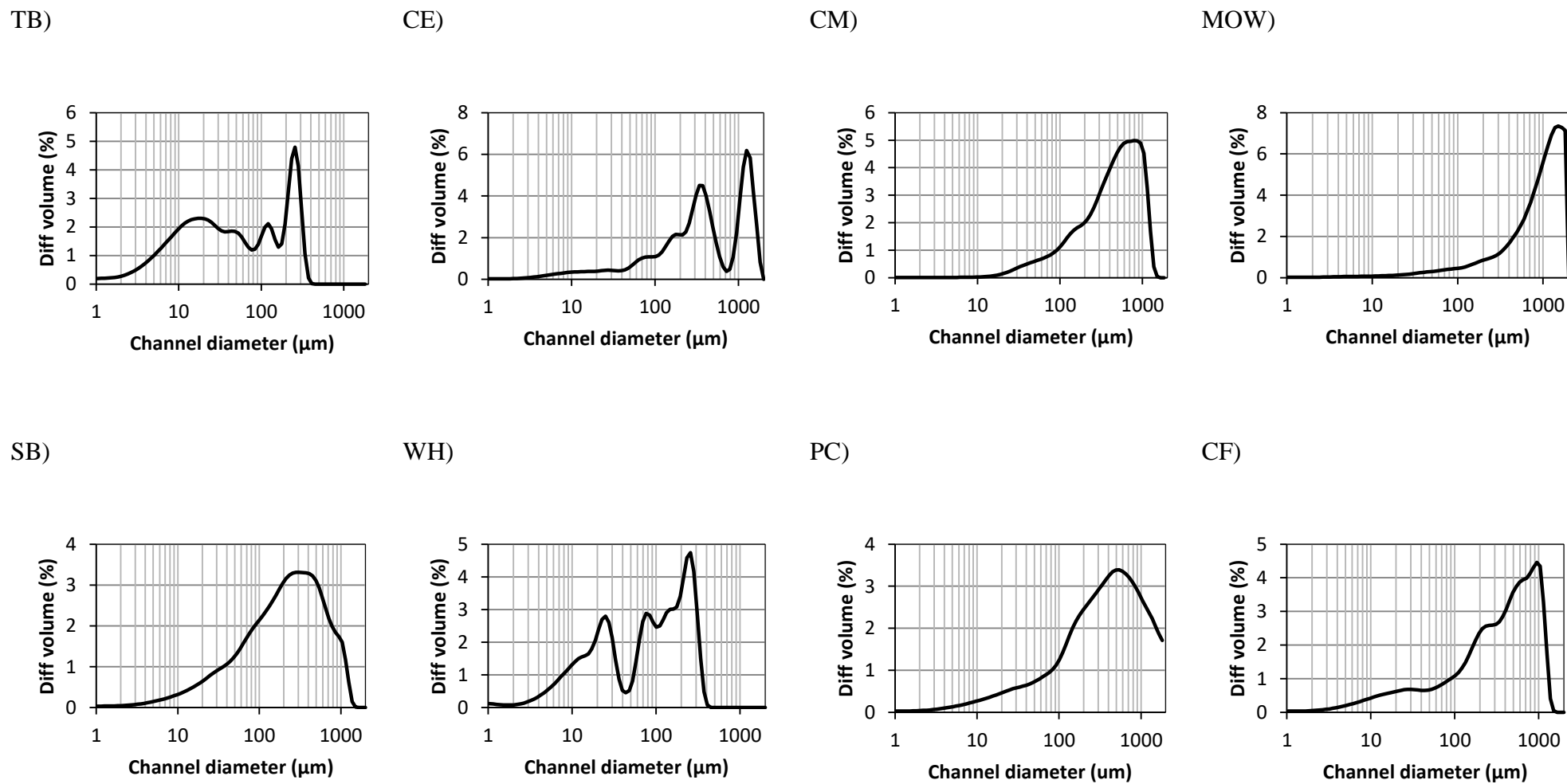
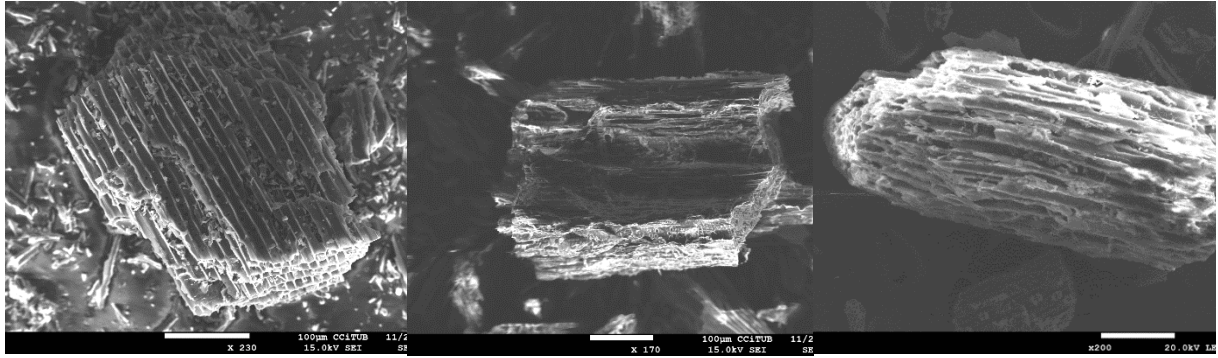


Figure 4.1 Particle size distribution of the sorbent materials.

TB)

CE)

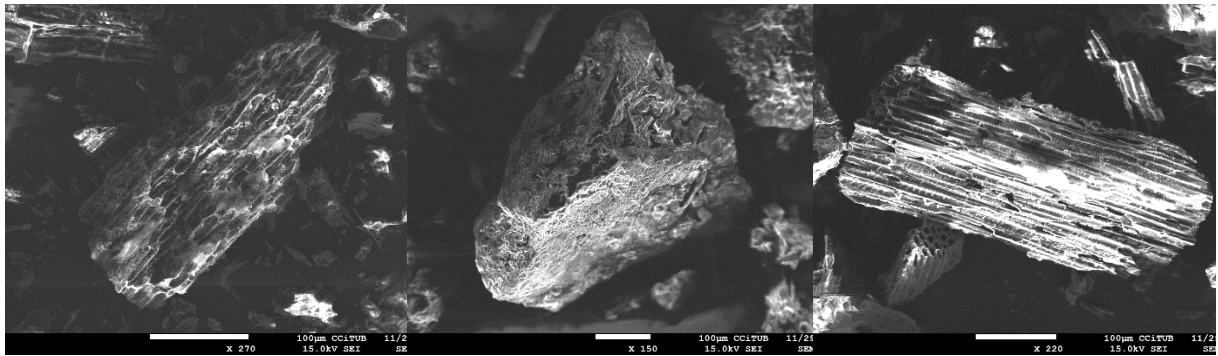
SB)



WH)

CM)

PC)



NGAC)

CF)

GAC)

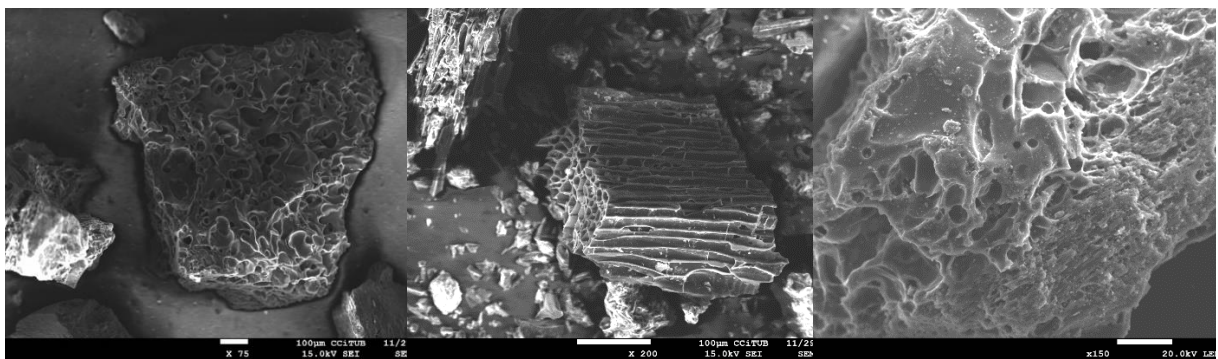
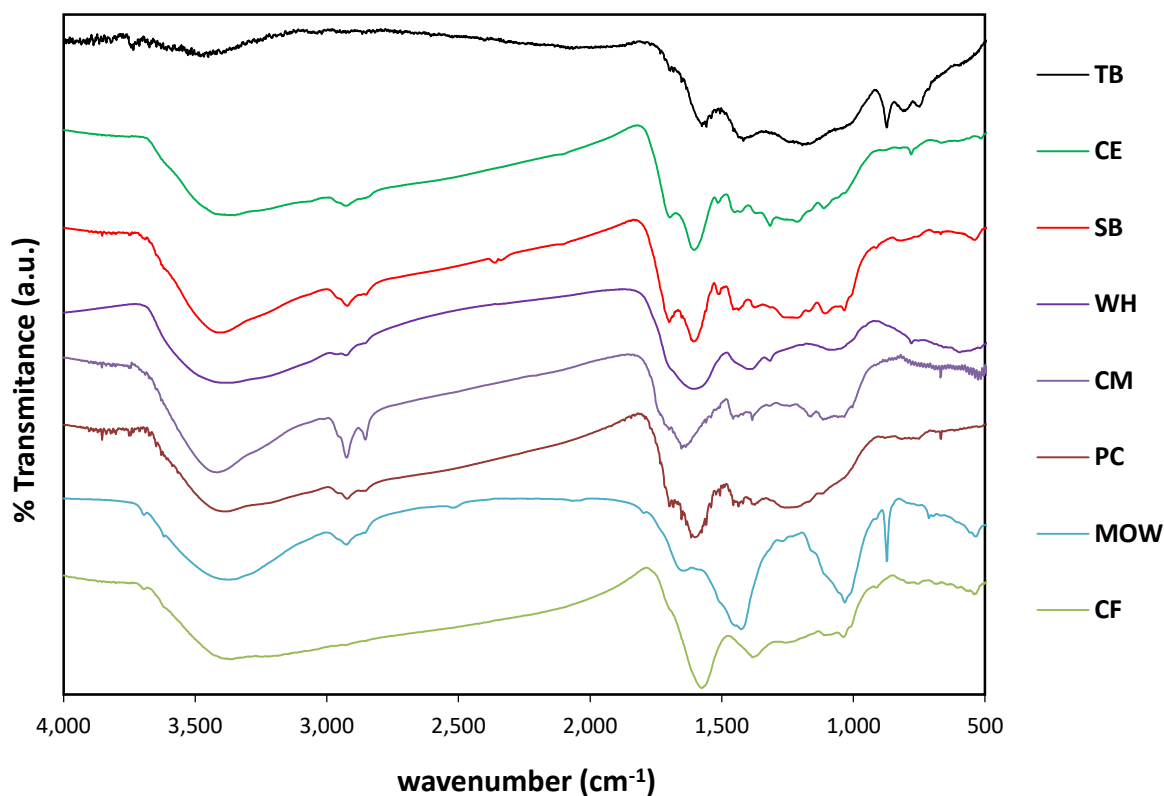


Figure 4.2 SEM images of the sorbent materials.

Table 4.4 Water soluble cations and anions of the sorbents.

	TB	CE	SB	WH	CM	PC	MOW	CF	GAC	NGAC
<i>Soluble cations</i>										
Ca (meq L ⁻¹)	0.90	0.79	0.33	2.2	1.4	0.06	1.6	0.34	1.0	0.14
Mg (meq L ⁻¹)	0.22	1.8	0.38	25	2.0	0.35	1.8	0.31	1.6	0.02
K (meq L ⁻¹)	0.33	0.76	0.47	31	2.3	5.3	3.0	1.6	0.68	0.01
Na (meq L ⁻¹)	0.07	0.26	0.04	12	0.06	2.7	5.7	0.05	0.29	0.03
<i>Soluble anions</i>										
Cl (meq L ⁻¹)	0.20	1.4	0.07	58	0.85	12	8.8	0.31	0.33	0.05
SO ₄ (meq L ⁻¹)	0.25	2.3	0.03	1.8	1.1	0.08	1.8	0.22	1.9	0.04
NO ₃ (meq L ⁻¹)	0.41	0.17	N.D.	N.D.	N.D.	N.D.	0.25	1.7	0.02	0.01
PO ₄ (meq L ⁻¹)	0.03	N.D.	N.D.	N.D.	1.6	1.6	0.19	N.D.	0.01	N.D.

N.D.: not detected

**Figure 4.3** FTIR spectra of the sorbent materials.

4.3.2. Effect of equilibration time on PFOS sorption

The evaluation of the sorption kinetics of PFOS in the four tested materials revealed that equilibrium was reached within the first 12 – 24 hours (see **Figure 4.4**), except for MOW, which required longer times. Thus, sorption experiments were carried out during 48 hours, in agreement with previous kinetic studies evaluating PFOS sorption in biochars with contrasting properties (Guo et al., 2017). The kinetic data were fitted to a PSOM, obtaining Pearson correlation coefficients close to one (**Table 4.5**). The PSOM results confirmed that PFOS sorption was faster in biochars than in compost and charcoal fines, although MOW showed a stronger affinity at longer times than the biochar CE. It has been hypothesized that in activated carbons particle size is one of the major factors controlling kinetic adsorption rates (Zhi and Liu, 2015). The V_0 values obtained followed the trend: TB > CE > CF > MOW, which were roughly negatively correlated with the material median particle size. This may confirm that sorption rates increase with decreasing particle size, and therefore, that materials with smaller particle size could be better candidates for remediation purposes.

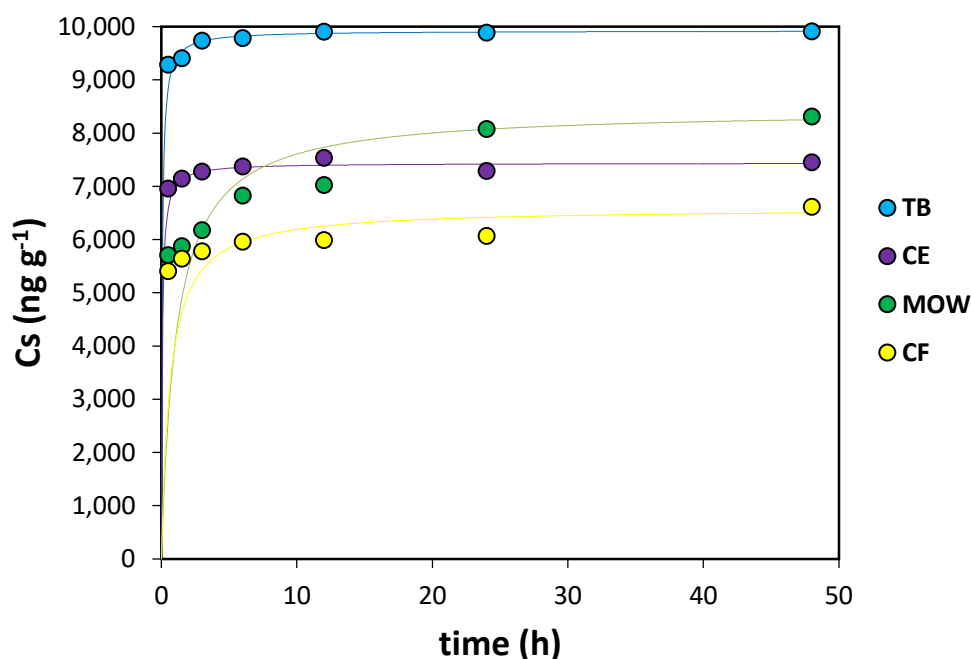


Figure 4.4 Sorption kinetics of PFOS in TB, CE, MOW and CF. Solid lines indicate the PSOM fitting.

Table 4.5 PSOM kinetic fitting results for PFOS sorption in materials TB, CE, MOW and CF.

Material	$C_{S,eq}$ (ng g ⁻¹)	V_0 (ng g ⁻¹ h ⁻¹)	K_2 (g ng ⁻¹ h ⁻¹)	r^2
TB	$9.9 \cdot 10^3$	$1.6 \cdot 10^5$	$1.6 \cdot 10^{-3}$	0.999
CE	$7.4 \cdot 10^3$	$1.1 \cdot 10^5$	$2.0 \cdot 10^{-3}$	0.999
MOW	$8.4 \cdot 10^3$	$7.7 \cdot 10^3$	$0.11 \cdot 10^{-3}$	0.998
CF	$6.6 \cdot 10^3$	$1.0 \cdot 10^4$	$0.24 \cdot 10^{-3}$	0.998

$C_{S,eq}$ = sorbed concentration at equilibrium; V_0 = initial PSOM rate constant; K_2 = PSOM rate constant

4.3.3. Effect of initial concentration on PFOS sorption

Sorption isotherm plots (C_S vs. C_{eq} plots) were constructed to evaluate the effect of the initial PFOS concentration on K_d (see **Figure 4.5**). Whereas previous reports have indicated saturated PFOS sorption in biochar and activated carbon samples at mg L⁻¹ levels (Guo et al., 2017; Ochoa-Herrera and Sierra-Alvarez, 2008), and also close-to-linear isotherms for PFOS on activated carbon (Zhang et al., 2016), linear sorption isotherms were obtained under our experimental conditions ($r^2 > 0.98$) for all the tested materials (see **Table 4.6**). The linearity of the isotherms was further confirmed after obtaining Freundlich N parameters statistically equal to one. This could be attributed to both the higher solid-to-solution ratio (40 g L⁻¹) and the lower initial PFOS concentration used in our experiments, providing a sufficient amount of sorption sites for the PFAS and, thus, ensuring a linear sorption pattern.

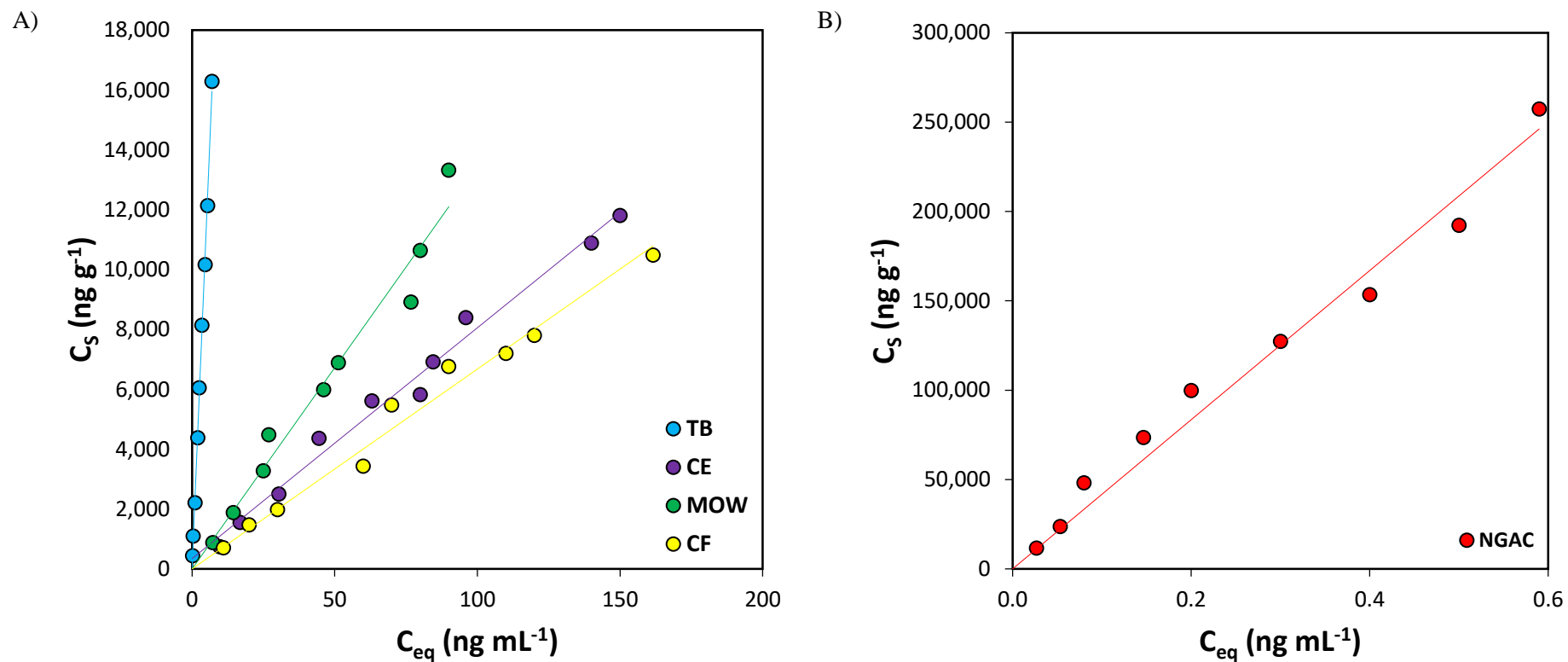


Figure 4.5 Sorption isotherms of PFOS in the materials TB, CE, MOW and CF (A); Sorption isotherms of PFOS in the material NGAC (B);

Solid lines indicate the linear fitting .

Table 4.6 PFOS sorption parameters (\pm 95% confidence interval) derived from the linear and Freundlich fitting of the sorption isotherms.

Material	K_d (L kg ⁻¹)	r^2	K_F (mg kg ⁻¹) / (mg L ⁻¹) ^N	N (dimensionless)	r^2
TB	2,290 \pm 54	0.998	2,290 \pm 234	1.02 \pm 0.06	0.998
CE	78 \pm 6	0.989	120 \pm 62	0.91 \pm 0.11	0.989
MOW	140 \pm 10	0.991	130 \pm 110	1.01 \pm 0.20	0.978
CF	67 \pm 4	0.995	89 \pm 68	0.94 \pm 0.16	0.983
NGAC	4.17 \cdot 10 ⁵ \pm 3.00 \cdot 10 ⁴	0.982	3.85 \cdot 10 ⁵ \pm 5.98 \cdot 10 ⁴	1.07 \pm 0.17	0.982

4.3.4. Effects of pH, Ca concentration and DOC content on PFOS sorption

The sorption percentages of PFOS under different experimental conditions are shown in **Figure 4.6**. For a given Ca concentration, PFOS sorption generally decreased with increasing pH, in agreement with previous findings (Saeidi et al., 2020a). This may be partly due to the increasing number of repulsions between the negatively-charged surface and PFOS at increasing pH values. This decrease was more significant between pH 5 and pH 7 for the CE and CF materials, which had the lowest pH_{ZPC} , highlighting the importance of the chemical groups present at the material surface for PFAS sorption (Saeidi et al., 2020a). The sorption percentages under acidic conditions for each material were high and relatively constant, regardless of the calcium concentration. This is in contrast to what was observed at neutral and, especially, alkaline pH values, where the sorption percentages increased with the Ca concentration. This might be attributed to two complementary mechanisms: the shielding effect of calcium ions under alkaline conditions that reduces the negative repulsions between the PFOS and the material surface and the presence of electrostatic bridge interactions between the negatively-charged surface and PFOS assisted by divalent cations (Du et al., 2014).

DOC has been reported to negatively affect PFOS sorption in activated carbons at levels over 10 mg C L^{-1} (Yu et al., 2012), which may be explained by both the competition between DOC and the PFAS for the solid material, whereas other authors attributed this effect to the blocking effect of DOC on the sorption sites present in the microporous (Saeidi et al., 2020b). For our materials, the DOC contents ranged from 10 to 250 mg C L^{-1} under acidic and neutral conditions depending on the material and regardless of the calcium concentration, although these levels significantly increased up to $1,100 \text{ mg C L}^{-1}$ under alkaline conditions and low ionic strength conditions for some materials such as MOW (see **Figure 4.6**). The DOC content was reduced under acidic conditions likely due to the protonation of the carboxyl and alkoxy functional groups present at the surface of the materials. Under alkaline conditions, such acidic functional groups were deprotonated, thus increasing the solubility of the organic compounds and leading to an increase in the DOC level. An increase in ionic strength reduced the DOC content by decreasing DOC solubility and promoting organic matter flocculation. Therefore, according to the DOC contents in our experiments, a sorption inhibition due to DOC increasing concentration was anticipated for certain scenarios. At the highest Ca concentration, the DOC content remained low and much less dependent on pH, whereas a decrease in PFOS sorption percentages with pH could be partially explained by increasing DOC content for a given Ca concentration.

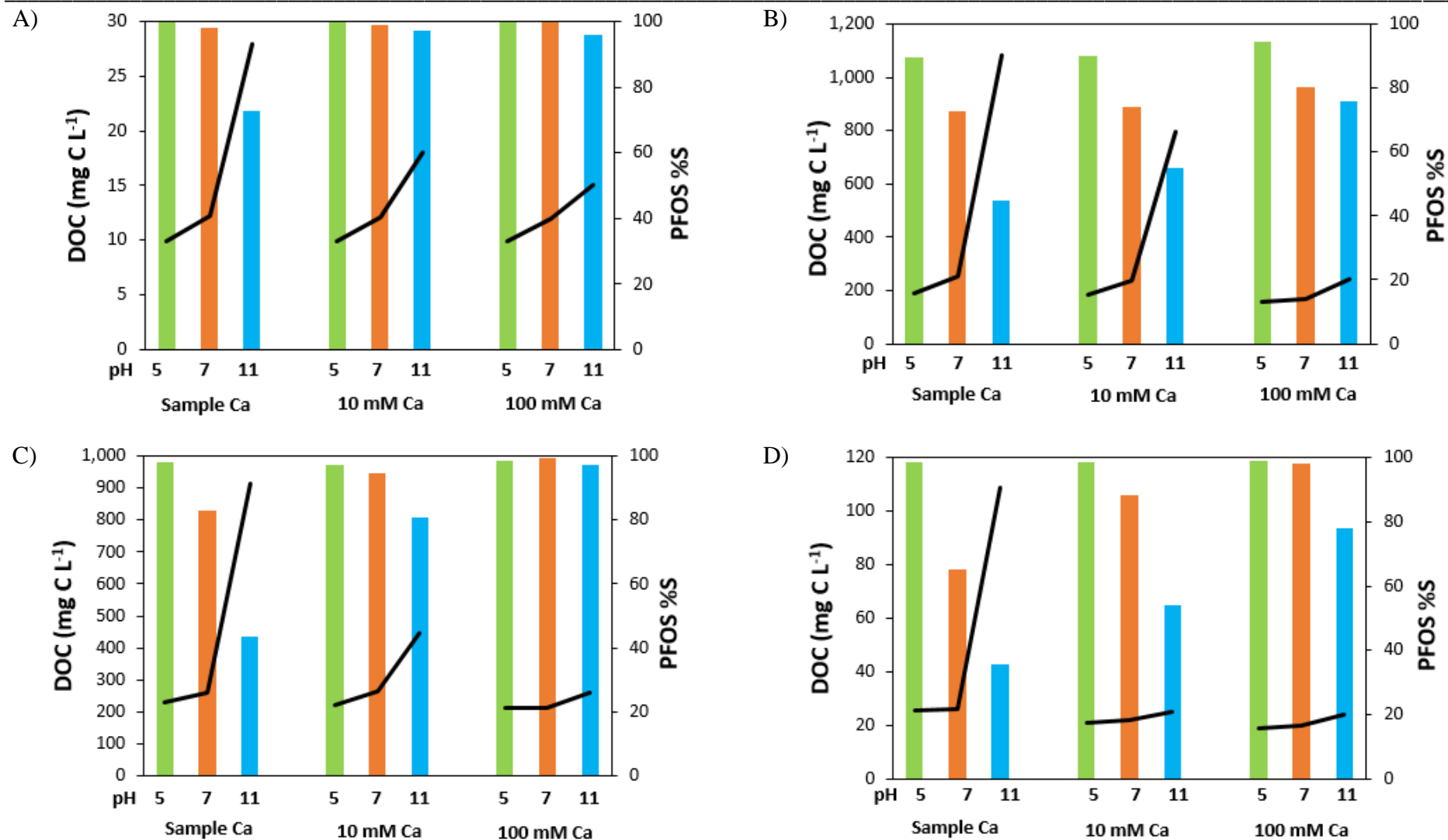


Figure 4.6 Effects of pH and Ca concentration on DOC content (solid line) and PFOS sorption percentage (bars) for: (A) TB; (B) CE; (C) MOW; (D) CF. Green bars: pH 5.0; orange bars: pH 7.0; blue bars: pH 11.0.

4.3.5. Effect of PFASs chain length

Since the K_d of PFOS was constant at the concentration ranges tested, further experiments aiming to calculate the sorption parameters for other PFASs were carried out at a single spiking concentration ensuring the quantification of K_d within the linear sorption range.

The results of these experiments are in **Table 4.7**. PFBS, PFHxA and PFHxS had K_d values up to 50 L kg^{-1} in the compost, charcoal fines and most biochars samples, being slightly lower than the K_d value of 100 L kg^{-1} reported for PFBA in a peach pit biochar with similar pH (6.5), C_{ORG} (69 %) and SSA ($6 \text{ m}^2 \text{ g}^{-1}$, Inyang and Dickenson, 2017), although they eventually increased up to 115 L kg^{-1} in the biochar TB. On the other hand, K_d values for PFOA, PFOS and PFNA were higher than those of the previous short-chained PFAS (up to 145 L kg^{-1}) and increased up to $2,900 \text{ L kg}^{-1}$ in the biochar TB. This is within the range of K_d values reported for these PFASs in different biochar samples ($0.2 - 2,400 \text{ L kg}^{-1}$, Chen et al., 2011; Söregård et al., 2020). PFDoA was the PFAS presenting highest K_d values, which ranged from 190 to $1,800 \text{ L kg}^{-1}$ for all materials excepting for TB, for which K_d value was over the 10^4 L kg^{-1} range, suggesting a moderate to high affinity between PFDoA and most carbon-rich materials. MOW showed a higher sorption affinity for those PFASs reported in **Table 4.7** than other composted wood fibres and barks of unknown properties (K_d values up to 7 L kg^{-1}), while CF also presented a higher sorption compared to similar materials rejected from the steel industry (K_d values up to 2 L kg^{-1} , Söregård et al., 2020), although, overall, their sorption K_d values were relatively low. The K_d values for all PFASs in the two activated carbon samples were much higher than for the rest of materials. These ranged from $8,0 \cdot 10^3$ to $2,6 \cdot 10^6 \text{ L kg}^{-1}$, in agreement with other reported literature values ($5,6 \cdot 10^3 - 4,8 \cdot 10^5 \text{ L kg}^{-1}$, Xiao et al., 2017), and indicated a very high PFAS sorption affinity for these materials. Moreover, FLSD test revealed that the sorption of PFASs for a given material increased when increasing PFAS chain length, in agreement with previous findings (Söregård et al., 2020; Xiao et al., 2017).

Table 4.7 K_d values of the PFASs for the 10 carbon-rich materials. Uppercase letters indicate significant differences ($p < 0.05$) among the K_d (PFAS) for a given material among the PFAS tested, as determined by the FLSD test.

Material	PFBS	PFHxA	PFHxS	PFOA	PFNA	PFOS	PFDoA
TB	19 ^A	25 ^B	115 ^C	450 ^D	1.2×10^3 ^E	2.9×10^3 ^F	$5.6 \cdot 10^4$ ^G
CE	8 ^A	20 ^B	23 ^B	35 ^C	61 ^D	75 ^D	395 ^E
SB	9 ^A	17 ^B	22 ^{BC}	27 ^C	110 ^D	110 ^D	$1.3 \cdot 10^3$ ^E
WH	10 ^A	19 ^B	29 ^C	41 ^D	68 ^E	145 ^F	$1.8 \cdot 10^3$ ^G
CM	16 ^A	38 ^B	47 ^{BC}	53 ^C	74 ^D	89 ^D	185 ^E
PC	11 ^A	15 ^{AB}	20 ^{BC}	30 ^{CD}	38 ^D	75 ^D	355 ^F
MOW	9 ^A	21 ^B	33 ^C	41 ^C	105 ^D	130 ^D	680 ^E
CF	8 ^A	10 ^A	16 ^B	31 ^C	42 ^C	63 ^D	360 ^E
GAC	$8.0 \cdot 10^3$ ^A	$1.6 \cdot 10^4$ ^B	$5.3 \cdot 10^4$ ^C	$1.3 \cdot 10^5$ ^D	$1.7 \cdot 10^5$ ^{DE}	$2.3 \cdot 10^5$ ^E	$1.7 \cdot 10^6$ ^F
NGAC	$8.9 \cdot 10^4$ ^A	$1.2 \cdot 10^5$ ^B	$1.9 \cdot 10^5$ ^C	$2.7 \cdot 10^5$ ^D	$3.2 \cdot 10^5$ ^{DE}	$4.3 \cdot 10^5$ ^E	$2.6 \cdot 10^6$ ^F

4.3.6. Multivariate analyses between material properties and PFASs sorption parameters

To better identify the key sorbent properties affecting PFAS sorption in carbon-rich materials, a PCA was performed with the data obtained in our experiments (**Table 4.7**) and material properties. Using three principal components, 84% of the data variance was explained (48%, 26% and 10% by the first, second and third principal components, respectively). The election of three principal components, all of them with eigenvalues higher than 1.0, allowed to describe a high amount of variation of the original data without overexplaining data noise (**Figure 4.7A**). The influence plot allows the identification of samples with extreme variation of each sample within the PCA model (Hotelling T^2 statistic index) or samples with a high error (Q statistic index) between a sample and its projection into the principal components retained in the model. Most of score samples were within the limits defined by the Q residuals vs. Hotelling T^2 plot, indicating that the PCA only contained a few extreme samples (**Figure 4.7B**).

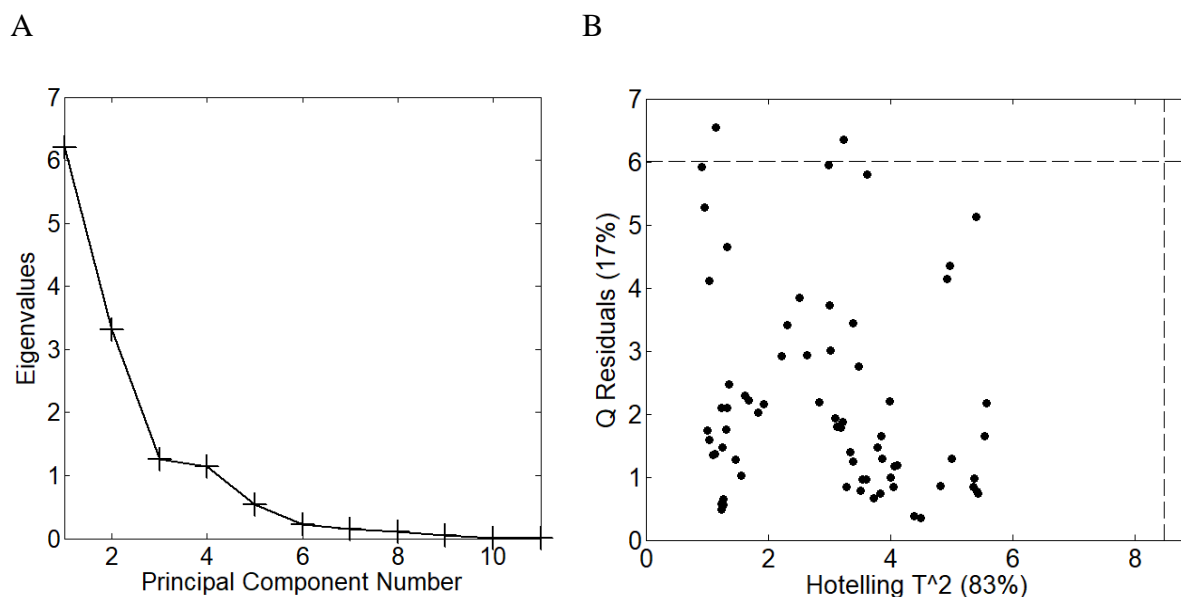


Figure 4.7 Eigenvalues of each principal component (A) and Q residuals vs. Hotelling T^2 influencing plot (B).

The results of the PCA are represented in a biplot of the first two principal components (**Figure 4.8**). According to the relative positions of the loading variables in the first two principal components, the C_{ORG}/O molar ratio, which may be related to the aromaticity of the material, had a positive effect on K_d . Unlike soils, in which the C_{ORG} content is the main parameter governing sorption, this agrees with previous findings that the basic sites in π -electron-rich regions in activated carbons materials are important for PFAS sorption, which may be explained by the adsorption of protons in π systems, thus providing sites for electrostatic interaction (Saeidi et al., 2020a), the presence of hydrophobic interactions (Li et al., 2019), or even the presence of additional stabilization mechanisms such as anion – π interactions. Further spectroscopic analysis are required to elucidate the interaction with these in π – electron-rich regions.

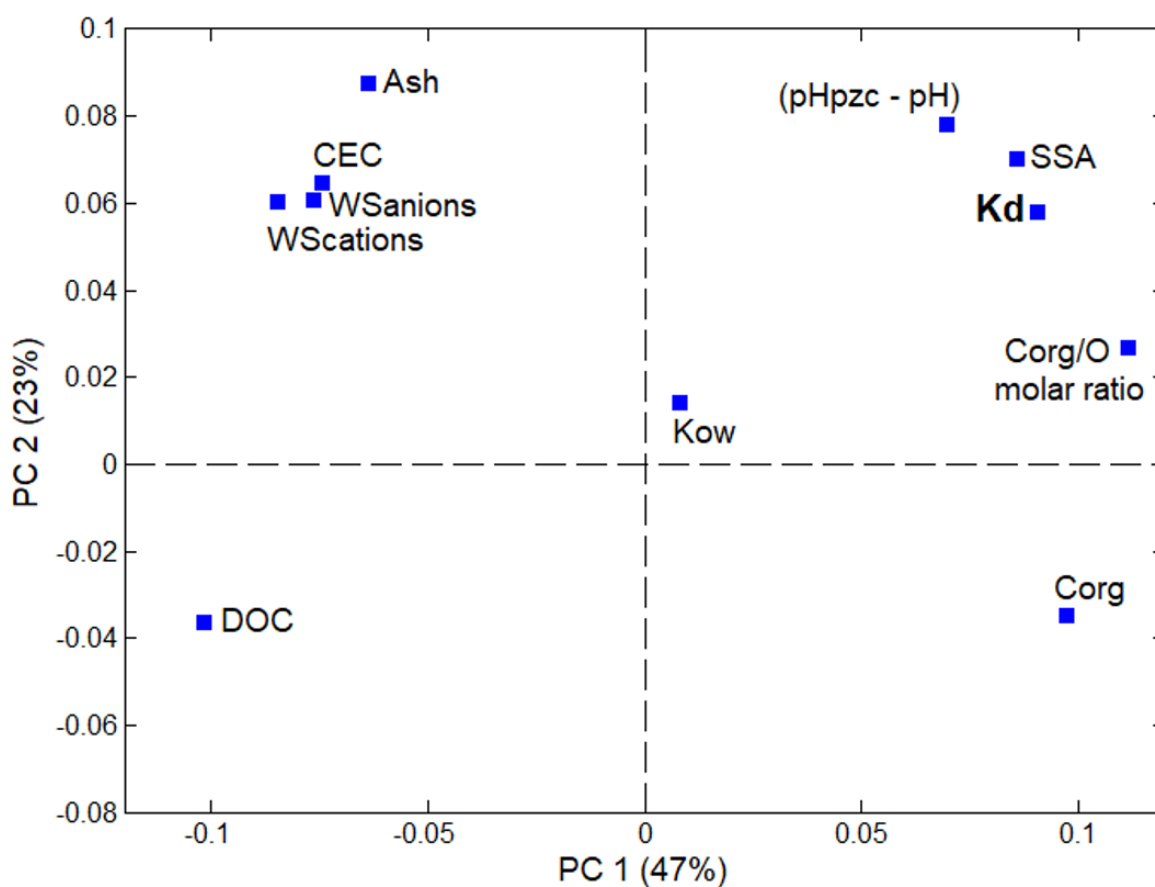


Figure 4.8 Results of the PCA according to PFASs sorption and material properties data.

Blue points indicate the loading variables.

Additionally, a higher C_{ORG}/O ratio indicates a lower amount of functional groups able to repel PFAS due to negative electrostatic repulsions. The SSA (with all values originating from N_2 -BET measurements) also had a positive effect on K_d in the PCA, in agreement with previous findings (Saeidi et al., 2020a). As the SSA is affected by both particle size distribution and porosity, this parameter may be considered an indicator of the number of sorption sites that can interact with PFASs. According to the PFASs molecular size ($150 - 300 \text{ cm}^3 \text{ mol}^{-1}$, Kim et al., 2015) and the pore width of the sorbents (**Table 4.3**), all PFASs molecules were expected to have access to the microporous structure.

As discussed in Section 4.3.4, PFAS sorption is favoured when $\text{pH} < \text{pH}_{\text{ZPC}}$. According to our PCA results, the difference between pH_{ZPC} and pH had a positive influence on K_d . This may be explained by the presence of interaction mechanisms such as electrostatic interactions in the case of positively-charged surfaces (Du et al., 2014), highlighting the additional influence of polar surface functional groups on PFAS sorption (Saeidi et al., 2020a). Both CEC and ash content did not have a direct effect on K_d . However, DOC content had a negative effect on K_d , as previously discussed in Section 4.3.4. Despite the influence of ionic strength, as discussed in Section 4.3.4, water-soluble cations did not have a significant influence on K_d according to our PCA data. This suggests that despite shielding repulsions and/or cation bridge interactions possibly play a role in PFAS sorption under certain experimental conditions for a single material (Du et al., 2014), these interactions are, overall, not predominant when considering all the materials. Similarly, although anion exchange interactions have been suggested to play a role in PFAS sorption in activated carbons (Saeidi et al., 2020a), our PCA results showed that water-soluble anions did not have a direct effect on K_d .

The third principal component to the PCA explained an additional 11% of the data variance, which mostly accounted for the contribution of PFAS hydrophobicity, represented by its $\log K_{\text{OW}}$. Similar results were obtained by evaluating PFAS hydrophobicity with its number

of CF₂. These findings agree with the increase in sorption observed in Section 4.3.5 with an increasing PFAS chain length, which might be due to the stronger binding of long-chained PFASs to carbon-rich materials through hydrophobic interactions (Li et al., 2019).

4.3.7. Development of a prediction model

A simple linear model was developed to predict K_d using specific physicochemical properties of the PFAS and the carbon-rich materials. The significant sorbent properties affecting PFAS sorption previously identified with the PCA (C_{ORG}/O molar ratio, SSA, $\log K_{OW}$, ($pH_{ZPC} - pH$) and DOC) were considered. As shown in **Table 1.1**, the hydrophobicity of the PFASs, expressed as $\log K_{OW}$, increased linearly with each fluorinated carbon added to the alkyl chain ($\log K_{OW} = 0.75 (\pm 0.07) \times \text{number of CF}_2$, $r^2 = 0.98$, $p < 0.001$, $n = 15$). Due to this strong correlation, PFAS hydrophobicity could be reasonably evaluated based on either the number of CF₂ or the $\log K_{OW}$. In principle, K_{OW} values differentiate better between PFASs that have the same number of CF₂, but different functional groups (*e.g.*, PFOS and PFNA). However, and although all $\log K_{OW}$ values in **Table 1.1** were calculated values, they may vary from experimental determinations. Therefore, CF₂, an easily available parameter that is descriptive of PFASs, was chosen as the descriptor for hydrophobicity in the development of the prediction model.

The small number of studies in the literature reporting DOC levels led to the exclusion of DOC content from the model. Subsequently, robust SMLR with the 85 entries of the calibration set was performed after a \log_{10} transformation of the data (with the exception of pH_{ZPC} and pH). By considering only the C_{ORG}/O molar ratio, SSA and CF₂ 90% of the K_d (PFAS) data variance was explained. The inclusion of the variable ($pH_{ZPC} - pH$) resulted in a non-significant coefficient and did not increase the explained variance, and therefore was excluded from the model, also because pH_{ZPC} may be affected for some materials with high ash

contents. Accordingly, the final model included the $C_{\text{ORG/O}}$ molar ratio and SSA, which may be indicative of the quality and quantity of the sorption sites available for PFAS sorption through hydrophobic interactions, respectively. In addition, the inclusion of the variable CF_2 allowed the model to be applicable to a wide range of PFASs. The robust SMLR resulted in the following equation, which defined the prediction model:

$$\log K_d = 1.87 (\pm 0.39) \log C_{\text{ORG/O}} + 0.49 (\pm 0.14) \log \text{SSA} + 0.25 (\pm 0.06) \text{CF}_2 - 0.94 (\pm 0.46) \quad (4.7)$$

$$r^2 = 0.90, n = 85; p < 0.001$$

The range of values of the model variables included in the calibration set establish the application range of the K_d (PFAS) prediction model. Specifically, the $C_{\text{ORG/O}}$ molar ratio ranged 1.3 – 104, SSA (measured in all cases by N_2 -BET) ranged 0.06 – 2,450 $\text{m}^2 \text{g}^{-1}$, and PFASs chain length ranged 3 – 11 CF_2 units. Although not included in the prediction model, the sample pH in the calibration set ranged 4 – 10, which suggests that the prediction model can be applicable to a wide range of environmentally relevant pH values. According to the expected maximum sorption capacities of carbon-rich products (up to several hundred g kg^{-1} , Gagliano et al., 2020), and maximum PFASs concentrations in contaminated soils (up to several mg kg^{-1} , Brusseau et al., 2020) the model should be applicable to most environmental conditions, since materials are not likely to reach saturation and, therefore, sorption would fall within the linear range of the isotherms, thus being K_d a good descriptor of the sorption process.

4.3.8. External validation of the prediction model

The K_d (PFAS) prediction model was externally validated with the validation set by splitting the data into two sets according to the type of materials (biochars and activated carbons), as shown in **Figure 4.9**. A satisfactory prediction was obtained in both cases, generating a slope between predicted and experimental $\log K_d$ values statistically equal to one and a null y-intercept, as well as explaining 75% and 68% of the data variance, respectively.

According to RMSE and RPD values, the model was of an acceptable quality for predicting K_d (PFAS) values in both biochars and activated carbons, especially considering that the validation dataset was affected by different sources of uncertainty, including the intrinsic variability of the literature data and the derivation of K_d values from different sorption parameters. The external validation of the model considering the overall dataset without refining data among materials also led to a satisfactory prediction, generating a slope between predicted and experimental $\log K_d$ statistically equal to one (0.94 ± 0.19) and a null y-intercept, as well as explaining 71% of the variance, and obtaining RMSE and RPD values of 0.53 and 1.57, respectively.

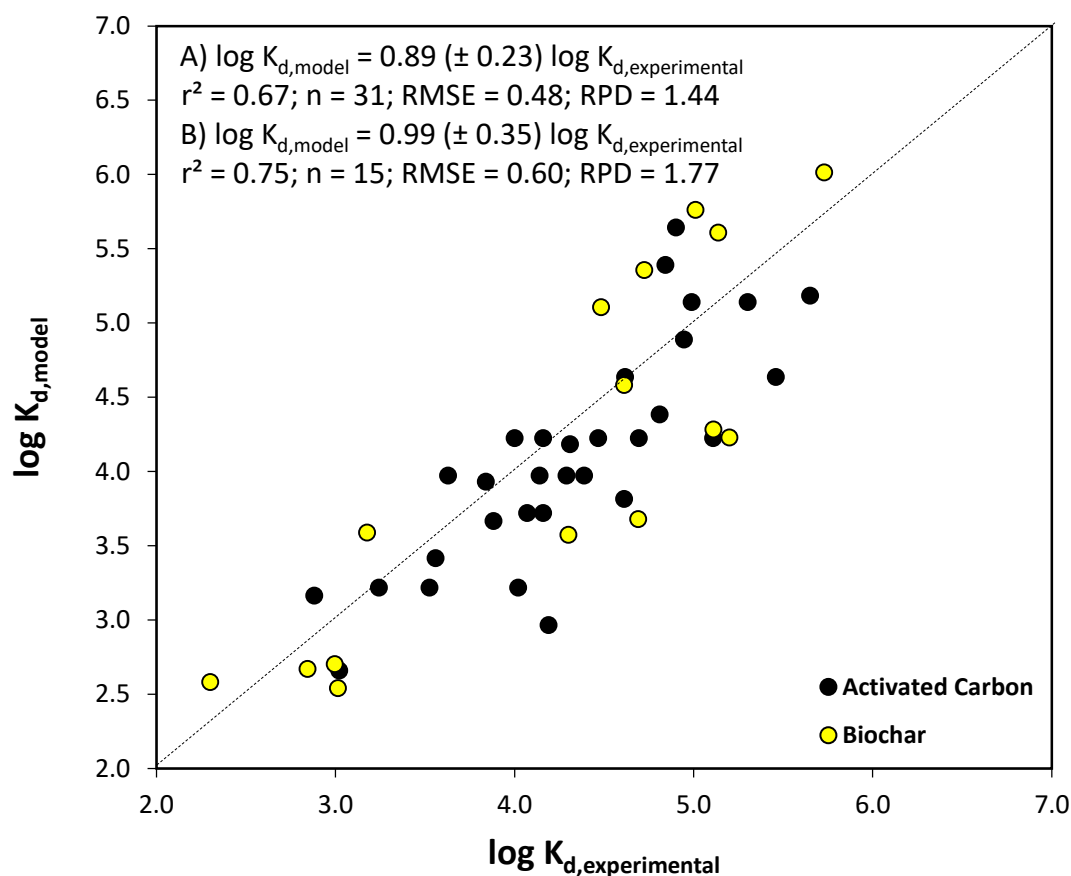


Figure 4.9 External validation of the prediction model, with separated validation sets for (A) activated carbons and (B) biochars.

The prediction errors were mostly around 0.5 $\log K_d$ units, increasing up to 1.2 $\log K_d$ units in the worst-case scenario. According to these results, the quality of the model was considered acceptable taking into account the variability of the validation dataset and that the

model aims to roughly group materials according to their PFAS sorption affinity that may vary over six orders of magnitude. All these results suggest that the $\log K_d$ values of PFASs for carbon-rich materials can be predicted with an acceptable accuracy using easily-derived physicochemical properties of the sorbent ($C_{\text{ORG/O}}$ and SSA) and PFAS (number of CF_2 units)

4.4. Conclusions

In this chapter, it has been demonstrated that the sorption of anionic PFASs by carbon-rich materials (biochars, activated carbon, compost and charcoal fines), although affected by solution-specific properties (*i.e.*, pH, concentration of divalent cations and DOC content), was mainly controlled by hydrophobic interactions. According to the proposed model, K_d values for PFASs in carbon-rich materials (biochars and activated carbons) can be predicted with acceptable accuracy using only a few physicochemical properties of the sorbent ($C_{\text{ORG/O}}$ molar ratio and SSA) and the PFAS (number of CF_2). The successful external validation of the proposed model using literature data, although affected by intrinsic sources of variability, suggests that the model may be useful in assessing the potential affinity of carbon-rich materials for PFASs in the early screening of candidate materials for environmental remediation. However, additional sorption data of PFASs of different chain-length in extensively characterized carbon-rich materials will be valuable to further improve the application range of the model. In addition, the identification of key sorbent properties affecting PFAS sorption may be useful in optimizing industrial processes (*i.e.*, pyrolysis/composting conditions or the physicochemical activation methods) to magnify these properties to increase sorbent affinity.

4.5. References

- Ahmad, M., Upamali, A., Eun, J., Zhang, M., Bolan, N., Mohan, D., Vithanage, M., Soo, S., Sik, Y., 2014. Biochar as a sorbent for contaminant management in soil and water: A review. *Chemosphere*, 99, 19–33. <https://doi.org/10.1016/j.chemosphere.2013.10.071>
- Askeland, M., Clarke, B. O., Cheema, S. A., Mendez, A., Gasco, G., Paz-Ferreiro, J., 2020. Biochar sorption of PFOS, PFOA, PFHxS and PFHxA in two soils with contrasting texture. *Chemosphere*, 249, 126072. <https://doi.org/10.1016/j.chemosphere.2020.126072>
- Brusseau, M. L., Anderson, R. H., Guo, B., 2020. PFAS concentrations in soils: Background levels versus contaminated sites. *Sci. Total Environ.* 740, 140017. <https://doi.org/10.1016/j.scitotenv.2020.140017>
- Carballo, T., Gil, M. V., Gómez, X., González-Andrés, F., Morán, A., 2008. Characterization of different compost extracts using Fourier-transform infrared spectroscopy (FTIR) and thermal analysis. *Biodegradation*, 19 (6), 815–830. <https://doi.org/10.1007/s10532-008-9184-4>
- Carter, K. E., Farrell, J., 2010. Removal of perfluorooctane and perfluorobutane sulfonate from water via carbon adsorption and ion exchange. *Sep. Sci. Technol.* 45 (6), 762–767. <https://doi.org/10.1080/01496391003608421>
- Chen, X., Xia, X., Wang, X., Qiao, J., Chen, H., 2011. A comparative study on sorption of perfluorooctane sulfonate (PFOS) by chars, ash and carbon nanotubes. *Chemosphere*, 83 (10), 1313–1319. <https://doi.org/10.1016/j.chemosphere.2011.04.018>
- Colomer-Vidal, P., Jiang, L., Mei, W., Luo, C., Lacorte, S., Rigol, A., Zhang, G., 2022. Plant uptake of perfluoroalkyl substances in freshwater environments (Dongzhulong and Xiaoqing Rivers, China). *J. Hazard. Mater.* 421, 126768. <https://doi.org/10.1016/j.jhazmat.2021.126768>

- Deng, S., Nie, Y., Du, Z., Huang, Q., Meng, P., Wang, B., Huang, J., Yu, G., 2015. Enhanced adsorption of perfluorooctane sulfonate and perfluorooctanoate by bamboo-derived granular activated carbon. *J. Hazard. Mater.* 282, 150–157. <https://doi.org/10.1016/j.jhazmat.2014.03.045>
- Doumer, M. E. M., Arízaga, G. G. C., da Silva, D. A., Yamamoto, C. I., Novotny, E. H., Santos, J. M., dos Santos, L. O., Wisniewski, Jr. A., de Andrade, J. B., Mangrich, A. S., 2015. Slow pyrolysis of different Brazilian waste biomasses as sources of soil conditioners and energy, and for environmental protection. *J. Anal. Appl. Pyrol.* 113, 434–443. <https://doi.org/10.1016/j.jaap.2015.03.006>
- Doumer, M. E., Rigol, A., Vidal, M., Mangrich, A. S., 2016. Removal of Cd, Cu, Pb, and Zn from aqueous solutions by biochars. *Environ. Sci. Pollut. R.* 23 (3), 2684–2692. <https://doi.org/10.1007/s11356-015-5486-3>
- Du, Z., Deng, S., Bei, Y., Huang, Q., Wang, B., 2014. Adsorption behavior and mechanism of perfluorinated compounds on various adsorbents — A review. *J. Hazard. Mater.* 274, 443–454. <https://doi.org/10.1016/j.jhazmat.2014.04.038>
- Du, Z., Deng, S., Chen, Y., Wang, B., Huang, J., Wang, Y., Yu, G., 2015. Removal of perfluorinated carboxylates from washing wastewater of perfluorooctanesulfonyl fluoride using activated carbons and resins. *J. Hazard. Mater.* 286, 136–143. <https://doi.org/10.1016/j.jhazmat.2014.12.037>
- Fagbayigbo, B. O., Opeolu, B. O., Fatoki, O. S., Akenga, T. A., Olatunji, O. S., 2017. Removal of PFOA and PFOS from aqueous solutions using activated carbon produced from *Vitis vinifera* leaf litter. *Environ. Sci. Pollut. R.* 24 (14), 13107–13120. <https://doi.org/10.1007/s11356-017-8912-x>

- Gagliano, E., Sgroi, M., Falciglia, P. P., Vagliasindi, F. G. A., Roccaro, P., 2020. Removal of poly- and perfluoroalkyl substances (PFAS) from water by adsorption: Role of PFAS chain length, effect of organic matter and challenges in adsorbent regeneration. *Water Res.* 171, 115381. <https://doi.org/10.1016/j.watres.2019.115381>
- Gellrich, V., Stahl, T., Knepper, T. P., 2012. Behavior of perfluorinated compounds in soils during leaching experiments. *Chemosphere*, 87 (9), 1052–1056. <https://doi.org/10.1016/j.chemosphere.2012.02.011>
- Guo, W., Huo, S., Feng, J., Lu, X., 2017. Adsorption of perfluorooctane sulfonate (PFOS) on corn straw-derived biochar prepared at different pyrolytic temperatures. *J. Taiwan Inst. Chem. Eng.* 78, 265–271. <https://doi.org/10.1016/j.jtice.2017.06.013>
- Horikawa, Y., Hirano, S., Mihashi, A., Kobayashi, Y., Zhai, S., Sugiyama, J., 2019. Prediction of Lignin Contents from Infrared Spectroscopy: Chemical Digestion and Lignin/Biomass Ratios of *Cryptomeria japonica*. *App. Biochem. Biotechnol.* 188 (4), 1066–1076. <https://doi.org/10.1007/s12010-019-02965-8>
- Inyang, M., Dickenson, E. R. V., 2017. The use of carbon adsorbents for the removal of perfluoroalkyl acids from potable reuse systems. *Chemosphere*, 184, 168–175. <https://doi.org/10.1016/j.chemosphere.2017.05.161>
- Jamieson, T., Sager, E., Guéguen, C., 2014. Characterization of biochar-derived dissolved organic matter using UV-visible absorption and excitation-emission fluorescence spectroscopies. *Chemosphere*, 103, 197–204. <https://doi.org/10.1016/j.chemosphere.2013.11.066>
- Kim, M., Li, L. Y., Grace, J. R., Yue, C., 2015. Selecting reliable physicochemical properties of perfluoroalkyl and polyfluoroalkyl substances (PFASs) based on molecular descriptors. *Environ. Pollut.* 196, 462–472. <https://doi.org/10.1016/j.envpol.2014.11.008>

- Knight, E. R., Janik, L. J., Navarro, D. A., Kookana, R. S., McLaughlin, M. J., 2019. Predicting partitioning of radiolabelled ^{14}C -PFOA in a range of soils using diffuse reflectance infrared spectroscopy. *Sci. Total Environ.* 686, 505–513. <https://doi.org/10.1016/j.scitotenv.2019.05.339>
- Kupryianchyk, D., Hale, S. E., Breedveld, G. D., Cornelissen, G., 2016. Treatment of sites contaminated with perfluorinated compounds using biochar amendment. *Chemosphere*, 142, 35–40. <https://doi.org/10.1016/j.chemosphere.2015.04.085>
- Lesmeister, L., Lange, F. T., Breuer, J., Biegel-Engler, A., Giese, E., Scheurer, M., 2020. Extending the knowledge about PFAS bioaccumulation factors for agricultural plants – A review. *Sci. Total Environ.* 766, 142640. <https://doi.org/10.1016/j.scitotenv.2020.142640>
- Li, M., Sun, F., Shang, W., Zhang, X., Dong, W., Liu, T., Pang, W., 2019. Theoretical studies of perfluorochemicals (PFCs) adsorption mechanism on the carbonaceous surface. *Chemosphere*, 235, 606–615. <https://doi.org/10.1016/j.chemosphere.2019.06.191>
- Limousin, G., Gaudet, J. P., Charlet, L., Szenknect, S., Barthès, V., Krimissa, M., 2007. Sorption isotherms: A review on physical bases, modeling and measurement. *Appl. Geochem.* 22, 249–275. <https://doi.org/10.1016/j.apgeochem.2006.09.010>
- Meng, P., Fang, X., Maimaiti, A., Yu, G., Deng, S., 2019. Efficient removal of perfluorinated compounds from water using a regenerable magnetic activated carbon. *Chemosphere*, 224, 187–194. <https://doi.org/10.1016/j.chemosphere.2019.02.132>
- Morlay, C., Quivet, E., Pilshofer, M., Faure, R., Joly, J. P., 2012. Adsorption of Imazamox herbicide onto Filtrasorb 400 activated carbon. *J. Porous Mat.* 19 (1), 79–86. <https://doi.org/10.1007/s10934-011-9450-4>

- Ochoa-Herrera, V., Sierra-Alvarez, R., 2008. Removal of perfluorinated surfactants by sorption onto granular activated carbon, zeolite and sludge. *Chemosphere*, 72 (10), 1588–1593. <https://doi.org/10.1016/j.chemosphere.2008.04.029>
- OECD, 2000. OECD 106 Adsorption - Desorption Using a Batch Equilibrium Method. OECD Guideline for the Testing of Chemicals. <https://doi.org/10.1787/9789264069602-en>
- Prevedouros, K., Cousins, I. T., Buck, R. C., Korzeniowski, S. H., 2006. Sources, fate and transport of perfluorocarboxylates. *Environ. Sci. Technol.* 40 (1), 32–44. <https://doi.org/10.1021/es0512475>
- Qian, J., Shen, M., Wang, P., Wang, C., Li, K., Liu, J., Lu, B., Tian, X., 2017. Perfluorooctane sulfonate adsorption on powder activated carbon: Effect of phosphate (P) competition, pH, and temperature. *Chemosphere*, 182, 215–222. <https://doi.org/10.1016/j.chemosphere.2017.05.033>
- Saeidi, N., Kopinke, F. D., Georgi, A., 2020a. Understanding the effect of carbon surface chemistry on adsorption of perfluorinated alkyl substances. *Chem. Eng. J.* 381, 122689. <https://doi.org/10.1016/j.cej.2019.122689>
- Saeidi, N., Kopinke, F. D., Georgi, A., 2020b. What is specific in adsorption of perfluoroalkyl acids on carbon materials? *Chemosphere*, 273. <https://doi.org/10.1016/j.chemosphere.2020.128520>
- Senevirathna, S. T. M. L. D., Tanaka, S., Fujii, S., Kunacheva, C., Harada, H., Ariyadasa, B. H. A. K. T., Shivakoti, B. R., 2010. Adsorption of perfluorooctane sulfonate (n-PFOS) onto non ion-exchange polymers and granular activated carbon: Batch and column test. *Desalination*, 260 (1–3), 29–33. <https://doi.org/10.1016/j.desal.2010.05.005>

- Silvani, L., Cornelissen, G., Smebye, A. B., Zhang, Y., Okkenhaug, G., Zimmerman, A. R., Thune, G., Saevarsson, H., Hale, S. E., 2019. Can biochar and designer biochar be used to remediate per- and polyfluorinated alkyl substances (PFAS) and lead and antimony contaminated soils? *Sci. Total Environ.* 694, 133693. <https://doi.org/10.1016/j.scitotenv.2019.133693>
- Siriwardena, D. P., Crimi, M., Holsen, T. M., Bellona, C., Divine, C., Dickenson, E., 2019. Changes in adsorption behavior of perfluorooctanoic acid and perfluorohexanesulfonic acid through chemically-facilitated surface modification of granular activated carbon. *Environ. Eng. Sci.* 36 (4), 453–465. <https://doi.org/10.1089/ees.2018.0319>
- Söregård, M., Östblom, E., Köhler, S., Ahrens, L., 2020. Adsorption behavior of per- And polyfluoroalkyl substances (PFASs) to 44 inorganic and organic sorbents and use of dyes as proxies for PFAS sorption. *J. Environ. Chem. Eng.* 8 (3), 103744. <https://doi.org/10.1016/j.jece.2020.103744>
- Sormo, E., Silvani, L., Bjerkli, N., Hagemann, N., Zimmerman, A. R., Hale, S. E., Hansen, C. B., Hartnik, T., Cornelissen, G., 2021. Stabilization of PFAS-contaminated soil with activated biochar. *Sci. Total Environ.* 763, 144034. <https://doi.org/10.1016/j.scitotenv.2020.144034>
- Stebel, E. K., Pike, K. A., Nguyen, H., Hartmann, H. A., Klonowski, M. J., Lawrence, M. G., Collins, R. M., Hefner, C. E., Edmiston, P. L., 2019. Absorption of short-chain to long-chain perfluoroalkyl substances using swellable organically modified silica. *Environ. Sci. Water Res. Technol.* 5 (11), 1854–1866. <https://doi.org/10.1039/c9ew00364a>

- Steigerwald, J. M., Ray, J. R., 2021. Adsorption behavior of perfluorooctanesulfonate (PFOS) onto activated spent coffee grounds biochar in synthetic wastewater effluent. *J. Hazard. Mater. Letters*. 2, 100025. <https://doi.org/10.1016/j.hazl.2021.100025>
- Ulrich, B. A., Im, E. A., Werner, D., Higgins, C. P., 2015. Biochar and activated carbon for enhanced trace organic contaminant retention in stormwater infiltration systems. *Environ. Sci. Technol.* 49 (10), 6222–6230. <https://doi.org/10.1021/acs.est.5b00376>
- Venegas, A., Rigol, A., Vidal, M., 2015. Viability of organic wastes and biochars as amendments for the remediation of heavy metal-contaminated soils. *Chemosphere*, 119, 190–198. <https://doi.org/10.1016/j.chemosphere.2014.06.009>
- Weishaar, J. L., Aiken, G. R., Bergamaschi, B. A., Fram, M. S., Fujii, R., Mopper, K., 2003. Evaluation of specific ultraviolet absorbance as an indicator of the chemical composition and reactivity of dissolved organic carbon. *Environ. Sci. Technol.* 37 (20), 4702–4708. <https://doi.org/10.1021/es030360x>
- Xiao, X., Ulrich, B. A., Chen, B., Higgins, C. P., 2017. Sorption of Poly- and Perfluoroalkyl Substances (PFASs) Relevant to Aqueous Film-Forming Foam (AFFF)-Impacted Groundwater by Biochars and Activated Carbon. *Environ. Sci. Technol.* 51 (11), 6342–6351. <https://doi.org/10.1021/acs.est.7b00970>
- Yan, B., Munoz, G., Sauv e, S., Liu, J., 2020. Molecular mechanisms of per- and polyfluoroalkyl substances on a modified clay: a combined experimental and molecular simulation study. *Water Res.* 184, 116166. <https://doi.org/10.1016/j.watres.2020.116166>
- Yao, Y., Volchek, K., Brown, C. E., Robinson, A., Obal, T., 2014. Comparative study on adsorption of perfluorooctane sulfonate (PFOS) and perfluorooctanoate (PFOA) by different adsorbents in water. *Water Sci. Technol.* 70 (12), 1983–1991. <https://doi.org/10.2166/wst.2014.445>

- Yu, J., Lv, L., Lan, P., Zhang, S., Pan, B., Zhang, W., 2012. Effect of effluent organic matter on the adsorption of perfluorinated compounds onto activated carbon. *J. Hazard. Mater.* 225–226, 99–106. <https://doi.org/10.1016/j.jhazmat.2012.04.073>
- Yu, Q., Zhang, R., Deng, S., Huang, J., Yu, G., 2009. Sorption of perfluorooctane sulfonate and perfluorooctanoate on activated carbons and resin: Kinetic and isotherm study. *Water Res.* 43 (4), 1150–1158. <https://doi.org/10.1016/j.watres.2008.12.001>
- Zhang, D., Luo, Q., Gao, B., Chiang, S. Y. D., Woodward, D., Huang, Q., 2016. Sorption of perfluorooctanoic acid, perfluorooctane sulfonate and perfluoroheptanoic acid on granular activated carbon. *Chemosphere*, 144, 2336–2342. <https://doi.org/10.1016/j.chemosphere.2015.10.124>
- Zhang, Q., Zhang, W. L., Liang, Y. N., 2020. Adsorption of perfluoroalkyl and polyfluoroalkyl substances (PFASs) from aqueous solution - A review. *Sci. Total Environ.* 694, 133606. <https://doi.org/10.1016/j.scitotenv.2020.142354>
- Zhi, Y., Liu, J., 2015. Adsorption of perfluoroalkyl acids by carbonaceous adsorbents: Effect of carbon surface chemistry. *Environ. Pollut.* 202, 168–176. <https://doi.org/10.1016/j.envpol.2015.03.019>
- Zhi, Y., Liu, J., 2018. Sorption and desorption of anionic, cationic and zwitterionic polyfluoroalkyl substances by soil organic matter and pyrogenic carbonaceous materials. *Chem. Eng. J.* 346, 682–691. <https://doi.org/10.1016/j.cej.2018.04.042>

CHAPTER IV

SORPTION OF FQs IN PURE SOIL

COMPONENTS

5.1. Introduction

The antimicrobial applications of quinolones were discovered in the early 1960s, although their industrial production increased during the 1970s and 1980s. Currently, FQs are prescribed for treating human and animal diseases against Gram positive and Gram negative pathogens (Andersson and MacGowan, 2003). Due to their widespread use, partial excretion by organisms and low photo and biodegradation (Girardi et al., 2011; Lin et al., 2018), high levels of FQs have been reported in environmental compartments. Specifically, FQs have been detected at mg kg^{-1} levels in animal manure such as chicken droppings, poultry and piggery, at levels up to few hundreds $\mu\text{g kg}^{-1}$ in soils and at levels up to few hundreds of ng L^{-1} in freshwater systems (Riaz et al., 2018). These concentrations may affect bacterial communities and provoke bacterial resistance against these drugs, then disrupting the balance of the original ecosystem with direct consequences to human health and other initially non-targeted organisms.

The environmental fate of FQs is mainly controlled by their sorption to soil particles (Chen et al., 2015). They have been suggested to have a low mobility and high accumulation in soils, although their sorption affinity to soil particles is pH dependent (Vasudevan et al., 2009; Pan and Chu, 2017). Evaluating the sorption of FQs in pure soil organic and mineral phases, in addition to elucidate their main interaction mechanisms, may be a first, preliminary step to assess and understand their environmental fate and overall interaction in soils.

FQs have shown a strong affinity to bind with humic and fulvic acids within the SOM phase. This process appears to depend on the physicochemical properties of the humic and fulvic acid (*i.e.*, amount and nature of functionalities, degree of aromaticity), in addition to the physicochemical properties of the aqueous solution (*i.e.*, pH, ionic strength and DOC content) and of the target FQ (*i.e.*, $\text{pK}_{\text{a}1}$; $\text{pK}_{\text{a}2}$) (Aristilde and Sposito, 2013; Martínez-Mejía et al., 2017). Although some results seem to indicate that the sorption affinity of FQs with similar chemical structures may differ (Zhao et al., 2019a), their overall sorption analogy in SOM has not yet

fully assessed. Regarding interaction mechanisms of FQs sorption in humic and fulvic acids, it has been hypothesized that cation exchange interactions are the main sorption mechanisms, although contributions of hydrogen bonding and hydrophobic interactions may play a role in sorption (Zhang et al., 2012; Martínez-Mejía et al., 2017; Liu et al., 2017a). Finally, scarce desorption data of FQs on humic acids have been reported to date (Martínez-Mejía et al., 2017). Therefore, systematic studies evaluating FQ sorption process in humic acids of contrasting properties are still required.

Regarding the role of mineral phases in FQ sorption in soils, the sorption of FQs in different metal oxides has been evaluated (Zhang and Huang, 2005; Rakshit et al., 2013; Qin, et al., 2014a), and a wide range of K_d values for specific oxides (*i.e.*, Fe oxides) has been reported (Zhang and Huang, 2007; Carrasquillo et al., 2008). Despite these studies, a comprehensive compilation of FQ sorption data in metal oxides, along with a discussion of their sorption patterns, the identification of key physicochemical properties affecting sorption and the development of K_d prediction models in these materials are still lacking.

Clay minerals may also play a relevant role in FQ sorption in soils. In fact, FQ sorption in acidic soils has been proved to positively correlate with the clay content (Leal et al., 2013). FQs have been found to strongly sorb at phyllosilicate minerals, which are the main components of the clay fraction, although the FQ sorption, quantified in terms of K_d , varied within orders of magnitude depending on the clay nature (Wan et al., 2013). Therefore, sorption of FQs in phyllosilicate minerals such as kaolinite, illite, vermiculite, palygorskyte and montmorillonite has been individually evaluated in several studies (Wu et al., 2010; Li et al., 2011; Chang et al., 2016; Liu et al., 2017) but there is still a lack of studies assessing and comparing the sorption at these phyllosilicates (Nowara et al., 1997; Wan et al., 2013). Besides, sorption of FQs in phyllosilicate minerals is expected to be pH-dependent, but K_d prediction models in different clays applicable to environmentally relevant pH ranges are scarce in the literature. Thus, to

build up a compilation of sorption K_d (FQ) data in phyllosilicate minerals and a subsequent systematic elucidation of the main physicochemical properties affecting FQ sorption is crucial to better assess the role of the clay fraction in the overall sorption of FQs in soils.

In this chapter, the sorption of the most common FQs (*i.e.*, NOR, CIP, ENR and OFL) in pure soil organic and mineral phases (specifically, humic and fulvic acids, metal oxides and phyllosilicate minerals) are discussed through data compilations originated by both own experiments and literature available data. Regarding FQ sorption at humic and fulvic acids, the sorption analogy among common FQs, the main factors affecting their sorption and their main interaction mechanisms are discussed after obtaining new sorption data in a total of seven humic acids of contrasting properties, which helped to feed a compilation of K_d (FQ) database in humic substances. Additionally, the FQ sorption in pure mineral phases and the effect of several properties (*e.g.*, pH; composition of the contact solution) are discussed on the basis of literature-compiled data, and moreover, prediction K_d (FQ) equations based on the K_d (FQ) - phase property correlations are suggested.

5.2. Sorption of FQs in humic substances

5.2.1. Materials and methods

5.2.1.1. Reagents and materials characterization

NOR (> 99%), CIP (> 99%), ENR (> 99%) and OFL (> 95%) were purchased from Sigma-Aldrich (Germany). Their main physicochemical properties are summarized in **Table 1.5**. Milli-Q double deionized water ($18.2 \text{ M}\Omega \text{ cm}^{-1}$) was obtained from a water purification system (USF PureLaB Plus, Spain). A $1,000 \text{ mg L}^{-1}$ individual FQ stock solution was prepared in acidified (pH 4.0) Milli-Q water using diluted HCl (37%, Panreac, Spain), and working solutions were prepared by appropriate dilution. Extra pure ($\geq 99\%$) dihydrated calcium chloride, sodium azide and potassium bromide were supplied by Merck (Germany). HPLC-

grade ACN, formic acid (98%) and triethanolamine ($\geq 99\%$) were purchased at Panreac (Spain). Pahokee Peat (PPHA, 1S103H), Leonardite (LHA, 1S104H), Elliot Soil (ESHA, 4S102H) and Suwannee River (SRHA, 3S101H) humic acids (HA) were purchased at the International Humic Substances Society (IHSS, <https://humic-substances.org/>), whereas additional humic acids were purchased at Janssen Chimica Belgium (JHA, 12.086.58), Sigma-Aldrich (AHA, H1,675-2, sodium salt) and Fluka Chemika Switzerland (FHA, 53680).

Besides the properties already reported for the HA samples, additional properties were characterized. The DOC content of the HA blank aqueous solutions was quantified using a DOC analyser (Analytic Jena Multi N/C) with previous acidification to pH 3.0 using HCl. Specific ultraviolet absorbance at 254 nm ($SUVA_{254}$), was acquired using a UV-spectrometer (Varian Cary 100) using a 1 cm optical cell and calculated as described elsewhere (Weishaar et al., 2003). The main physicochemical properties of the HA are summarized in **Table 5.1**.

Table 5.1 Physicochemical properties of the commercial humic acids

	LHA	ESHA	PPHA	SRHA	FHA	AHA	JHA
% C	63.8 ^a	59.5 ^a	56.4 ^a	54.6 ^a	45.9 ^b	42.2 ^b	39.2 ^b
% O	31.3 ^a	32.2 ^a	37.3 ^a	40.0 ^a	49.8 ^b	53.4 ^b	56.3 ^b
Molar C/O ratio	2.72	2.47	2.01	1.82	1.23	1.05	0.93
Aromatic C (%) ^c	58 ^a	41 ^a	47 ^a	35 ^a	N.R.	54 ^d	N.R.
Carboxyl (meq g C ⁻¹)	7.46 ^a	8.28 ^a	9.01 ^a	9.59 ^a	N.R.	N.R.	N.R.
Phenolic (meq g C ⁻¹)	2.31 ^a	1.87 ^a	1.91 ^a	4.24 ^a	N.R.	N.R.	N.R.
DOC (mg C L ⁻¹)	3.7	6.2	7.5	70	13	23	18
$SUVA_{254}$ (L mg ⁻¹ m ⁻¹)	5.0	3.0	2.8	1.5	2.1	1.8	1.2

^a Data extracted from the IHSS official webpage; ^b Data obtained from Rigol et al. (1994);

^c Referred to total carbon; ^d Data obtained from Huculak-Mączka et al. (2018). N.R.: not reported

The carbon content of the HA samples ranged 39 – 64%, and the C/O molar ratio ranged 0.9 – 2.7. Both carboxyl and phenolic contents increased with decreasing C/O molar ratio. DOC content was relatively low (4 – 23 mg C L⁻¹) under experimental conditions, although increased to 70 mg C L⁻¹ for SRHA. The SUVA₂₅₄ index ranged 1.2 – 5.0 and was comparable to other reported values (0.6 – 5.3) in a set of ten humic and fulvic acids (Weishaar et al., 2003).

FTIR spectra (Thermo Nicolet 5700) were obtained in selected samples by mixing the dried residues derived from the sorption isotherm experiments containing the maximum NOR sorbed concentration with solid KBr. The peaks in the FTIR spectra were identified using the OMNIC™ software.

5.2.1.2. Batch sorption experiments

Whereas three HA samples (LHA, ESHA and PPHA) were selected as representative materials to evaluate NOR (as representative for the rest of FQs) sorption kinetics, NOR sorption isotherms were subsequently obtained for all HA samples. Following this, the same three selected HA were used to evaluate NOR desorption and the effect of pH, DOC content, and Ca concentration (as subrogate for the ionic strength) in NOR sorption. Additional sorption experiments were carried out in the three HAs with other FQs (CIP, ENR and OFL) to test FQ sorption analogy.

Batch sorption experiments were conducted according to a procedure described elsewhere (OECD, 2000). Briefly, 6 mg of HA sample were weighed in a 50 mL PP centrifuge tube. Then, 30 mL of 10 mM CaCl₂ solution containing 1 g L⁻¹ of NaN₃ adjusted to pH 5.0 ± 0.2 (being NOR mainly under its cationic form), using 0.1 N HCl were added to achieve a 0.20 g L⁻¹ suspension of HA. After, a certain amount of NOR working solution was added to achieve a concentration of 10 mg L⁻¹ for the sorption kinetics and a concentration ranging 1–10 mg L⁻¹ for the sorption isotherms, which ensured a reliable determination of FQ concentration in the

supernatant after the sorption process. For the other sorption experiments, the single initial concentration was of 1 mg L^{-1} , which fell within the linear range of the sorption isotherms. For the experiments aiming to evaluate the effect of pH, the contact solution was adjusted using either HCl or NaOH to achieve a pH ranging from 3 to 11 after equilibrium. For the experiments aiming to evaluate the effect of Ca as a representative for changes in the ionic strength, different calcium additions were tested: 0 (use of Milli-Q water), and 5, 10 and 20 mM CaCl_2 . With the exception of the experiments under Milli-Q water, all aqueous solutions contained NaN_3 at 1 g L^{-1} . Control samples were run in parallel at the same pH/Ca status, and the DOC content in solution was monitored.

After the FQ addition, the tubes were end-over-end shaken at 30 rpm and room temperature ($25 \pm 1 \text{ }^\circ\text{C}$) and wrapped with aluminium foil to avoid photodegradation. At selected times, tubes were centrifuged for 15 min at 4°C and $7,800 \text{ g}$ (AJ2-HS, Beckman Coulter, USA). Supernatants were filtered through $0.45 \text{ }\mu\text{m}$ and analysed as described in Section 5.2.1.3. Desorption experiments were performed after drying the residues of the respective sorption experiments at $40 \pm 1 \text{ }^\circ\text{C}$. Then, 30 mL of contact solution containing 10 mM CaCl_2 and 1 g L^{-1} NaN_3 were added to the tubes, which were shaken during 48 hours, assuming that would be enough to reach desorption equilibrium according to previous studies evaluating desorption kinetics in HAs (Martínez-Mejía et al., 2017). After, tubes were centrifuged and supernatants were filtered and analysed as described previously.

Both sorption and desorption experiments were run in triplicate, and quality control samples were run in parallel in each batch. These controls included blank samples, to ensure that no background FQs were present in the HA samples, and control samples run without any suspended HA to account for possible losses through the experimental stages. Blank samples revealed that no FQ was present in the HA samples, whereas control samples revealed null FQ losses due to the experimental setup.

5.2.1.3. FQs determination by HPLC-FLD

An Agilent 1200 chromatograph was used for the FQ determination in both sorption and desorption supernatants, using an isocratic 85:15 0.1% formic acid (adjusted to pH 3.0 using triethanolamine):ACN mobile phase and a ZORBAX SB-C₁₈ (5 μm, 4.6 x 250 mm) separation column. Flow rate and injection volume were set at 1 mL min⁻¹ and 10 μL, respectively. NOR, CIP, ENR and OFL detection was carried using a FLD set at an excitation/emission wavelength of 280/447, 284/449, 284/467 and 298/499 nm, respectively. LOQ, determined as a signal-to-noise ratio of 10:1, were 0.01 mg L⁻¹ for all FQs. In order to avoid biased results due to possible matrix effects (Peruchi et al., 2015), matrix-matched calibration curves were prepared for each pH, Ca concentration, HA sample and FQ combination. Seven-point calibration curves were prepared in each case, and Pearson coefficients were in all cases up to 0.99. The precision of 10 consecutive injections of a 0.2 mg L⁻¹ NOR aqueous standard was 3.8% RSD, whereas the precision of 10 injections of 0.2 mg L⁻¹ NOR aqueous standards during 10 different days was 6.1% RSD. Similar results were obtained for CIP, ENR and OFL.

5.2.1.4. Data treatment

The kinetic data was fitted to the PSOM equation:

$$\frac{t}{C_{S,t}} = \frac{1}{K_2 C_{S,eq}^2} + \frac{t}{C_{S,eq}} = \frac{1}{V_0} + \frac{t}{C_{S,eq}} \quad (5.1)$$

where $C_{S,t}$ (mg kg⁻¹) is the sorbed concentration at time t (h), K_2 (kg mg⁻¹ h⁻¹) is the PSOM rate constant and $C_{S,eq}$ is the sorbed amount at equilibrium (mg kg⁻¹). The initial PSOM rate constant (V_0 , mg kg⁻¹ h⁻¹) can be further calculated as the product of K_2 and $C_{S,eq}^2$ (Ho and McKay, 1998). The sorbed concentration on the solid phase (C_s , mg kg⁻¹) was calculated as the difference between the initial FQ spiked concentration (C_{in} , mg L⁻¹) and the FQ concentration determined in supernatants (C_{eq} , mg L⁻¹) by HPLC-FLD, according to Equation 5.2:

$$C_S = \frac{(C_{in} - C_{eq}) \cdot V}{m} \quad (5.2)$$

where V (L) is the total volume of contact solution and m (kg) refers to the dry mass of HA. Similarly, the concentration remaining in the solid phase after running the desorption experiments ($C_{S,des}$, mg kg^{-1}) was calculated as:

$$C_{S,des} = C_{in,des} - \frac{C_{eq,des} \cdot V}{m} \quad (5.3)$$

where $C_{eq,des}$ (mg L^{-1}) is the FQ concentration in the aqueous phase quantified by HPLC-FLD after desorption experiments, whereas $C_{in,des}$ (mg kg^{-1}) is the initial FQ concentration in the solid after sorption step. Thus, $C_{in,des}$ is C_S corrected by the amount of FQ present in the residual volume of solution (V_{res} , L^{-1}) and incorporated into the solid after drying the residues of the sorption experiments:

$$C_{in,des} = C_S + \frac{C_{eq} \cdot V_{res}}{m} \quad (5.4)$$

The experimental data from the sorption and desorption isotherms were fitted to the Freundlich model, which has been applied to describe the sorption of different pollutants on heterogeneous surfaces containing sites with different affinities (Limousin et al., 2007):

$$C_S = K_F (C_{eq})^N \quad (5.5)$$

where K_F ($(\text{mg kg}^{-1})/(\text{mg L}^{-1})^N$) and N (dimensionless) are the fitted Freundlich parameters, representative of the sorption affinity and the heterogeneity of sorption sites available in the sorbent surface, respectively. An $N < 1$ value is indicative of the presence of heterogeneous sorption sites with different affinities for the sorbate, being the sites with higher affinity the first to be involved in the sorption process (Limousin et al, 2007).

K_d (L kg^{-1}), defined in Equation 5.6, and $K_{d,des}$ (L kg^{-1}), defined in Equation 5.7, were calculated within the linear range of the respective sorption isotherm as:

$$K_d = \frac{C_s}{C_{eq}} \quad (5.6)$$

$$K_{d,des} = \frac{C_{s,des}}{C_{eq,des}} \quad (5.7)$$

Lastly, sorption and desorption percentages (%S and %D, respectively) were calculated as:

$$\%S = \frac{(C_{in} - C_{eq})}{C_{eq}} \cdot 100 \quad (5.8)$$

$$\%D = \frac{C_{eq,des} \cdot V}{C_{in,des} \cdot m} \cdot 100 \quad (5.9)$$

The kinetic and isotherm data were fitted using the least squares method using Matlab (cftoolbox, Matlab® R2009a (MathWorks Inc., USA)).

5.2.1.5. Creation of a dataset of K_d (FQ) and data treatment

A dataset compiling sorption K_d (FQ) values in different humic substances was created to complete the dataset originated from our sorption experiments. Literature data of sorption K_d values for humic and fulvic acids were pooled in the dataset. Acceptance criteria to include a K_d (FQ) value in the dataset were: (i) sorption parameters for FQs in humic and fulvic acids not only originate from batch sorption experiments, as other approaches can be followed, such as dialysis experiments (Carmosini et al., 2009), fluorescence quenching spectroscopy (Wang et al., 2015), cyclic voltammetry (Antilen et al., 2016) and affinity capillary electrophoresis (ACE, Schmitt-Kopplin et al., 1999); (ii) K_d (FQ) values were derived when necessary from other reported sorption parameters as described in Section 4.2.7 of this thesis; (iii) for those studies reporting sorption parameters at different ionic strengths and/or temperatures, 0.01 M CaCl_2 and 25 °C were preferably selected. The overall number of K_d (FQ) entries of the resulting dataset was 119. When testing sorption analogy among different FQs, in case of having various K_d (FQ) entries obtained at varying pH, only one K_d (FQ) value was used (the one most representative for environmental conditions, as marked in bold in **Table 5.2**).

Table 5.2. List of references used to build up the K_d (FQ) sorption database in humic substances.

Reference	Methodology	Type of HS samples	FQ	Experimental conditions	Total entries (*)
Aristilde and Sposito, 2013	Fluorescence quenching	3 HA; 1 FA	CIP	Synthetic freshwater; pH = 4.0; 5.0 ; 6.0; 7.0; 8.0	20 (4)
Carmosini and Lee, 2009	Dialysis + HPLC (FLD)	2 HA; 2 FA	CIP	0.01 M KCl; pH = 4.0 ; 6.0; 7.5	12 (4)
Antilen et al., 2016	Cyclic voltammetry	2 HA	CIP	0.01 M PO ₄ ³⁻ buffer; pH = 7.0	2 (2)
Martínez-Mejía et al., 2017	Batch + HPLC (FLD)	3 HA	ENR	0.01 M CaCl ₂ ; pH = 3.0; 4.5 ; 7.0	9 (3)
Zhang et al., 2012	Batch + HPLC (FLD)	1 HA	NOR	0.01 M CaCl ₂ ; pH = 2.0; 3.0; 4.0; 5.0 ; 6.0; 7.0; 8.0	7 (1)
Zhu et al., 2018	Batch + HPLC (MS/MS)	4 HA	NOR	0.01 M CaCl ₂ ; pH = 6.0	4 (4)
Peng et al., 2015	Batch + HPLC (UV-Vis)	1 HA	NOR, OFL	0.02 M NaCl; pH = 5.8	2 (2)
Zhang et al., 2011	Batch + HPLC (UV-Vis)	1 HA	NOR	0.01 M CaCl ₂ ; pH = 5.0	1 (1)
Wu et al., 2013	Batch + HPLC (UV-Vis)	5 HA	NOR	0.01 M CaCl ₂ ; pH = 7.0	5 (5)
Zhao et al., 2019b	Batch + HPLC (FLD)	1 HA	NOR	0.1 M NaNO ₃ ; pH = 5.0	1 (1)
Wang et al., 2017	Batch + HPLC (UV-Vis)	1 HA	OFL	0.01 M CaCl ₂ ; pH = 4.7	1 (1)
Lei et al., 2014	Fluorescence quenching	4 HA	OFL	0.01 M NaCl; pH = 7.1	4 (4)
Wang et al., 2015	Fluorescence quenching	4 HA	OFL	0.01 M NaCl; pH = 7.0	4 (4)
Pan et al., 2012a	Dialysis + HPLC (UV-Vis)	1 HA	OFL	0.01 M NaCl; pH = 7.0	1 (1)
Pan et al., 2012b	Dialysis + HPLC (UV-Vis)	1 HA	OFL	Aqueous solution, pH = 7.0	1 (1)
Pan et al., 2012c	Batch + HPLC (UV-Vis)	1 HA	OFL	0.01 M CaCl ₂ ; pH = 4.7	1 (1)
Schmitt-Kopplin et al., 1999	ACE	1 HA	NOR, CIP, ENR, OFL	Carbonate buffer; pH = 9.2	4 (0)
This study	Batch + HPLC (FLD)	7 HA	NOR, CIP, ENR, OFL	0.01 M CaCl ₂ ; pH = 3.0; 4.0; 5.0 ; 6.0; 7.0; 8.0; 9.0; 10.0; 11.0	40 (16)

HA: Humic acid; FA: Fulvic acid; ACE: Affinity capillary electrophoresis; (*) selected number of entries to assess sorption analogy.

A two-way ANOVA ($\alpha = 0.05$) was used to statistically compare FQ sorption data for NOR, CIP, ENR and OFL derived from our experiments, whereas FLSD (run at $\alpha = 0.05$) was applied to evaluate the sorption analogy among FQ populations. Both tests were applied using Statgraphics Centurion 18.1.14 (Statgraphics Technologies, USA).

5.2.2. Results and discussion

5.2.2.1. Sorption kinetics of NOR in humic acids

The results of the kinetic sorption experiments of NOR on LHA, ESHA and PPHA are shown in **Figure 5.1**. The variation of C_s over time indicated that a contact time of 48 hours was enough to achieve the sorption equilibrium, in agreement with that observed in previous kinetic experiments (Pan et al., 2012c; Zhang et al., 2012).

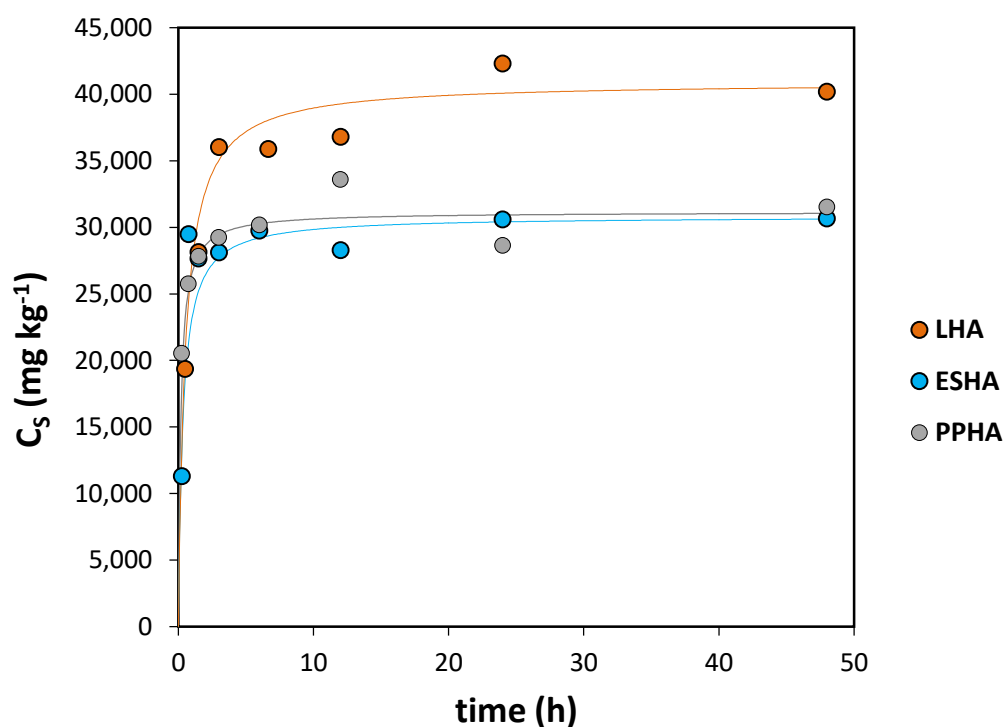


Figure 5.1 Sorption kinetics of NOR on LHA, ESHA and PPHA. Solid lines indicate the PSOM fitting.

The kinetic data was successfully fitted to the PSOM (see **Table 5.3**), thus indicating that sorption may have occurred mainly by chemisorption processes (Ho and McKay, 1998). In addition, the obtained PSOM rate constants and initial rate constants were comparable to those reported in the literature (Pan et al., 2012c; Zhang et al., 2012).

Table 5.3 PSOM fitting parameters of NOR in LHA, ESHA and PPHA samples.

Humic acid	$C_{S,eq}$ (mg kg^{-1})	K_2 ($\text{kg mg}^{-1} \text{h}^{-1}$)	V_0 ($\text{mg kg}^{-1} \text{h}^{-1}$)	r^2
LHA	$4.09 \cdot 10^4$	$0.49 \cdot 10^{-4}$	$8.16 \cdot 10^4$	0.998
ESHA	$3.06 \cdot 10^4$	$1.13 \cdot 10^{-4}$	$1.06 \cdot 10^5$	0.999
PPHA	$6.12 \cdot 10^4$	$1.84 \cdot 10^{-4}$	$1.79 \cdot 10^5$	0.997

$C_{S,eq}$ = sorbed concentration at equilibrium; K_2 = PSOM rate constant; V_0 = PSOM initial rate constant

According to these results, the subsequent sorption experiments were conducted at 48 hours.

5.2.2.2. Sorption isotherms of NOR in humic acids

Sorption isotherms of NOR in the seven HA samples were conducted under equilibrium conditions (see **Figure 5.2**).

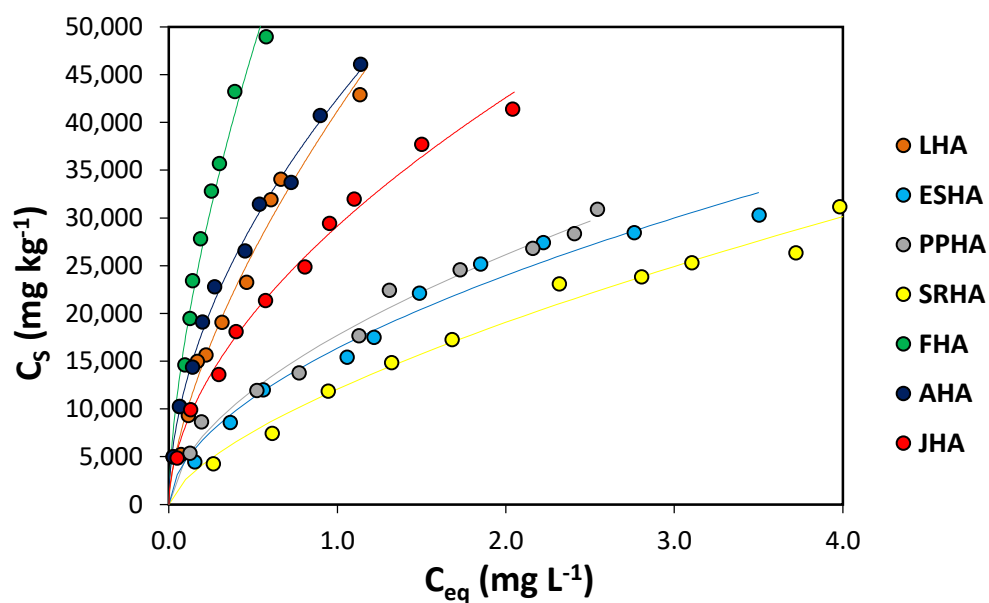


Figure 5.2 Sorption isotherms for NOR in the seven HA samples. Solid lines indicate the Freundlich fitting.

The isotherm sorption data was fitted to the Freundlich model and the resulting fitting parameters are summarized in **Table 5.4**.

Table 5.4 Sorption parameters of NOR in the seven HA samples.

HA	K_F (mg L ⁻¹) / (mg kg ⁻¹) ^N	N (dimensionless)	r ²	%S	K _d (L kg ⁻¹)
LHA	$4.12 \cdot 10^4 \pm 3.24 \cdot 10^3$	0.64 ± 0.10	0.98	94 ± 0.9	$7.45 \cdot 10^4 \pm 5.64 \cdot 10^3$
ESHA	$1.64 \cdot 10^4 \pm 1.53 \cdot 10^3$	0.55 ± 0.11	0.96	84 ± 1.6	$2.46 \cdot 10^4 \pm 4.38 \cdot 10^3$
PPHA	$1.77 \cdot 10^4 \pm 1.11 \cdot 10^3$	0.56 ± 0.08	0.98	85 ± 1.1	$4.38 \cdot 10^4 \pm 1.77 \cdot 10^3$
SRHA	$1.21 \cdot 10^4 \pm 1.36 \cdot 10^3$	0.66 ± 0.10	0.98	80 ± 1.9	$1.11 \cdot 10^4 \pm 2.02 \cdot 10^3$
FHA	$7.30 \cdot 10^4 \pm 8.30 \cdot 10^3$	0.62 ± 0.02	0.97	97 ± 0.5	$1.74 \cdot 10^5 \pm 3.38 \cdot 10^4$
AHA	$4.25 \cdot 10^4 \pm 1.72 \cdot 10^3$	0.53 ± 0.05	0.99	97 ± 1.2	$1.54 \cdot 10^5 \pm 5.36 \cdot 10^4$
JHA	$2.91 \cdot 10^4 \pm 9.80 \cdot 10^2$	0.55 ± 0.05	0.99	93 ± 2.8	$7.38 \cdot 10^4 \pm 2.99 \cdot 10^3$

Good fittings were observed for all the isotherms, with N values < 1, indicating sorption site heterogeneity and, thus, non-linear sorption within the concentration range tested. Both linear and non-linear sorption isotherms have been previously observed for FQs in HA (Aristilde and Sposito, 2013; Zhang et al., 2012). At low initial concentrations, FQ are sorbed at high-affinity sorption sites, whereas when higher concentrations are tested, the saturation of the high-affinity sites permits that other sites with lower affinity participate in the sorption process. This suggests that different interaction mechanisms may govern FQ sorption in HA.

Table 5.4 also shows the K_d values derived from the respective sorption isotherms, as well as the related sorption percentages. As all the isotherms were non-linear, sorption parameters (K_d and %S) were calculated from specific experimental points (those with C_{in} = 1 – 3 mg L⁻¹) that were ensured to fall within the linear range. The K_d values agreed with previous values observed for NOR and CIP in HAs at acidic pH (Aristilde and Sposito, 2013; Zhang et al., 2012), and were indicative of a high sorption affinity of FQs to SOM fractions, also in agreement with the high sorption percentages (> 80%) quantified.

5.2.2.3. Desorption isotherms of NOR in humic acids

NOR desorption isotherms were obtained for a selection of HA samples (**Figure 5.3**).

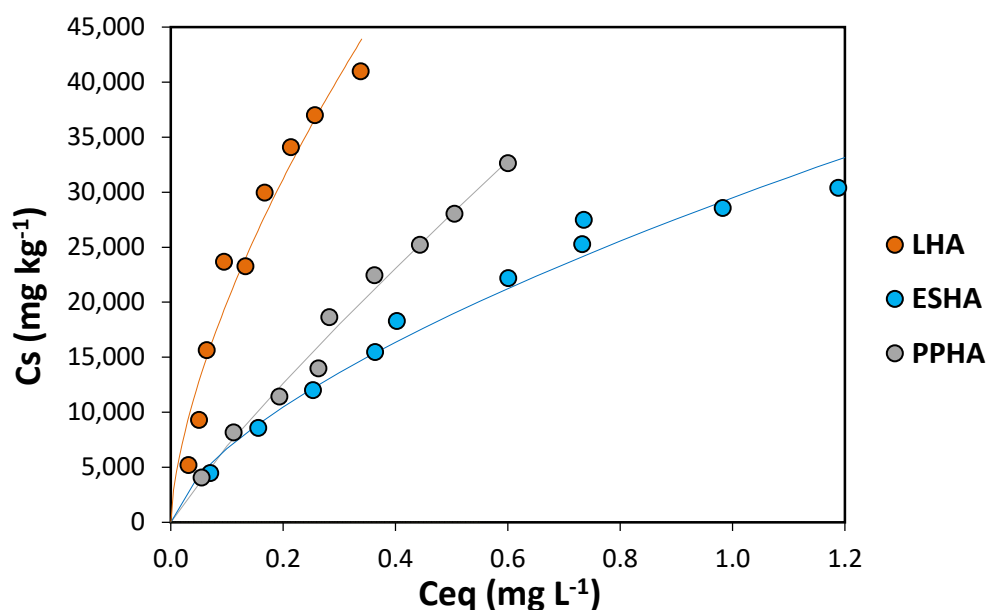


Figure 5.3 NOR desorption isotherms for LHA, ESHA and PPHA samples. Solid lines indicate the Freundlich fitting.

The desorption isotherm data were successfully fitted by the Freundlich model (**Table 5.5**).

Table 5.5 Desorption parameters for NOR in LHA, ESHA and PPHA samples.

HA	K_F (mg L ⁻¹) / (mg kg ⁻¹) ^N	N (dimensionless)	r ²	%D	$K_{d,des}$ (L kg ⁻¹)	H
LHA	$8.79 \cdot 10^4 \pm 2.50 \cdot 10^4$	0.64 ± 0.17	0.95	2.7 ± 0.9	$1.99 \cdot 10^5 \pm 4.66 \cdot 10^4$	2.7
ESHA	$2.95 \cdot 10^4 \pm 2.91 \cdot 10^3$	0.64 ± 0.17	0.94	8.4 ± 2.0	$5.55 \cdot 10^4 \pm 9.30 \cdot 10^3$	2.3
PPHA	$5.12 \cdot 10^4 \pm 5.64 \cdot 10^3$	0.87 ± 0.12	0.99	6.3 ± 1.5	$6.88 \cdot 10^4 \pm 9.48 \cdot 10^3$	1.6

Desorption isotherms displaying a Freundlich behaviour have been previously described for FQs in humic acids (Martínez-Mejía et al., 2017), suggesting that the fraction of FQ sorbed at less affinity sites are more likely to be mobilized to the liquid phase, which is observed at increasing FQ concentration. Similarly to Section 5.2.2.2, $K_{d,des}$ values were derived from those

experimental points ($C_{in} = 1 - 3 \text{ mg L}^{-1}$) which fell within the linear range of the respective desorption isotherms, and all cases were higher than the respective sorption K_d . Desorption percentages were relatively low ($< 8.4\%$). The hysteresis coefficient (H) was higher than one in all materials, suggesting a strong sorption irreversibility at the low FQ initial concentration.

5.2.2.4. Effect of Ca concentration and DOC content on NOR sorption in humic acids

The K_d values of NOR in LHA, ESHA and PPHA obtained at calcium concentrations ranging 0 – 20 mM (where 0 refers to natural sample soluble Ca, which is $< 0.003 \text{ mM}$ in all cases) and pH 5.0 are shown in **Figure 5.4**.

At pH 5.0, NOR is mainly present under its cationic form, and thus, calcium cations may compete with NOR for the available sorption sites present in the HA. In agreement with previous findings for ENR in a set of three HA samples extracted from soils (Martínez-Mejía et al., 2017), NOR sorption was reduced in all HA samples when increasing Ca concentrations. This reduction differed slightly among materials: whereas LHA and ESHA suffered a strong inhibition in K_d when increasing Ca concentration from sample Ca to 5 mM, NOR sorption in PPHA was less affected by the presence of Ca, thus indicating a different weight of the different interaction mechanisms among NOR and the HAs. The reduction of the observed K_d at increasing Ca concentrations from 5 to 20 mM was similar for the three tested materials.

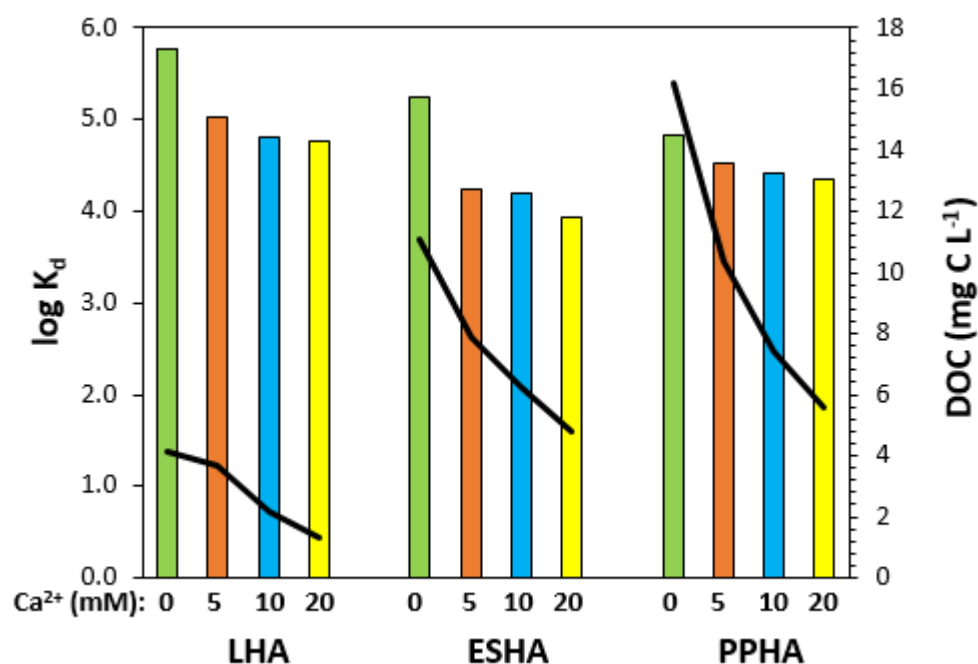


Figure 5.4 Effect of Ca concentration (bars) and DOC content (solid lines) on NOR sorption in LHA, ESHA and PPHA samples.

On the other hand, the increase in Ca concentration (and thus in the ionic strength) of the contact solution reduced the DOC content, likely by an associated decrease in organic compounds solubility and increase in organic matter flocculation. The DOC pattern decrease was similar to K_d (NOR) decrease. It has been observed that sorption of NOR was reduced at DOC contents around 20 mg C L⁻¹ likely due to FQ-DOC interactions (Zhang et al., 2018). The NOR sorption pattern observed for the three HA in the absence of additional Ca could be nicely explained by DOC competitive effects, as the sequence of K_d (NOR) among the three HA samples was inversely related to the sequence of DOC content. However, when Ca concentration increased, the K_d (NOR) reduction observed for the three HA could not be only explained by DOC competitive effects, as the DOC content also decreased, thus suggesting that the increase in Ca concentration was the main responsible factor inhibiting NOR sorption from sample Ca to 5 mM Ca, with a minor additional effect for higher Ca concentrations.

The interaction mechanisms suggested to play a role in the sorption of FQs in HA are mainly electrostatic interactions, cation exchange, hydrogen, cation bridge and hydrophobic interactions (Aristilde and Sposito, 2010; Liu et al., 2017a; Martínez-Mejía et al., 2017; Zhang et al., 2012; Zhao et al., 2019a). In addition, cation – π and π – π interactions may also occur in highly aromatic HA (Zhao et al., 2017). To better elucidate the interaction mechanisms between FQs and LHA, ESHA and PPHA responsible for the effect of Ca and DOC on K_d (NOR) values, FTIR analysis were conducted to analyse HA samples before and after NOR sorption. The spectra of the HA samples prior and after NOR sorption were recorded, and specific bands of the spectra representative of the hydrophobic and hydrophilic regions were identified according to previous reports (Rodríguez and Núñez, 2011), and the shift of these bands before and after NOR sorption were semi quantified (**Table 5.6**).

Table 5.6. Wavenumber and chemical shifts (into brackets) observed for specific bands in HA samples before and after NOR sorption.

HA sample	O – H stretch (phenol, carboxyl)	C = C stretch (aromatic rings)	O – H bend (carboxyl)	C – O stretch (phenol, carboxyl)	C – O stretch (alcohols)
LHA	3,389 (1)	1,585 (7)	1,385 (1)	1,269 (1)	1,046 (4)
ESHA	3,383 (1)	1,582 (1)	1,384 (0)	1,261 (7)	1,034 (0)
PPHA	3,388 (4)	1,577 (8)	1,385 (3)	1,266 (4)	1,044 (3)

The aromatic regions of the HA were likely to be a significant sorption domain for LHA and PPHA, which were the HA with a higher aromatic carbon contents (see **Table 5.1**), as revealed by the significant shifts in the aromatic C = C stretch bands. These interactions may be driven by cation – π rather than by π – π interactions at acidic to neutral pH (Zhao et al., 2017), which could also explain the enhanced sorption observed for FQ in highly aromatic HA (Aristilde and Sposito, 2013). Hydrophilic domains also played a role in sorption in PPHA. Protonated carboxyl and phenol groups of the HA at pH 5 may participate in hydrogen bonding

with the fluorine moiety of the FQ structure, whereas carboxylate groups may participate in electrostatic and cation exchange interactions, in addition to participate in hydrogen bonding with the protonated carboxylate of the FQ. Sorption of NOR in ESHA, which was the tested HA with the lowest aromatic carbon content (see **Table 5.1**) was mainly in the hydrophilic domains, likely through the abovementioned interaction mechanisms. Furthermore, the presence of all cation – π , electrostatic and cation exchange mechanisms could support the sorption decrease observed due to competition of Ca cations for the sorption sites.

5.2.2.5. Sorption analogy of FQs in humic substances

The K_d (FQ) values from the additional sorption experiments for CIP, ENR and OFL in LHA, ESHA and PPHA samples are summarized in **Table 5.7**.

Table 5.7 K_d (FQ) values ($L\ kg^{-1}$) of NOR, CIP, ENR and OFL in LHA, ESHA and PPHA samples. RSD of the replicates was $\leq 20\%$.

HA	NOR	CIP	ENR	OFL
LHA	$6.31 \cdot 10^4$	$6.46 \cdot 10^4$	$3.10 \cdot 10^4$	$1.91 \cdot 10^4$
ESHA	$2.57 \cdot 10^4$	$1.07 \cdot 10^4$	$7.25 \cdot 10^3$	$4.17 \cdot 10^3$
PPHA	$2.19 \cdot 10^4$	$2.34 \cdot 10^4$	$1.29 \cdot 10^4$	$7.42 \cdot 10^3$

A general sorption trend was observed in which the sequence of K_d (FQ) was $NOR \approx CIP > ENR > OFL$, which is inversely related to the molecular weight and/or the $\log K_{ow}$ of the FQs (see **Table 1.5**). This trend agrees with the binding capacity revealed by thermodynamic sorption data in HAs (Zhao et al., 2019). A two-way ANOVA with replicates revealed that both HA material and FQ significantly affected K_d (FQ) values, confirming that

sorption of FQs may not be analogous when tested in similar materials at specific experimental conditions.

The overall assessment of FQ sorption analogy (at pH 4 – 7) should include humic and fulvic acid samples with contrasting properties, as well as data affected by additional sources of K_d (FQ) variability (as the replicate data dispersion quantified in our experiments was extremely low). To better assess the sorption analogy among these four FQs in humic substances, 55 entries of those gathered in the built-up dataset were selected for such analyses, including data from own experiments. Only those FQs with a sufficient number of entries ($n > 10$) were used to compare FQ populations. **Figure 5.5** shows the comparison among literature-derived K_d values for NOR, CIP and OFL in a box and whisker plot. FLSD tests applied in the three FQ populations confirmed that the overall sorption in humic substances at varying experimental conditions was analogous for the three FQ.

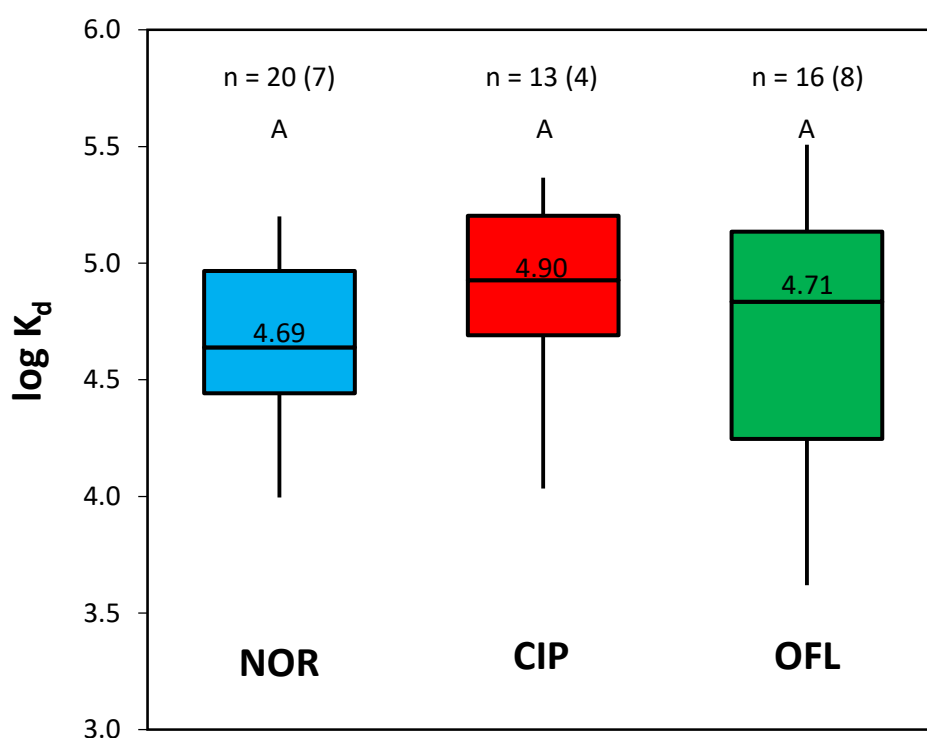


Figure 5.5 Compiled K_d values for NOR, CIP and OFL in humic substances at pH 4 - 7.

Capital letters indicate FLSD test results, n are the total entries and the number of studies these entries were derived from are into brackets. Central values are median values.

Thus, it could be concluded that the effect of minor differences in FQ structure on K_d (FQ) is of a lesser significance than humic and fulvic acid characteristics and experimental procedure applied to quantify the given K_d (FQ) values.

5.2.2.6. Effect of pH on FQs sorption in humic substances

The sorption of NOR in LHA, ESHA and PPHA at pH ranging 3 – 11 was evaluated, as pictured in **Figure 5.6**, which shows a sort of U-shaped variation of $\log K_d$ (NOR) with pH increase that agrees with the changes in NOR species at varying pH. The %RSD of the replicates was < 20%. The fitting of the experimental data with a second-order polynomic equation confirmed that NOR sorption was maximized at pH 5.2 – 5.5, indicating that sorption of the positively charged FQ specie was favoured. A further increase in pH led to a decrease in NOR sorption, likely due to electrostatic repulsions between the negatively charged functional groups present in the HA surface and the NOR zwitterion form. The sorption decrease was further observed at $\text{pH} > \text{pK}_{a2}$, in which NOR existed mainly under its negative form, leading to $\log K_d$ values around 2.3, in agreement with reported K_d (FQ) values in HA at basic conditions (Schmitt-Kopplin et al., 1999). In fact, at basic pH the role of the HA characteristics diminished, and the K_d (NOR) values approached in the three HA samples tested. Overall, these pH-dependent sorption trends highlighted the significant role of FQ speciation in the sorption process.

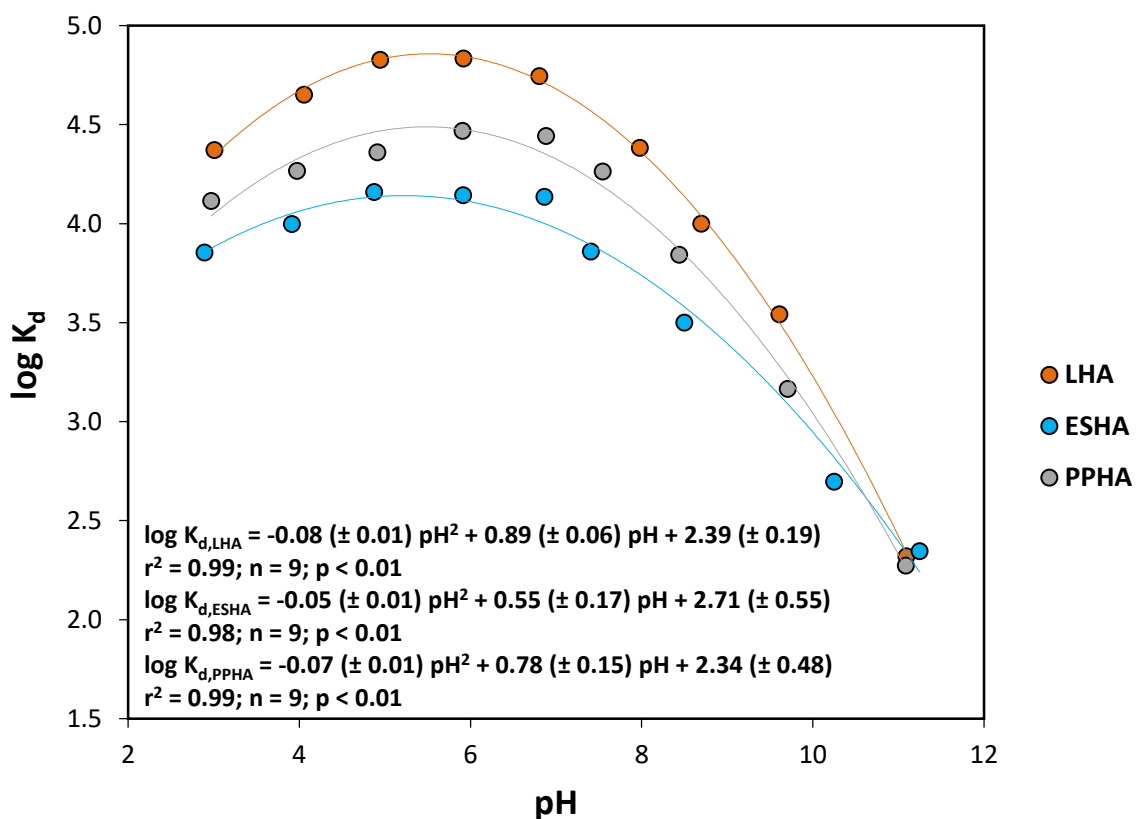


Figure 5.6 Effect of pH on NOR sorption in LHA, PPHA and ESHA. Solid lines indicate the second-order polynomial fitting.

The good fitting of our own experimental data to a second-order polynomial equation encouraged the exploration of the role of pH in the overall available K_d (FQ) entries in the built-up dataset. Sorption data for NOR, CIP, OFL and ENR was pooled after showing their sorption analogy. Log K_d (FQ) entries were grouped in intervals of 1.0 pH unit to facilitate visualization of the K_d (FQ) vs. pH dependence, although the fitting was done for all the individual entries (n=119). The resulting fitting is also plotted in **Figure 5.7**.

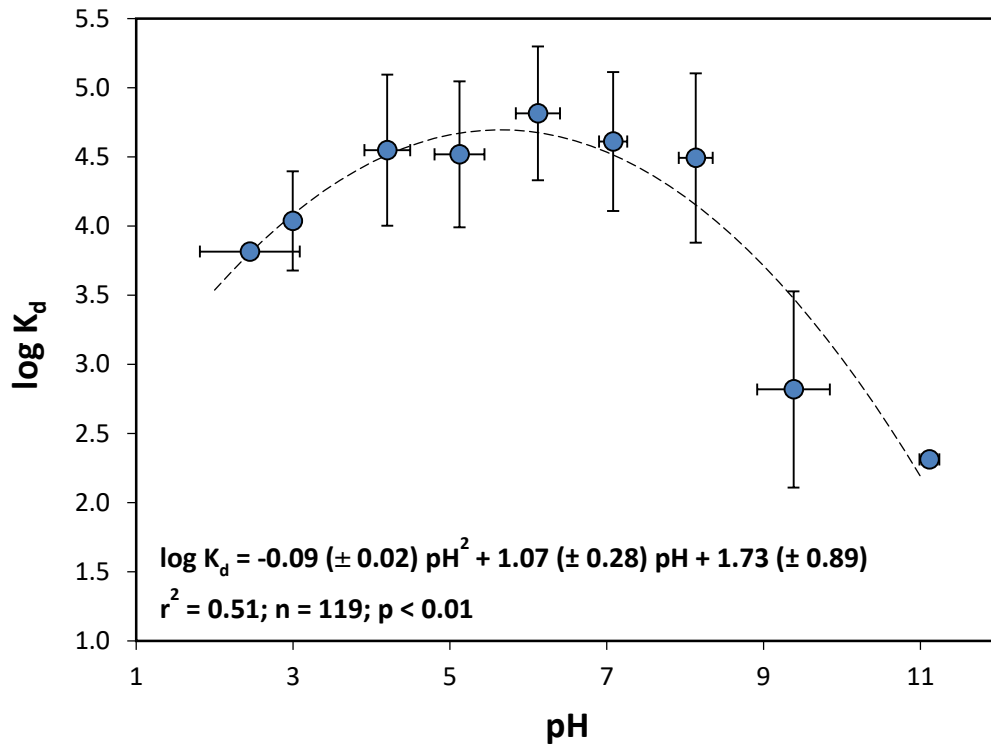


Figure 5.7 Effect of pH on K_d (FQ) in humic and fulvic acids. Solid lines indicate standard deviation of data grouped for visualization purposes. Dashed line indicates the second-order polynomial fitting.

The fitting of the overall FQ (K_d) sorption data by the second-order polynomial equation revealed that maximum sorption occurred at pH 5.9 and showed that pH alone could describe around 50% of K_d (FQ) variability regardless the nature and characteristic of the humic substance, the tested methodology and the selected experimental conditions, which confirmed the crucial role of pH in the FQ sorption process in SOM fractions.

5.3. Sorption of FQs in metal oxides

5.3.1. Creation of a K_d (FQ) dataset and data treatment

Sorption K_d (FQ) values in metal oxides and ancillary information about material physicochemical properties and experimental conditions was compiled from available literature data. Acceptance criteria to include a K_d (FQ) value in the database were: (i) sorption data in metal oxides of Cu, Fe (including data on Fe oxyhydroxides (FeO(OH); goethite)), Ti, Al, Mn, Mg and Si were accepted, although a few of these oxides may be present at trace levels in soils. (ii) sorption data was included regardless of the origin of the material (*i.e.*, synthetic or natural oxides), and ancillary information of the sorbents and experimental conditions was also collected. As most sorption data were obtained at slightly acidic/neutral (5 – 7) pH, this pH range was used to evaluate the role of metal nature and material characteristics responsible for sorption, thus ruling out the pH effect in FQ sorption. (iii) for those studies reporting sorption parameters at different ionic strengths or temperatures, 0.01 M CaCl₂ and 25 °C were preferably selected; (iv) only sorption data for NOR, CIP, ENR and OFL was accepted, as their sorption was assumed to be analogous according to previous analyses performed in humic substances. Besides, as levofloxacin (LEV) and OFL are two isomeric FQs, sorption of OFL and LEV was assumed to be analogous and were pooled into OFL data; (v) K_d (FQ) values were derived when necessary from other reported sorption parameters as described in Section 4.2.7 of this thesis.

Expert judgement was applied to carefully select K_d (FQ) entries of the overall dataset when elucidating the individual role of significant factors, such as the role of metal or SSA in FQ sorption. When required, data were fitted using the least-squares method using Matlab (cftoolbox, Matlab® R2009a (MathWorks Inc., USA)).

5.3.2. Evaluating the role of metal on FQs sorption in metal oxides

Different metal oxides have been tested for their ability to sorb FQs (Fries et al., 2016; Tan et al., 2015). **Table 5.8** summarize some selected studies in which K_d (FQ) on metal oxides at neutral pH were derived.

Table 5.8 Sorption parameters (K_d and surface area-normalized K_d ($K_{d,SSA}$)) of FQs in metal oxides and ancillary information of the batch experiments.

Reference	FQ	Material	SSA ($m^2 g^{-1}$)	Contact solution; pH	K_d ($L kg^{-1}$)	$K_{d,SSA}$ ($mL m^2$)
Goyne et al., 2005	OFL	SiO ₂	7.5	0.02 M CaCl ₂ , pH 7.2	0.87	0.12
Khoshnamvand et al., 2017	CIP	MgO	1,236	Aqueous solution, pH 6.0	277	0.22
Zhang and Huang, 2005	ENR	MnO ₂	255	0.01 M NaCl, pH 6.0	188	0.73
Goyne et al., 2005	OFL	Al ₂ O ₃	37	0.02 M CaCl ₂ , pH 7.2	55	1.5
Fries et al., 2016	CIP	TiO ₂	45	0.001 M NaCl, pH 8.0	275	6.1
Peng et al., 2015	NOR	Fe ₂ O ₃	45	0.02 M NaCl, pH 5.8	916	20
Ahmadi et al., 2017	CIP	CuO	20	Aqueous solution, pH 7.0	2,100	105

The K_d (FQ) values in metal oxides were generally much lower than those quantified in humic substances. Therefore, when both types of phases may be present in soils, the role of the SOM can be anticipated to be more significant than that of the metal oxides. Nevertheless, it is worth to elucidate the main factors affecting FQ sorption in metal oxides.

Computational studies have suggested that FQs are capable to bind metallic atoms through covalent bonds by forming FQ-M complexes (Aristilde and Sposito, 2008). To test this and facilitate the comparison among metal oxides, K_d (FQ) values in **Table 5.8** were normalized to the material surface area ($K_{d,SSA}$) to remove the influence of SSA in the assessment of metal nature in FQ sorption. These SSA-normalized K_d values followed the trend: Cu >> Fe >> Ti > Al > Mn > Mg \approx Si, which roughly agree with the Irving – Williams series describing the

complexation stability of organic ligands by metallic atoms (Irving and Williams, 1949). These results suggest an increasing binding affinity of FQ under neutral conditions with specific metallic atoms in the mineral surface through covalent bonds, besides the key role of SSA metal oxides in FQ sorption, which is further explored in the following section.

5.3.3. Factors affecting FQs sorption: the case of Fe oxides and (hydro)oxides

As the metal atom present in the mineral surface plays a role sorption, K_d (FQ) in Fe oxides and (hydro)oxides were selected to discuss the role of other factors in FQ sorption in oxides. The sorption of FQ (specifically CIP) in goethite ($pH_{ZPC} = 9$; Qin et al., 2014b) has been shown to be affected by pH, reaching its maximum sorption at pH 6 – 7, where the zwitterion CIP species is predominant. At $pH < pK_{a1}$, electrostatic repulsion occurs between the positive FQs and the mineral surface, although FQ sorption could be attributed to complexation mechanisms with Fe atoms, since goethite can promote the deprotonation of the FQ carboxylate moiety at $pH < pK_{a1}$ (Trivedi and Vasudevan, 2007). At $pH > pK_{a1}$, these complexation mechanisms may become predominant, and in addition, electrostatic interactions between the negatively charged FQ and the positively charged goethite surface may further contribute to sorption. At $pH > pH_{ZPC}$, electrostatic repulsions between the anionic FQ specie and the negatively charged goethite surface leads to an abrupt decrease in sorption.

Ionic strength and composition of the aqueous solution also affect FQs sorption in goethite. Whereas some authors found that the presence of dissolved Ca cations enhanced CIP sorption through ternary complexes assisted by cation bridging mechanisms (FQ-Ca-HA, Tan et al., 2015), other authors reported that dissolved Ca cations decreased FQ sorption due to the formation of soluble Ca-FQ complexes in solution (Qin et al., 2014a). The different Ca concentrations used in each study (0.1 and 10 mM, respectively) may explain these differences: at low Ca concentrations, cation-bridging mechanisms may be more likely to occur, whereas at high Ca concentrations Ca-FQ complexes may be more prone to form in solution.

As concluded in the former section, material surface seems to play a major role in the sorption of FQ in metal oxides. **Table 5.9** summarizes the list of references used to build up a partial dataset for FQs in Fe-containing minerals (including Fe_2O_3 , Fe_3O_4 and $\text{FeO}(\text{OH})$), as well as additional information on specific material properties and the experimental conditions in which K_d (FQ) values were derived.

Table 5.9 Literature-derived K_d (FQ) values in common Fe-minerals present in soils.

Reference	FQ	Material	SSA ($\text{m}^2 \text{g}^{-1}$)	Experimental conditions	K_d (L kg^{-1})
Mackay and Seremet, 2008	CIP	$\text{FeO}(\text{OH})$	15	PIPES buffer, pH 7.0	100
Carrasquillo et al., 2008	CIP	$\text{FeO}(\text{OH})$	10	0.01 M PIPES, pH 6.6	214
Shi et al., 2013	CIP	Fe_3O_4	24	Aqueous solution, pH 7.0	276
Yu et al., 2019	OFL	$\text{FeO}(\text{OH})$	20	PIPES buffer, pH 6.6	314
Tan et al., 2015	CIP	$\text{FeO}(\text{OH})$	64	0.01 M NaNO_3 , pH 6.0	333
Zhang and Huang, 2007	CIP	$\text{FeO}(\text{OH})$	49	0.01 M NaCl , pH 5.0	416
Paul et al., 2014	OFL	$\text{FeO}(\text{OH})$	64	0.01 M NaCl , pH 7.0	514
Rakshit et al., 2013	CIP	Fe_3O_4	40	0.01 M NaCl , pH 6.0	852
Peng et al., 2015	NOR	Fe_2O_3	45	0.02 M NaCl , pH 5.8	916
Qin et al., 2014a	LEV	$\text{FeO}(\text{OH})$	84	0.01 M NaCl , pH 5.2	1,180
Lin and Lee, 2020	CIP	$\text{FeO}(\text{OH})$	140	Aqueous solution, pH 7.0	1,270
Qin et al., 2014b	LEV	$\text{FeO}(\text{OH})$	98	0.01 M NaCl , pH 6.6	1,310
Gu and Karthikeyan, 2005	CIP	$\text{FeO}(\text{OH})$	332	0.01 M NaCl , pH 7.1	5,010
Zhang and Huang, 2007	CIP	$\text{FeO}(\text{OH})$	159	0.01 M NaCl , pH 5.0	12,300

PIPES = 1,4-piperazinediethanesulfonic acid; Fe_2O_3 = hematite; Fe_3O_4 = magnetite; $\text{FeO}(\text{OH})$ = goethite

The K_d (FQ) values for these Fe-containing minerals at pH ranging 5 – 7 varied within a 100 – 12,300 L kg^{-1} range. As FQs were mostly in their zwitterion form under these conditions, surface complexation with the Fe atoms present in the mineral surface could be

expected (Paul et al., 2014). A bidentate complex involving both carboxylate and the carbonyl moieties of CIP with the Fe atoms present in the mineral surface was suggested for hematite and magnetite (Rakshit et al., 2013; Martin et al., 2015), whereas other bi- and tridentate complexes were hypothesized for goethite (Paul et al., 2014).

Differences in K_d (FQ) values could be attributed to specific surface properties. As shown in **Table 5.9**, SSA varied within the 10 – 330 $\text{m}^2 \text{g}^{-1}$ range. In this sense, a significant linear relationship between \log_{10} -transformed K_d and SSA data was found, which described nearly 75% of the K_d (FQ) variability (**Figure 5.8**). This positive relationship between K_d and SSA confirmed the key role of SSA in the sorption of FQs in Fe-containing minerals.

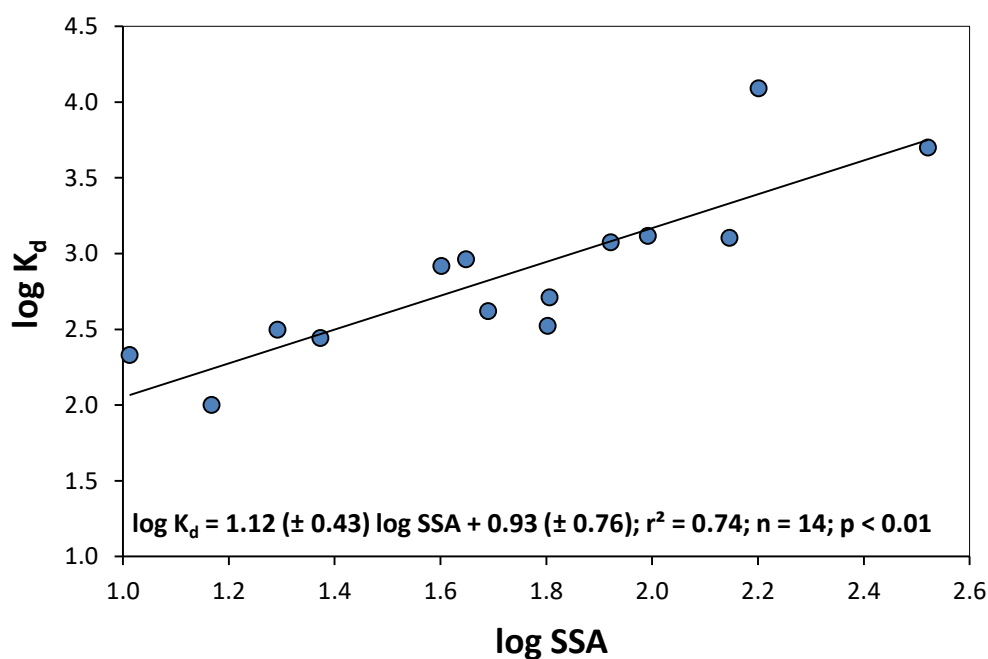


Figure 5.8 Correlation between K_d (FQ) and SSA for Fe minerals. Solid line indicate the Linear fitting.

The resulting relationship may be of interest for K_d (FQ) predicting purposes. However, in the context of soils, the SSA of naturally occurring Fe-minerals are expected to be low ($\approx 10 \text{ m}^2 \text{g}^{-1}$, Jacobson and Fan, 2019), and then low K_d (FQ) values are also expected. Therefore, a low contribution of metal oxides in the overall FQ sorption in bulk soils can be anticipated.

5.4. Sorption of FQs in phyllosilicate minerals

5.4.1. Creation of a K_d (FQ) dataset and data treatment

Sorption K_d (FQ) values in phyllosilicate minerals and ancillary information about material physicochemical properties and experimental conditions was compiled from the literature. Acceptance criteria to include a K_d (FQ) value in the dataset were: (i) only sorption data in 1:1 and 1:2 dioctahedral phyllosilicates (*i.e.*, kaolinite, illite, vermiculite, palygorskyte and montmorillonite) was considered; (ii) only data from NOR, CIP, ENR and OFL were considered, as their sorption was assumed to be analogous according to previous analyses performed in humic substances. Besides, as LEV and OFL are two isomeric FQs, sorption of OFL and LEV was assumed to be analogous and were pooled into OFL data; (iii) sorption K_d values at different pH values was included in the database, although for those studies reporting sorption at different ionic strengths or temperatures, 0.01 M CaCl_2 and 25 °C were preferably selected; (iv) K_d (FQ) values were derived when necessary from other sorption parameters as described in Section 4.2.7 of this thesis.

Table 5.10 summarizes the list of references included in the dataset. Phyllosilicates were grouped as 1:2 swelling (*i.e.*, montmorillonite), 1:2 non-swelling (*i.e.*, palygorskyte, illite, and vermiculite) and 1:1 phyllosilicates (*i.e.*, kaolinite). When various K_d (FQ) values were reported at varying pH for a single FQ and phyllosilicate group, a unique K_d value was selected for every FQ and phyllosilicate combination, preferably at an environmentally relevant pH (4.5 – 7.5) in which the FQs are under cationic or zwitterion forms, to examine the role of the phyllosilicate. If different sorption isotherms were reported within this pH range, the derived K_d values from the best fitted isotherm were selected. All entries in **Table 5.10** were used to model the K_d dependence with pH. The overall number of entries and those selected to statistically compare sorption among phyllosilicates (in brackets) were: 38 (20) for 1:2 swelling phyllosilicates; 11 (7) for 1:2 non-swelling phyllosilicates; and 20 (12) for 1:1 phyllosilicates.

Table 5.10. List of references used to build up the K_d (FQ) dataset in phyllosilicates.

Reference	FQ	Experimental conditions	Number of entries
<i>Montmorillonite</i>			
Rivagli et al., 2014	ENR	Tap water; 0.01 M CaCl ₂ ; pH = 2.0; 7.5	8 (4)
Wan et al., 2013	ENR	Aqueous solution; pH = 4.5	1 (1)
Wu et al., 2010	CIP	Aqueous solution; pH = 3.0; 4.5 ; 11.0	3 (1)
Roca et al., 2015	CIP	Aqueous solution; pH = 3.0; 6.0 ; 7.5; 10.0	4 (1)
Yan et al., 2012	ENR	0.01 M KCl; pH = 3.5; 4.5; 5.5 ; 6.5; 7.5; 8.5	6 (1)
Wu et al., 2014	CIP	Aqueous solution; pH = 4.0 ; 11.0	2 (1)
Genç et al., 2013a	CIP	Aqueous solution; pH = 4.5, 5.5	1 (1)
Septian et al., 2018	CIP	Aqueous solution; pH = 5.0 ; 8.0	2 (1)
Genç et al., 2013b	CIP	Aqueous solution; pH = 5.5	1 (1)
Wang et al., 2010	CIP	Aqueous solution; pH = 5.8	1 (1)
Nowara et al., 1997	ENR	Aqueous solution; pH = 5.9	1 (1)
Zhou et al., 2014	OFL	0.1 M CaCl ₂ ; pH = 6.1	1 (1)
Wu et al., 2012	CIP	Aqueous solution; pH = 6.4	1 (1)
Hanamoto and Ogawa, 2019	LEV	0.005 M CaCl ₂ ; pH = 6.5	1 (1)
Carrasquillo et al., 2008	CIP	0.01 M PIPES buffer; pH = 6.6	1 (1)
Pei et al., 2011	NOR	0.01 M NaNO ₃ ; pH = 7.0 ; 9.0	2 (1)
Gulen and Demircivi, 2020	CIP	Aqueous solution; pH = 7.0	1 (1)
Jalil et al., 2017	CIP	Aqueous solution; pH = 10.0	1 (0)
<i>Palygorskyte</i>			
Chang et al., 2016	CIP	Aqueous solution; pH = 2.0; 7.0 ; 11.0	3 (1)
Quan and Bi, 2017	OFL	0.01 M NaCl; pH = 2.0; 7.4 ; 9.5	3 (1)
Berhane et al., 2016	CIP	0.01 M CaCl ₂ ; pH = 7.0	1 (1)

PIPES = 1,4-piperazinediethanesulfonic acid;

Table 5.3 (Continued)

Reference	FQ	Experimental conditions	Number of entries
<i>Illite</i>			
Wan et al., 2013	ENR	Aqueous solution; pH = 4.5	1 (1)
Nowara et al., 1997	ENR	Aqueous solution; pH = 5.9	1 (1)
<i>Vermiculite</i>			
Nowara et al., 1997	ENR	Aqueous solution; pH = 5.9	1 (1)
Liu et al., 2017b	CIP	Aqueous solution; pH = 5.0	1 (1)
<i>Kaolinite</i>			
Rivagli et al., 2014	ENR	Tap water; 0.01 M CaCl ₂ ; pH = 2.0; 7.5	4 (2)
Li et al., 2011	CIP	Aqueous solution; pH = 3.8	1 (1)
Wan et al., 2013	ENR	Aqueous solution; pH = 4.5	1 (1)
Li et al., 2017a	OFL	0.01 M NaCl; pH = 4.5 ; 7.0; 11.0	3 (1)
Li et al., 2017b	OFL	0.01 M NaCl; pH = 4.5 ; 7.0; 9.5	3 (1)
Nowara et al., 1997	ENR	Aqueous solution; pH = 6.0	1 (1)
Pan et al., 2012c	OFL	0.01 M CaCl ₂ ; pH = 6.4	1 (1)
Wu et al., 2012	CIP	Aqueous solution; pH = 6.4	1 (1)
Zhou et al., 2014	OFL	0.1 M CaCl ₂ ; pH = 6.6	1 (1)
Carrasquillo et al., 2008	CIP	0.01 M PIPES buffer; pH = 6.6	1 (1)
Zhang et al., 2020	CIP	0.001 M NaCl; pH = 5.0; 7.0 ; 9.0	3 (1)

PIPES = 1,4-piperazinediethanesulfonic acid;

Among the 69 total entries included in the database, most of the sorption data was attributed to CIP and ENR (42% and 36%, respectively), whereas few data were available for NOR. When required, data were fitted using the least-squares method using Matlab (cftoolbox, Matlab® R2009a (MathWorks Inc., USA)). FLSD test was run at a significance level of $\alpha = 0.05$ to statistically assess sorption differences among types of phyllosilicate using Statgraphics Centurion 18.1.14 (Statgraphics Technologies, USA).

5.4.2. Influence of the type of phyllosilicate in FQs sorption

The selected K_d (FQ) values from the overall dataset were classified and compared in terms of box and whisker plots and FLSD analyses (**Figure 5.9**).

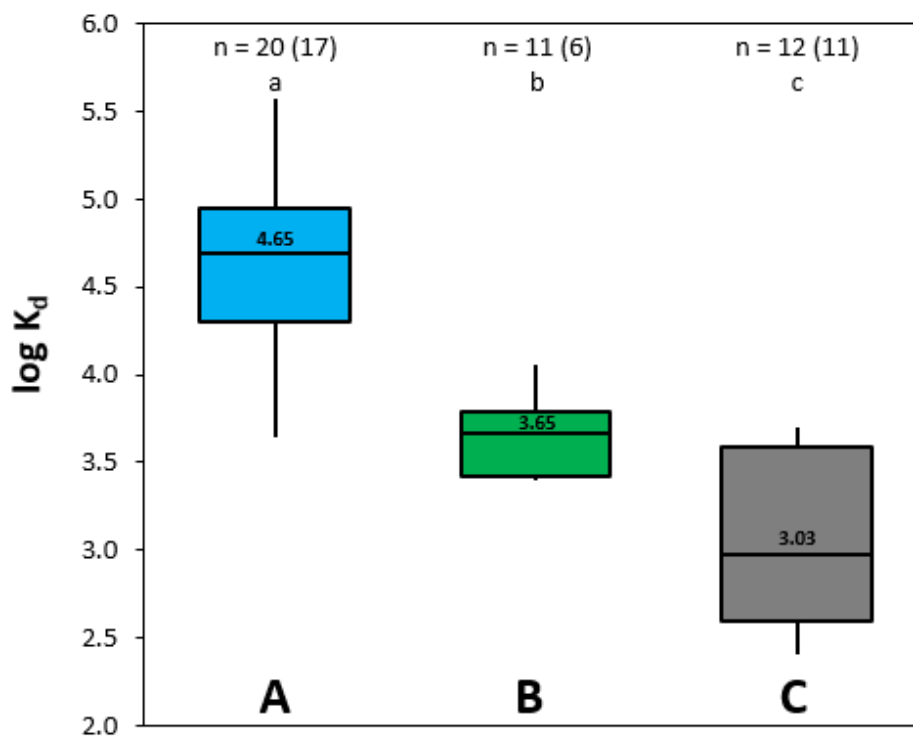


Figure 5.9 Compiled K_d (FQ) values in (A) 1:2 swelling phyllosilicates; (B) 1:2 non-swelling phyllosilicates; (C) 1:1 phyllosilicates; n are the entries tested (in brackets the number of the studies they were derived); lower case letters indicate FLSD-test results; central values are median values.

K_d (FQ) depended significantly on the nature of the phyllosilicates: the highest K_d (FQ) values corresponded to 1:2 phyllosilicate swelling clays (over one order of magnitude higher than the rest of phyllosilicate materials), with values similar to those observed for SOM substances. This finding agrees with previous studies that showed the key role of montmorillonite in FQ sorption, as the interlayer space of montmorillonite may contain specific sites with a high affinity for FQ sorption, as revealed by the observed interlayer expansion after X-ray diffraction analyses along FQ sorption (Nowara et al., 1997). In contrast, this was not observed for illite, vermiculite or palygorskite (Chang et al., 2016; Liu et al., 2017b; Wan et al., 2013).

5.4.3. Effect of pH on FQs sorption in phyllosilicate minerals

Sorption of FQs in phyllosilicate minerals is pH-dependent. Specifically, FQ sorption increases with pH, reaching its maximum at pH 3 – 5 in which the FQ is mostly under its cationic form. At $\text{pH} < \text{pK}_{a1}$, the cationic FQ species strongly sorb at the clay surface due to cationic exchange mechanisms (Li et al., 2011). At $\text{pH} > \text{pK}_{a1}$, despite the FQ molecules still participate in cation exchange, sorption may decrease due to increasing negative electrostatic repulsions between the negatively charged clay surface and the carboxylate moiety of the FQ. These repulsions are maximized at increasing pH above pK_{a2} and may differ among clays depending on their specific pH_{ZPC} (Wan et al., 2013).

To examine the role of pH in the overall sorption of FQs in clay minerals, K_d (FQ) values from the dataset were grouped within ± 1 pH unit and plotted against the pH (**Figure 5.10**). The pH trend observed when grouping literature data by the phyllosilicates classes defined before agreed with could be expected on the basis of changes in FQ speciation when varying pH (Wan et al., 2013). A second-order polynomial fitting of the overall dataset resulted in an explained K_d (FQ) variance of 50%, 70% and 48% for 1:2 swelling phyllosilicates, 1:2 non-swelling phyllosilicates and 1:1 phyllosilicates, respectively, although for visualization purposes data in **Figure 5.10** were grouped in 1 pH-unit intervals. This explained variance of the data was relatively high taking into account the different sources of variability of the original data (*i.e.*, materials from different procedences; sorption data obtained at varying experimental conditions; K_d values derived in some cases from other reported sorption parameters), thus confirming the key role of pH on FQ sorption in phyllosilicate minerals.

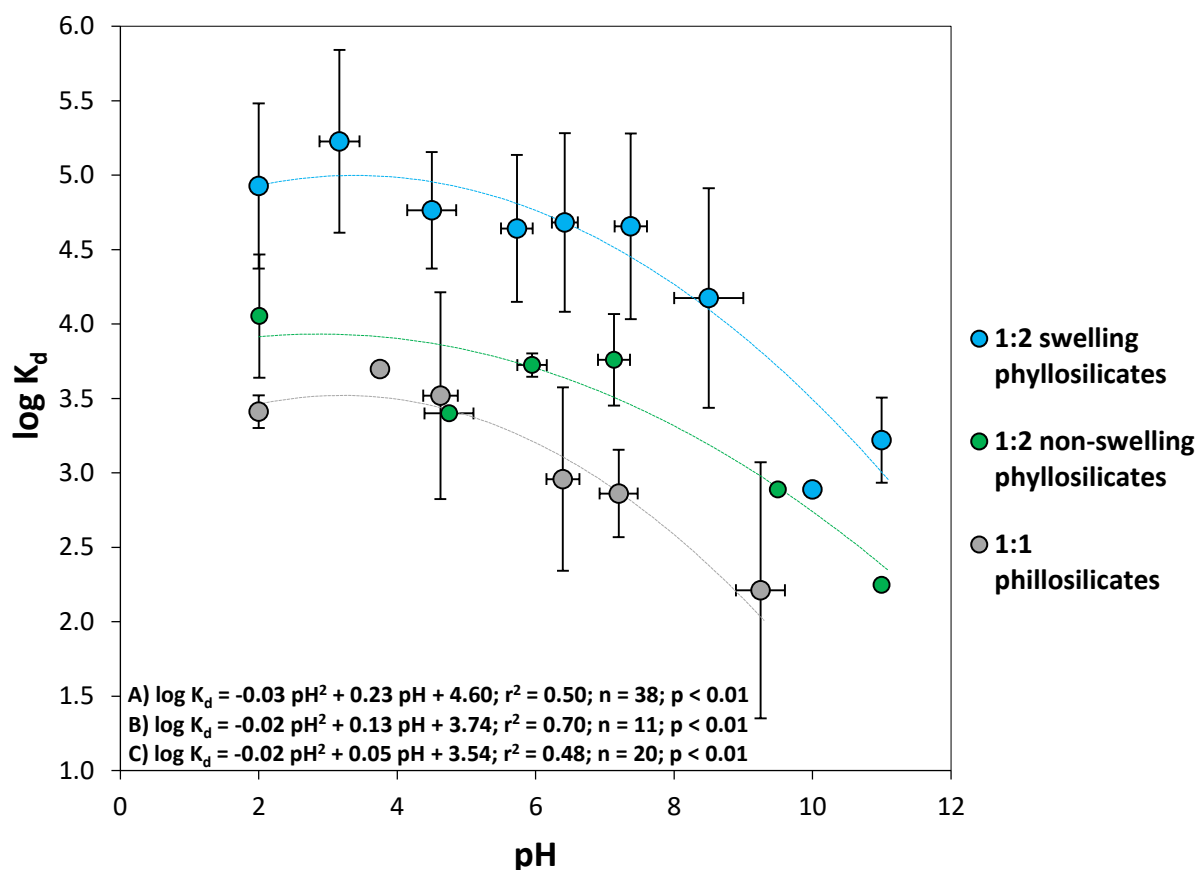


Figure 5.10 Correlation between K_d (FQ) and pH for 1:2 swelling phyllosilicates (A, blue); 1:2 non-swelling phyllosilicates (B, green); 1:1 phyllosilicates (C, red); dashed lines indicate the second-order polynomial fitting.

The second-order polynomial fitting allowed to calculate the pH values in which maximum FQ sorption is achieved. These pH values were 3.4, 3.2 and 2.9 for 1:2 swelling phyllosilicates, 1:2 non-swelling phyllosilicates and 1:1 phyllosilicates, respectively. These values are close to the pH_{ZPC} of these respective clays (Chang et al., 2016; Pan, et al., 2012c), which also indirectly highlighted the role pH_{ZPC} in FQ sorption in phyllosilicates.

5.4.4. Elucidating interaction mechanisms and additional phyllosilicate properties governing FQs sorption

The role of secondary properties of the phyllosilicates, such as CEC and SSA, was examined when the information was available in the built-up dataset. **Table 5.11** summarizes the CEC, SSA and the density of exchangeable sites per m². Besides, it is reported FQ sorption data for a number of phyllosilicates, specifically K_d (FQ) values and maximum sorption capacities, C_{S,MAX}, derived from Langmuir fitting performed in the cited publications.

Table 5.11. Physicochemical properties and FQ sorption parameters in selected studies.

Reference	FQ	Material	Physicochemical Properties	Solution nature and pH	Sorption Parameters
Wu et al., 2010	CIP	Montmorillonite	CEC = 110 ceq kg ⁻¹ SSA = 35 m ² g ⁻¹ CEC/SSA = 3.1 ceq m ²	Aqueous solution pH = 3.0	K _d = 56,000 L kg ⁻¹ C _{S,MAX} = 120 ceq kg ⁻¹
Chang et al., 2016	CIP	Palygorskyte	CEC = 18 ceq kg ⁻¹ SSA = 173 m ² g ⁻¹ CEC/SSA = 0.10 ceq m ²	Aqueous solution pH = 7.0	K _d = 11,232 L kg ⁻¹ C _{S,MAX} = 16 ceq kg ⁻¹
Liu et al., 2017b	CIP	Vermiculite	CEC = 86 ceq kg ⁻¹ SSA = 3.5 m ² g ⁻¹ CEC/SSA = 25 ceq m ²	Aqueous solution pH = 5.0	K _d = 2,507 L kg ⁻¹ C _{S,MAX} = 5.5 ceq kg ⁻¹
Wang et al., 2011	CIP	Illite	CEC = 12 ceq kg ⁻¹ SSA = 22 m ² g ⁻¹ CEC/SSA = 0.55 ceq m ²	Aqueous solution pH = 4.5	K _d = 2,456 L kg ⁻¹ C _{S,MAX} = 10 ceq kg ⁻¹
Li et al., 2017a	OFL	Kaolinite	CEC = 1.3 ceq kg ⁻¹ SSA = 65 m ² g ⁻¹ CEC/SSA = 0.02 ceq m ²	0.01 M NaCl pH = 7.0	K _d = 1,111 L kg ⁻¹ C _{S,MAX} = 0.91 ceq kg ⁻¹

CEC: cation exchange capacity; SSA = specific surface area; C_{S,MAX} = maximum sorption capacity

Cation exchange of FQs and clays is supposed to be the main interaction mechanism at acidic to neutral pH, as already proved (Wu et al., 2010; Li et al., 2011; Chang et al., 2016), in agreement with the FQ sorption inhibition due to the increase in the concentration of competing cations in solution (Rivagli et al., 2014). As seen in **Table 5.11**, K_d (FQ) generally increased with CEC and SSA, although the individual effect of every property was difficult to be assessed as a high CEC was not necessarily related to a high SSA. In accordance, maximum sorption capacities derived from Langmuir fittings ($C_{S,MAX}$) in these clays usually reached values close to their CEC, from which can be deduced that the CEC of the phyllosilicates play a role in restricting FQ sorption extension under these pH conditions.

An exception to this pattern was the sorption of CIP in a vermiculite clay, for which the $C_{S,MAX}$ reached only 6% of the CEC. Although CIP molecules may also access to the interlayer space of vermiculite (Turel and Golobic, 2003; Liu et al., 2017b), the low sorption capacity compared to the CEC value could be due to its high density of CEC sites per square meter in comparison to the other clays reported in **Table 5.11**, which may compromise FQ fully access to all the sorbing sites due to steric effects. SSA values of the clays reported in **Table 5.11** may significantly vary depending on clay nature and origin. Hence, it may be concluded that CEC is the main factor affecting FQ sorption capacity in phyllosilicates at acidic to neutral pH, although depending on exchangeable sites density, SSA contributes to determine the FQ sorption capacity of the phyllosilicate.

5.5. Conclusions

The sorption of FQs in pure soil organic and mineral phases has been evaluated through compiled datasets originated from own experiments and literature data. It has been revealed that sorption of NOR, CIP and OFL in humic substances can be considered analogous, being this sorption process relatively fast, strong (with K_d (FQ) values usually within the $10^4 - 10^5$ L kg^{-1} range), irreversible and affected by specific solution physicochemical properties (*i.e.*, dissolved Ca concentration, DOC content and pH). Mechanisms involved in FQ sorption in humic substances were electrostatic, cation- π , hydrogen and halogen bonding interactions at slightly acidic pH. Sorption in metal oxides was, however, driven by complexation mechanisms, and varied according to both metal nature and surface area. The resulting sorption parameters in these materials pointed to a low contribution in the overall fate of FQs in bulk soils according to the low surface areas observed in metal oxides present in soils and the related lower K_d (FQ) values than for humic substances. Contrarily, sorption of FQs in phyllosilicate minerals, although dependent on clay nature and pH, was much higher than for metal oxides and similar to the values observed for humic substances. The main physicochemical property influencing sorption was pH, affecting both FQ speciation and clay surface charge. Clay property limiting maximum sorption capacity was CEC at acidic pH, although for those minerals with a high exchangeable site density, SSA became the main limiting factor due to steric effects among FQ molecules. The high K_d values observed in both humic acids and phyllosilicate minerals, although being highly pH-dependent, suggested that pH, organic matter and clay contents significantly contribute to the sorption FQ in bulk soils.

5.6. References

- Ahmadi, S., Banach, A., Mostafapour, F. K., Balarak, D., 2017. Study survey of cupric oxide nanoparticles in removal efficiency of ciprofloxacin antibiotic from aqueous solution: adsorption isotherm study. *Desalin. Water Treat.* 89, 297–303. <https://doi.org/10.5004/dwt.2017.21362>
- Andersson, M., I., MacGowan, A., P., 2003. Development of the quinolones. *J. Antimicrob. Chemoth.*, 51 (90001), 1–11. <https://doi.org/10.1093/jac/dkg212>
- Antilen, M., Bustos, O., Ramirez, G., Canales, C., Faundez, M., Escudey, M., Pizarro, C., 2016. Electrochemical evaluation of ciprofloxacin adsorption on soil organic matter. *New J. Chem.* 40, 7132–7139. <https://doi.org/10.1039/C6NJ00207B>
- Aristilde, L., Sposito, G., 2008. Molecular modeling of metal complexation by a fluoroquinolone antibiotic. *Environ. Toxicol. Chem.* 27 (11), 2304–2310. <https://doi.org/10.1897/08-059.1>
- Aristilde, L., Sposito, G., 2010. Binding of ciprofloxacin by humic substances: A molecular dynamics study. *Environ. Toxicol. Chem.* 29 (1), 90–98. <https://doi.org/10.1002/etc.19>
- Aristilde, L., Sposito, G., 2013. Complexes of the antimicrobial ciprofloxacin with soil, peat, and aquatic humic substances. *Environ. Toxicol. Chem.* 32 (7), 1467–1478. <https://doi.org/10.1002/etc.2214>
- Berhane, T. M., Levy, J., Krekeler, M. P. S., Danielson, N. D., 2016. Adsorption of bisphenol A and ciprofloxacin by palygorskite-montmorillonite: Effect of granule size, solution chemistry and temperature. *Appl. Clay Sci.* 132–133, 518–527. <https://doi.org/10.1016/j.clay.2016.07.023>
- Carmosini, N., Lee, L. S., 2009. Ciprofloxacin sorption by dissolved organic carbon from reference and bio-waste materials. *Chemosphere*, 77 (6), 813–820. <https://doi.org/10.1016/j.chemosphere.2009.08.003>

- Carrasquillo, A. J., Bruland, G. L., Mackay, A. A., Vasudevan, D., 2008. Sorption of Ciprofloxacin and Oxytetracycline Zwitterions to Soils and Soil Minerals: Influence of Compound Structure. *Environ. Sci. Technol.* 42 (20), 7634–7642. <https://doi.org/10.1012/es801277y>
- Chang, P. H., Jiang, W. T., Li, Z., Kuo, C. Y., Wu, Q., Jean, J. S., Lv, G., 2016. Interaction of ciprofloxacin and probe compounds with palygorskite PFI-1. *J. Hazard. Mater.* 303, 55–63. <https://doi.org/10.1016/j.jhazmat.2015.10.012>
- Chen, G., Li, M., Liu, X., 2015. Fluoroquinolone Antibacterial Agent Contaminants in Soil/Groundwater: A Literature Review of Sources, Fate, and Occurrence. *Water Air Soil Poll.* 226 (12). <https://doi.org/10.1007/s11270-015-2438-y>
- Fries, E., Crouzet, C., Michel, C., Togola, A., 2016. Interactions of ciprofloxacin (CIP), titanium dioxide (TiO₂) nanoparticles and natural organic matter (NOM) in aqueous suspensions. *Sci. Total Env.* 563–564, 971–976. <https://doi.org/10.1016/j.scitotenv.2015.12.023>
- Genç, N., Dogan, E. C., Yurtsever, M., 2013a. Bentonite for ciprofloxacin removal from aqueous solution. *Water Sci. Technol.* 68 (4), 848–855. <https://doi.org/10.2166/wst.2013.313>
- Genç, N., Dogan, E. C., 2013b. Adsorption kinetics of the antibiotic ciprofloxacin on bentonite, activated carbon, zeolite, and pumice. *Desal. Water Treat.* 1–9. <https://doi.org/10.1080/19443994.2013.842504>
- Girardi, C., Greve, J., Lamshöft, M., Fetzer, I., Miltner, A., Schäffer, A., Kästner, M., 2011. Biodegradation of ciprofloxacin in water and soil and its effects on the microbial communities. *J. Hazard Mater.* 198, 22–30. <https://doi.org/10.1016/j.jhazmat.2011.10.004>

- Goyne, K. W., Chorover, J., Kubicki, J. D., Zimmerman, A. R., Brantley, S. L., 2005. Sorption of the antibiotic ofloxacin to mesoporous and nonporous alumina and silica. *J. Colloid Interf. Sci.* 283 (1), 160–170. <https://doi.org/10.1016/j.jcis.2004.08.150>
- Gu, C., Karthikeyan, K. G., 2005. Sorption of the antimicrobial ciprofloxacin to aluminum and iron hydrous oxides. *Environ. Sci. Technol.* 39 (23), 9166–9173. <https://doi.org/10.1021/es051109f>
- Gulen, B., Demircivi, P., 2020. Adsorption properties of fluoroquinolone type antibiotic ciprofloxacin into 2:1 dioctahedral clay structure: Box-Behnken experimental design. *J. Mol. Struct.* 1206, 127659. <https://doi.org/10.1016/j.molstruc.2019.127659>
- Hanamoto, S., Ogawa, F., 2019. Predicting the sorption of azithromycin and levofloxacin to sediments from mineral and organic components. *Environ. Pollut.* 255, 113180. <https://doi.org/10.1016/j.envpol.2019.113180>
- Ho, Y. S., McKay, G., 1998. Sorption of dye from aqueous solution by peat. *Chem. Eng. J.* 70 (2), 115–124. [https://doi.org/10.1016/S1385-8947\(98\)00076-X](https://doi.org/10.1016/S1385-8947(98)00076-X)
- Huculak-Mączka, M., Hoffmann, J., Hoffmann, K., 2018. Evaluation of the possibilities of using humic acids obtained from lignite in modern water treatment. *Desalin. Water Treat.* 134, 296–304. <https://doi.org/10.5004/dwt.2018.23223>
- Irving, H., Williams, R. J. P., 1953. The stability of transition metal complexes. *J. Chem. Soc.* 637, 3192 - 3210. <https://doi.org/10.1039/JR9530003192>
- Jacobson, A. T., Fan, M., 2019. Evaluation of natural goethite on the removal of arsenate and selenite from water. *J. Environ. Sci-China*, 76, 133–141. <https://doi.org/10.1016/j.jes.2018.04.016>
- Jalil, M. E. R., Baschini, M., Sapag, K., 2017. Removal of ciprofloxacin from aqueous solutions using pillared clays. *Materials*, 10 (12), 17–19. <https://doi.org/10.3390/ma10121345>

- Khoshnamvand, N., Ahmadi, S., Mostafapour, F. K., 2017. Kinetic and isotherm studies on ciprofloxacin adsorption using magnesium oxide nanoparticles. *J. Appl. Pharm. Sci.* 7 (11), 79–83. <https://doi.org/10.7324/JAPS.2017.71112>
- Leal, R. M. P., Alleoni, L. R. F., Tornisielo, V. L., Regitano, J. B., 2013. Sorption of fluoroquinolones and sulfonamides in 13 Brazilian soils. *Chemosphere*, 92 (8), 979–985. <https://doi.org/10.1016/j.chemosphere.2013.03.018>
- Lei, K., Han, X., Fu, G., Zhao, J., Yang, L., 2014. Mechanism of ofloxacin fluorescence quenching and its interaction with sequentially extracted dissolved organic matter from lake sediment of Dianchi, China. *Environ. Monit. Assess.* 186 (12), 8857–8864. <https://doi.org/10.1007/s10661-014-4049-2>
- Li, Z., Hong, H., Liao, L., Ackley, C. J., Schulz, L. A., Macdonald, R. A., Mihelich, A. L., Emard, S. M., 2011. A mechanistic study of ciprofloxacin removal by kaolinite. *Colloid. Surface. B.* 88 (1), 339–344. <https://doi.org/10.1016/j.colsurfb.2011.07.011>
- Li, Y., Bi, E., Chen, H., 2017a. Sorption Behavior of Ofloxacin to Kaolinite: Effects of pH , Ionic Strength, and Cu (II). *Water Air Soil Poll.* 228, 46 - 56 <https://doi.org/10.1007/s11270-016-3236-x>
- Li, Y., Bi, E., Chen, H., 2017b. Effects of dissolved humic acid on fluoroquinolones sorption and retention to kaolinite. *Ecotox. Environ. Safe.* 178, 43 - 50 <https://doi.org/10.1007/s11270-016-3236-x>
- Limousin, G., Gaudet, J. P., Charlet, L., Sznknect, S., Barthès, V., Krimissa, M., 2007. Sorption isotherms: A review on physical bases, modeling and measurement. *Appl. Geochem.* 22, 249–275. <https://doi.org/10.1016/j.apgeochem.2006.09.010>

- Lin, Y. C., Hsiao, K. W., Lin, A., Y. C., 2018. Photolytic degradation of ciprofloxacin in solid and aqueous environments: kinetics, phototransformation pathways, and byproducts. *Environ. Sci. Pollut. R.* 25 (3), 2303–2312. <https://doi.org/10.1007/s11356-017-0666-y>
- Lin, C. C., Lee, C. Y., 2020. Adsorption of ciprofloxacin in water using Fe₃O₄ nanoparticles formed at low temperature and high reactant concentrations in a rotating packed bed with co-precipitation. *Mater. Chem. Phys.* 240, 122049. <https://doi.org/10.1016/j.matchemphys.2019.122049>
- Liu, X., Lu, S., Liu, Y., Meng, W., Zheng, B., 2017a. Adsorption of sulfamethoxazole (SMZ) and ciprofloxacin (CIP) by humic acid (HA): characteristics and mechanism. *RSC Adv.*, 7 (80), 50449–50458. <https://doi.org/10.1039/C7RA06231A>
- Liu, S., Wu, P., Yu, L., Li, L., Gong, B., Zhu, N., Dang, Z., Yang, C., 2017b. Preparation and characterization of organo-vermiculite based on phosphatidylcholine and adsorption of two typical antibiotics. *Appl. Clay Sci.* 137, 160–167. <https://doi.org/10.1016/j.clay.2016.12.002>
- Mackay, A. A., Seremet, D. E., 2008. Probe Compounds to Quantify Cation Exchange and Complexation Interactions of Ciprofloxacin with Soils. *Environ. Sci. Technol.* 2008, 42 (22), 8270–8276.
- Martin, S., Shchukarev, A., Hanna, K., Boily, J-F., 2015. Kinetics and Mechanisms of Ciprofloxacin Oxidation on Hematite Surfaces. *Environ. Sci. Technol.* 49 (20), 12197–12205. <https://doi.org/10.1021/acs.est.5b02851>
- Martínez-Mejía, M. J., Sato, I., Rath, S., 2017. Sorption mechanism of enrofloxacin on humic acids extracted from Brazilian soils. *Environ. Sci. Pollut. R.* 24 (19), 15995–16006. <https://doi.org/10.1007/s11356-017-9210-3>

- Nowara, A., Burhenne, J., Spitteller, M., 1997. Binding of Fluoroquinolone Carboxylic Acid Derivatives to Clay Minerals. *J. Agr. Food Chem.* 45 (4), 1459–1463. <https://doi.org/10.1021/jf9602151>
- OECD, 2000. OECD 106 Adsorption - Desorption Using a Batch Equilibrium Method. OECD Guideline for the Testing of Chemicals. <https://doi.org/10.1787/9789264069602-en>
- Pan, B., Qiu, M., Wu, M., Zhang, D., Peng, H., Wu, D., Xing, B., 2012a. The opposite impacts of Cu and Mg cations on dissolved organic matter-ofloxacin interaction. *Environ. Pollut.* 161, 76–82. <https://doi.org/10.1016/j.envpol.2011.09.040>
- Pan, B., Liu, Y., Xiao, D., Wu, F., Wu, M., Zhang, D., Xing, B., 2012b. Quantitative identification of dynamic and static quenching of ofloxacin by dissolved organic matter using temperature-dependent kinetic approach. *Environ. Pollut.* 161, 192–198. <https://doi.org/10.1016/j.envpol.2011.10.026>
- Pan, B., Wang, P., Wu, M., Li, J., Zhang, D., Xiao, D., 2012c. Sorption kinetics of ofloxacin in soils and mineral particles. *Environ. Pollut.* 171, 185–190. <https://doi.org/10.1016/j.envpol.2012.07.037>
- Pan, M., Chu, L. M., 2017. Leaching behavior of veterinary antibiotics in animal manure-applied soils. *Sci. Total Environ.* 579, 466–473. <https://doi.org/10.1016/j.scitotenv.2016.11.072>
- Paul, T., Liu, J., Machesky, M. L., Strathmann, T. J., 2014. Adsorption of zwitterionic fluoroquinolone antibacterials to goethite: A charge distribution-multisite complexation model. *J. Colloid Interf. Sci.* 428, 63–72. <https://doi.org/10.1016/j.jcis.2014.04.034>
- Pei, Z. G., Shan, X. Q., Zhang, S. Z., Kong, J. J., Wen, B., Zhang, J., Zheng, L. R., Xie, Y. N., Janssens, K., 2011. Insight to ternary complexes of co-adsorption of norfloxacin and Cu(II) onto montmorillonite at different pH using EXAFS. *J. Hazard. Mater.* 186 (1), 842–848. <https://doi.org/10.1016/j.jhazmat.2010.11.076>

- Peng, H., Liang, N., Li, H., Chen, F., Zhang, D., Pan, B., Xing, B., 2015. Contribution of coated humic acids calculated through their surface coverage on nano iron oxides for ofloxacin and norfloxacin sorption. *Environ. Pollut.* 204, 191–198.
<https://doi.org/10.1016/j.envpol.2015.04.029>
- Peruchi, L. M., Fostier, A. H., Rath, S.. 2015. Sorption of norfloxacin in soils: Analytical method, kinetics and Freundlich isotherms. *Chemosphere*, 119, 310–317.
<https://doi.org/10.1016/j.chemosphere.2014.06.008>
- Qin, X., Liu, F., Wang, G., Li, L., Wang, Y., Weng, L., 2014a. Modeling of levofloxacin adsorption to goethite and the competition with phosphate. *Chemosphere*, 111, 283–290.
<https://doi.org/10.1016/j.chemosphere.2014.04.032>
- Qin, X., Liu, F., Wang, G., Weng, L., Li, L., 2014b. Adsorption of levofloxacin onto goethite: Effects of pH, calcium and phosphate. *Colloid. Surface. B.* 116, 591–596.
<https://doi.org/10.1016/j.colsurfb.2013.09.056>
- Quan, Y., Bi, E., 2017. Adsorption Characteristics of Different Forms of Ofloxacin to Attapulgitite (in chinese). *Chem. J. Chin. Uni.* Vol. 38 (4), 622–630.
<https://doi.org/10.7503/cjcu20160773>
- Rakshit, S., Sarkar, D., Elzinga, E. J., Punamiya, P., Datta, R., 2013. Mechanisms of ciprofloxacin removal by nano-sized magnetite. *J. Hazard. Mater.* 246–247, 221–226.
<https://doi.org/10.1016/j.jhazmat.2012.12.032>
- Riaz, L., Mahmood, T., Khalid, A., Rashid, A., Siddique, M. B. A., Kamal, A., Coyne, M. S., 2018. Fluoroquinolones (FQs) in the environment: A review on their abundance, sorption and toxicity in soil. *Chemosphere*, 191, 704–720.
<https://doi.org/10.1016/j.chemosphere.2017.10.092>

- Rigol, A., Vidal, M., Rauret, G., 1998. Ultrafiltration-capillary zone electrophoresis for the determination of humic acid fractions. *J. Chromatogr. A.* 807, 275-284. [https://doi.org/10.1016/S0021-9673\(98\)00088-0](https://doi.org/10.1016/S0021-9673(98)00088-0)
- Rivagli, E., Pastorello, A., Sturini, M., Maraschi, F., Speltini, A., Zampori, L., Setti, M., Malavasi, L., Profumo, A., 2014. Clay minerals for adsorption of veterinary FQs: Behavior and modeling. *J. Env. Chem. Eng.* 2 (1), 738-744. <https://doi.org/10.1016/j.jece.2013.11.017>
- Roca, M. E. J., Baschini, M., Sapag, K., 2015. Influence of pH and antibiotic solubility on the removal of ciprofloxacin from aqueous media using montmorillonite. *Appl. Clay Sci.* 114, 69-76. <https://doi.org/10.1016/j.clay.2015.05.010>
- Rodríguez, F. J., Núñez, L. A., 2011. Characterization of aquatic humic substances. *Water Environ. J.* 25 (2), 163-170. <https://doi.org/10.1111/j.1747-6593.2009.00205.x>
- Schmitt-Kopplin, P., Burhenne, J., Freitag, D., Spiteller, M., Kettrup, A., 1999. Development of capillary electrophoresis methods for the analysis of fluoroquinolones and application to the study of the influence of humic substances on their photodegradation in aqueous phase. *J. Chromatogr. A.* 837 (1-2), 253-265. [https://doi.org/10.1016/S0021-9673\(99\)00079-5](https://doi.org/10.1016/S0021-9673(99)00079-5)
- Septian, A., Oh, S., Shin, W. S., 2018. Sorption of antibiotics onto montmorillonite and kaolinite: competition modelling. *Environ. Technol.* 1-14. <https://doi.org/10.1080/09593330.2018.1459870>
- Shi, S., Fan, Y., Huang, Y., 2013. Facile low temperature hydrothermal synthesis of magnetic mesoporous carbon nanocomposite for adsorption removal of ciprofloxacin antibiotics. *Ind. Eng. Chem.* 52 (7), 2604-2612. <https://doi.org/10.1021/ie303036e>
- Turel, I., Golobic, A., 2003. Crystal Structure of Ciprofloxacin Hydrochloride 1.34-Hydrate. *Anal. Sci.* 19, 329-330. <https://doi.org/10.2116/analsci.19.329>

- Tan, Y., Guo, Y., Gu, X., Gu, C., 2015. Effects of metal cations and fulvic acid on the adsorption of ciprofloxacin onto goethite. *Environ. Sci. Pollut. R.* 22 (1), 609–617. <https://doi.org/10.1007/s11356-014-3351-4>
- Trivedi, P., Vasudevan, D., 2007. Spectroscopic investigation of ciprofloxacin speciation at the goethite-water interface. *Environ. Sci. Technol.* 41 (9), 3153–3158. <https://doi.org/10.1021/es061921y>
- Vasudevan, D., Bruland, G. L., Torrance, B. S., Upchurch, V. G., Mackay, A. A., 2009. pH-dependent ciprofloxacin sorption to soils: Interaction mechanisms and soil factors influencing sorption. *Geoderma* 151, 68–76. <https://doi.org/10.1016/j.geoderma.2009.03.007>
- Wan, M., Li, Z., Hong, H., Wu, Q., 2013. Enrofloxacin uptake and retention on different types of clays. *J. Asian Earth Sci.* 77, 287–294. <https://doi.org/10.1016/j.jseaes.2013.02.032>
- Wang, C. J., Li, Z., Jiang, W. T., Jean J. S., Liu, C. C., 2010. Cation exchange interaction between antibiotic ciprofloxacin and montmorillonite. *J. Hazard. Mat.* 183, 309 - 314, <https://doi.org/10.1016/j.jhazmat.2010.07.025>
- Wang, C. J., Li, Z., Jiang, W. T., 2011. Adsorption of ciprofloxacin on 2:1 dioctahedral clay minerals. *Appl. Clay Sci.* 53 (4), 723–728. <https://doi.org/10.1016/j.clay.2011.06.014>
- Wang, L., Liang, N., Li, H., Yang, Y., Zhang, D., Liao, S., Pan, B., 2015. Quantifying the dynamic fluorescence quenching of phenanthrene and ofloxacin by dissolved humic acids. *Environ. Pollut.* 196, 379–385. <https://doi.org/10.1016/j.envpol.2014.10.029>
- Wang, C., Ma, L., Liu, B., Zhang, D., Pan, B., 2017. Co-contaminant effects on ofloxacin adsorption onto activated carbon, graphite, and humic acid. *Environ. Sci. Pollut. R.* 23834–23842. <https://doi.org/10.1007/s11356-017-0038-7>

- Weishaar, J. L., Aiken, G. R., Bergamaschi, B. A., Fram, M. S., Fujii, R., Mopper, K., 2003. Evaluation of specific ultraviolet absorbance as an indicator of the chemical composition and reactivity of dissolved organic carbon. *Environ. Sci. Technol.* 37 (20), 4702–4708. <https://doi.org/10.1021/es030360x>
- Wu, Q., Li, Z., Hong, H., Yin, K., Tie, L., 2010. Adsorption and intercalation of ciprofloxacin on montmorillonite. *Appl. Clay Sci.* 50, 204–211. <https://doi.org/10.1016/j.clay.2010.08.001>
- Wu, Q., Li, Z., Hong, H., Li, R., Jiang, W. T., 2012. Desorption of ciprofloxacin from clay mineral surfaces. *Water Res.* 47 (1), 259–268. <https://doi.org/10.1016/j.watres.2012.10.010>
- Wu, M., Ning, P., Liu, S., 2013. Adsorption characteristics of Norfloxacin in soil organic matter fractions (in chinese). *Environ. Chem.* 32 (1), 112–117, <https://doi.org/10.7524/j.issn.0254-6108.2013.01.017>
- Wu, Q. F., Zhang, T., Li, Z., Hong, H. L., Yin, K., Jean, J. S., Jiang, W. T., 2014. Using probing compounds to investigate adsorption mechanism of ciprofloxacin on montmorillonite. *Mater. Technol. Adv. Biomat.* 29 (B2), B100–B107. <https://doi.org/10.1179/1753555714Y.0000000154>
- Yan, W., Hu, S., Jing, C., 2012. Enrofloxacin sorption on smectite clays: Effects of pH, cations, and humic acid. *J. Colloid Interf. Sci.* 372 (1), 141–147. <https://doi.org/10.1016/j.jcis.2012.01.016>
- Yu, C., Devlin, J. F., Bi, E., 2019. Bonding of monocarboxylic acids, monophenols and nonpolar compounds onto goethite. *Chemosphere*, 214, 158–167. <https://doi.org/10.1016/j.chemosphere.2018.09.080>

- Zhang, H., Huang, C-H., 2005. Oxidative transformation of fluoroquinolone antibacterial agents and structurally related amines by manganese oxide. *Environ. Sci. Technol.* 39 (12), 4474–4483. <https://doi.org/10.1021/es048166d>
- Zhang, H., Huang, C. H., 2007. Adsorption and oxidation of fluoroquinolone antibacterial agents and structurally related amines with goethite. *Chemosphere*, 66 (8), 1502–1512. <https://doi.org/10.1016/j.chemosphere.2006.08.024>
- Zhang, Q., Huang, G. Y., Zhao, L., Dong, Y. H., 2011. Thermodynamics and kinetics of Norfloxacin Sorption on Humic Acid (in chinese). *J. Agro-Environ. Sci.* 30 (1), 65-70.
- Zhang, Q., Zhao, L., Dong, Y-H., Huang, G-Y., 2012. Sorption of norfloxacin onto humic acid extracted from weathered coal. *J. Environ. Manage.* 102, 165–172. <https://doi.org/10.1016/j.jenvman.2011.12.036>
- Zhang, J., Lu, M., Wan, J., Sun, Y., Lan, H., Deng, X., 2018. Effects of pH, dissolved humic acid and Cu^{2+} on the adsorption of norfloxacin on montmorillonite-biochar composite derived from wheat straw. *Biochem. Eng. J.* 130, 104–112. <https://doi.org/10.1016/j.bej.2017.11.018>
- Zhang, H., Lu, T., Zhang, R., Wang, M., Krishnan, S., Liu, S., Zhou, Y., Li, D., Qi, Z., 2020. Effects of clay colloids on ciprofloxacin transport in saturated quartz sand porous media under different solution chemistry conditions. *Ecotox. Environ. Safe.* 199, 110754. <https://doi.org/10.1016/j.ecoenv.2020.110754>
- Zhao, Q., Zhang, S., Zhang, X., Lei, L., Ma, W., Ma, C., Song, L., Chen, J., Pan, B., Xing, B., 2017. Cation-Pi Interaction: A Key Force for Sorption of Fluoroquinolone Antibiotics on Pyrogenic Carbonaceous Materials. *Environm. Sci. Technol.* 51 (23), 13659–13667. <https://doi.org/10.1021/acs.est.7b02317>

- Zhao, L., Liu, J., Wang, H., Dong, Y. H., 2019a. Sorption of copper and norfloxacin onto humic acid: effects of pH, ionic strength, and foreign ions. *Environ. Sci. Pollut. R.* 26 (11), 10685–10694. <https://doi.org/10.1007/s11356-019-04515-5>
- Zhao, X., Hu, Z., Yang, X., Cai, X., Wang, Z., Xie, X., 2019b. Noncovalent interactions between fluoroquinolone antibiotics with dissolved organic matter: A ¹H NMR binding site study and multi-spectroscopic methods. *Environ. Pollut.* 248, 815–822. <https://doi.org/10.1016/j.envpol.2019.02.077>
- Zhou, D., Chen, B., Wu, M., Liang, N., Zhang, D., Li, H., Pan, B., 2014. Ofloxacin sorption in soils after long-term tillage: The contribution of organic and mineral compositions. *Sci. Total Env.* 497–498, 665–670. <https://doi.org/10.1016/j.scitotenv.2014.07.130>
- Zhu, Y., Yang, K., Shan, R., Han, Z., Shao, Y., Tian, C., 2018. The Influence of Humification Degree of Humic Acid on Its Sorption of Norfloxacin During Sewage Sludge Composting. *Water Air Soil Poll.* 229 (5). <https://doi.org/10.1007/s11270-018-3821-2>

CHAPTER VI

SORPTION OF FQs IN SOILS

6.1. Introduction

FQs are currently prescribed for treating human and animal diseases caused by Gram positive and Gram negative pathogens (Andersson and MacGowan, 2003). Due to their widespread use, partial elimination in the organism, and low photo and biodegradation (Girardi et al., 2011; Lin et al., 2018), high levels of FQs have been reported in environmental compartments. Specifically, FQs have been detected at mg kg^{-1} levels in animal manure such as chicken droppings, poultry and piggery, and the application of manure as a soil amendment is considered an important FQ input pathway in the environment (Picó and Andreu, 2007). Thus, FQs have been detected in soils at levels of up to a few hundred $\mu\text{g kg}^{-1}$ (Riaz et al., 2018); these levels may lead to bacterial resistance against these drugs (Redgrave et al., 2014), and thus disrupt the balance of the original ecosystems.

The environmental fate of FQs is mainly controlled by their sorption to soil particles (Chen et al., 2015). As seen in the previous chapter, sorption of FQs in pure soil components, including humic acids, phyllosilicate minerals and metal oxides is highly pH-dependent. Fluoroquinolone sorption increases in acidic soils with clay content (Leal et al., 2013), being sorption on pure clay minerals is mainly controlled by cation exchange interactions at acidic to neutral pH. The addition of humic acid to soils also increases FQ sorption at acidic to neutral pH (Teixidó et al., 2014), involving cation exchange, electrostatic and hydrogen bonding interactions. Besides, the presence of metal oxides may increase FQ sorption at neutral to basic pH through surface complexation mechanisms (Paul et al., 2014), although this contribution is suspected to be negligible in average soils due to the low K_d values expected in naturally occurring metal oxides. Besides, soluble metals may decrease FQ sorption due to competition for exchangeable sites (Kong et al., 2014).

Due to the multiple interaction mechanisms involved in FQ sorption, the development of models to predict K_d (FQ) based on the soils physicochemical properties as descriptors of

these chemical interactions is challenging. Based on the results obtained in the previous chapter, all soil pH, clay and organic matter content may play a significant role in the sorption process of FQs in soils, whereas the role of other soil and FQ physicochemical properties in the overall sorption in bulk soils is still unclear. In addition, some of the currently available commercial FQs differ slightly in their chemical structure (Van Doorslaer et al., 2014), and it is not yet clear whether their sorption in bulk soils can be considered analogous.

A few empirical equations aiming to predict K_d for FQs in soils have been reported. For instance, a set of five equations have been proposed at different pH aiming to predict CIP sorption by multiple linear regressions (MLR) (Vasudevan et al., 2009). However, these equations were developed after forcing CIP sorption in 30 soils at different pH, thus modifying the surface charge of the original soil particles, and they may not be totally representative of real environmental scenarios. In addition, a parametric model aiming to predict NOR sorption was proposed after a PLS regression (Gong et al., 2012). The model included the following predictive variables: pH, clay, Fe, OM and exchangeable Ca content, and led to a satisfactory prediction of their own K_d (FQ) data. However, the model was not tested against external validation data, and so its predictive effectiveness for other scenarios not contemplated in its construction is unclear.

Alternatively to parametric models based on specific physicochemical properties, to consider probabilistic tools allowing the derivation of best-estimate K_d values with their associated variability through CDFs are also of interest (USEPA, 2014). CDFs describe the population and variability of a given property, here K_d (FQ), and their related accumulated frequency through a continuous function. CDFs have been successfully used to describe K_d variability and to derive best-estimate K_d values of several pollutants after refining datasets according to the key soil properties governing interaction, instead of suggesting an overall K_d value regardless of soil properties (Ramírez-Guinart et al., 2020a, 2020b, 2020c).

In this chapter, we aimed to obtain K_d values for four FQs (NOR, CIP, ENR and OFL) in seven soils with contrasting physicochemical properties. The K_d (FQ) values were subsequently incorporated in a dataset built up with data gathered from the literature. Sorption analogy among FQs was assessed and a PLS prediction model was constructed. Due to the low predictive quality of the PLS model, we derived best-estimate K_d (FQ) values through CDFs by grouping K_d (FQ) data according to the most relevant soil properties affecting sorption. This strategy made it possible to reduce K_d (FQ) variability compared to that of the overall K_d (FQ) dataset, and thus appears better suited for risk assessment of a specific soil scenario.

6.2. Materials and methods

6.2.1. Reagents and materials

NOR (> 99%), CIP (> 99%), ENR (> 99%) and OFL ($\geq 95\%$) were purchased from Sigma-Aldrich (Germany). Their main physicochemical properties are summarized in **Table 1.5**. Milli-Q double deionized water ($18.2\text{ M}\Omega\text{ cm}^{-1}$) was obtained from a water purification system (USF PureLaB Plus, Spain). A $1,000\text{ mg L}^{-1}$ FQ stock solution was prepared in HCl-acidified (pH 4.0) Milli-Q water. HPLC-grade methanol, formic acid (> 95%), HCl (37%) and NaOH (> 95%) were purchased from Panreac (Spain).

The soil samples used in this study were selected to cover a wide range of physicochemical properties, especially pH, CEC, OC and clay contents. The main soil properties are summarized in **Table 6.1**, and exchangeable and water-soluble cation contents for Na, K, Ca and Mg are provided in **Table 6.2**. Additional soil characterization information can be found elsewhere (Gil-García et al., 2008; Ramírez-Guinart et al., 2017).

The pH of the blank soils was determined in a 40 g L^{-1} Milli-Q water suspension slurry after being shaken during 48 hours, whereas OC content was determined by elemental analysis (EA-1108 C.E Instruments, Thermo Fisher Scientific). Soil texture (sand, silt and clay contents)

was deduced after analysing the particle size of the soil particles by the pipette method (Burt, 2004). CEC was determined by BaCl₂-triethanolamine exchange at pH 8.2, accounting for the sum of exchangeable K, Na, Mg, Ca, NH₄⁺, Fe and Al (Burt, 2004). The amount of amorphous Fe was determined by ascorbic extraction (Kotska and Luther, 1994), whereas the amount of amorphous Al and Mn was determined by oxalate extraction (Carter and Gregorich, 2006). The calcium carbonate content, CaCO₃, was determined by the Bernard method (Müller and Gastner, 1971).

The DOC content in the blank soil suspensions was determined using a DOC analyser (Shimadzu TOC-5000 A, Japan) after acidification to pH 2.0 using HCl 1 N. Main water-soluble cations in the blank samples (including K, Na, Mg and Ca) were determined by ICP-OES (Thermo-Jarrell Ash 25 and Perkin Elmer Optima 3200 RL, USA) in a 40 g L⁻¹ Milli-Q water suspension slurry. The pH of the samples ranged from 3.9 to 9.9, whereas the OC varied from 0.3% to 41%. The CEC of the soils ranged from 22 to 185 cmol_c kg⁻¹, and sand and clay contents ranged from 12% to 86% and from 0.2% to 28%, respectively. Amorphous Fe, Al and Mn contents ranged 60 – 20,000; 120 – 580 and 110 – 390 mg kg⁻¹, respectively. The sum of water-soluble and exchangeable cations ranged from 0.90 to 9.5 mmol_c L⁻¹ and from 5.9 to 116 cmol_c kg⁻¹, respectively. DOC contents in the supernatants ranged from 4 to 187 mg C L⁻¹ and correlated with soil OC ($p < 0.05$, data derived from **Table 6.1**).

Table 6.1 Physicochemical properties of the soils

Soil	pH	CEC ^a (cmol _c kg ⁻¹)	OC ^b (%)	Sand ^c (%)	Clay ^c (%)	Fe ^d (mg kg ⁻¹)	Al ^d (mg kg ⁻¹)	Mn ^d (mg kg ⁻¹)	CaCO ₃ (%)	DOC ^e (mg L ⁻¹)	∑ Ex cations (cmol _c kg ⁻¹)	∑ WS cations (mmol _c L ⁻¹)
RED STONE	3.9	68	9.3	46	6	4.42 · 10 ³	584	114	1.3	180	17	0.90
ALM	5.5	23	1.6	54	10	1.01 · 10 ³	404	204	2.0	15	5.9	1.6
KOM	5.7	185	41	20	0.2	1.97 · 10 ⁴	481	393	0.5	187	116	4.5
BAD1	7.7	22	0.9	50	19	580	493	168	2.0	11	8.3	3.5
DELTA2	8.0	87	7.7	12	28	2.97 · 10 ³	230	330	51	39	66	9.5
ZORITA	8.5	27	1.0	41	20	56	118	199	40	7	11	4.3
VAN1	9.9	25	0.3	86	6	238	138	150	5	4	15	4.1

^a CEC = Cation Exchange Capacity; ^b OC = Organic Carbon; ^c Sand and Clay contents referred to mineral phase; ^d Amorphous metal content; ^e DOC = Dissolved Organic Carbon; ∑ Ex cations: sum of exchangeable Na, K, Ca and Mg concentrations; ∑ WS cations: sum of water-soluble Na, K, Ca and Mg concentrations.

Table 6.2 Exchangeable and water-soluble cation concentrations for Na, K, Ca and Mg.

	Exchangeable cations (cmol _c kg ⁻¹)				Water-soluble cations (mmol _c L ⁻¹)			
	Na	K	Ca	Mg	Na	K	Ca	Mg
RED STONE	14	0.60	1.0	1.7	0.09	0.18	0.30	0.33
ALM	0.60	0.41	4.1	0.76	0.04	0.08	1.2	0.25
KOM	8.8	0.50	100	6.7	0.17	0.13	3.5	0.67
BAD1	0.48	0.62	5.5	1.7	0.06	0.10	2.2	1.1
DELTA2	2.2	3.5	52	8.6	4.0	0.13	4.0	1.4
ZORITA	0.13	0.48	9.3	1.2	0.01	0.08	4.0	0.17
VAN1	0.77	0.34	13	0.93	0.06	0.03	3.8	0.25

6.2.2. Batch experiments

Batch experiments were applied to construct sorption isotherms for NOR and to determine K_d at a single initial concentration for CIP, ENR and OFL (OECD, 2000). Briefly, 25 mL of Milli-Q water were added in 50 mL PP centrifuge tubes containing 1.00 g of soil. Tubes were shaken in an end-over-end shaker at 30 rpm and room temperature (22 – 25°C) for 24 hours to reach a pre-equilibrium state. Next, a certain amount of NOR solution was added to achieve a concentration range of 10 – 80 mg L⁻¹ (1 – 8 mg L⁻¹ for the VAN1 soil), whereas for CIP, ENR and OFL a concentration of 50 mg L⁻¹ (5 mg L⁻¹ for the VAN1 soil) was used, after ensuring that the selected concentrations fell within the NOR sorption linear range. After the spike, the tubes were shaken again wrapped with aluminium foil. After 48 hours, a period identified in previous kinetic studies as sufficiently long to achieve the equilibrium stage (Pan et al., 2012; Peruchi et al., 2015), tubes were centrifuged at 7,800 g at 4 °C for 15 min (AJ2-HS, Beckman Coulter, USA), and then the supernatants were filtered through 0.45 µm and analysed as described in Section 6.2.3. Desorption experiments were run similarly with the solid residues obtained for the NOR sorption isotherms, after drying the residues at 40 ± 1 °C. It was

also anticipated that desorption equilibrium would be reached after 48 hours in the light of previous kinetic studies in pure soil components (Martínez-Mejía et al., 2017; Wu et al., 2012). The pH of the resulting sorption and desorption supernatants did not significantly differ (± 0.2) from the soil pH reported in **Table 6.1**.

Both sorption and desorption experiments were run in triplicate, and quality control samples were run in parallel in each batch. These controls included blank samples, to ensure that no background FQs were present in the soils, and control samples run without any soil to account for possible losses through the experimental stages. Blank samples revealed that no FQs were present in the soils prior to analysis, and control samples revealed null FQ losses during the experimental setup.

6.2.3. FQs analysis by HPLC-FLD

The HPLC separation conditions were adapted from elsewhere (Teixidó et al., 2014). An Agilent 1200 chromatograph was used for the FQ determination in both sorption and desorption supernatants, using an isocratic 75:25 0.01 M oxalic acid:MeOH mobile phase and a ZORBAX SB-C₁₈ (5 μm , 4.6 x 250 mm) separation column. Flow rate and injection volume were set at 1 mL min⁻¹ and 10 μL respectively. NOR, CIP, ENR and OFL detection was carried out using a FLD set at excitation/emission wavelengths of 280/447, 284/449, 284/467 and 298/499 nm respectively.

LOQ, determined as a signal-to-noise ratio of 10:1, were 0.01 mg L⁻¹ for all FQs. In order to avoid biased results during the HPLC determination due to possible matrix effects (Peruchi et al., 2015), matrix-matched calibration curves were prepared during both sorption and desorption experiments for each soil and FQ pair. Seven-point calibration curves were prepared for each case, and Pearson coefficients rose to 0.99. The quantification precision of 10 consecutive injections of a 0.2 mg L⁻¹ NOR aqueous standard was 3.8% RSD, whereas the

quantification precision of 10 injections of 0.2 mg L⁻¹ NOR aqueous standards on 10 different days was 6.1% RSD. Similar results were obtained for CIP, ENR and OFL.

6.2.4. Creation of a K_d (FQ) dataset

A critically-reviewed dataset was created including batch sorption K_d data of FQs in soils, subsoils and sediments, all environmental matrices considered as analogues, in addition to ancillary information on physicochemical properties such as pH, OC and mineral contents. The dataset also included information on the experimental conditions in which the batch experiments were carried out. The sorption data obtained in this study for NOR, CIP, ENR and OFL were also included in the dataset. Other geochemical materials, such as pure organic and oxide and clay phases, were not considered. The percentages of sand, silt and clay of the soils, often reported referred to the mineral phase, were recalculated in this study when necessary to ensure that all mineral data was referred to the bulk soil. Acceptance criteria for the entries of the dataset were: (i) Only data originated from batch experiments was contemplated; (ii) For those studies reporting both the soil pH and the final pH after the sorption experiments, the latter pH was considered. Those studies reporting the pH of the aqueous solution but not the pH of the soil were included in the dataset, but excluded when grouping samples according to pH. Since changes in the pH of the contact solution may change some of the physicochemical properties of the soil, as well as affect the speciation of the FQs, for those studies reporting K_d (FQ) values at varying pH values only the sorption data obtained at ± 1 pH units differing from soil pH were considered; (iii) For those studies in which the organic matter was reported instead of OC, a conversion factor of 2.0 was applied (Pribyl, 2010); (iv) For those studies where the organic or mineral contents were modified (either removing one of the phases or adding pure components as surrogates), only the unmodified soils were included; (v) For those studies reporting K_d values at different ionic strengths only those K_d values attributed to the lowest

ionic strength were considered; (vi) Those studies reporting soil classification but not the specific percentages of sand, silt and clay were not considered when grouping according to mineral content; (vii) For those studies in which K_d values were not provided but Freundlich fitting parameters were reported, K_d values were calculated at an aqueous concentration of 100 ng L^{-1} , which is representative for FQs concentration in freshwaters (Massey et al., 2010). (viii) As LEV and OFL are two isomeric FQs, sorption of OFL and LEV was assumed to be analogous and was pooled into OFL data. As only a few sorption data were found for other FQs such as danofloxacin (*i.e.*, Leal et al., 2013; Rath et al., 2019) the final dataset included only entries for NOR, CIP, ENR, OFL.

The dataset had a total of 312 entries, and the list of references used to build up the dataset can be found in **Table 6.3**.

Table 6.3 List of references used to build up the sorption dataset

Matrix	Number of samples	NOR	CIP	ENR	OFL	Number of entries	Reference
Soil	4	X				4	Peruchi et al., 2015
Soil	4		X	X		8	Rath et al., 2019
Soil	30		X			30	Vasudevan et al., 2009
Soil	5	X		X		10	Figueroa-Diva et al., 2010
Soil	13	X	X	X		39	Leal et al., 2013
Soil	1		X	X		2	Parpounas et al., 2017
Soil	1			X		1	Graouer-Bacart et al., 2015
Soil	2				X	2	Wu et al., 2014
Soil	3	X				3	Kong et al., 2014
Soil	3	X				3	Zhang et al., 2009
Soil	2				X	2	Drillia et al., 2005
Soil	3	X				3	Zhang and Dong, 2008
Soil	1	X				1	Pan and Chu, 2016
Soil	1	X	X	X		3	Conkle et al., 2010
Soil	11				X	11	Zhou et al., 2014
Soil	3		X	X		6	Uslu et al., 2008
Soil	3			X		3	Sturini et al., 2012
Soil	1	X	X	X		3	Leal et al., 2012
Soil	5		X	X	X	7	Nowara et al., 1997
Soil	2		X	X		4	Teixidó et al., 2014
Soil	4		X			4	Dalkmann et al., 2014
Soil	4				X	4	Li et al., 2017
Soil	23	X				23	Gong et al., 2012
Soil	8	X				8	Williams et al., 2009
Soil	3	X				3	Peng et al., 2014
Soil	4	X		X	X	12	Chen et al., 2016
Soil	4	X				4	Zhang and Dong, 2007
Soil	3		X			3	Sidhu et al., 2019
Soil	1		X			1	Zhao et al., 2017
Soil	1		X	X	X	3	Riaz et al., 2019
Soil	20			X		20	Álvarez-Esmorís et al., 2020
Soil	4		X		X	8	Kiecak et al., 2019
Soil	9				X	9	Hanamoto and Ogawa, 2019
Soil	2			X		2	Aldana et al., 2021
Soil	1				X	1	Wei et al., 2021
Soil	7	X	X	X	X	28	This study
Sediment	7		X			7	Mutavd et al., 2017
Sediment	3	X				3	Cao et al., 2015
Sediment	6	X				6	Jin et al., 2011
Sediment	1				X	1	Wang et al., 2017
Sediment	1	X				1	Hari et al., 2005
Sediment	1	X				1	Dong et al., 2018
Sediment	3		X			3	Córdova-Kreylos and Scow, 2007
Sediment	4	X				4	Williams et al., 2009
Sediment	2	X		X	X	6	Chen et al., 2016
Sediment	1				X	1	Zhang et al., 2019
Sediment	1		X			1	Belden, 2007
Total	226	97	87	74	54	312	

OC was reported in all entries, and soil/sediment pH was reported in 295. pH, OC and textural mineral (sand/silt/clay) data were simultaneously available in only 251 entries, which

where V (L) is the total volume of contact solution and m (kg) refers to the dry mass of soil added. The K_d ($L\ kg^{-1}$), was calculated as follows:

$$K_d = \frac{C_S}{C_{eq}} \quad (6.2)$$

Similarly, the concentration remaining in the solid phase after running the desorption experiments ($C_{S,des}$, $mg\ kg^{-1}$) was calculated according to Equation 6.3:

$$C_{S,des} = C_{in,des} - \frac{C_{eq,des} \cdot V}{m} \quad (6.3)$$

where $C_{eq,des}$ ($mg\ L^{-1}$) is the FQ concentration in the solid and aqueous phases after desorption experiments, whereas $C_{in,des}$ ($mg\ kg^{-1}$) is the sorbed concentration in the solid phase before running the desorption experiments. Thus, $C_{in,des}$ is C_S corrected by the amount of FQ present in the residual volume of solution (V_{res} , L^{-1}) removed after drying the residues of the sorption experiments:

$$C_{in,des} = C_S + \frac{C_{eq} \cdot V_{res}}{m} \quad (6.4)$$

Desorption percentage was calculated as:

$$\% D = \frac{C_{eq,des} \cdot V}{C_{in,des} \cdot m} \cdot 100 \quad (6.5)$$

The experimental data obtained after the isotherm experiments were fitted to the Linear (Equation 6.2) and Freundlich (Equation 6.6) models. This last model considers a parameter (K_F , $(mg\ kg^{-1}) / (mg\ L^{-1})^N$) related to the affinity of the sorbate-sorbent interaction and a dimensionless parameter, N , related to the heterogeneity of sorption sites. For $N = 1$, the model assumes that the sorbent has a sufficient amount of equally-affine sorption sites able to bind the sorbate, and therefore, Equation 6.2 equals to Equation 6.6 and K_F equals to K_d (Limousin et al., 2007).

$$C_S = K_F (C_{eq})^N \quad (6.6)$$

The sorption data for NOR, CIP, ENR and OFL for our own experiments were compared by a two-way ANOVA with replicates at $\alpha = 0.05$, whereas the sorption data derived from the literature dataset were examined by classifying $\log K_d$ values in box and whisker plots, and FLSD test run at $\alpha = 0.05$ (Statgraphics Technologies, USA) was used for statistical comparison of the FQ populations.

6.2.6. Development of a partial least squares prediction model

PLS is a multivariate regression method that builds a model for predictive purposes in a low-dimensional space formed by Latent Variables (LVs). PLS can also be used to determine which variables are more important for correlating with the Y property, here K_d (FQ), by checking certain indexes such as the Variable Importance in Projection (VIP) scores. In addition, the influence plot allows the identification of samples with extreme properties for the model (those with a high Hotelling T^2 value) or samples with a high error between observed and predicted K_d (those with a high Q residual value). The PLS regression was run using Matlab (PLS Toolbox703, Matlab® R2009a (MathWorks 181 Inc., USA)), and all data were \log_{10} transformed (with the exception of pH) and autoscaled prior to running the PLS analysis.

To build the model, selected literature data were used to complement part of our data to construct a “calibration set” representative for a wide range of soil properties. The calibration set comprised 80 soils and 92 entries, all of them reporting pH, soil texture, CEC, OC and Fe content, and included K_d data for NOR, CIP, ENR and OFL (**Table 6.4**). The fraction of each FQ species at a given pH was calculated as described elsewhere (Septian et al., 2018) and were also included in the model. Only the K_d values of a single representative FQ were considered for soils for which sorption K_d data of different FQ were reported, but K_d values for different FQs obtained in the same soil were accepted in the calibration matrix only for those soils that could improve the calibration set due to their having extreme soil property values (*e.g.*, pH and OC).

Table 6.4 List of references to build up the calibration set.

Reference	FQ	soils	pH	OC (%)	Sand (%)	Silt (%)	Clay (%)	CEC (ceq kg ⁻¹)	Fe (g kg ⁻¹)
This study*	NOR	4	5.7 – 9.9	0.30 – 41	3.6 – 86	8.0 – 51	0.04 - 24	25 – 185	0.06 – 20
	CIP	4	5.7 – 9.9	0.30 – 41	3.6 – 86	8.0 – 51	0.04 - 24	25 – 185	0.06 – 20
	ENR	4	5.7 – 9.9	0.30 – 41	3.6 – 86	8.0 – 51	0.04 - 24	25 – 185	0.06 – 20
	OFL	7	3.9 – 9.9	0.30 – 41	3.6 – 86	8.0 – 51	0.04 – 24	22 – 185	0.06 – 20
Riaz et al., 2019	OFL	1	5.8	2.7	9.5	68	17	2.1	8.3
Vasudevan et al., 2009	CIP	30	3.2 – 7.5	0.04 - 9	8.9 – 92	3.7 – 66	1.2 – 60	0.98 – 62	0.04 – 31
Leal et al., 2013	ENR	13	3.7 – 6.9	0.67 – 21	6.5 – 86	3.9 – 41	3.9 – 57	28 – 218	3 – 192
Aldana et al., 2021	ENR	2	8.1 – 8.2	1.7 – 2.9	26 – 37	35 – 40	20 – 33	28 – 70	0.05 – 0.18
Gong et al., 2012	NOR	23	4.7 – 7.8	0.12 - 24	0.97 – 89	10 – 68	0.40 – 21	2.5 – 41	12 – 364
Zhang and Dong, 2007	NOR	4	5.2 – 8.1	0.3 – 1.5	34 – 62	24 – 47	13 – 28	10 – 24	10 – 50
Total		92	3.2 – 9.9	0.04 - 41	0.97 - 92	1.8 - 72	0.04 - 60	0.98 - 218	0.01 - 364

* Additional data for NOR, CIP and ENR in soils KOM, DELTA2, ZORITA and VAN1 was contemplated.

The samples selected for the calibration set had pH and OC values ranging from 3.2 to 9.9 and from 0.04 to 41% respectively. Besides, sand, silt and clay percentages, all of them referring to the bulk soil, ranged 1.0 – 92%, 1.8 – 72% and 0.04 – 60% respectively. Soil CEC ranged 0.98 – 218 $\text{cmol}_c \text{kg}^{-1}$, whereas Fe contents ranged 0.01 – 364 g kg^{-1} . The histograms of the selected properties revealed a good distribution of their values within the calibration set (see **Figure 6.2**).

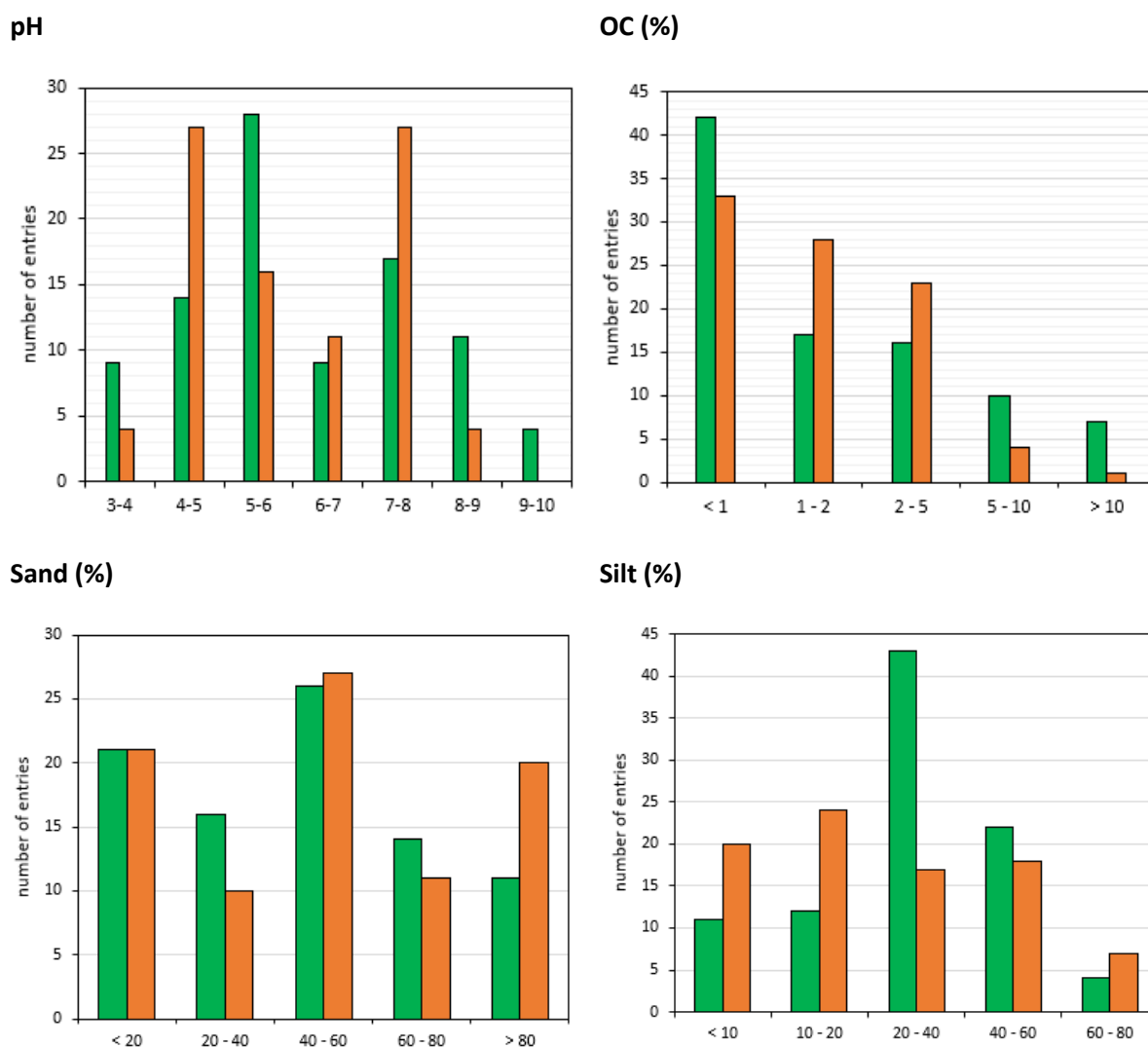


Figure 6.2 Histograms displaying the range of selected soil properties for the calibration (green) and validation (orange) datasets.

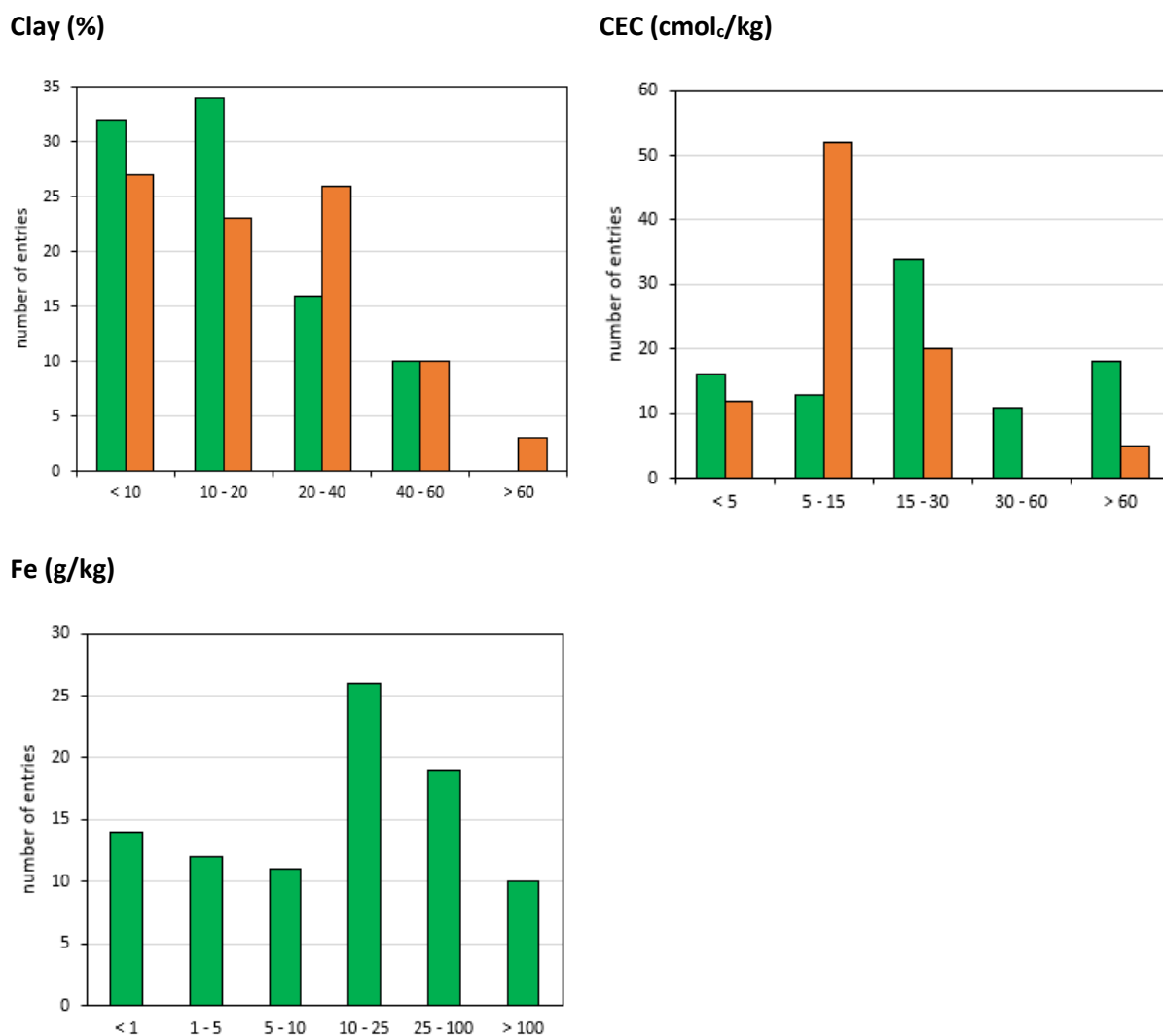


Figure 6.2 (Continued)

The model used only the variables that significantly described K_d (FQ) (those with VIP scores > 1) and it was validated using both cross-validation (using the venetian blind method with 10 data splits) and external data. This external validation included data from the literature not considered in the calibration set with the reported physicochemical properties of the variables selected in the final model (**Table 6.5**).

Table 6.5 List of references to build up the external validation set

Reference	FQ	soils	Entries	pH	%OC	% Sand	CEC
Parpounas et al., 2017	ENR, CIP	1	2	7.2	0.60	19	190
Graouer-Bacart et al., 2015	ENR	1	1	8.1	3.4	45	18
Uslu et al., 2008	ENR, CIP	3	6	6.0 – 6.6	0.59 – 2.3	78 – 93	4.0 – 9.0
Sturini et al., 2012	ENR	3	3	6.4 – 6.5	1.1 – 1.8	43 – 46	13 – 18
Leal et al., 2012	NOR, CIP, ENR	1	3	5.9	1.6	12	128
Nowara et al., 1997	ENR, CIP, OFL	5	7	4.9 – 7.5	0.70 – 1.6	27 – 84	7.4 – 19
Teixidó et al., 2014	ENR, CIP	2	4	7.4 – 7.4	1.0 – 1.6	14 – 37	8.9 – 16
Peng et al., 2014	OFL	3	3	4.8 – 8.7	0.52 – 2.1	9.8 – 42	6.4 – 26
Chen et al., 2016	NOR, ENR, OFL	6	18	7.1 – 7.9	0.39 – 3.3	6.5 – 92	8.9 – 25
Zhao et al., 2017	CIP	1	1	7.1	2.8	34	7.7
Álvarez-Esmorís et al., 2020	ENR	20	20	4.1 – 7.3	0.30 – 11	35 – 70	3.3 – 28
Córdova-Kreylos and Scow, 2007	CIP	3	3	5.1 – 8.6	2.0 – 2.8	27 – 56	5.1 – 11
Jin et al., 2011	NOR	2	2	6.2 – 8.7	0.25 – 2.8	31 – 56	7.9 – 20
Peruchi et al., 2015	NOR	4	4	4.1 – 5.0	0.89 – 1.9	15 – 91	1.9 – 6.6
Rath et al., 2019	CIP, ENR	4	8	4.1 – 5.0	0.89 – 1.9	15 – 91	1.9 – 6.6
Belden, 2007	CIP	1	1	5.6	1.3	16	16
Zhang and Dong, 2008	NOR	3	3	4.8 – 4.9	0.21 – 0.35	42 – 47	5.3 – 8.9
TOTAL		59	89	4.1 – 8.7	0.21 - 11	6.5 – 92	1.9 – 190

The external validation set comprised 59 soils, with a total number of entries of K_d (FQ) of 89. The samples in this external validation set had pH, OC, sand and CEC values ranging 4.1 – 8.7%, 0.21 – 11%, 6.5 – 92% and 1.9 – 190 $\text{cmol}_c \text{kg}^{-1}$ respectively, and fell within the variable ranges contemplated in the calibration set (see **Figure 6.2**).

To evaluate the predictive accuracy of the model, the root square mean error (RMSE) and the residual predictive deviation (RPD) were calculated as:

$$\text{RMSE} = \sqrt{\frac{\sum_{i=1}^n (\log K_{d,\text{measured},i} - \log K_{d,\text{predicted},i})^2}{N}} \quad (6.6)$$

where $\log K_{d,\text{measured},i}$ are the measured experimental $\log K_d$ values, $\log K_{d,\text{predicted},i}$ are the predicted $\log K_d$ values by the model, i is the entry being tested and N is the total number of entries included in the model.

The RPD was calculated as:

$$\text{RPD} = \frac{\text{SD}}{\text{RMSE}} \quad (6.7)$$

where SD is the standard deviation of the original experimental $\log K_{d,\text{measured}}$ data. RPD values therefore relate the variability of the original data to the variability of the prediction errors, and are indicative of the quality of the model. Despite RPD thresholds are subjective and dependent on imposed quality requirements, usually RPD values < 1.5 are considered as models with poor prediction ability; RPD values from 1.5 to 2.0 are considered as models with acceptable prediction ability; RPD values between 2.0 and 3.0 are considered as models with good prediction ability, and RPD values > 3.0 are considered as models with excellent prediction ability (Knight et al., 2019).

6.2.7. Construction of cumulative distribution functions

Since K_d is a ratio between concentrations (see Equation 6.2), K_d data are expected to follow a \log_{10} normal distribution (Sheppard, 2011). Therefore, the statistical parameters describing a symmetrical $\log K_d$ distribution are the location parameter (μ), considered as the most probable $\log K_d$ value corresponding to the 50th percentile (which permits derivation of the best-estimate value of a K_d population), and the scale parameter (σ), which gives an estimation of the dispersion among $\log K_d$ values.

The overall dataset was refined according to a few soil physicochemical properties affecting FQs sorption. The $\log K_d$ data within each dataset were sorted by increasing value and an empirical frequency ($f_{\text{exp},i}$) equal to $1/N$ (where N is the total number of entries) was assigned to each entry. Experimental cumulative frequency distribution was constructed by assigning to each sorted $\log K_d$ value its corresponding cumulative frequency ($F_{\text{exp},i}$), *i.e.*, the sum of the preceding frequencies ($F(K_{d,j}) = \sum_{i=0}^j f(K_{d,i})$). The Kolmogorov-Smirnov test was applied to ensure the lognormal distribution of each resulting CDF, and then these were fitted to the theoretical normal CDF equation (Equation 6.8) using the *cftool* toolbox of Matlab (Matlab® R2009a (MathWorks Inc., USA)):

$$P(\log K_{d,i} \leq \log K_{d,j}) = \sum_{\log K_{d,i} \leq \log K_{d,j}} p(\log K_{d,i}) = \frac{1}{2} + \frac{1}{2} \operatorname{erf}\left(\frac{\log(K_{d,i}) - \mu}{\sigma \sqrt{2}}\right); K_{d,i} > 0 \quad (6.8)$$

where P is the cumulative probability, *erf* is the error function, and subscripts i and j represent two different K_d values in the ranked grouping (Ramírez-Guinart et al., 2020a). Both μ and σ were derived from each dataset after fitting the data to Equation 6.8, and the 5th and 95th percentiles were calculated accordingly.

As the overall sorption dataset was split into partial datasets according to the threshold values of the soil variables that were relevant in FQ sorption, CDFs were obtained for the overall and partial datasets, the latter aiming to derive representative best-estimate K_d (FQ)

values with a lower associated variability than that of the overall dataset. As the construction of reliable CDFs requires a minimum number of entries (around $N \geq 7-10$ entries, Ramírez-Guinart et al., 2020a), the thresholds of the variable ranges to define the partial datasets were adapted to ensure a minimum number of entries in the partial datasets. For cases for which a CDF could not be constructed, the reported K_d best estimates were straightforwardly calculated from the geometrical mean (GM) and geometrical standard deviation (GSD) of the original data. Finally, FLSD tests were run at $\alpha = 0.05$ (Statgraphics Technologies, USA) to complete the CDF analyses and to carry out a statistical comparison with the populations resulting from the partial datasets defined according to the thresholds of each soil variable considered.

6.3. Results and discussion

6.3.1 Sorption and desorption pattern of NOR in soils

Figure 6.3 shows the NOR sorption isotherms in the seven soils and summarizes the results of the fitting of the isotherms to the linear and Freundlich model. Although previous studies performing sorption of NOR on soils found non-linear isotherms (Kong et al., 2014; Peruchi et al., 2015), the isotherms in the present study had a linear trend, as revealed by their high Pearson coefficients (> 0.98) and the N values resulting from Freundlich fitting equals to one (see **Table 6.6**). The linearity of the isotherms obtained could be attributed to both the lower initial concentration range ($\leq 80 \text{ mg L}^{-1}$) tested and to the higher soil-to-solution ratio (40 g L^{-1}) than those used in previous works, leading to a higher number of available sorption sites able to interact with NOR. Therefore, the linearity of the isotherms validated the derivation of K_d values from the slope of the respective sorption isotherm.

The derived K_d values varied within the $44 - 5,600 \text{ L kg}^{-1}$ range, and in general they indicated a strong sorption and therefore a low expected mobility of FQs in soils, with the exception of the ZORITA and (especially) VAN1 soils.

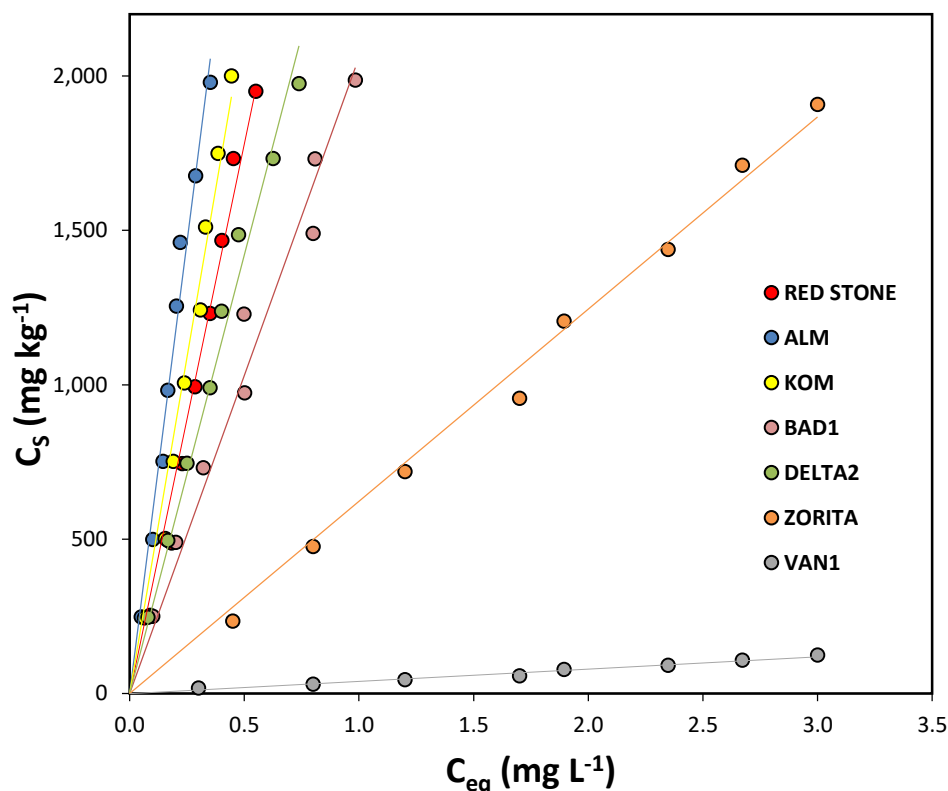


Figure 6.3 Sorption isotherm of NOR in the seven studied soils. Solid lines indicate the Linear fitting.

The sequence of K_d (NOR) variation between soils agreed with the changes in the soil properties that are expected to govern NOR sorption.

Table 6.6 Sorption K_d values and desorption percentages for NOR in the studied soils.

Soil	K_d (L kg ⁻¹)	r^2	K_F (mg kg ⁻¹) / (mg L ⁻¹) ^N	N (dimensionless)	r^2	%D
RED STONE	3,940 ± 400	0.989	4,010 ± 560	1.13 ± 0.18	0.991	0.37 ± 0.10
ALM	5,600 ± 560	0.988	5,870 ± 1,470	1.00 ± 0.18	0.984	0.36 ± 0.16
KOM	4,810 ± 530	0.988	5,320 ± 770	1.13 ± 0.14	0.991	0.25 ± 0.11
BAD	2,080 ± 200	0.989	1,990 ± 165	0.88 ± 0.17	0.983	1.1 ± 0.08
DELTA2	2,920 ± 290	0.988	2,650 ± 230	0.89 ± 0.12	0.991	0.50 ± 0.10
ZORITA	640 ± 37	0.996	575 ± 45	1.09 ± 0.09	0.997	1.5 ± 0.09
VAN1	44 ± 4	0.989	37 ± 6	1.09 ± 0.18	0.989	20 ± 2.4

ALM presented the highest K_d , followed by KOM, despite their contrasting mineral and organic contents. However, these two soils had a pH around 5.5, at which FQ sorption is favoured at both clay minerals and humic substances sites (Martínez-Mejía et al., 2017; Wan et al., 2013). RED STONE presented a slightly lower K_d value than KOM probably due to its lower pH (3.9), which does not favour sorption of NOR cationic species due both to a decrease in the negative charges in the soil surface particles and to the competition of protons for exchangeable sites (Wan et al., 2013). BAD1 presented a lower K_d value than ALM, despite containing a higher clay content, probably due to its lower OC and its slightly basic pH, which strongly affects the sorption in mineral phases due to the negative repulsions of the zwitterion NOR form and the negative charges present in mineral particles (Wan et al., 2013). DELTA2, although slightly more alkaline than BAD1, presented a higher K_d value. Albeit the presence of mono- and divalent cations in solution may compete for exchangeable sorption sites with the zwitterion NOR species (Kong et al., 2014), its higher K_d could be attributed both to its higher Fe content, which may favour sorption at this pH due to complexation mechanisms with Fe-minerals (Paul et al., 2014), and to its higher OC content. The much lower K_d value found in ZORITA than in DELTA2 could therefore be attributed to higher pH, lower OC and Fe contents and higher sand content, which all negatively affect sorption of FQs (Vasudevan et al., 2009). Finally, the K_d value found for VAN1 was the lowest among the soils analysed. Although no sorption data obtained in soils at pH 10 could be found in the literature, this extremely low sorption could be attributed to its alkaline pH, low OC and high sand content.

Since NOR sorption is affected by multiple soil properties including pH, OC, sand, Fe, DOC contents and concentration of water-soluble cations, our sorption K_d data for NOR were correlated with soil properties. A preliminary overview of our data revealed that K_d (NOR) values were not linearly correlated to any single property of the soils at $\alpha = 0.05$, with the exception of pH ($r^2 = 0.72$). In this regard, **Figure 6.4** displays the K_d (NOR) values for all

tested soils along with soil pH, superimposed over the NOR speciation diagram over pH, to illustrate the key role of pH and NOR speciation in K_d (NOR) variability. For soil pH below pK_{a1} , NOR sorption increased with pH, as is often observed for cationic species. Sorption increased when approaching pK_{a1} , regardless of other soil characteristics, as NOR was present in the soil under its cationic and zwitterion forms.

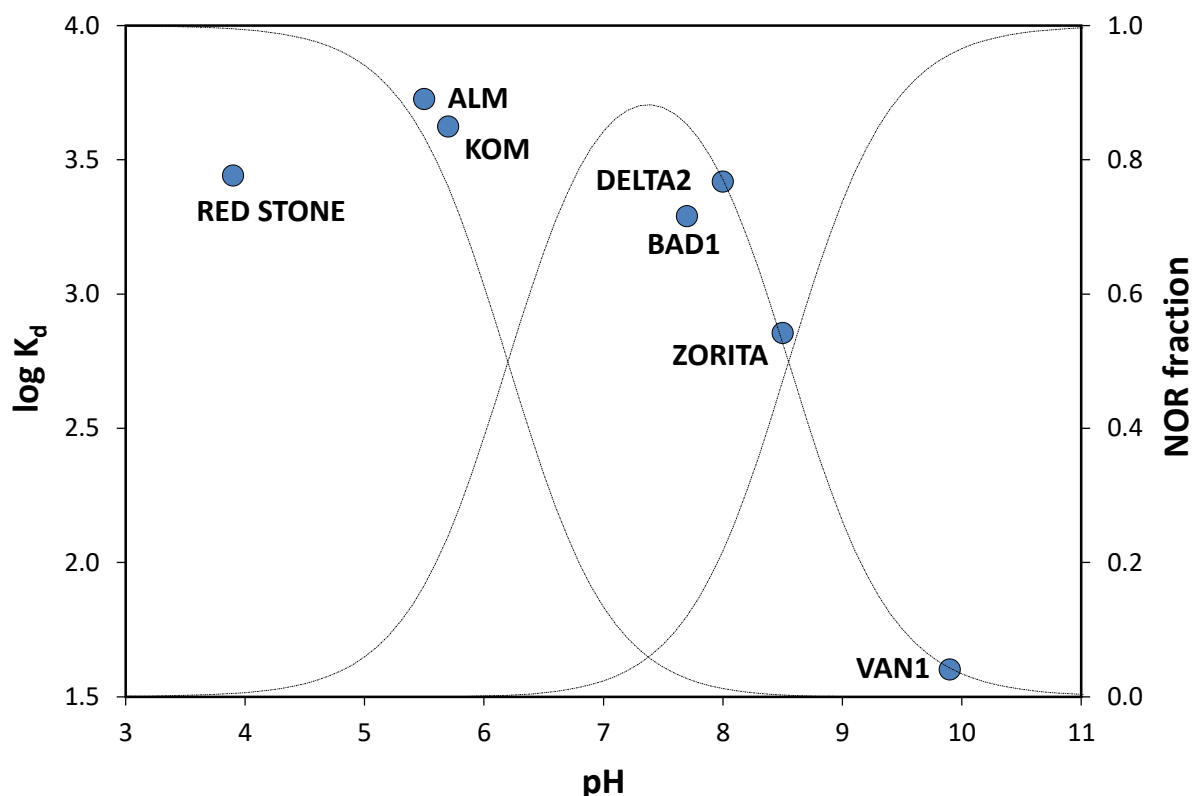


Figure 6.4 Dependence of K_d (NOR) values with soil pH superimposed with NOR speciation diagram. Dashed lines indicate the respective NOR fraction of each NOR species at each pH.

At pH above pK_{a1} , sorption started to decrease likely due to the increase in electrostatic repulsions between the carboxylate group of the increasingly predominant zwitterion species and the negatively charged soil particles; these repulsions were further maximized for scenarios with $pH > pK_{a2}$, for which the anionic form gradually became the majority species.

NOR desorption percentages are also given in **Table 6.6**. They were extremely low (generally $< 1\%$), with the exception of VAN1 (20%). In fact, the sequence of desorption yields

roughly agreed with the inverse of the sequence of K_d (FQ) in the soils tested. These results, combined with the previous sorption data, strongly suggest a low leaching potential of FQs in slightly acidic soils, but a higher mobility is expected, and therefore a higher environmental risk, for basic sandy soils with low OC content, in agreement with previous leaching data obtained in the laboratory (Pan and Chu, 2017; Domínguez et al., 2014).

6.3.2. Assessing the sorption analogy between NOR, CIP, ENR and OFL

In order to test sorption analogy between FQs in the tested soils, K_d values for CIP, ENR and OFL were derived using the same batch methodology. Since K_d (NOR) was constant along the range of concentrations tested, the K_d values for CIP, ENR and OFL could be obtained at a single initial concentration within the range tested for NOR. The %RSD of the K_d (FQ) replicates was $\leq 20\%$. **Figure 6.5** displays the K_d values derived for the four FQs. Smaller differences were observed between FQs for a given soil than between soils for a given FQ, suggesting a lesser role of the FQ structure for the tested FQs in soil sorption. A two-way ANOVA analysis confirmed that K_d (FQ) was significantly affected by the soil factor but not by the FQ factor.

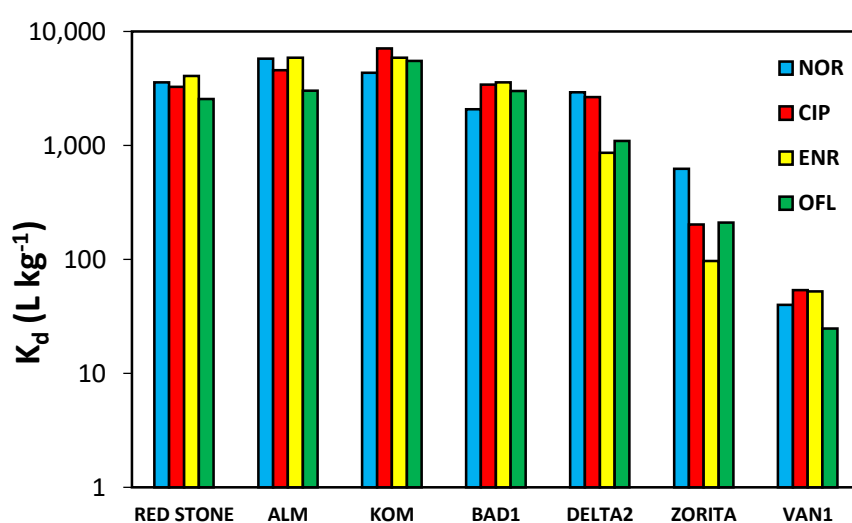


Figure 6.5 Comparison of K_d values obtained for NOR, CIP, ENR and OFL in the seven soils.

In order to extend these comparisons to a larger scale, the sorption data for NOR, CIP, ENR and OFL gathered in the literature dataset were analysed by box and whisker plots (see **Figure 6.6**).

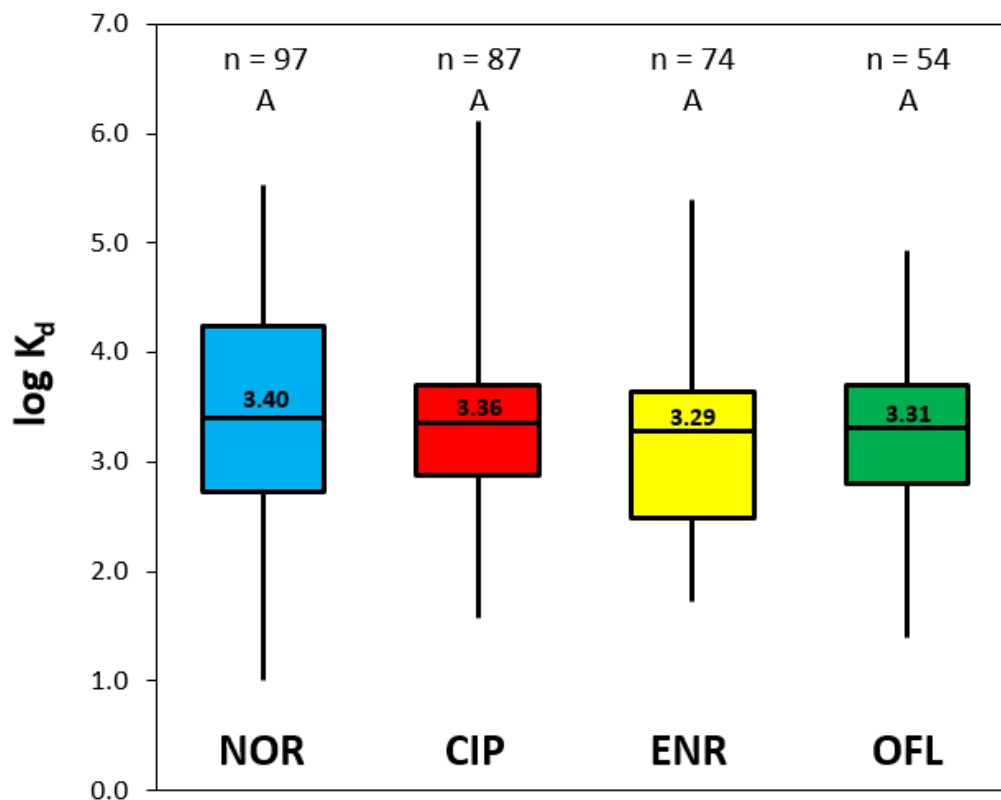


Figure 6.6 Box and whisker plots of K_d values for NOR, CIP, ENR and OFL derived from the overall dataset; Central values are the calculated median values.

FLSD results showed that sorption of these four FQs was statistically comparable, with median K_d ($L\ kg^{-1}$) values of 2,500, 2,300, 1,900 and 2,000 for NOR, CIP, ENR and OFL respectively, suggesting that sorption differences that could be attributed to target FQs have a much lower contribution to K_d (FQ) variability than that caused by soil physicochemical properties.

6.3.3. Development of a multivariate K_d (FQ) prediction model

As K_d (FQ) is affected by multiple soil and FQ physicochemical properties, PLS regression was used to construct a multivariate K_d (FQ) prediction model. Considering the data in the calibration dataset (**Table 6.4**), the PLS explained 75% of the K_d (FQ) data variance using five LVs. The influence plot revealed that most of the data was within the acceptance range of the Q residuals vs. Hotelling T^2 statistics, suggesting the presence of minor extreme soils samples in the calibration set (**Figure 6.7**).

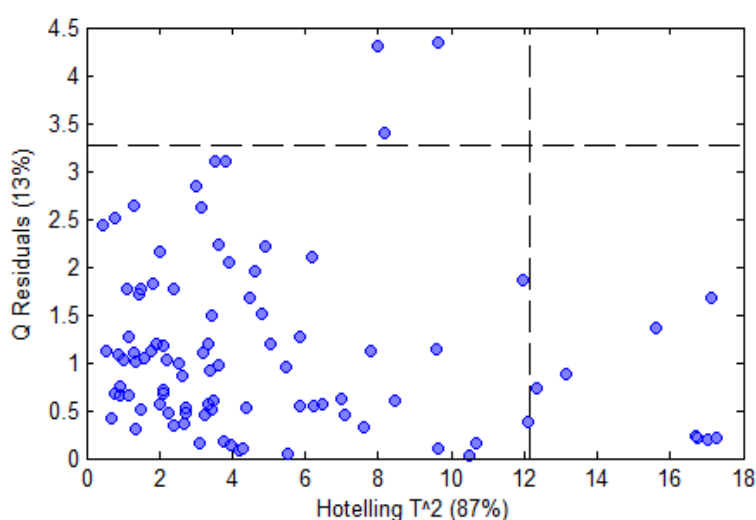


Figure 6.7 Influence plot (Q Residuals vs. Hotelling T^2) of the PLS-based K_d (FQ) model.

The VIP projection of the original variables are displayed in **Figure 6.8**.

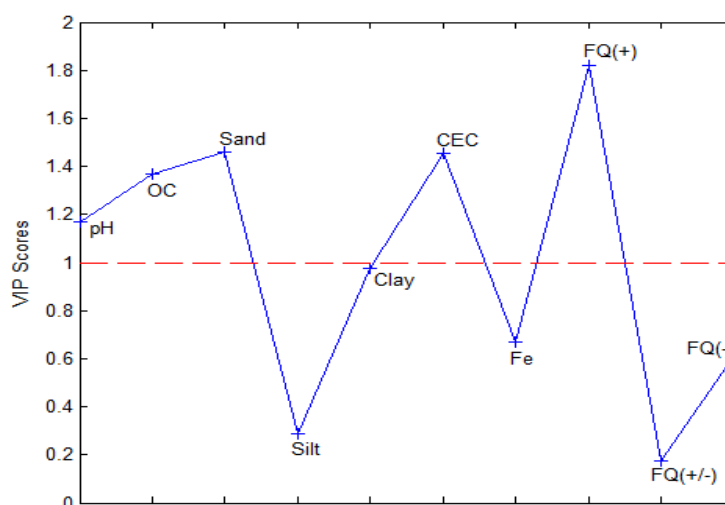


Figure 6.8 VIP scores of the original variables of the PLS-based K_d (FQ) model.

The VIP scores confirmed that pH, CEC, OC and sand contents were good descriptors (VIP score > 1) of K_d (FQ), while silt, clay and Fe contents did not significantly describe the K_d (FQ) of the calibration dataset (VIP score < 1). Among the three FQ species (cationic, zwitterion and anionic), only the cationic species (FQ(+)) contributed significantly (VIP score > 1) to K_d (FQ).

Accordingly, a new simplified model considering only the relevant properties (VIP score > 1) describing K_d (FQ) was created. The new PLS model explained 61% of the K_d (FQ) data variance using three LVs, and the model resulted in the following equation:

$$\log K_d = -0.06 \text{ pH} - 0.17 \log \text{OC} - 0.48 \log \text{Sand} + 0.79 \log \text{CEC} + 0.34 \log \text{FQ(+)} + 3.54 \quad (6.9)$$

Cross-validation revealed that the prediction ability of the model was acceptable, obtaining RMSE and RPD values of 0.44 and 1.88 respectively, although a slope and y-intercept between the experimental and modelled \log_{10} -transformed K_d values statistically differed to one and zero respectively (see **Figure 6.9**).

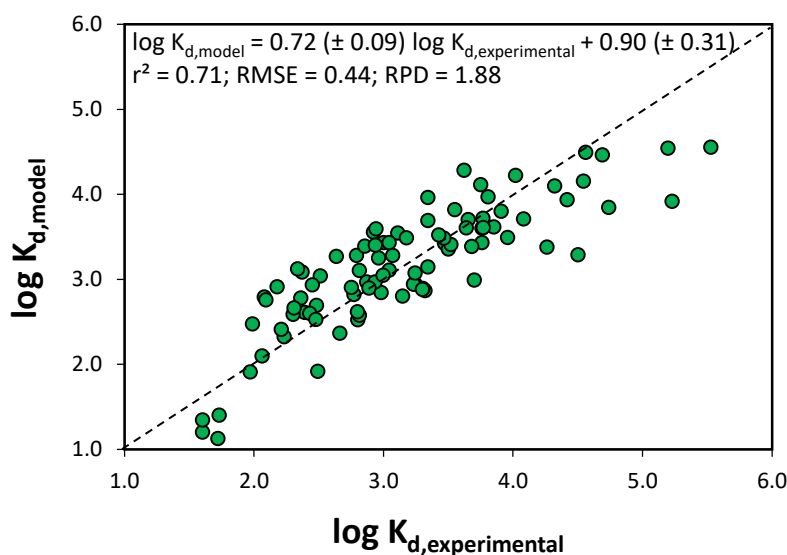


Figure 6.9 Cross-validation results of the PLS-based FQ (K_d) model.

The predictive ability of the model was lower when the external validation set was tested, describing only 32% of the K_d (FQ) data variance, and obtaining RMSE and RPD values of 0.57 and 1.13 respectively and a slope and y-intercept between the experimental and modelled \log_{10} -transformed K_d values statistically different to one and zero respectively (see **Figure 6.10**).

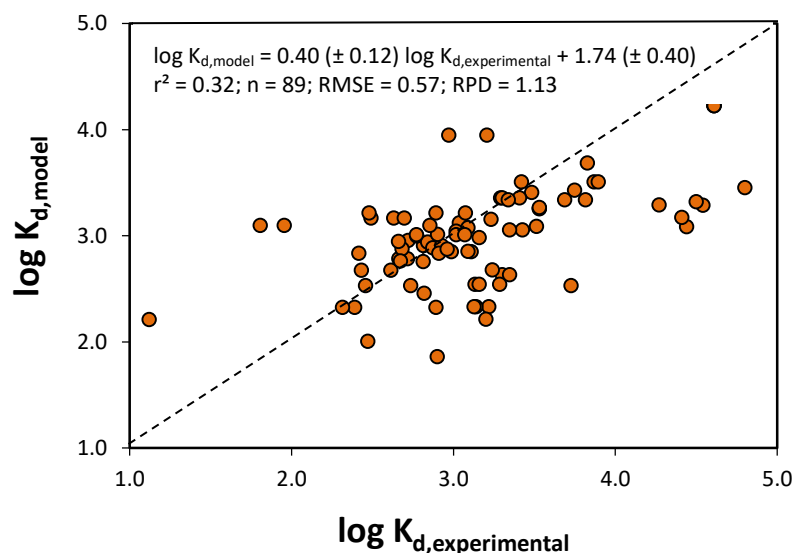


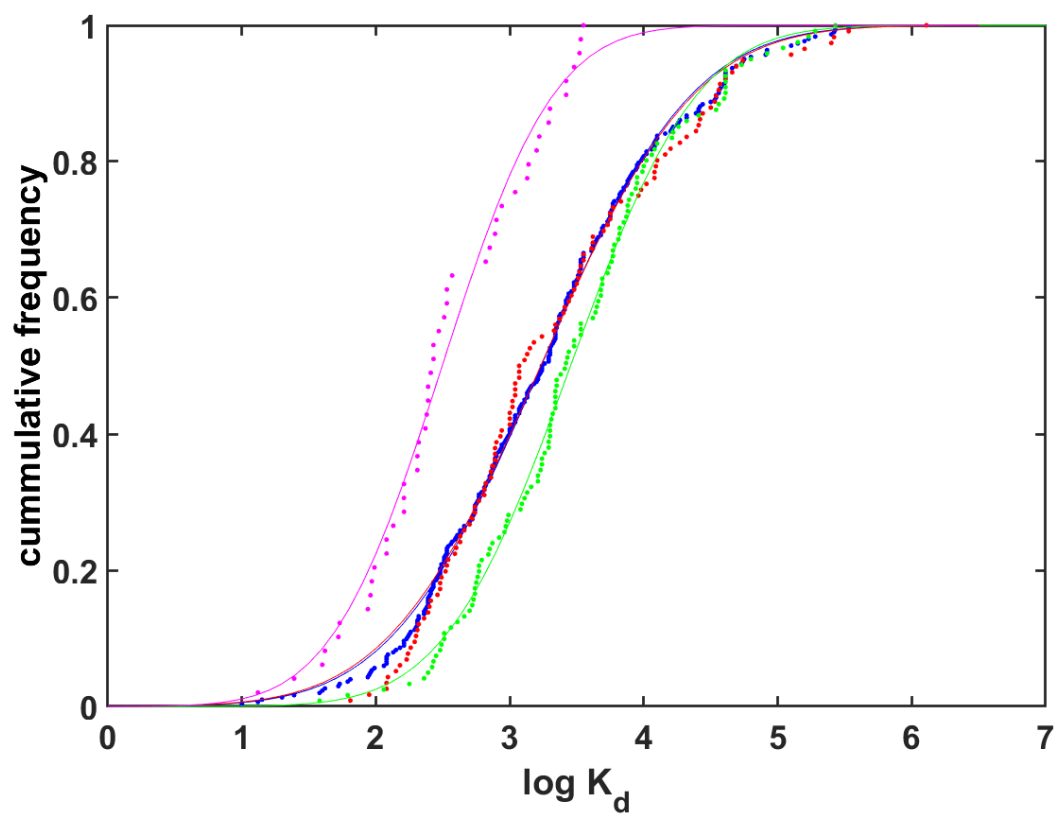
Figure 6.10 External validation results of the PLS-based FQ (K_d) model.

The low predictive quality of the PLS-based model could be attributed to its inability to explain the non-linear sorption trend with pH observed in Section 6.3.1. Hence, due to the low predictive quality of the PLS-based prediction model, best-estimate K_d (FQ) values with informed variability were derived by a probabilistic approach.

6.3.4. Deriving best-estimate K_d (FQ) values in soils

CDFs were constructed to derive best-estimate K_d values for soils grouped according to the values of specific soil properties, to reduce the variability affecting the proposal of K_d (FQ) values for risk assessment, and to better describe K_d (FQ) variability for a given soil group. Therefore, the literature dataset was split into partial datasets according to pH as the main relevant parameter, OC, and sand content. These three properties, besides being key soil properties affecting FQ sorption, are the ones for which the most information is available in the literature dataset.

Regarding pH grouping criteria, the thresholds of every pH group were defined according to FQ pK_a values in order to represent the effect of each FQ species on sorption. The first group comprised soils with $pH < 5.5$, whereas the second group was formed by soils with pH ranging from 5.5 to 7.5. This latter pH threshold also ensured that there were sufficient data to assess the sorption of the negatively charged FQ species in soils with $pH \geq 7.5$. The median pH values of the entries in each group were 4.7, 6.6 and 7.8 respectively, thus confirming that these partial datasets could be considered descriptors of the presence of cationic, zwitterion and anionic FQ species. As regards the OC variable, soils were grouped as those with $OC < 2\%$ (representative for mineral soils) and those with $OC \geq 2\%$. The soils with $OC > 10\%$ could not be grouped due to the lack of sorption data for organic soils. The textural characteristics of soil affect FQ sorption, which is mainly driven by clay minerals. Since clay minerals may also be found in the silt fraction of the soil, sand content was chosen as the K_d (FQ) descriptor for the overall dataset refinements to derive CDFs based on textural information. Thus, soil K_d (FQ) data were grouped according to soils having $< 50\%$ and $\geq 50\%$ sand content, which obtained a sufficient amount of data in each partial dataset to allow the construction of CDFs. **Figure 6.11** displays the CDFs derived for the overall dataset and for pH partial datasets.



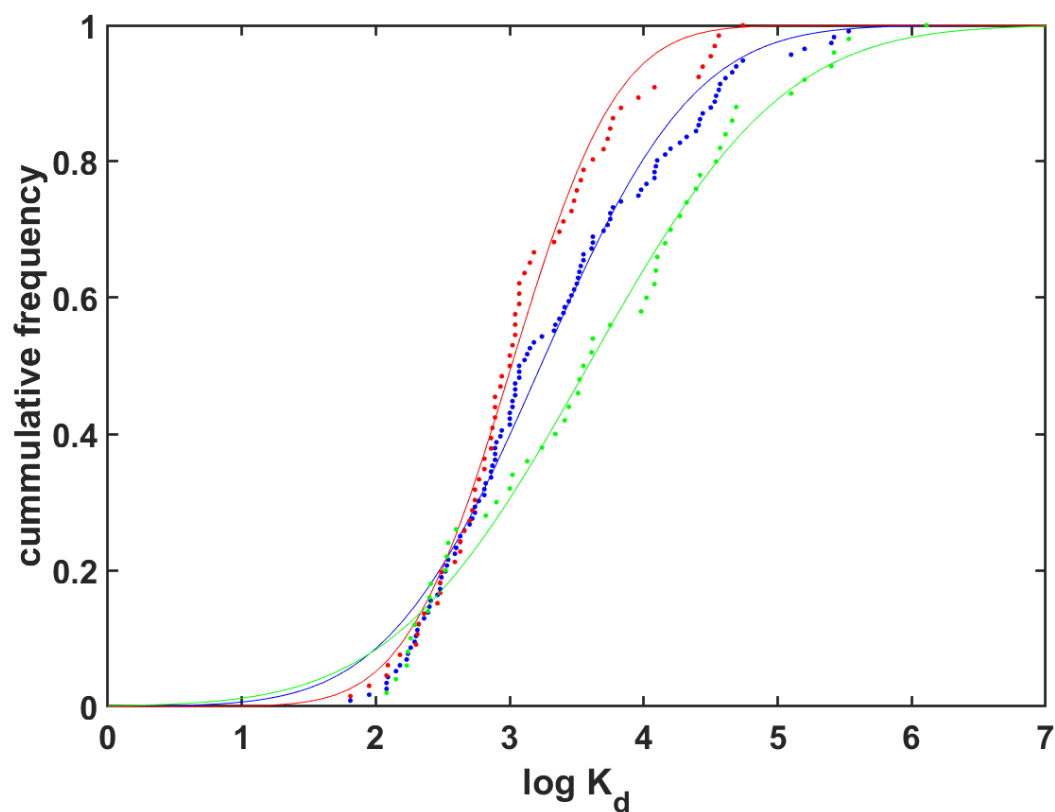
Soil groups	Colour	N	μ (K_d , L kg ⁻¹)	σ	r^2	FLSD ¹
Overall	Blue	312	1,679	7.59	0.998	
pH < 5.5	Red	117	1,690	7.88	0.998	A
pH 5.5 – 7.5	Green	127	3,390	5.80	0.995	B
pH \geq 7.5	Pink	51	324	4.49	0.989	C

N = number of observations; μ : best-estimate K_d (50th percentile); σ = geometric standard deviation; ¹Different letters in the datasets compared indicate statistically significant differences between GMs according to the Fisher's Least Significant Differences test.

Figure 6.11 CDFs of $\log K_d$ (FQ) distributions for soil groups according to the pH criterion.

This approach permitted the derivation of best-estimate K_d (FQ) values of approximately 1,700 and 3,400 L kg⁻¹ for the acidic and neutral soil datasets respectively, whereas for basic soils the best-estimate K_d (FQ) value was nearly one order of magnitude lower (320 L kg⁻¹; see **Table 6.6**). These values agree with the pH trend observed in Section 6.3.1, in which sorption was maximized at pH 5 – 7. Moreover, the FLSD test revealed that all three resulting datasets led to the quantification of statistically different descriptors, confirming that pH was an important parameter affecting sorption and that K_d (FQ) best estimates may change within one order of magnitude solely based on changes in pH, besides generally decreasing the data variability with respect to that of the overall dataset.

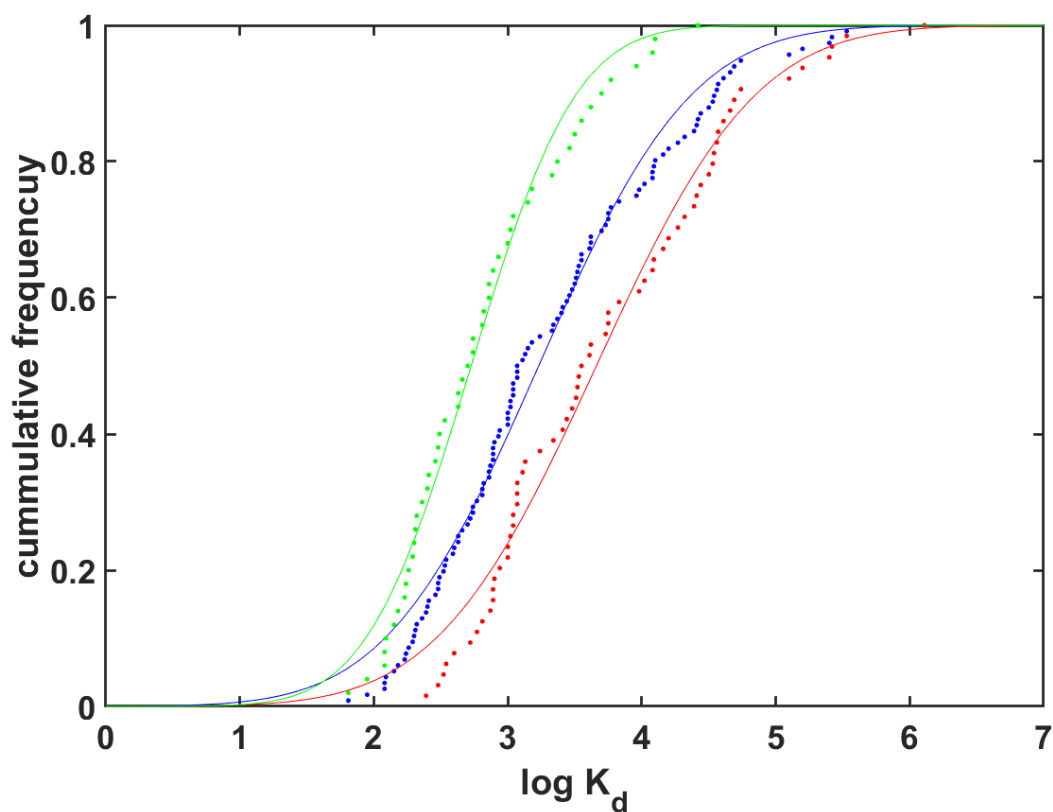
To reduce data variability further, double groupings were tested according to pH_OC and pH_Sand criteria. Refining the overall dataset by pH_OC and pH_Sand criteria led to datasets that were significantly different according to FLSD tests for soils with pH < 5.5 (see **Figure 6.12** and **Figure 6.13**) and pH 5.5 – 7.5 (see **Figure 6.14** and **Figure 6.15**). For soils with pH > 7.5, the application of both the pH_OC and pH_Sand criteria did not result in significantly different datasets (**Figure 6.16** and **Figure 6.17**), suggesting a minor effect of the organic matter and textural characteristics in K_d (FQ) for these scenarios. The best estimate K_d (FQ) results from the application of the pH_OC criterion (see **Table 6.6**) agreed with the pH-dependent sorption of FQs in soil organic matter components (Martínez-Mejía et al., 2017) and confirmed the positive effect of OC on FQ sorption in soils (Teixidó et al., 2014). In addition, application of the pH_OC criterion allowed the derivation of K_d (FQ) best estimates with a generally lower variability than the overall data. Similarly, the refinement by the pH_Sand criterion revealed lower best-estimate K_d (FQ) values with increasing sand contents, which confirm the higher FQ leaching observed in sandy soils than in other loamy and clay soils (Pan and Chu, 2017), and data variability was generally reduced in each refinement.



Soil groups	Colour	N	μ (K_d , L kg ⁻¹)	σ	r^2	FLSD ¹
pH < 5.5	Blue	117	1,690	7.88	0.998	
pH < 5.5; OC < 2 %	Red	67	1,028	4.16	0.984	A
pH < 5.5; OC \geq 2 %	Green	50	3,837	14.0	0.989	B

N = number of observations; μ : best-estimate K_d (50th percentile); σ = geometric standard deviation; 5th, 95th: 5% and 95% percentiles. ¹Different letters among the datasets compared indicate statistically significant differences between GMs according to the Fisher's Least Significant Differences test.

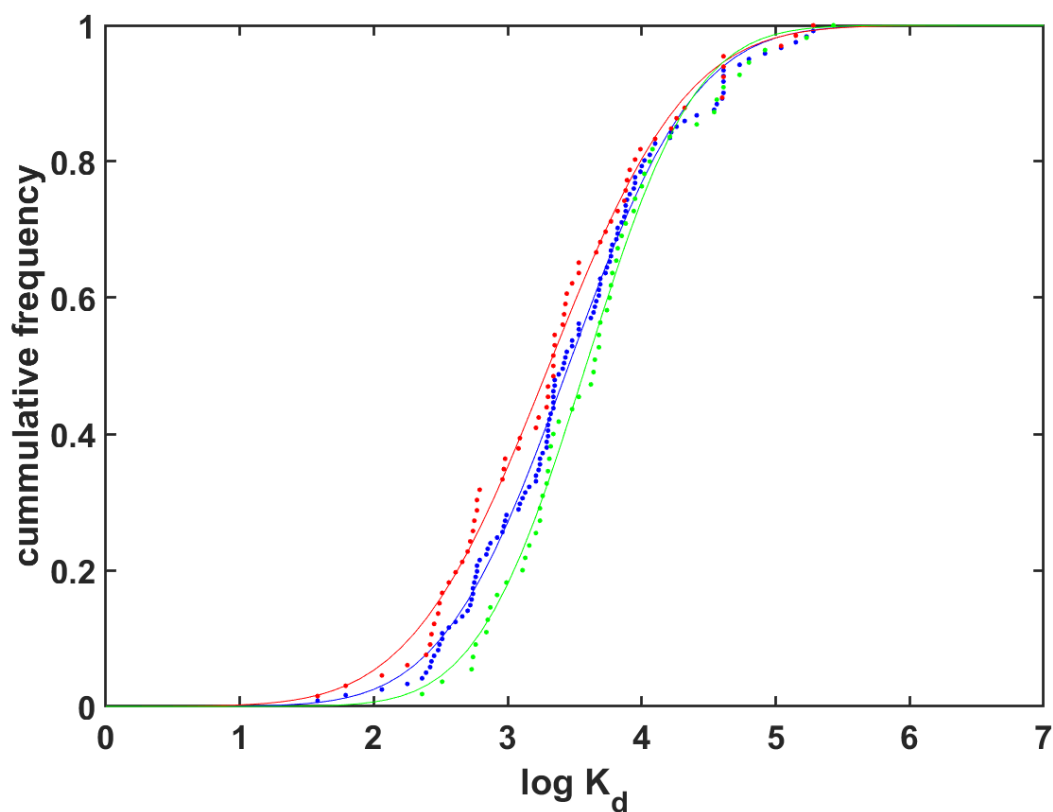
Figure 6.12 Resulting CDFs after splitting the soils by the pH_OC criteria for those soils with pH < 5.5.



Soil groups	Colour	N	μ (K_d , L kg ⁻¹)	σ	r^2	FLSD ¹
pH < 5.5	Blue	117	1,690	7.88	0.998	
pH < 5.5; Sand < 50 %	Red	64	4,581	8.59	0.983	A
pH < 5.5; Sand \geq 50 %	Green	50	478	4.11	0.983	B

N = number of observations; μ : best-estimate K_d (50th percentile); σ = geometric standard deviation; 5th, 95th: 5% and 95% percentiles. ¹Different letters among the datasets compared indicate statistically significant differences between GMs according to the Fisher's Least Significant Differences test.

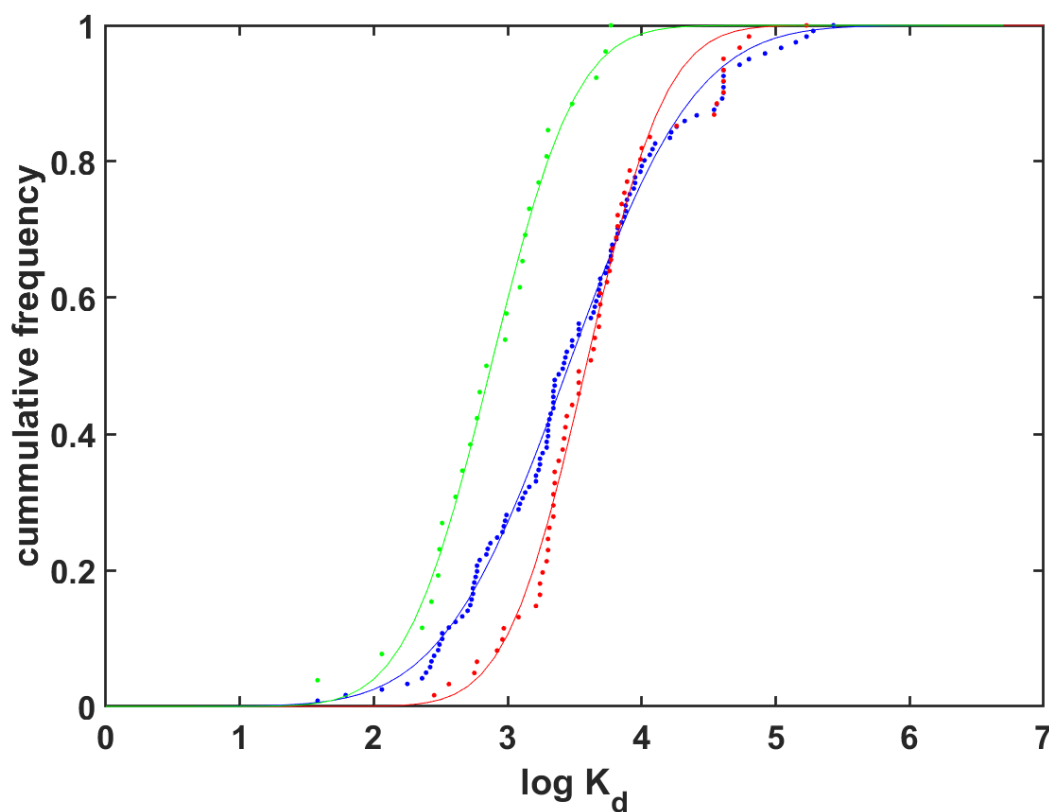
Figure 6.13 Resulting CDFs after splitting the soils by the pH_Sand criteria for those soils with pH < 5.5.



Soil groups	Colour	N	μ (K_d , L kg ⁻¹)	σ	r^2	FLSD ¹
pH 5.5 – 7.5	Blue	127	3,390	5.80	0.995	
pH 5.5 – 7.5; OC < 2 %	Red	71	2,028	6.45	0.993	A
pH 5.5 – 7.5; OC \geq 2 %	Green	56	3,828	4.34	0.992	B

N = number of observations; μ : best-estimate K_d (50th percentile); σ = geometric standard deviation; 5th, 95th: 5% and 95% percentiles. ¹Different letters among the datasets compared indicate statistically significant differences between GMs according to the Fisher's Least Significant Differences test.

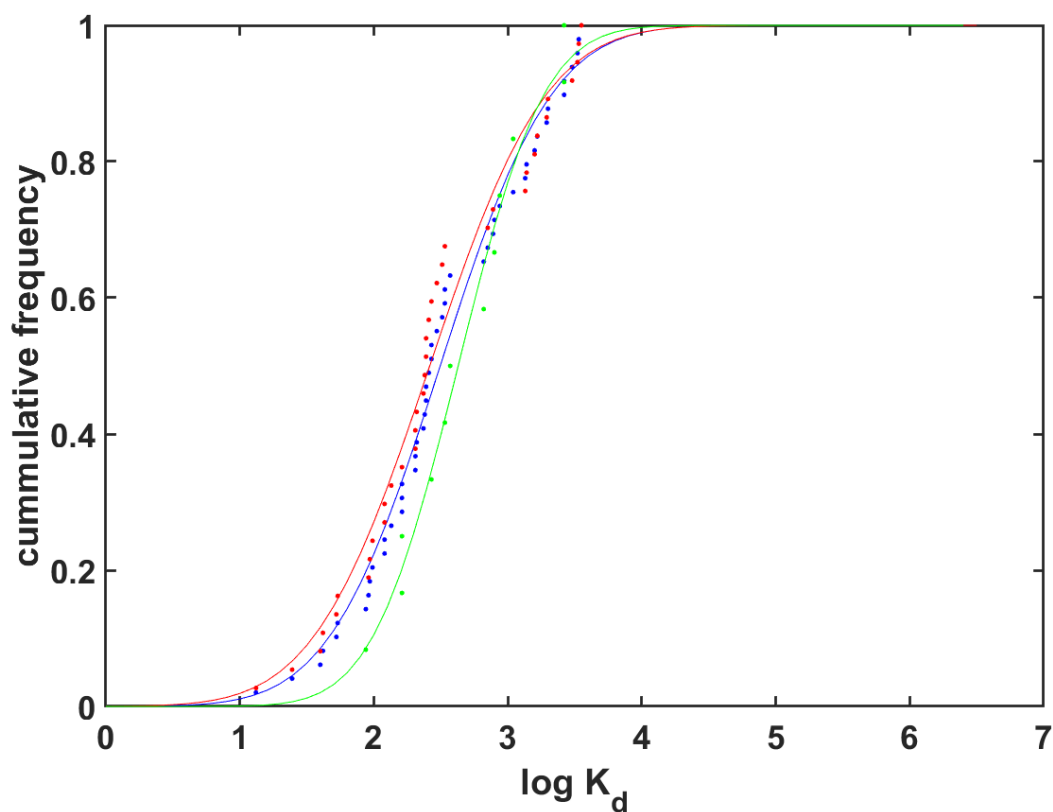
Figure 6.14 Resulting CDFs after splitting the soils by the pH_OC criteria for those soils with pH 5.5 - 7.5.



Soil groups	Colour	N	μ (K_d , L kg ⁻¹)	σ	r^2	FLSD ¹
pH 5.5 – 7.5	Blue	127	3,390	5.80	0.995	
pH 5.5 – 7.5; Sand < 50 %	Red	61	3,846	2.93	0.984	A
pH 5.5 – 7.5; Sand \geq 50 %	Green	26	750	3.16	0.992	B

N = number of observations; μ : best-estimate K_d (50th percentile); σ = geometric standard deviation; 5th, 95th: 5% and 95% percentiles. ¹Different letters among the datasets compared indicate statistically significant differences between GMs according to the Fisher's Least Significant Differences test.

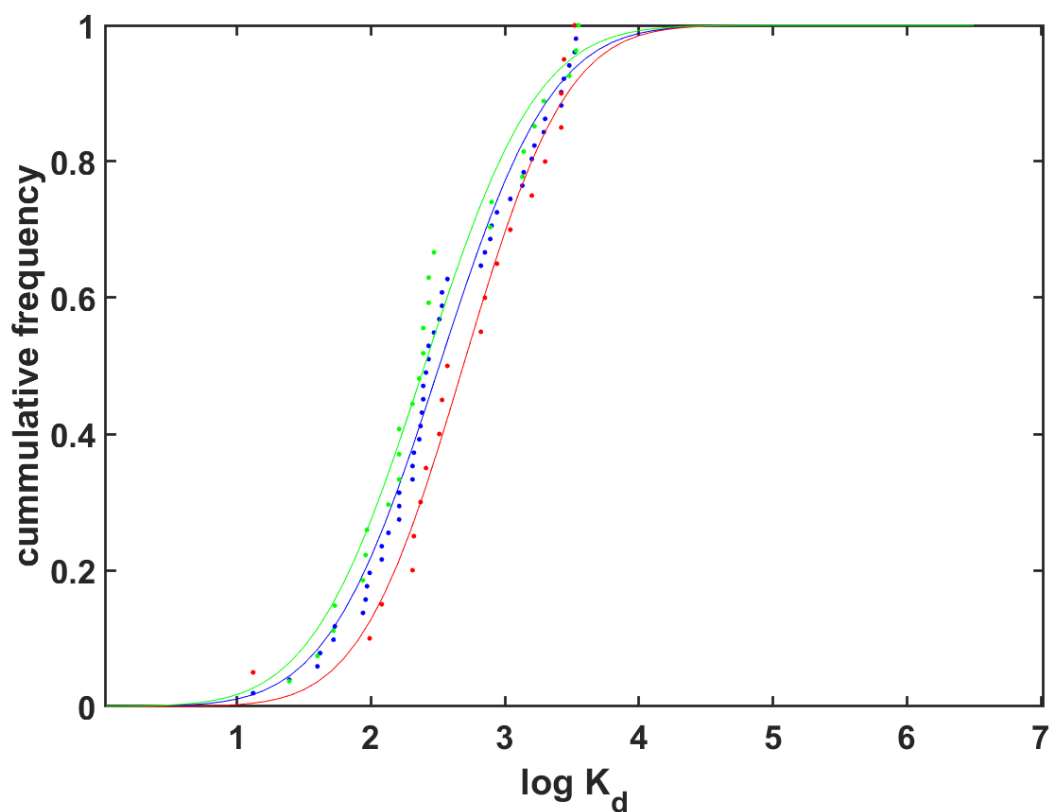
Figure 6.15 Resulting CDFs after splitting the soils by the pH_Sand criteria for those soils with pH 5.5 – 7.5.



Soil groups	Colour	N	μ (K_d , L kg ⁻¹)	σ	r^2	FLSD ¹
pH \geq 7.5	Blue	51	324	4.49	0.989	
pH \geq 7.5; OC < 2 %	Red	38	261	4.82	0.971	A
pH \geq 7.5; OC \geq 2 %	Green	13	427	3.18	0.982	A

N = number of observations; μ : best-estimate K_d (50th percentile); σ = geometric standard deviation; 5th, 95th: 5% and 95% percentiles. ¹Different letters among the datasets compared indicate statistically significant differences between GMs according to the Fisher's Least Significant Differences test.

Figure 6.16 Resulting CDFs after splitting the soils by the pH_OC criteria for those soils with pH \geq 7.5.

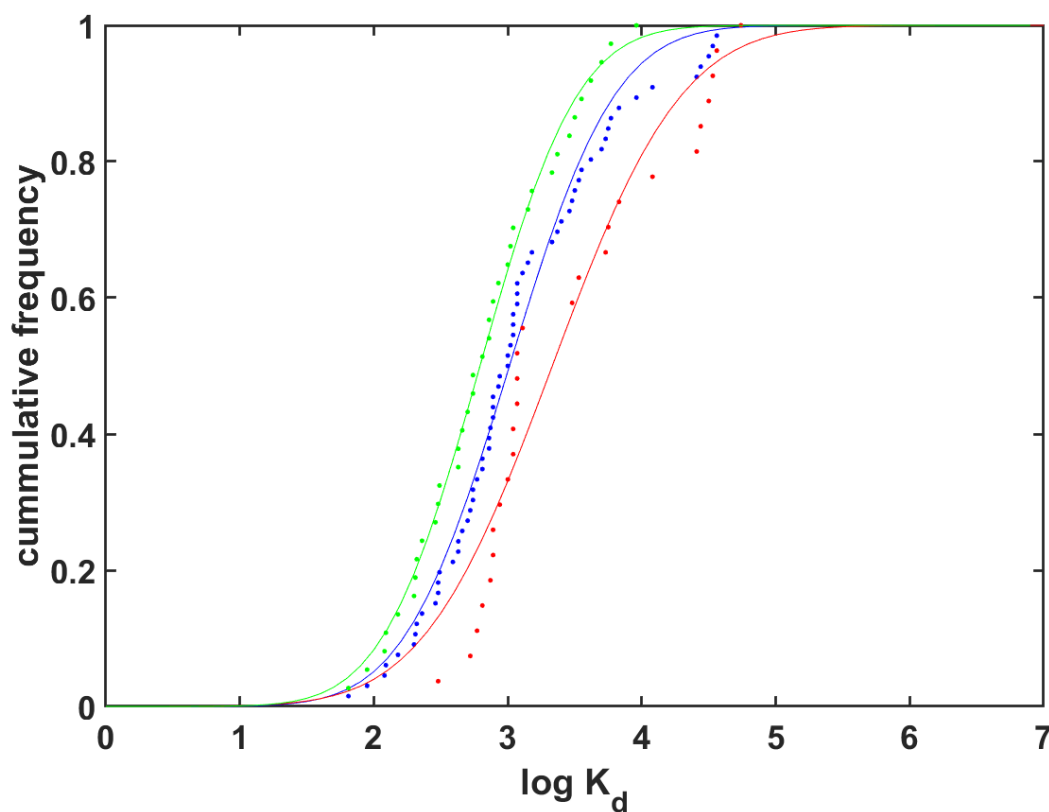


Soil groups	Colour	N	μ (K_d , L kg ⁻¹)	σ	r^2	FLSD ¹
pH \geq 7.5	Blue	51	324	4.49	0.989	
pH \geq 7.5; Sand < 50 %	Red	24	459	6.07	0.966	A
pH \geq 7.5; Sand \geq 50 %	Green	26	175	3.11	0.977	A

N = number of observations; μ : best-estimate K_d (50th percentile); σ = geometric standard deviation; 5th, 95th: 5% and 95% percentiles. ¹Different letters among the datasets compared indicate statistically significant differences between GMs according to the Fisher's Least Significant Differences test.

Figure 6.17 Resulting CDFs after splitting the soils by the pH_Sand criteria for those soils with pH \geq 7.5.

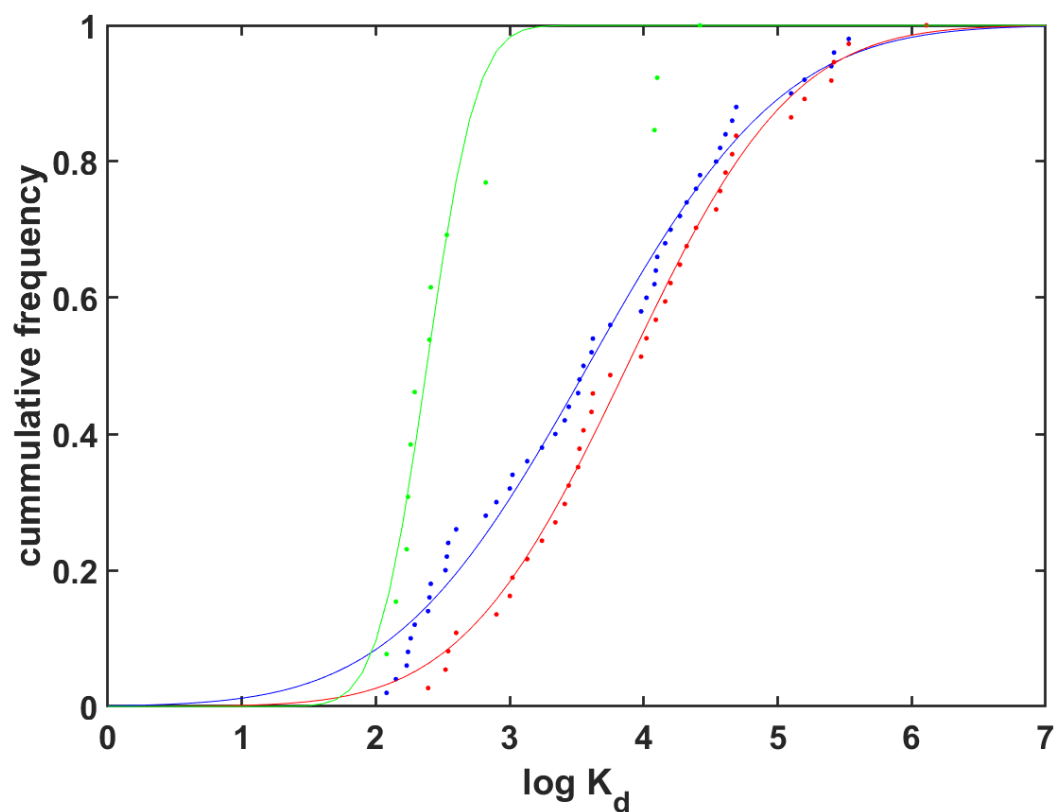
Triple groupings according to the pH_OC_Sand criterion were examined (see **Figure 6.18**, **Figure 6.19**, **Figure 6.20**, **Figure 6.21** and **Figure 6.22**). As revealed by the FLSD tests, this allowed the derivation of significantly different best-estimate K_d (FQ) values for those soils with $\text{pH} < 5.5$ and $\text{pH} 5.5 - 7.5$, with OC contents either below or above 2% (see **Table 6.6**). In addition, best-estimate K_d (FQ) values for a given OC content were consistent with the previously observed pH-dependent sorption, for sand contents either below or above 50%, and moreover, the variability of the original data was generally reduced in each refinement. For those soils with $\text{pH} \geq 7.5$, although best-estimate K_d (FQ) values followed the same pattern as those soils with $\text{pH} < 5.5$ and $\text{pH} 5.5 - 7.5$, refining the dataset with the pH_OC_Sand criterion did not result in statistically significant datasets for soils with $\text{OC} < 2\%$ and varying sand contents. For those soils with $\text{OC} > 2\%$ and varying sand contents, the low number of entries did not allowed a proper statistical analysis of both datasets.



Soil groups	Colour	N	μ (K_d , L kg ⁻¹)	σ	r^2	FLSD ¹
pH < 5.5; OC < 2%	Blue	67	1,028	4.16	0.986	
pH < 5.5; OC < 2%; sand < 50 %	Red	27	2,148	5.76	0.926	A
pH < 5.5; OC < 2%; sand \geq 50 %	Green	37	621	3.72	0.995	B

N = number of observations; μ : best-estimate K_d (50th percentile); σ = geometric standard deviation; 5th, 95th: 5% and 95% percentiles. ¹Different letters among the datasets compared indicate statistically significant differences between GMs according to the Fisher's Least Significant Differences test.

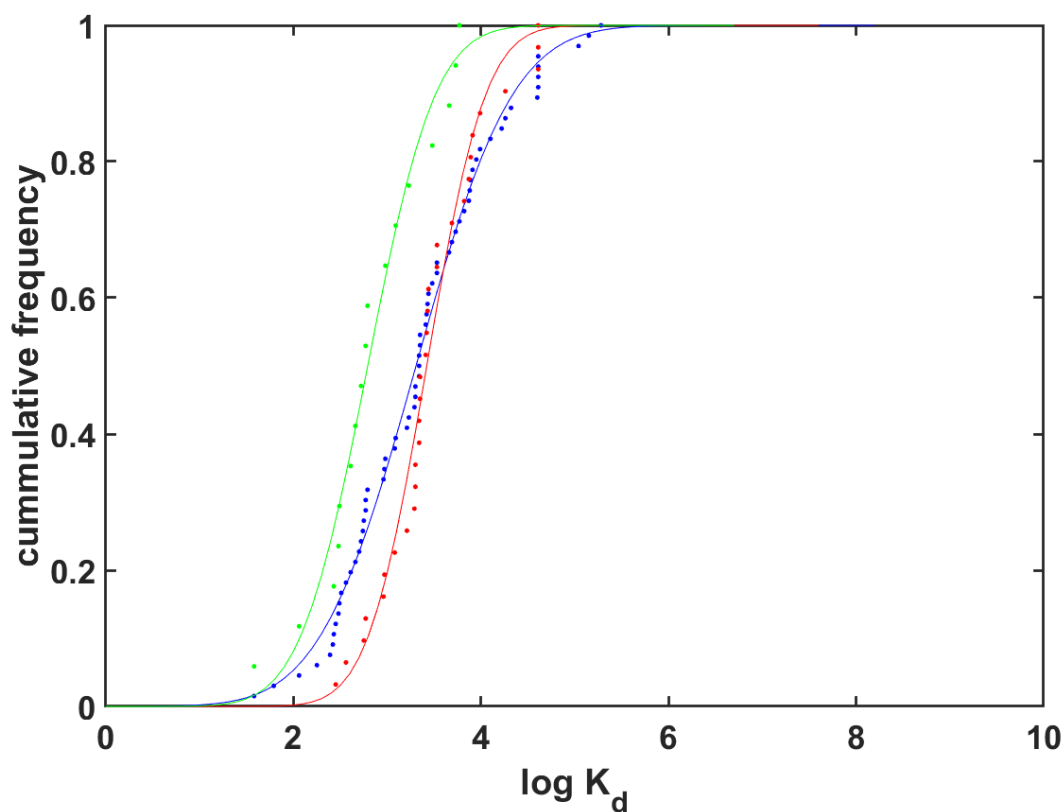
Figure 6.18 Resulting CDFs after splitting the soils by the pH_OC_Sand criteria for those soils with pH < 5.5 and OC < 2%.



Soil groups	Colour	N	μ (K_d , L kg ⁻¹)	σ	r^2	FLSD ¹
pH < 5.5; OC \geq 2%	Blue	50	3,837	14.0	0.989	
pH < 5.5; OC \geq 2%; sand < 50 %	Red	37	7,516	9.35	0.994	A
pH < 5.5; OC \geq 2%; sand \geq 50 %	Green	13	240	1.96	0.920	B

N = number of observations; μ : best-estimate K_d (50th percentile); σ = geometric standard deviation; 5th, 95th: 5% and 95% percentiles. ¹Different letters among the datasets compared indicate statistically significant differences between GMs according to the Fisher's Least Significant Differences test.

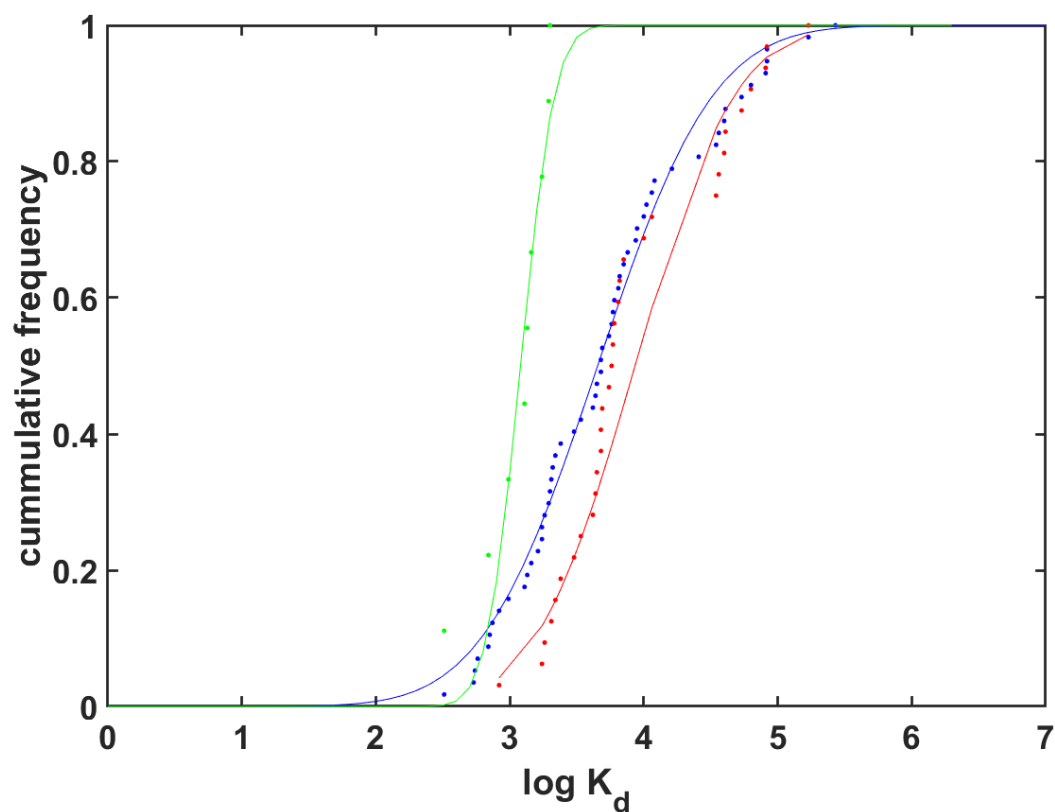
Figure 6.19 Resulting CDFs after splitting the soils by the pH_OC_Sand criteria for those soils with pH < 5.5 and OC \geq 2%.



Soil groups	Colour	N	μ (K_d , L kg ⁻¹)	σ	r^2	FLSD ¹
pH 5.5 – 7.5; OC < 2%	Blue	71	2,028	6.45	0.993	
pH 5.5 – 7.5; OC < 2%; sand < 50 %	Red	31	2,636	3.12	0.972	A
pH 5.5 – 7.5; OC < 2%; sand \geq 50 %	Green	17	619	3.68	0.977	B

N = number of observations; μ : best-estimate K_d (50th percentile); σ = geometric standard deviation; 5th, 95th: 5% and 95% percentiles. ¹Different letters among the datasets compared indicate statistically significant differences between GMs according to the Fisher's Least Significant Differences test.

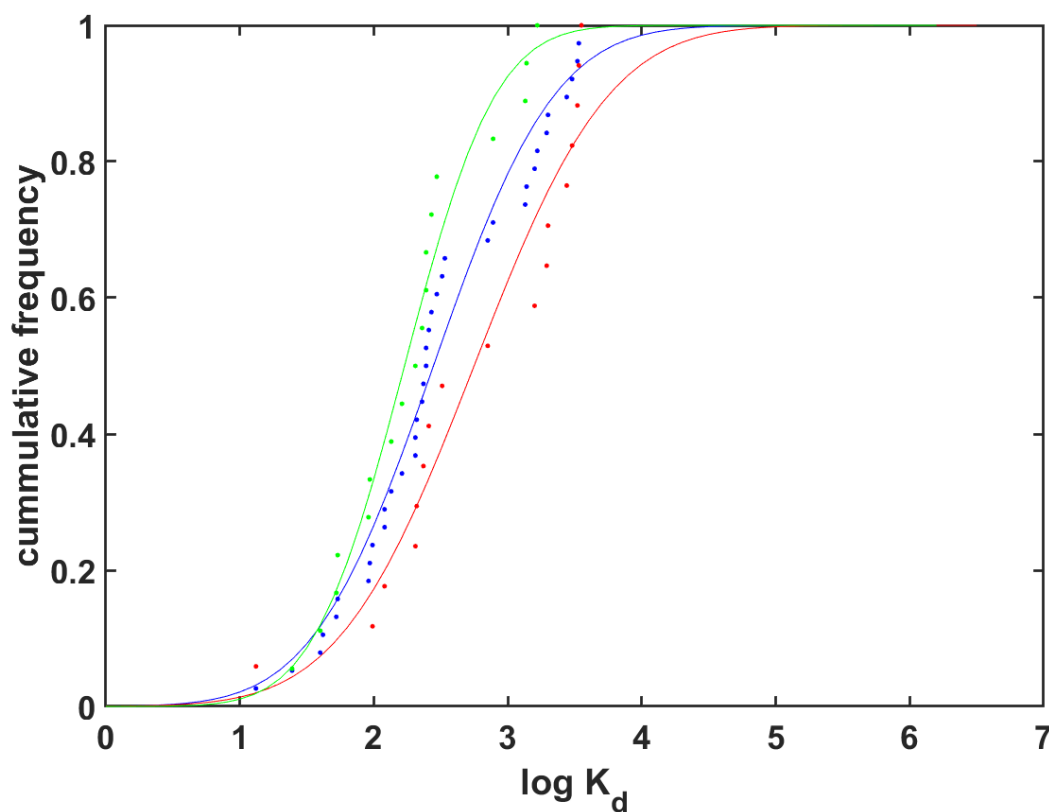
Figure 6.20 Resulting CDFs after splitting the soils by the pH_OC_Sand criteria for those soils with pH 5.5 – 7.5 and OC < 2%.



Soil groups	Colour	N	μ (K_d , L kg ⁻¹)	σ	r^2	FLSD ¹
pH 5.5 – 7.5; OC \geq 2%	Blue	56	3,828	4.34	0.992	
pH 5.5 – 7.5; OC \geq 2%; sand < 50 %	Red	30	6,561	3.63	0.937	A
pH 5.5 – 7.5; OC \geq 2%; sand \geq 50 %	Green	9	914	2.17	0.921	B

N = number of observations; μ : best-estimate K_d (50th percentile); σ = geometric standard deviation; 5th, 95th: 5% and 95% percentiles. ¹Different letters among the datasets compared indicate statistically significant differences between GMs according to the Fisher's Least Significant Differences test.

Figure 6.21 Resulting CDFs after splitting the soils by the pH_OC_Sand criteria for those soils with pH 5.5 – 7.5 and OC \geq 2%.



Soil groups	Colour	N	μ (K_d , $L\ kg^{-1}$)	σ	r^2	FLSD ¹
pH \geq 7.5; OC < 2%	Blue	38	261	4.82	0.971	
pH \geq 7.5; OC < 2%; sand < 50 %	Red	20	560	6.17	0.935	A
pH \geq 7.5; OC < 2%; sand \geq 50 %	Green	17	165	3.64	0.980	A
pH \geq 7.5; OC \geq 2 %	-	13	427	3.18	0.982	
pH \geq 7.5; OC \geq 2%; sand < 50 %	-	8	765*	2.53*	N.A.	N.A.
pH \geq 7.5; OC \geq 2%; sand \geq 50 %	-	5	219*	2.28*	N.A.	N.A.

N = number of observations; μ : best-estimate K_d (50th percentile); σ = geometric standard deviation; 5th, 95th: 5% and 95% percentiles. ¹Different letters among the datasets compared indicate statistically significant differences between GMs according to the Fisher's Least Significant Differences test. * Data derived from GM and GSD of the original data; N.A. = non analysed.

Figure 6.22 Resulting CDFs after splitting the soils by the pH_OC_Sand criteria for those soils with pH \geq 7.5 and OC < 2%.

All the resulting best-estimate K_d (FQ) values with associated uncertainty derived from the CDFs are summarized in **Table 6.6**:

Table 6.6: Best-estimate K_d (FQ) values (μ , $L\ kg^{-1}$), geometrical standard deviation (σ , $L\ kg^{-1}$), 5th and 95th percentiles ($L\ kg^{-1}$) and maximum and minimum values for each partial dataset defined according to relevant soil properties affecting FQ sorption in soils.

Group 1	Group 2	Group 3	N	μ (K_d , $L\ kg^{-1}$)	σ	5 th	95 th	Min	Max
Overall			312	1,680	7.6	93	56,234	10	1,288,250
pH < 5.5			117	1,690	7.9	141	125,892	65	1,288,250
pH < 5.5	Sand < 50		64	4,580	8.6	347	251,189	245	1,288,250
pH < 5.5	Sand \geq 50		50	480	4.1	120	12,022	65	26,303
pH < 5.5	OC < 2		67	1,030	4.2	123	33,884	65	54,954
pH < 5.5	OC \geq 2		50	3,84	14	170	263,027	120	1,288,250
pH < 5.5	Sand < 50	OC < 2	27	2,150	5.8	525	36,307	302	54,954
pH < 5.5	Sand \geq 50	OC < 2	37	620	3.7	89	5,888	65	9,120
pH < 5.5	Sand < 50	OC \geq 2	37	7,520	9.4	331	45,708	245	1,288,250
pH < 5.5	Sand \geq 50	OC \geq 2	13	240	2.0	141	12,589	120	26,303
pH 5.5 – 7.5			127	3,390	5.8	269	83,176	38	269,153
pH 5.5 – 7.5	Sand < 50		61	3,850	2.9	654	22,579	282	169,284
pH 5.5 – 7.5	Sand \geq 50		26	750	3.2	115	5,370	38	5,888
pH 5.5 – 7.5	OC < 2		71	2,030	6.4	354	40,738	38	190,546
pH 5.5 – 7.5	OC \geq 2		56	3,830	4.3	324	83,176	229	269,153
pH 5.5 – 7.5	Sand < 50	OC < 2	31	2,640	3.1	363	18,197	282	40,738
pH 5.5 – 7.5	Sand \geq 50	OC < 2	17	620	3.7	115	5,370	38	5,888
pH 5.5 – 7.5	Sand < 50	OC \geq 2	30	6,560	3.6	1,738	63,096	832	169,824
pH 5.5 – 7.5	Sand \geq 50	OC \geq 2	9	910	2.2	254	1,445	229	1,995
pH \geq 7.5			51	320	4.5	40	3,311	13	3,548

N = number of observations; μ : best-estimate K_d (50th percentile); σ : geometric standard deviation; 5th, 95th: 5% and 95% percentiles; Min, Max: minimum and maximum K_d value of the distribution

In brief, the application of CDFs to the overall K_d (FQ) dataset allowed the derivation of more accurate best-estimates K_d (FQ) values according to specific environmental scenarios. Specifically, these best-estimates K_d (FQ) values ranged from 320 to 7,500 L kg⁻¹ depending on easily-derivable soil physicochemical properties (pH, OC and sand contents), indicating that the most suitable best-estimate K_d (FQ) values for use as input data for risk assessment might vary within more than one order of magnitude just according to properties of the target soils.

6.4. Conclusions

K_d (NOR) values in soils followed a non-linear pattern along changes in pH, reaching a peak at pH 5 – 7, in which the cationic and zwitterion FQ species were predominant, confirming that pH was the main soil parameter affecting FQ sorption, both by modifying soil surface charges and affecting FQ speciation. The construction of a literature-assembled sorption K_d (FQ) dataset, including K_d data from NOR, CIP, ENR and OFL, confirmed that their sorption was statistically comparable. The development of a PLS-based prediction model based on relevant soil and FQ properties affecting sorption (pH, fraction of cationic FQ, CEC, OC and sand contents) led to a poor prediction of the K_d (FQ) when externally tested with literature data. Therefore, CDFs were constructed to derive best-estimate K_d (FQ) values with a known associated variability as input data for environmental risk assessment according to the specific characteristics of the scenario to be assessed, specifically pH, OC and sand content. Refining the sorption K_d dataset according to soil properties permitted derivation of more representative K_d (FQ), often with a lower related variability than that derived from the overall dataset. These K_d values were above 1,000 L kg⁻¹ under most environmental conditions, suggesting a strong sorption to soil particles and therefore a low predicted mobility, although higher environmental mobility might be expected in scenarios with alkaline pH, low OC and high sand contents.

6.5. References

- Aldana, G. O., Hazlerigg, C., Lopez-Capel, E., Werner, D., 2021. Agrochemical leaching reduction in biochar-amended tropical soils of Belize. *Eur. J. Soil Sci.* 72 (3), 1243–1255. <https://doi.org/10.1111/ejss.13021>
- Álvarez-Esmorís, C., Conde-Cid, M., Ferreira-Coelho, G., Fernández-Sanjurjo, M. J., Núñez-Delgado, A., Álvarez-Rodríguez, E., Arias-Estévez, M., 2020. Adsorption/desorption of sulfamethoxypyridazine and enrofloxacin in agricultural soils. *Sci. Total Environ.* 706, 136015. <https://doi.org/10.1016/j.scitotenv.2019.136015>
- Andersson, M., I., MacGowan, A., P., 2003. Development of the quinolones. *J. Antimicrob. Chemoth.*, 51 (90001), 1–11. <https://doi.org/10.1093/jac/dkg212>
- Belden, J. B., 2007. Partitioning and photodegradation of ciprofloxacin in aqueous systems in the presence of organic matter. *Chemosphere* 66, 1390–1395. <https://doi.org/10.1016/j.chemosphere.2006.09.032>
- Burt, R., 2004. Soil survey laboratory methods manual. Investigation report No 42, Version 4.0, Natural resources Conservation Service. USDA, Washington, USA.
- Cao, X., Pang, H., Yang, G., 2015. Sorption behaviour of norfloxacin on marine sediments. *J. Soils Sediments* 1, 1635–1643. <https://doi.org/10.1007/s11368-015-1124-4>
- Carter, M. R., Gregorich, E. G., 2006. Extractable Al, Fe, Mn and Si. From: *Soil Sampling and Methods of Analysis*, second edition. Canadian Society of Soil Science, CRC Press, Boca Raton, USA. <https://doi.org/10.1201/9781420005271>
- Chen, G., Li, M., Liu, X., 2015. Fluoroquinolone Antibacterial Agent Contaminants in Soil/Groundwater: A Literature Review of Sources, Fate, and Occurrence. *Water Air Soil Poll.* 226 (12). <https://doi.org/10.1007/s11270-015-2438-y>
- Chen, G., Liu, X., Tartakovsky, D., Li, M., 2016. Risk assessment of three fluoroquinolone antibiotics in the groundwater recharge system. *Ecotox. Environ. Safe.* 133, 18–24. <https://doi.org/10.1016/j.ecoenv.2016.05.030>

- Conkle, J. L., Latta, C., White, J. R., Cook, R. L., 2010. Competitive sorption and desorption behavior for three fluoroquinolone antibiotics in a wastewater treatment wetland soil. *Chemosphere*, 80 (11), 1353–1359. <https://doi.org/10.1016/j.chemosphere.2010.06.012>
- Córdova-Kreylos, A. L., Scow, K. M., 2007. Effects of ciprofloxacin on salt marsh sediment microbial communities. *The ISME Journal*, 1, 585-595. <https://doi-org.sire.ub.edu/10.1038/ismej.2007.71>
- Dalkmann, P., Willaschek, E., Schiedung, H., Bornemann, L., Siebe, C., Siemets, J., 2014. Long-term Wastewater Irrigation Reduces Sulfamethoxazole Sorption, but Not Ciprofloxacin Binding, in Mexican Soils. *J. Environ. Qual.* 43, 964–970. <https://doi.org/10.2134/jeq2013.11.0473>
- Domínguez, C., Flores, C., Caixach, J., Mita, L., Piña, B., Comas, J., Bayona, J. M., 2014. Evaluation of antibiotic mobility in soil associated with swine-slurry soil amendment under cropping conditions. *Environ. Sci. Pollut. R.* 21 (21), 12336–12344. <https://doi.org/10.1007/s11356-014-3174-3>
- Dong, D., Li, L., Zhang, L., Hua, X., Guo, Z., 2018. Effects of lead, cadmium, chromium, and arsenic on the sorption of lindane and norfloxacin by river biofilms, particles, and sediments. *Environ. Sci. Pollut. R.* 25 (5), 4632–4642. <https://doi.org/10.1007/s11356-017-0840-2>
- Drillia, P., Stamatelatou, K., Lyberatos, G., 2005. Fate and mobility of pharmaceuticals in solid matrices. *Chemosphere*, 60 (8), 1034–1044. <https://doi.org/10.1016/j.chemosphere.2005.01.032>
- Figuerola-Diva, R. A., Vasudevan, D., MacKay, A. A., 2010. Trends in soil sorption coefficients within common antimicrobial families. *Chemosphere*, 79 (8), 786–793. <https://doi.org/10.1016/j.chemosphere.2010.03.017>
- Gil-García, C. J., Rigol, A., Rauret, G., Vidal, M., 2008. Radionuclide sorption-desorption pattern in soils from Spain. *Appl. Radiat. Isotopes*, 66 (2), 126–138. <https://doi.org/10.1016/j.apradiso.2007.07.032>

- Girardi, C., Greve, J., Lamshöft, M., Fetzner, I., Miltner, A., Schäffer, A., Kästner, M., 2011. Biodegradation of ciprofloxacin in water and soil and its effects on the microbial communities. *J. Hazard. Mater.* 198, 22–30. <https://doi.org/10.1016/j.jhazmat.2011.10.004>
- Gong, W., Liu, X., He, H., Wang, L., Dai, G., 2012. Quantitatively modeling soil-water distribution coefficients of three antibiotics using soil physicochemical properties. *Chemosphere*, 89 (7), 825–831. <https://doi.org/10.1016/j.chemosphere.2012.04.064>
- Graouer-Bacart, M., Sayen, S., Guillon, E., 2015. Adsorption of enrofloxacin in presence of Zn (II) on a calcareous soil. *Ecotox. Environ. Safe.* 122, 470–476. <https://doi.org/10.1016/j.ecoenv.2015.09.019>
- Hanamoto, S., Ogawa, F., 2019. Predicting the sorption of azithromycin and levofloxacin to sediments from mineral and organic components. *Environ. Pollut.* 255, 113180. <https://doi.org/10.1016/j.envpol.2019.113180>
- Hari, A. C., Paruchuri, R. A., Sabatini, D. A., Kibbey, T. C. G., 2005. Effects of pH and Cationic and Nonionic Surfactants on the Adsorption of Pharmaceuticals to a Natural Aquifer Material. *Environ. Sci. Technol.* 39 (8), 2592–2598. <https://doi.org/10.1021/es048992m>
- Jin, L., He, M., Zhang, J., Xia, X., 2011. Norfloxacin Sorption to Different Fractions in Sediments from Typical Water Systems in China. *Soil Sediment Contam.* 20, 564–580. <https://doi.org/10.1080/15320383.2011.587045>
- Kiecak, A., Sassine, L., Boy-Roura, M., Elsner, M., Mas-Pla, J., LA Salle, C. L. G., Stumpp, C., 2019. Sorption properties and behaviour at laboratory scale of selected pharmaceuticals using batch experiments. *J. Contaminant Hydrol.* 225, 103500. <https://doi.org/10.1016/j.jconhyd.2019.103500>
- Knight, E. R., Janik, L. J., Navarro, D. A., Kookana, R. S., McLaughlin, M. J., 2019. Predicting partitioning of radiolabelled ¹⁴C-PFOA in a range of soils using diffuse reflectance infrared spectroscopy. *Sci. Total Environ.* 686, 505–513. <https://doi.org/10.1016/j.scitotenv.2019.05.339>

- Kong, X., Feng, S., Zhang, X., Li, Y., 2014. Effects of bile salts and divalent cations on the adsorption of norfloxacin by agricultural soils. *J. Environ. Sci.* 26 (4), 846–854. [https://doi.org/10.1016/S1001-0742\(13\)60480-5](https://doi.org/10.1016/S1001-0742(13)60480-5)
- Kotska, J. E., Luther III, G. W., 1994. Partitioning and speciation of solid phase Fe in saltmarsh sediments. *Geochim. Cosmochim. Acta*, 58 (7), 1701 - 1710. [https://doi.org/10.1016/0016-7037\(94\)90531-2](https://doi.org/10.1016/0016-7037(94)90531-2)
- Leal, R. M. P., Figueira, R. F., Tornisielo, V. L., Regitano, J. B., 2012. Occurrence and sorption of fluoroquinolones in poultry litters and soils from São Paulo State, Brazil. *Sci. Total Environ.* 432, 344–349. <https://doi.org/10.1016/j.scitotenv.2012.06.002>
- Leal, R. M. P., Alleoni, L. R. F., Tornisielo, V. L., Regitano, J. B., 2013. Sorption of fluoroquinolones and sulfonamides in 13 Brazilian soils. *Chemosphere*, 92 (8), 979–985. <https://doi.org/10.1016/j.chemosphere.2013.03.018>
- Li, F., Pan, B., Liang, N., Chang, Z., Zhou, Y., Wang, L., Li, H., Xing, B., 2017. Reactive mineral removal relative to soil organic matter heterogeneity and implications for organic contaminant sorption. *Environ. Pollut.* 227, 49–56. <https://doi.org/10.1016/j.envpol.2017.04.047>
- Limousin, G., Gaudet, J. P., Charlet, L., Sznknect, S., Barthès, V., Krimissa, M., 2007. Sorption isotherms: A review on physical bases, modeling and measurement. *Appl. Geochem.* 22, 249–275. <https://doi.org/10.1016/j.apgeochem.2006.09.010>
- Lin, Y. C., Hsiao, K. W., Lin, A. Y. C., 2018. Photolytic degradation of ciprofloxacin in solid and aqueous environments: kinetics, phototransformation pathways, and byproducts. *Environ. Sci. Pollut. R.* 25 (3), 2303–2312. <https://doi.org/10.1007/s11356-017-0666-y>
- Martínez-Mejía, M. J., Sato, I., Rath, S., 2017. Sorption mechanism of enrofloxacin on humic acids extracted from Brazilian soils. *Environ. Sci. Pollut. R.* 24, 15995–16006. <https://doi.org/10.1007/s11356-017-9210-3>

- Massey, L. B., Haggard, B. E., Galloway, J. M., Loftin, K. A., Meyer, M. T., Green, W. R., 2010. Antibiotic fate and transport in three effluent-dominated Ozark streams. *Ecol. Eng.* 36 (7), 930–938. <https://doi.org/10.1016/j.ecoleng.2010.04.009>
- Müller, G., Gastner, M., 1971. The "Karbonate-bomber", a simple device for the determination of the carbonate content in sediments, soils, and other materials. *Neues Jb. Mineral. Monat.* 10, 466–469.
- Mutavd, D., Lidija, Ć., Gr, I., Iva, Š., 2017. Isotherm, kinetic, and thermodynamic study of ciprofloxacin sorption on sediments. *Environ. Sci. Pollut. R.* 24, 10091–10106. <https://doi.org/10.1007/s11356-017-8461-3>
- Nowara, A., Burhenne, J., Spitteller, M., 1997. Binding of Fluoroquinolone Carboxylic Acid Derivatives to Clay Minerals. *J. Agr. Food Chem.* 45 (4), 1459–1463. <https://doi.org/10.1021/jf9602151>
- OECD, 2000. OECD 106 Adsorption - Desorption Using a Batch Equilibrium Method. OECD Guideline for the Testing of Chemicals. <https://doi.org/10.1787/9789264069602-en>
- Pan, B., Wang, P., Wu, M., Li, J., Zhang, D., Xiao, D., 2012. Sorption kinetics of ofloxacin in soils and mineral particles. *Environ. Pollut.* 171, 185–190. <https://doi.org/10.1016/j.envpol.2012.07.037>
- Pan, M., Chu, L. M., 2016. Adsorption and degradation of five selected antibiotics in agricultural soil. *Sci. Total Environ.* 545–546, 48–56. <https://doi.org/10.1016/j.scitotenv.2015.12.040>
- Pan, M., Chu, L. M., 2017. Leaching behavior of veterinary antibiotics in animal manure-applied soils. *Sci. Total Environ.* 579, 466–473. <https://doi.org/10.1016/j.scitotenv.2016.11.072>
- Parpounas, A., Litskas, V., Hapeshi, E., Michael, C., Fatta-Kassinou, D., 2017. Assessing the presence of enrofloxacin and ciprofloxacin in piggery wastewater and their adsorption behaviour onto solid materials, with a newly developed chromatographic method. *Environ. Sci. Pollut. R.* 24, 23371–23381. <https://doi.org/10.1007/s11356-017-9849-9>

- Paul, T., Liu, J., Machesky, M. L., Strathmann, T. J., 2014. Adsorption of zwitterionic fluoroquinolone antibacterials to goethite: A charge distribution-multisite complexation model. *J. Colloid Interf. Sci.* 428, 63–72. <https://doi.org/10.1016/j.jcis.2014.04.034>
- Peng, F. J., Zhou, L. J., Ying, G. G., Liu, Y. S., Zhao, J. L., 2014. Antibacterial activity of the soil-bound antimicrobials oxytetracycline and ofloxacin. *Environ. Toxicol. Chem.* 33 (4), 776–783. <https://doi.org/10.1002/etc.2513>
- Peruchi, L. M., Fostier, A. H., Rath, S., 2015. Sorption of norfloxacin in soils: Analytical method, kinetics and Freundlich isotherms. *Chemosphere*, 119, 310–317. <https://doi.org/10.1016/j.chemosphere.2014.06.008>
- Picó, Y., Andreu, V., 2007. Fluoroquinolones in soil-risks and challenges. *Anal. Bioanal. Chem.* 387 (4), 1287–1299. <https://doi.org/10.1007/s00216-006-0843-1>
- Pribyl, D. W., 2010. A critical review of the conventional SOC to SOM conversion factor. *Geoderma*, 156 (3–4), 75–83. <https://doi.org/10.1016/j.geoderma.2010.02.003>
- Ramírez-Guinart, O., Kaplan, D., Rigol, A., Vidal, M., 2020a. Deriving probabilistic soil distribution coefficients (K_d). Part 1: General approach to decreasing and describing variability and example using uranium K_d values. *J. Environ. Radioact.* 222, 106362. <https://doi.org/10.1016/j.jenvrad.2020.106362>
- Ramírez-Guinart, O., Kaplan, D., Rigol, A., Vidal, M., 2020b. Deriving probabilistic soil distribution coefficients (K_d). Part 2: Reducing caesium K_d uncertainty by accounting for experimental approach and soil properties. *J. Environ. Radioact.* 223–224. <https://doi.org/10.1016/j.jenvrad.2020.106407>
- Ramírez-Guinart, O., Kaplan, D., Rigol, A., Vidal, M., 2020c. Deriving probabilistic soil distribution coefficients (K_d). Part 3: Reducing variability of americium K_d best estimates using soil properties and chemical and geological material analogues. *J. Environ. Radioact.* 223–224, 106378. <https://doi.org/10.1016/j.jenvrad.2020.106378>

- Ramírez-Guinart, O., Salaberria, A., Vidal, M., Rigol, A., 2017. Assessing soil properties governing radiosamarium sorption in soils: Can trivalent lanthanides and actinides be considered as analogues? *Geoderma*, 290, 33–39. <https://doi.org/10.1016/j.geoderma.2016.12.010>
- Rath, S., Fostier, A. H., Pereira, L. A., Dioniso, A. C., de Oliveira Ferreira, F., Doretto, K. M., Maniero Peruchi, L., Viera, A., de Oliveira Neto, O. F., Dal Bosco, S. M., Martínez-Mejía, M. J., 2019. Sorption behaviors of antimicrobial and antiparasitic veterinary drugs on subtropical soils. *Chemosphere*, 214, 111–122. <https://doi.org/10.1016/j.chemosphere.2018.09.083>
- Redgrave, L. S., Sutton, S. B., Webber, M. A., Piddock, L. J. V., 2014. Fluoroquinolone resistance: Mechanisms, impact on bacteria, and role in evolutionary success. *Trends Microbiol.* 22 (8), 438–445. <https://doi.org/10.1016/j.tim.2014.04.007>
- Riaz, L., Mahmood, T., Khalid, A., Rashid, A., Ahmed Siddique, M. B., Kamal, A., Coyne, M. S., 2018. Fluoroquinolones (FQs) in the environment: A review on their abundance, sorption and toxicity in soil. *Chemosphere*, 191, 704–720. <https://doi.org/10.1016/j.chemosphere.2017.10.092>
- Riaz, L., Mahmood, T., Yang, Q., Yasir, M. W., Rashid, A., Coyne, M. S., D'angelo, E., 2019. Sorption and Desorption Behavior of Fluoroquinolone Antibiotics in an Agricultural Soil. *Pedosphere*, 29 (5), 676–680. [https://doi.org/10.1016/S1002-0160\(19\)60831-3](https://doi.org/10.1016/S1002-0160(19)60831-3)
- Septian, A., Oh, S., Shin, W. S., 2018. Sorption of antibiotics onto montmorillonite and kaolinite: competition modelling. *Environ. Technol.* 1–14. <https://doi.org/10.1080/09593330.2018.1459870>
- Sheppard, S. C., 2011. Robust prediction of K_d from soil properties for environmental assessment. *Human Ecol. Risk Assess.* 17 (1), 263–279. <https://doi.org/10.1080/10807039.2011.538641>
- Sidhu, H., Angelo, E. D., Connor, G. O., 2019. Retention-release of ciprofl oxacin and azithromycin in biosolids and biosolids-amended soils. *Sci. Total Environ.* 650, 173–183. <https://doi.org/10.1016/j.scitotenv.2018.09.005>

- Sturini, M., Speltini, A., Maraschi, F., Profumo, A., Pretali, L., Fasani, E., Ibini, A., 2012. Sunlight-induced degradation of soil-adsorbed veterinary antimicrobials Marbofloxacin and Enrofloxacin. *Chemosphere*, 86 (2), 130–137. <https://doi.org/10.1016/j.chemosphere.2011.09.053>
- Teixidó, M., Medeiros, J., Beltrán, J., Prat, M. D., Granados, M., 2014. Sorption of enrofloxacin and ciprofloxacin in agricultural soils: Effect of organic matter. *Adsorpt. Sci. Technol.* 32 (2–3), 153–163. <https://doi.org/10.1260/0263-6174.32.2-3.153>
- USEPA, 2014. Risk Assessment Forum White Paper: Probabilistic Risk Assessment Methods and Case Studies. U. S. Environmental Protection Agency, EPA/100/R-14/004.
- Uslu, M. Ö., Yediler, A., Balçioğlu, I. A., Schulte-Hostede, S., 2008. Analysis and sorption behavior of fluoroquinolones in solid matrices. *Water Air Soil Pollut.* 190 (1–4), 55–63. <https://doi.org/10.1007/s11270-007-9580-0>
- Van Doorsaler, X., Dewulf, J., Van Langenhove, H., Demeestere, K., 2014. Fluoroquinolone antibiotics: An emerging class of environmental micropollutants. *Sci Total Environ.* 500-501, 250-269. <https://10.1016/j.scitotenv.2014.08.075>
- Vasudevan, D., Bruland, G. L., Torrance, B. S., Upchurch, V. G., Mackay, A. A., 2009. pH-dependent ciprofloxacin sorption to soils: Interaction mechanisms and soil factors influencing sorption. *Geoderma* 151, 68–76. <https://doi.org/10.1016/j.geoderma.2009.03.007>
- Wan, M., Li, Z., Hong, H., Wu, Q., 2013. Enrofloxacin uptake and retention on different types of clays. *J. Asian Earth Sci.* 77, 287–294. <https://doi.org/10.1016/j.jseaes.2013.02.032>
- Wang, P., Zhang, D., Zhang, H., Li, H., Ghosh, S., Pan, B., 2017. Impact of concentration and species of sulfamethoxazole and ofloxacin on their adsorption kinetics on sediments. *Chemosphere* 175, 123 - 129. <https://doi.org/10.1016/j.chemosphere.2017.02.038>
- Wei, M., Lv, D., Cao, L. H., Zhou, K., Jiang, K., 2021. Adsorption behaviours and transfer simulation of levofloxacin in silty clay. *Environ. Sci. Pollut. R.* 28 (34), 46291–46302. <https://doi.org/10.1007/s11356-021-13955-x>

- Williams, M., Ong, P. L., Williams, D. B., Kookana, R. S., 2009. Estimating the sorption of pharmaceuticals based on their pharmacological distribution. *Environ. Toxicol. Chem.* 28 (12), 2572–2579.
- Wu, Q., Li, Z., Hong, H., Li, R., Jiang, W., 2012. Desorption of ciprofloxacin from clay mineral surfaces. *Water Res.* 47 (1), 259–268. <https://doi.org/10.1016/j.watres.2012.10.010>
- Wu, D., Li, H., Liao, S., Sun, X., Peng, H., Zhang, D., Pan, B., 2014. Co-sorption of ofloxacin and Cu (II) in soils before and after organic matter removal. *Sci. Total Environ.* 481 (1), 209–216. <https://doi.org/10.1016/j.scitotenv.2014.02.041>
- Zhang, J. Q., Dong, Y. H., 2007. Adsorption of Norfloxacin on Four Typical Soils in China (in chinese). *Environ. Sci.* Vol 28, No 9, 2134-2140. <https://doi.org/10.1016/j.jhazmat.2007.11.046>
- Zhang, J., Dong, Y., 2008. Effect of low-molecular-weight organic acids on the adsorption of norfloxacin in typical variable charge soils of China. *J. Hazard. Mater.* 151 (2–3), 833–839. <https://doi.org/10.1016/j.jhazmat.2007.11.046>
- Zhang J., Li, Z., Ge, G., Sun, W., Liang, Y., Wu, L., 2009. Impacts of soil organic matter, pH and exogenous copper on sorption behavior of norfloxacin in three soils. *J. Environ. Sci.* 21 (5), 632–640. [https://doi.org/10.1016/S1001-0742\(08\)62318-9](https://doi.org/10.1016/S1001-0742(08)62318-9)
- Zhang, L., Dong, D., Hua, X., Guo, Z., 2019. Sorption of the fluoroquinolone antibiotic ofloxacin by aquatic sediments : influence of biofilm development at the sediment-water interface. *J. Soils Sed.* 19, 4063–4072. <https://doi.org/10.1007/s11368-019-02356w>
- Zhao, H., Xiang, L., Wu, X., Jiang, Y., Li, H., Li, Y., Cai, Q., Mo, C., Liu, J., Wong, M., 2017. Low-molecular-weight organic acids correlate with cultivar variation in ciprofloxacin accumulation in Brassica. *Sci. Reports*, 1–11. <https://doi.org/10.1038/s41598-017-10701-7>
- Zhou, D., Chen, B., Wu, M., Liang, N., Zhang, D., Li, H., Pan, B., 2014. Ofloxacin sorption in soils after long-term tillage: The contribution of organic and mineral compositions. *Sci. Total Environ.* 497–498, 665–670. <https://doi.org/10.1016/j.scitotenv.2014.07.130>

CHAPTER VII
CONCLUSIONS

Regarding the identification of key parameters governing PFASs and FQs sorption in soils and other environmental matrices, the following conclusions can be drawn:

- Sorption of PFASs in soils is largely governed by soil organic carbon content through hydrophobic interactions, and it increases with increasing PFAS chain length. The contribution of the mineral phase (*i.e.*, silt and clay phases) can play a significant role in sorption for those soils with a low organic carbon content, but sorption in these scenarios is generally very low.
- Sorption of PFASs in carbon-rich materials (*e.g.*, biochars and activated carbons) is governed by hydrophobic interactions and it increases with increasing PFAS chain length. Contrarily to what was observed in soils, not only the quantity of organic carbon, but its quality (expressed by its aromaticity through the C_{ORG}/O molar ratio) is an important descriptor of PFAS sorption. Sorption increases when increasing material aromaticity, and additionally, material surface area plays an additional role in sorption providing extra sorption sites.
- Sorption of FQs in humic acids is fast, strong, irreversible, affected by calcium cations and highly pH-dependent. Sorption is driven by multiple interaction mechanisms, including cation – π , electrostatic and hydrogen and halogen bonding interactions. Moreover, the sorption of norfloxacin, ciprofloxacin and ofloxacin in humic and fulvic acids can be considered analogous. On the other hand, sorption of FQs in phyllosilicate minerals is relatively strong, although highly pH-dependent. This pH dependence is due to both the speciation of the FQs and the overall surface charge of the clay, related to its pH_{ZPC} . Under acid to neutral conditions, sorption is driven by cation exchange mechanisms, and follows the trend: 1:2 swelling clays (*e.g.*, montmorillonite) > 1:2 non-swelling clays (*e.g.*, palygorskyte, vermiculite, illite) > 1:1 clays (*e.g.*, kaolinite).

Lastly, sorption of FQs in metal oxides, although affected by pH and ionic strength, is mainly driven by complexation mechanisms with the metal atoms in the mineral surface under neutral pH conditions. The resulting sorption affinity is dependent on the metal nature (with increasing affinity according to the Irving-Williams series), whereas for a specific set of metal oxides and (hydro)oxides (*e.g.*, Fe), sorption increases when increasing mineral surface area.

- The identification of key properties affecting FQ sorption in pure soil components allowed to deduce the main phases responsible for sorption in soils. Besides confirming the sorption analogy among target FQs, it was confirmed that sorption of FQs in bulk soils is pH-dependent, being soil pH, clay and organic matter content key parameters descriptors of sorption.

Regarding the development of K_d prediction models for PFASs and FQs in environmental matrices, the following conclusions can be drawn:

- An empiric K_d prediction model for PFASs in soils was developed by accounting the relative contribution of organic and mineral phases in the overall K_d . The model, constructed by contemplating a wide range of PFAS and soils after gathering data from the literature, included only three variables: the organic carbon and the reactive mineral phase (silt + clay) contents, and the number of fluorinated carbons of the PFAS. A validation procedure ensured its ability to roughly predict K_d values for a wide range of scenarios and PFASs.
- An empiric K_d prediction model for PFASs in carbon-rich materials (applicable to biochars and activated carbons) was developed with our own sorption data supplemented with a few literature data to enhance its range of applicability. The model included only three variables: the quality and quantity of sorption sites (represented by the C_{ORG}/O molar

ratio and the specific surface area, respectively) and the number of fluorinated carbons of the PFAS. Validating the model against additional data gathered from the literature ensured its applicability to roughly predict the potential affinity of these materials to sorb PFASs. To our knowledge, this is the first available model with these features in the current literature.

- Using both experimental and literature data in the case of humic acids, and only literature data in the case of metal oxides and phyllosilicate minerals, several empirical equations have been proposed to predict the K_d of FQs in these pure soil components. Specifically, and despite the multiple sources of variability due to the contemplation of different materials and experimental conditions, the sorption K_d values in humic acids and different phyllosilicate minerals at different pH values were relatively well described by a second-grade polynomial fitting, highlighting the important role of pH on the sorption of FQs in these materials. Besides, a linear model was proposed to predict K_d values for FQs in metal oxides and (hydro)oxides of Fe at neutral pH according to its surface area. To our knowledge, these are the first proposed equations to predict the sorption of FQs in these pure soil components.
- An empiric K_d prediction model for FQs in soils was developed after multivariate analyses. The model was constructed with own and selected literature data to be applicable to a wide range of scenarios. Whereas similar, previously reported prediction models had not been externally validated, the external validation exercise applied to our model revealed a poor prediction ability when tested against additional literature data, likely due to its incapability to describe the non-linear sorption of FQs with pH.

- Due to the low prediction quality of the K_d (FQ) prediction model, alternatively, a set of best-estimate K_d values with associated uncertainty were proposed by refining an overall sorption K_d dataset for FQs in soils grouped according to specific key properties (pH, organic carbon and sand contents) through cumulative distribution functions. According to our knowledge, this is the first time that probabilistic K_d values for FQs in soils have been derived.

